Methodology for the Evaluation of Natural Ventilation in Buildings Using a Reduced-Scale Air Model

by
Christine E. Walker

M.S. Mechanical Engineering
University of Illinois at Chicago, 2001

B. S. Architectural Sciences
University of Illinois at Champaign-Urbana, 1998

Submitted to the Department of Architecture in
Partial Fulfillment of the Requirements for the Degree of

Doctor of Philosophy in Building Technology

at the

Massachusetts Institute of Technology

February 2006

Signature of Author .....
Department of Architecture
September 15, 2005

Certified by .....
Leon R. Glicksman, PhD
Professor of Mechanical Engineering and Building Technology
Thesis Supervisor

Accepted by .....
Yung Ho Chang
Department Head
Department of Architecture

Thesis Committee:
Leon R. Glicksman, Advisor, Professor of Mechanical Engineering and Building Technology
Leslie K. Norford, Professor of Building Technology
John H. Lienhard, Professor of Mechanical Engineering

Methodology for the Evaluation of Natural Ventilation in Buildings Using a Reduced-Scale Air Model

Submitted to the Department of Architecture on September 15th, 2005
In Partial Fulfillment of the Requirements for the Degree of
Doctor of Philosophy in Building Technology

ABSTRACT

Commercial office buildings predominantly are designed to be ventilated and cooled using mechanical systems. In temperate climates, passive ventilation and cooling techniques can be utilized to reduce energy consumption while maintaining occupant comfort using natural ventilation. However, current modeling techniques have limitations and assumptions that reduce their effectiveness in predicting internal building performance. There are few tools to predict the thermal performance of and resulting airflow patterns in naturally ventilated office buildings accurately.

This thesis presents three significant contributions for the evaluation of natural ventilation in buildings:

- A methodology for assessing the performance of naturally ventilated buildings through a reduced-scale air model was developed based on dimensional analysis and similitude criteria. Buoyancy, wind, and combined ventilation strategies for a multi-zoned commercial office building with an open floor plan layout were evaluated using the reduced-scale model.

- Guidelines were established for monitoring natural ventilated buildings as a means to evaluate their operation, based on field measurements of a prototype building were established.

- A framework for evaluating current techniques for modeling airflow patterns in naturally ventilated buildings was developed, including guidelines for model development and analysis.

Data from the reduced-scale model were compared to the data obtained from monitoring a prototype building and then used in creating numerical simulations. Certain building characteristics, such as atrium stack vents and railings, influenced the resulting simulation predictions and simple analytical model results. Lack of detailed temperature stratification and surface temperature data in the prototype building prohibited the exact comparison of the methodology for more complex design characteristics, such as thermal mass.

Thesis Supervisor: Leon R. Glicksman
Title: Professor of Mechanical Engineering and Building Technology

Table of Contents

List of Figures

List of Tables

Acknowledgements

Financial support for this research was provided by several sources, including the Cambridge-MIT Institute and the Dean for Graduate Students. The generous support was greatly appreciated.

I want to be sure to thank the Building Technology lab for the many discussions, laughs and moral support through the past four years. In particular, I would like to thank Rogelio Palomera-Arias, Harn-Wei Kua, Anubhav Gupta, Henry Spindler, Peter Armstrong, and all of the first years. Lisa Engblom and Wanda Lau, you guys have been great this past year. Rogelio and Harn, thank you for the discussions and late nights. Henry and Peter, your knowledge has always been helpful. To the Building Technology staff, thank you for assisting in all of the details, making things move usually seamlessly. Thank you to Kathleen Ross and Nancy Dalrymple, and Dorrit Schuchter and Sara MacDonald for taking care of so many details.

To my family and friends, thank you for always listening, supporting, and reviewing my efforts over the past four years. Michael, you have always been a true friend, willing to discuss and review my research, and supportive throughout. Paul, you have my gratitude for always pushing me to succeed and being a sounding board for concerns and questions. To my parents, I will always appreciate your listening and supporting me through this substantial milestone.

The Building Technology Program provided a great opportunity to collaborate with colleagues at the BP Institute in Cambridge, UK. Thank you to Stephen Livermore for the cooperation and hard work. I appreciate all of the discussions with Shaun Fitzgerald, Lotty Gladstone, Shweta Manchanda, and Andy Woods. This research has benefited from our partnership. I am grateful to the Aldwyck Housing Association for their acceptance of our equipment and presence in evaluating their building for this research.

I am indebted to my thesis committee members for their support and insight during my research, for their time, effort, and encouragement. Your suggestions and consideration was greatly appreciated. To my advisor, Leon Glicksman, your perceptiveness and our discussions were invaluable in the advancement of this research.

Chapter 1.0

Introduction

Energy consumption and building performance are key issues when evaluating the life cycle of commercial office buildings. As energy costs increase, there is a desire by owners, operators, and designers to reduce energy consumption and operating costs in commercial office buildings without impairing indoor air quality. Beginning with the energy crisis in 1973 attempts were made to make buildings more energy efficient, resulting in increased insulation levels and more tightly constructed buildings (Allard 2002). Subsequent building construction practices led to moisture entrainment issues, causing mold that negatively affected the health of occupants. After a series of problems with Sick Building Syndrome (SBS), building construction strategies were revised, and in the mid-1990s natural ventilation and low energy building design began to develop as an alternative approach, through innovative heating, cooling, and ventilation methods. In a study of office buildings in California comparing naturally ventilated buildings and mechanically ventilated and air-conditioned buildings, it was found that naturally ventilated buildings had the least number of health issues when compared to mechanically ventilated and air-conditioned ones overall (Fisk et al 1993, Seppanen and Fisk 2002). Certain building characteristics have emerged from the study of low energy and passive cooling designs as the means to ensure good building performance. However, problems have surfaced as well, including difficulties with the integration of building components, cooperation between engineers and architects, and having to develop new techniques for evaluating these passive and low energy designs.

Current aspects of low energy building design include lighting and controls, ventilation systems, and the improved building envelope. Lighting energy can be reduced through the use of high efficiency fixtures and controls such as occupancy sensors that turn banks of lights off when no movement is sensed, and photosensors that reduce the light output as needed to maintain a minimum light level. These technologies combined with design details like light shelves, high windows, external shading and atria, increase the natural daylight throughout the building while reducing energy consumption associated with artificial light. Systems that consume energy required for providing fresh air to meet indoor air quality requirements can be reduced or eliminated with the use of passive or hybrid technologies. Hybrid ventilation, or the use of natural and mechanical systems to cool and ventilate buildings, offer opportunities to take advantage of the external conditions when appropriate, but have a mechanical system to maintain the indoor environment when the external conditions are not adequate. Additionally, building envelope systems such as high levels of insulation or the use of thermal mass can help to temper the internal environment, reducing the amount of supplementary heating or cooling needed to maintain occupant comfort.

In addition to overall building performance, the indoor environment and occupant comfort has emerged as an important design consideration in both mechanically and naturally ventilated buildings. Passively cooled and ventilated buildings have many benefits not only in reduced

energy consumption and reduced first cost with ventilation equipment, but also in terms of the occupant environment. Occupant comfort, though difficult to quantitatively measure, has been evaluated through occupant surveys such as the PROBE studies (Bordass 2001). It has been found that the indoor temperature associated with thermal comfort of occupants has a larger range in naturally ventilated buildings (Braeger and de Dear 2000), extending the range of exterior temperatures at which natural ventilation is usable. The interior temperature is only one aspect of the indoor environment, which includes air velocities and surface temperatures as well. In the design of naturally ventilated buildings, concern over the disturbing of papers due to high air velocities is a factor, but slightly higher velocities can also help in maintaining comfort with higher internal temperatures. With slight increases in velocities, from 0.1 m/s to 0.25 m/s, occupants can tolerate a temperature increase of 3.6°C without any additional discomfort (Chandra et al 1986). For air velocities within the occupied space up to 0.4m/s occupants can tolerate interior temperatures of 28°C or 30°C as long as there are cooler surface temperatures on surrounding walls, floors or ceilings (Allard 2002). Cooler surface temperatures can be achieved through proper use of thermal mass in the building design. Passively cooled and ventilated environments have increased occupant satisfaction when occupants have the ability, or perceived ability, to control their own environment through the use of operable windows (Jones and West 2001).

The location of the building affects its performance as well. Climate influences the feasibility and usage period of natural ventilation as a means to cool a building. Buildings in temperate climates can use natural ventilation for most of the cooling season, May through October. In climates with a wider temperature range, including hot summers, passive cooling is still applicable, but greater attention to detail and design characteristics must be made. Lechner (1991) divided the United States into 17 different climate regions, based on maximum, minimum and average monthly temperatures, humidity, wind, sunshine and degree-days. Of the 17 climates identified, 12 regions could benefit from natural ventilation, at least for a portion of the cooling period (Jones and West 2001).

1.1 Building Energy Use

In temperate climates, the energy consumption required to cool and ventilate a building can be reduced by incorporating natural ventilation in the building design, though it is not often done. In the United Kingdom (UK), which has a climate suitable for naturally ventilated buildings, only a handful of naturally ventilated commercial office buildings exist. The number is even less in the United States (US). Thirteen percent of the UK total energy consumption is used in the service sector, which includes retail buildings. Of the 13 percent, 61 percent is consumed by the private commercial sector (DTI 2004), or commercial office buildings. Thus, commercial buildings consumed 7.9 percent of total energy used in the UK, as compared to 17 percent of the total energy usage consumed by commercial buildings in the US (EIA 2004). Though heating makes up most of the energy usage both in the US and UK, cooling energy is also a significant portion, representing almost 10 percent of all energy usage for commercial buildings (DTI 2004). In the US, only 3 percent of commercial office buildings do not have air-conditioning. The breakdown of energy usage by sub-system for commercial office buildings in both the US and the UK is presented in Table 1. The majority of the energy is used for heating, cooling, and ventilating occupied spaces. The US tends to have better envelope systems, but not necessarily high efficiency lighting or lighting controls. The UK, on the other hand, is known for its under-

insulated building envelopes with their substantially higher heating energy requirements. The adoption of passive cooling and ventilation methods in the United States could impact energy use, particularly for cooling and ventilation, which together make up almost 15 percent of commercial office building energy consumption.

Table 1. Energy End Use for Commercial Office Buildings, Percent of Total

	Space Heating	*Cooling and Ventilation*	*Water Heating*	*Lighting*	*Cooking*	*Office Equipment*	Other
United States	25.0	14.6	8.9	28.9	1.0	15.6	5.9
United Kingdom	59.2	9.0	6.6	13.6	2.7	6.3	2.6

The use of passive cooling techniques could be a potential design strategy component even in the United States. By incorporating energy efficient technologies, control schemes, and improved building envelope design required heating and cooling loads could be decreased. More energy-efficient lighting fixtures, combined with control systems that allow lighting to be turned off when not in use or dimmed when sufficient light levels exist, would address lighting-related energy efficiency issues and are commonly used in commercial office buildings. Designers and engineers continue to improve the building envelope and façade treatments to reduce heat loss through the envelope and solar gains through the windows, thereby decreasing heating and cooling requirements and minimizing the difference between indoor air and surface temperatures that may cause occupants discomfort. The increased use of thermal mass to temper the indoor air temperature has become more widely used in commercial building design.

1.2 Difficulties in Predicting Natural Ventilation

Although natural ventilation has the potential to significantly reduce energy consumption related to cooling buildings, several factors impede the application of this ventilation strategy in commercial office buildings. There is concern over building performance and occupant comfort, particularly in which occupants will not be subject to warm temperatures outside of their comfort area or uncomfortable interior environments during their workday. There is a lack of understanding of natural ventilation and the resulting temperatures and airflows for specific climates, a lack of comprehensive tools to analyze design strategies effectively, quickly and in detail, and a preconceived notion that appearance of a naturally ventilated building will be odd.

Currently there are limited tools to predict or assess the performance of natural ventilation in buildings, pre or post occupancy. Tools for use in the design stage, such as MIT's Design Advisor (http://designadvisor.mit.edu), provide preliminary data on the performance of a single space when building characteristics, such as orientation, materials, and location, are entered through the user interface. However, modeling programs do not adequately model natural ventilation effects. Some commercially available programs, such as AIDA and AIM-2 only model single zones and do not have the ability to set occupancy schedules. Other programs, such as AIOLOS and BREEZE are able to model multiple zones but still do not take into account occupancy schedules or conductive heat transfer into or out of the building (Emmerich et al 2001). These last two programs do allow the user to define opening schedules for windows as part of a simulation. The AIOLOS software, based on network modeling, is used for the

calculation of the airflow rate in naturally ventilated spaces configurations. The BREEZE software program estimates ventilation and airflows in multi-zone buildings, and calculates airflow rates based on user defined openings and leakage paths (Orme and Leksmono 2002).

COMIS and CONTAMW are two software programs that are multi-zone modeling tools with occupancy and opening schedules, but have underlying assumptions that make them less than ideal for the prediction of detailed information on a specific space within a building (Orme and Leksmono 2002). One of the major assumptions in both modeling systems is that of a well-mixed space, which does not necessarily occur in naturally ventilated buildings. Furthermore these software programs are meant to model the ventilation portion of the system based only on mass flow balances, not to consider any thermal loads which often overshadow mass flow effects. Ventilation models and thermal models are then 'coupled' together in an attempt to overcome this deficiency.

More complex software packages such as DOE-2 and EnergyPlus have some ability to model natural ventilation, but again assume a well-mixed environment. DOE-2 relies on a user-input for the ventilation rate, while EnergyPlus is integrated with the COMIS multi-zone airflow model to determine flow rates. These programs are considered whole building simulation programs, and account for conduction through the building envelope, occupancy, lighting and equipment schedules in addition to ventilation modeling issues.

Numerical software packages such as PHOENICS model airflow and thermal conditions for a range of applications, but do not account for conduction through the building envelope. They are unique in their ability to predict airflow patterns and temperature distributions throughout a single space or simple building, rather than bulk airflow rates (Orme 1999). Still, when inputting the boundary conditions and parameters describing the space, the user must take care to provide enough detail. The numerical solutions from these computational fluid dynamic models must be validated and results verified, as this limitation in their modeling structure can cause erroneous results.

1.3 Examples of Naturally Ventilated Buildings

There is a trend for more buildings to incorporate natural ventilation as a scheme for cooling and ventilating part of or a whole building. Some of these buildings emphasize design characteristics making them stand out in a typical streetscape, while others lean toward a more traditional building façade. Both strategies work and examples of each are presented here for comparison. Office buildings selected for comparison include each of three types of natural ventilation: buoyancy or stack driven flow, cross ventilation, and cross ventilation with an atrium. These examples demonstrate the application of natural ventilation to buildings that have schedules and heat loads typical of commercial office buildings, and show the effectiveness of natural ventilation in building design. Most naturally ventilated buildings are located in Europe, and the examples here are from the United Kingdom and the Netherlands.

Of the examples, one in particular accentuates the design characteristics on the façade of the building, the home of the British Research Establishment (BRE). This building incorporates stack vents into the ventilation scheme, and makes them pronounced in the architecture of the building. The BRE, designed by Fielden Clegg and built in 1997, is well known for its low

energy usage and efficient design. It combines the use of thermal mass, cross ventilation and stacks to passively cool the building. The building's stacks not only are a prominent feature in its façade, but also assist in driving buoyancy and stack driven air flow. They are constructed of glass block, shown in Figure 1, creating a greenhouse effect that warms up air within the shaft which as it rises, draws in cooler air through other openings on the façade. The occupants have control over the lights and window openings as shown in Figure 2.

The European Patent Office (EPO) is a naturally ventilated office building in The Hague that uses cross ventilation to passively cool and ventilate the tower portion of the building. The structure was built in 1972 by architect R.D. Bleeker, with a limited number of design requirements for the building. The design includes large amounts of thermal mass and exterior shading to temper the interior environment and shade it from large solar heat gains, as shown in Figure 3. Each perimeter office is equipped with manually controlled windows, two upper windows and two lower windows, shown in Figure 4.

The Pearson Education Building (Figure 5), otherwise known as the Edinburgh Gate building, combines an open office floor plan with operable windows and louvers to promote natural ventilation and airflow through the building. This building primarily relies on cross-ventilation to meet ventilation and summer cooling requirements. There are three atria located throughout the building to assist in ventilating the surrounding offices, and which supply warmer air in the winter and exhaust warm air in the summer. Built in 1995, the Pearson building incorporates solar shading, thermal mass, and uses awning type windows (Figure 6).

These examples are of buildings that have been in operation a minimum of 5 years and use a variety of natural ventilation strategies. Their performance has been monitored by organizations such as NatVent, which is a Pan-European project encouraging the use of natural ventilation in office-type buildings. The post-occupancy monitoring of these passively ventilated buildings provides critical insight into the functioning and performance of specific buildings that incorporate various design strategies. These buildings were assessed primarily based on remote monitoring, which only provides part of the overall performance.

Figure 1. BRE Office Building Facade with Stacks[1]

Figure 2. Building Interior

[1] Photos by Roger Chang, SMBT MIT, 2002

Figure 3. European Patent Office Building Exterior

Figure 4. Interior View of Windows

Figure 5. Edinburgh Gate Office Building Exterior Facade

Figure 6. Interior View of Window

1.4 Goals of this Research

Monitoring alone provides insight into the operation of a particular building over a determined amount of time, but monitoring alone does not enable that insight to be extended and use to predict the performance of other buildings. The focus of this research is to develop a methodology that can be used to evaluate and then predict the performance of natural ventilation in other buildings. The development starts with the monitoring of an existing naturally ventilated building with certain design characteristics. Through modeling and supported by data from monitoring, the operation of the building under certain environmental conditions can be understood. The natural ventilation strategies modeled are pure buoyancy-driven flow, wind-driven flow, and combined wind-buoyancy driven flow. By using data from a monitored building to calibrate the results of a reduced-scale air model through dimensional analysis and similitude, the configuration of the model then can be altered to determine what impact changes in certain design characteristics would have under the three natural ventilation strategies. In addition, the reduced-scale air model can provide a validation of models using computational fluid dynamic simulations. Once developed this new methodology will provide the framework for furthering the understanding of the performance of natural ventilation in buildings and improving current simulation methods to better predict temperatures and flow patterns within naturally ventilated buildings. First, the underlying driving forces of natural ventilation must be understood and applied to airflow in buildings. Then key design characteristics will be more easily identified so that their affect on the indoor environment can be enhanced. This increased predictive ability in turn will help in the development of better simulation tools for designers and engineers to assess the benefits of incorporating passive cooling in new or rehabilitated commercial buildings.

While this research has three parts (monitoring, modeling, and simulation), each part is used for comparing and evaluating a modeling procedure. Data from the monitoring of a naturally ventilated building is used in the development and construction of a reduced-scale air model that can then be utilized to evaluate design characteristics of the original building. The numerical simulations of the reduced-scale model provide verification of results from the experimental work, and identify issues in numerical modeling tools. The experimental work is non-dimensionalized to compare it to the original data from the full-scale building and numerical simulation of the full-scale building, and then applied to determine the influence of the three types of natural ventilation on temperature distribution and airflow patterns within the building.

1.5 Scope of document

This thesis presents the foundation of the methodology for modeling natural ventilation airflow in buildings. The focus is on the three natural ventilation cases: buoyancy-driven, wind-driven, and combined buoyancy-wind driven ventilation. A methodology is developed and used to evaluate natural ventilation in a commercial office building, using a reduced-scale air model. A numerical model using computational fluid dynamics was created to check the experimental results and better understand some of the heat transfer phenomena, not readily obtained through experimental work. With the validation of this methodology, other configurations of naturally ventilated buildings can be evaluated using reduced-scale air models (or CFD with care in

selecting boundary conditions) to enhance the performance of naturally ventilated buildings and improve simulation methods.

The organization of this thesis is as follows:

- Chapter 2 presents the three types of natural ventilation and building characteristics that are often considered in the design of naturally ventilated buildings. Also presented are the methods used to assessing the performance of a naturally ventilated commercial office building used as reference point for the development of the methodology.
- Chapter 3 describes the process and measurements taken in evaluating the reference, or prototype building, Houghton Hall. A description of the building and presentation of the data resulting from 16 months of monitoring are presented and will be used in part to validate the methodology in a later chapter.
- Chapter 4 explains the modeling and flow visualization techniques that are currently in use for models at a variety of scales and working fluids. An overview of the three main modeling techniques is presented, along with the impact of scale, fluid, and natural ventilation type under investigation. The principles of flow visualization and its application to buildings is discussed, along with the selection of the technique used in the reduced-scale modeling experiments.
- Chapter 5 provides dimensional analysis and similitude requirements for the use of scale modeling in simulating full-scale phenomena. The governing equations for the analysis of flow are presented and then non-dimensionalized to obtain the dimensionless parameters. The selection of which dimensionless parameters to match is discussed, along with other similarity requirements for reduced-scale modeling.
- Chapter 6 outlines the experiments conducted using the reduced-scale air model in the test chamber. Buoyancy, wind and combined natural ventilation experiments are described for several different configurations using both the physical model and the complimentary numerical model,. The equipment and model materials used in the construction and measurement of the reduced-scale air model are presented.
- Chapter 7 presents the data gathered from the experimental and computational models. Included in this chapter are the analyses and comparisons of the modeling techniques used, and issues that arose while conducting the experimental and simulation work. The results are presented in non-dimensionalized form for comparison.
- Chapter 8 provides guidelines for modeling airflow in naturally ventilated buildings. A comparison of the current techniques including the methodology developed for this research, how to apply those techniques in modeling, and the limitations of each technique are discussed.
- Chapter 9 concludes the thesis and provides suggestions for future research. A summary and evaluation of the method developed for evaluating natural ventilation in buildings using a reduced-scale air model are presented.
- References and appendices follow Chapter 9

Chapter 2.0

Natural Ventilation

2.1 Introduction

Natural ventilation has been used throughout history as a means to ventilate and passively cool structures. With the advent of more densely populated office buildings, with more computers, higher internal heat loads, and deeper floor plans, buildings have moved toward tighter construction, controlling the air introduced into the building, and are generally cooled mechanically. It is the increased heat load and concerns over occupant comfort that often restrict dependence on natural ventilation in commercial office buildings, even in temperate climates. The attainment of uniform internal temperatures for occupant comfort was thought to be possible only by controlling amount of air being supplied to an occupied space and its temperature.

Although summer conditions are of primary concern related to occupant comfort, attention has to be paid to the winter conditions to ensure that the building also performs well during periods with cold external temperatures. During the summer months, the goal is to bring in ventilation to meet comfort requirements and cool the space using purpose-provided openings. In the winter however, any infiltration will add to the cost of heating the space to meet comfort requirements. A well designed and constructed naturally ventilated building should be able to perform satisfactorily year round. The focus of this research is on summer conditions, evaluating the airflow patterns and velocities that can be created by natural ventilation in a commercial office building.

This chapter presents the foundation of natural ventilation from the types of ventilation to specific design elements. First the types of ventilation, buoyancy-driven and wind-driven, are presented. Then design characteristics included in low-energy and naturally ventilated buildings are outlined, followed by a brief description of the specific design characteristics that were used in the prototype building. The method used to evaluate the effectiveness of natural ventilation in the prototype building is then described, followed by a discussion of factors that are unique to naturally ventilated buildings.

2.2 Types of Natural Ventilation

There are two main forces that drive natural ventilation: stack or buoyancy-driven ventilation and wind-driven ventilation. Although these types can be found individually, more commonly both are found in naturally ventilated buildings, sometimes with one type dominating the other. In this section both buoyancy- and wind-driven natural ventilation will be defined individually, followed by a description of how they are defined when found together.

2.2.1 Buoyancy-Driven Ventilation

Ventilation driven by buoyancy is prevalent in many naturally ventilated buildings, with air flow caused by pressure differences across the building envelope. With buoyancy-driven ventilation the pressure differences are due to air density differences, which in turn are due to temperature differences. It is the magnitude of these temperature differences and resulting pressure differences, as well as the building opening characteristics that determine the magnitude of the airflow due to buoyancy. In stack-driven ventilation, the addition of stack increases the height, and therefore the pressure difference, between an inlet and outlet. A temperature difference between the inlet and outlet can enhance the effects of buoyancy-driven ventilation.

A neutral pressure level (NPL) is created at the point where the internal pressure is equal to the external pressure, resulting in no airflow in or out of an opening at that particular height. Above or below the NPL, the airflow and direction can be determined; the direction of the airflow is always from the region of higher pressure to the area of lower pressure. The NPL can be calculated based on the total inlet and outlet areas and respective resistances, and their relative height if more than one floor level exists. Roof openings and chimneys or raised stacks can shift the NPL, usually to higher levels. For buoyancy driven flow, the NPL is presented graphically in Figure 7.

The Bernoulli equation is used to derive the flow due to buoyancy-driven ventilation, calculating the pressure differential due to height, i.e. the hydrostatic head, for both the exterior environment and the interior environment. The overall pressure difference between the interior and exterior can be expressed in terms of the height difference, H, gravitational constant, g, density at a reference temperature, ρ_o, and the interior and exterior temperatures. The Bernoulli equation is given by:

$$\frac{v_O^2}{2} + \frac{P_O}{\rho} + gz_O = constant \tag{2.1}$$

For the buoyancy-driven case, there is no external velocity so the relationship reduces to:

$$\frac{P_O}{\rho_O} + gz_O = constant \tag{2.2}$$

The pressure difference is applied to the outside environment, using subscript E, and the internal environment, using subscript I. The resulting pressure differences due to height between an origin height, z_O, and at some height H, z_H, for the outside and inside become:

$$\Delta P_E = \rho_E g\left(z_H - z_O\right) \tag{2.3}$$

$$\Delta P_I = \rho_I g\left(z_H - z_O\right) \tag{2.4}$$

To determine the total pressure difference, ΔP_T, the pressure difference across the inlet and outlet openings is calculated. Figure 7 illustrates this, with it resulting in:

$$\left(P_{I,H} - P_{O,H}\right) + \left(P_{O,0} - P_{I,0}\right) = gH\left(\rho_O - \rho_I\right) \tag{2.5}$$

It is assumed that air is a perfect gas, so the ideal gas law is used:

$$\rho = \frac{P}{RT} \tag{2.6}$$

and substituted into equation 2.5 for the ρ_O and ρ_I terms. Since the difference between P_O and P_I is negligible compared to atmospheric pressure, the term P/RT_B is moved outside of the parenthesis, and the ideal gas law again applied. Equation 2.5 to describe the pressure difference due to buoyancy-driven flow then becomes:

$$\Delta P_T = \rho_O gH\left(\frac{T_I - T_O}{T_I}\right) \tag{2.7}$$

The Boussinesq approximation is used for ideal gases, so that $\beta=1/T_I$. The density differences are assumed to be negligible in the Boussinesq approximation except to determine ΔP_T, since the density of air does not vary significantly with temperature over the range of temperature differences found in the reference building. The value for β used is the inverse of an average internal temperature. The Boussinesq approximation is generally valid as long as $\Delta T<30°C$ (Etheridge 1996).

The ventilation rate is calculated by using the square root law (Etheridge 1996), using the Boussinesq approximation, and substituting in equation 2.7 to yield:

$$Q = c_d A\sqrt{2\frac{\Delta P}{\rho}} = c_d A^*\sqrt{gH\frac{T_I - T_O}{T_I}} = c_d A^*\sqrt{g\beta H T_I - T_O} \tag{2.8}$$

Where Q is the flow rate through a building or space, C_d is the coefficient of discharge, and A^* is the contribution of inlet and outlet areas. A* is defined by:

$$A^* = \sqrt{\frac{A_1^2 + A_2^2}{A_1^2 A_2^2}} \tag{2.9}$$

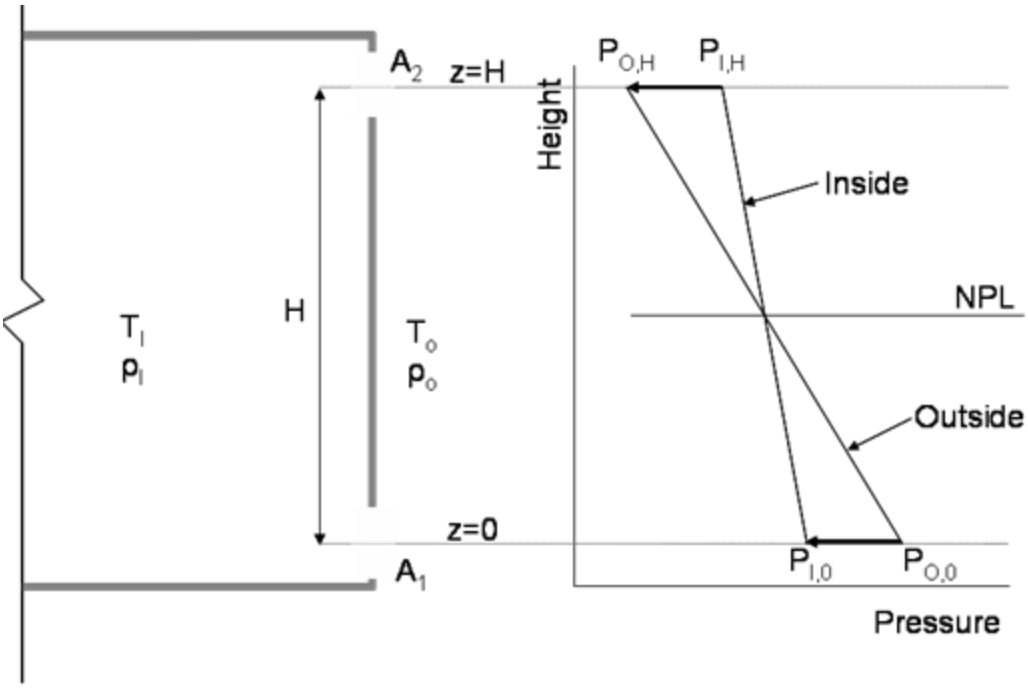

Figure 7. Neutral Pressure Level for Buoyancy Driven Ventilation

When natural ventilation is used as a means to ventilate a building under the buoyancy driven case, the airflow is not assisted with forced air from wind or mechanical systems. This is often considered the critical design situation, during warm summer months for applying this passive technique in buildings. In the buoyancy driven case, the following parameters are somewhat interdependent, making the analysis of this ventilation scheme more complicated. These include:

- the size of inlets and outlets,
- the height of the space,
- the strength of the heat sources driving the airflow,
- the resulting temperature difference between the interior and exterior spaces due to the interior heat source(s)

Additionally, complex building geometries, such as multiple floors that are directly or indirectly connected, increase the difficulty of evaluating the forces that drive natural ventilation flow. It is in part this complexity combined with the lack of understanding of the physical mechanisms involved in both buoyancy- and wind-driven natural ventilation that reduces the effective use of natural ventilation in building design.

2.2.2 Wind-Driven Ventilation

Natural ventilation is influenced by several environmental conditions, the most unpredictable being wind velocity, both its speed and its direction. Both of these factors are difficult to control and analyze, especially in a full scale building. In the actual environment, instantaneous wind speed varies with time, and the pressure difference varies with building geometry and location on the building surface. In most wind-driven natural ventilation experiments a constant, uniform wind speed is used. These design wind speeds are often the mean wind speeds for a given location over a specific period of time, often years or decades (Awbi 2003).

There are several equations that have been developed to describe pressure difference due to wind-driven flow. The equations below describe a case with a constant wind speed creating a situation where wind pressure does not fluctuate with time. However, for single-sided ventilation fluctuations in wind speed may be important. A diagram portraying wind-driven ventilation, the airflow direction and resulting pressure versus height is presented in Figure 8. If the openings on opposite sides are identical, the pressure differences across the openings are equal to half the pressure difference across the building when it is assumed that there is negligible pressure differential through the interior of the building. The Bernoulli equation applied between a point at some distance from the face of the building containing the window and the façade then reduces to the ideal equation:

$$P_w = P_O + \rho_O U_O^2/2 \tag{2.10}$$

where P_w is the pressure due to wind at the façade and P_O is the pressure away from the building, and U_O is a reference velocity away from the building. Any height differential for flow along a particular streamline is neglected, so both gz terms are zero, and the velocity at the face of the building is zero as it is the stagnation point. A pressure coefficient, c_p, is used in the actual case, and is a function of wind direction and location of the measurement on the building façade. The resulting equations are:

$$P_w = P_O + C_P \rho_O U_O^2/2 \tag{2.11}$$

$$Q = C_d A U_O \sqrt{\Delta C_P/2} \tag{2.12}$$

where Q is the flow entering or leaving through the openings. The value of c_p depends on the geometry of the building and the location on the façade, and values are often obtained through the use of wind tunnel experiments (Orme 1999). The pressure on the exterior of the building in Figure 8 is assumed to not vary significantly with height.

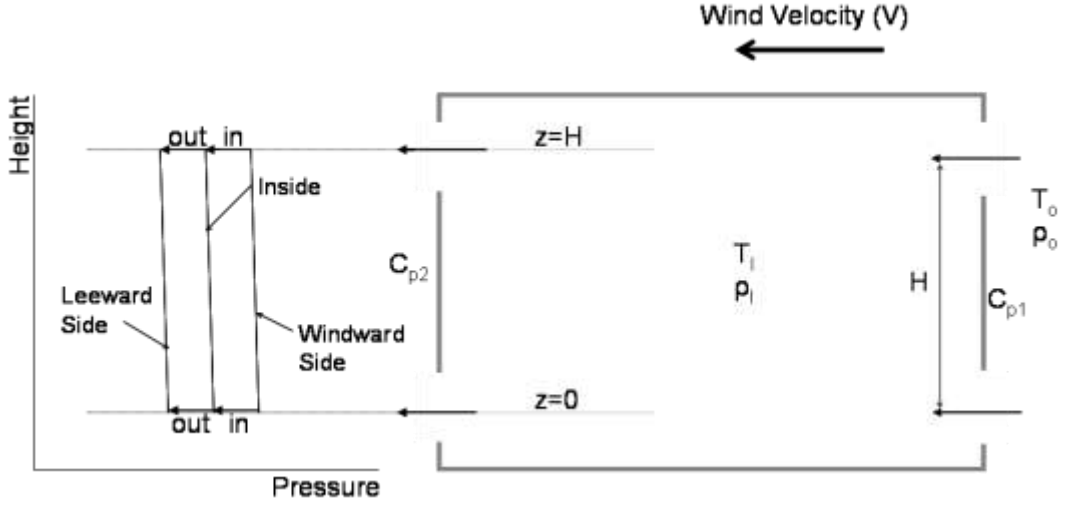

Figure 8. Wind Driven Ventilation: Airflow Direction and Pressure versus Height

Combined wind-buoyancy flow is more readily found in full-scale buildings, and these two natural ventilation types can work either together or in opposition. Figure 9 presents the airflow direction and the relation of pressure versus height in a combined buoyancy-wind natural ventilation case. The total pressures due to each case are added together to determine the total pressure across an opening:

$$\Delta P_T = \Delta P_W + \Delta P_B \tag{2.13}$$

Using the square root law presented in equation 2.8, the total flow rate through an opening is calculated by:

$$Q_T = C_D A \sqrt{2 \Delta P_T / \rho} \tag{2.14}$$

Substituting in the pressure differences for each case into equation 2.12 and then the total pressure difference into equation 2.13, the total flow rate, Q_T, becomes:

$$Q_T = C_D A \sqrt{\Delta C_P U_O^2 / 2 + g \beta H (T_B - T_O)} \tag{2.15}$$

$$Q_T = \left[Q_W^2 + Q_B^2 \right]^{1/2} \tag{2.16}$$

where Q_w is the flow rate component due to wind and Q_B is the component due to stack, or buoyancy flow (Awbi 2003).

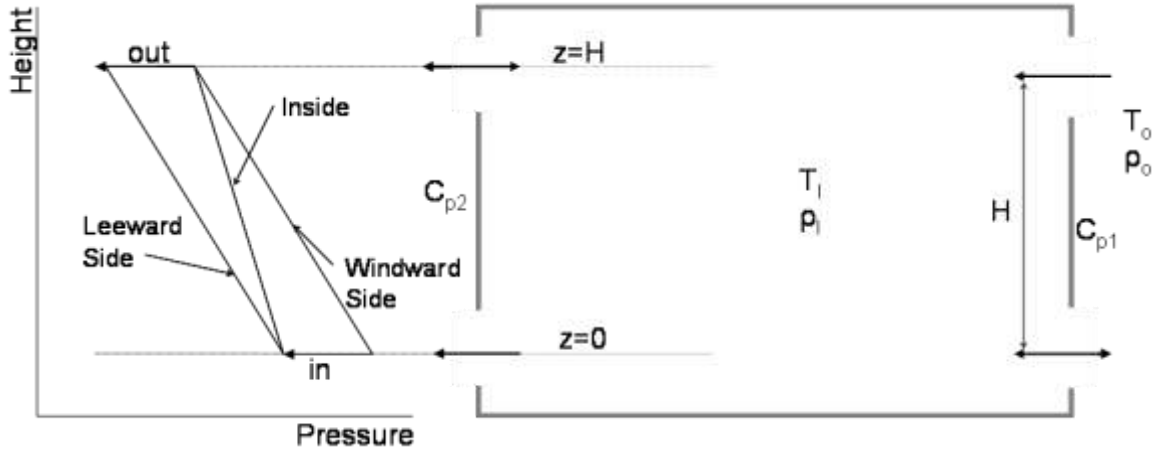

Figure 9. Combined Wind-Buoyancy Ventilation: Airflow Direction and Pressure versus Height

There are concerns with the accuracy of this equation (Etheridge 1996) in part due to the relative effects of wind and buoyancy. When the buoyancy and wind effects were approximately equal,

the error in using equation 2.15 was usually 50% (Etheridge 1996). The magnitude of the errors associated with equation 2.15 depends on the distribution of both inlet and outlet openings and the flow characteristics of those openings. However, at present there are not many simplified methods available for calculating the ventilation rate when wind and buoyancy are acting at the same time.

Air change is driven in part by thermal conditions, so it is important to include a ventilation component in an energy balance on a space. Performing an energy balance on a simple room, the total airflow, $\rho c_P Q_T \Delta T$, added to the conduction of heat through the building envelope must equal the interior heat loads under steady state conditions. The material properties, surface areas, and temperature difference between the interior and exterior environment are used to calculate the conduction through the walls and windows, $Q_{walls+windows}=UA\Delta T$. The internal loads, Q_{loads}, typically include heat due to occupants, equipment and lights. For steady state conditions, the energy balance equation is:

$$Q_{loads} = UA(T_I - T_O) + \rho c_P (T_I - T_O) \tag{2.17}$$

2.3 Design Characteristics

Building details, from the macro-scale, such as how to site the building, taking in to account its surroundings, to the micro-scale, as in the details of a window type and location, can impact the effectiveness of natural ventilation in an office building. Some of the design characteristics particular to naturally ventilated buildings, including the details of those used in the prototype building are presented in this section,.

2.3.1 Building Layout

Large-scale building design decisions, such as orientation and surrounding conditions, can impact both the thermal and ventilation performance of a naturally ventilated building. From the macroscopic perspective, this influence begins with the choice of a site location itself, and the characteristics of the surrounding area. Other building forms can impact the flow of air on the site, either enhancing or detracting from the airflow relative to the building under consideration. The orientation and geometry of the building is often determined by the lot of land on which the building will be sited, and can impact whether or not cross ventilation or single sided ventilation is an appropriate means to ventilate the building.

For natural ventilation to be effective, the depth and layout of the floor space must be considered along with the natural ventilation scheme used to ventilate the space. In cellular-type office plans, single sided ventilation is prevalent due to the configuration of offices, not allowing for cross-ventilation. With this configuration, air enters and leaves the space on the same façade of the building. If the window opening is only at one height, then the NPL falls in the mid-point of the window; air enters in the lower half and exits out of the upper half of the window. This design would have a tendency to create a concentration of warmer air at the ceiling and cooler air at the floor. An alternate configuration could use windows at two heights; the lower window then becomes the air inlet opening, while the upper window removes the exhaust air, thus having the capacity to remove more heat and lower the space temperature better than the single window

design. The depth of natural ventilation effectiveness in the single sided case is usually said to be limited to approximately 2.5 times the height of the space (Awbi 2003).

In open floor plans, cross-ventilation can be considered when there are openings on two sides of a space or building. In wind and combined wind-buoyancy driven cross ventilation flow, air enters through openings on one side of the building or space, traverses the space, and exits through openings on another side of the building or space, or through the atrium or upper floors. In cross ventilation, the airflow will be driven by wind if there is no significant height differential between inlet and outlet window openings and no vertical connection between floors. The airflow penetrates more deeply into the space than for single-sided ventilation, so the floor plans can be deeper. For cross-ventilation to work effectively, an open floor plan with few internal partitions is desired. The maximum depth of the space for effective ventilation by this method is said to be approximately five times the height of the space (Awbi 2003).

Often atria are included in the design of naturally ventilated office buildings because they not only increase the amount of natural daylight within the space, but also offer the potential to control and passively enhance buoyancy-driven ventilation. An increase in atrium height can enhance the buoyancy-based ventilation. This enhancement can be obtained by providing an increased height differential, and can be magnified by the use of glazing at the top of the atrium to increase the temperature of the air near the exhaust opening through solar gain. The use of glazing makes the stack flow more effective due to the increase in buoyancy-driven flow. Additionally, in the winter the atrium can act as a buffer to the external environment. However, care must be taken when designing stack vents and atria, since the position of the opening can reduce or even reverse the impact of the stack flow.

2.3.2 Window Characteristics

In naturally ventilated buildings purpose-provided openings allow fresh outside air to enter and exhaust air to exit a building in prescribed locations. Not only how the air enters and exits the building, but also how much air enters, is impacted by the window type, its location, and its orientation with respect to the dominant wind direction. Summer, spring and fall wind conditions are usually of most concern to designers using natural ventilation techniques, as occupant comfort is more dependent on passive ventilation to cool the building during months when cooling is required.

Each window type has its own effective opening area, or the percentage of the overall window area through which air can flow, and amount of leakage. Both of these factors can impact the selection of a window for a given climate and application. The three main types of windows are sliding, hinged, and rotating. These classifications also relate to the type of opening; simple opening, vertical-vane opening, and horizontal-vane opening (Allard 2002). Windows that use a track are either on a horizontal track, such as sliding windows, or a vertical track, as is the case with hung windows. Track mounted windows are often referred to as simple openings. Side-hinged casement windows or vertical-pivot windows pivot or hinge on the vertical axis. Horizontal-vane openings are similar to their vertical counterparts, except that the pivot or hinge is on the horizontal axis. Rotating windows can have either vertical or horizontal pivots, but the pivot is located at the center of the window, so that the window rotates about a central axis. A summary of the window types and their characteristics is presented in Table 2 and Table 3.

Table 2. Window Types by Opening Type

	Sliding	*Hinged (at edge)*	*Rotating (center pivot)*
Simple opening	X		
Vertical vane		X	X
Horizontal vane		X	X

Simple opening windows do not tend to affect the airflow patterns of the entering air much, except near the window edges as the air is forced through the opening. However, with horizontal-vane openings in particular, the airflow can be directed either upwards or downwards, depending on the location of the pivot or hinge. Horizontal-pivoted windows, with the pivot located in the center of the window offer a larger flow are than the other hinged or pivoted windows, as air is able to enter the lower half, and exit at the upper half. For vertical-vane openings airflow pattern and velocity is mostly impacted in the horizontal direction, due to the location of the pivot or hinge.

Table 3. Window Geometry and Characteristics

Window Geometry	*Relative Flow Area*	*Ventilation Effectiveness*
Horizontal Pivot	Larger flow area	Very effective for single-sided
Side-Hung	Smaller effective area	Lower airflow
Vertical Pivot	Smaller effective area	Effective for directing wind
Top/Bottom Hung	Smallest effective area	Effective for single-sided
Horizontal/Vertical Sliding	Larger flow area	Effective for both types of ventilation

As discussed previously, the window or opening location can impact the type and effectiveness of the airflow rate. Windows that are at a single height are not as efficient for buoyancy driven flow, as they have decreased height differential, unless very tall windows are used. Windows at two heights, a lower and upper opening, have a larger potential for flow through a space. Stack openings have the potential to enhance buoyancy-driven ventilation when designed correctly, i.e. taking into account the dominant wind direction, slope of the roof, and location of the opening on the roof.

The discharge coefficient, which takes into account the effect of contraction at a window opening, affects the amount of uncertainty within modeling naturally ventilated windows. The hydraulic resistance across an opening influences the airflow through that opening and depends on the geometry of the window and the Reynolds number. Normally, a discharge coefficient of 0.6 is used, approximating the window as a sharp edged orifice (ASHRAE 2001). The majority of research has been on a rectangular opening, and not other geometries, such as the awning type window (Karava 2004). The consensus for use with calculating flow rates through windows for natural ventilation is 0.6±0.1, based on: full-scale experiments (Flourentzou 1998), analytical calculations (Andersen 2002), and experimental compared with numerical simulations (Fracastoro 2002). If the flow rate, pressure difference, and area are known, equations 2.11 and 2.13 can be rearranged to calculate the discharge coefficient for a particular window geometry.

2.3.3 Thermal Mass

Thermal mass can be used for its capacity to store heating or cooling energy, depending on the season. The use of heavy mass materials strategically placed in a building can reduce the amount

of cooling required by 30 percent or more, and decrease internal room temperatures by 5°C (Daniels 2003) when compared to lower mass buildings. During summer months thermal mass can be exposed to the lower, nighttime temperatures, in effect pre-cooling the interior space during un-occupied hours. This effect is often created by drawing in cooler night air, and thereby pre-cooling the thermal mass. The pre-cooled thermal mass is then able to temper the interior temperature during occupied hours, counteracting the build up of heat due to interior loads. The cooling period takes advantage of the natural diurnal swings of the exterior environment, capturing the cooling energy provided by the lower outside temperatures. In this way, the internal temperature of the building is moderated; not getting as cold as the environment during the nighttime, but also not reaching the high temperatures occurring during midday to early afternoon. Thermal mass is known for causing 'peak shifting', when the peak internal temperature occurs well after the peak outside temperature. Sometimes the peak internal temperature occurs at the end of the workday when there are fewer occupants. In the heating season, the thermal mass retains heat generated by the internal loads during the daytime hours, and releases the heat during nighttime hours so that the building does not get as cold or require as much additional heating during un-occupied hours.

2.3.4 Integration of Design Details

The above described techniques are important to the enhancement of natural ventilation individually; however they can increase the performance of a naturally ventilated building much more when two or more are integrated in the building design. It is not uncommon to have window type and location selected based on the layout of the building floor plan due to the type of ventilation, single-sided or cross ventilation, that is planned. Through careful design, many of these building characteristics can be incorporated into the overall design of a naturally ventilated building to ensure proper airflow, occupant comfort, and overall building performance.

2.3.5 Prototype Building Characteristics

The prototype building, described in detail in Chapter 3, included several of the above natural ventilation enhancing techniques. The building was located in a relatively open office park, with buildings of similar height. Attention to details such as the selection of building material, increasing daylight within the office space, decreasing solar gain and glare, and office layout resulted in a naturally ventilated commercial office building that functions well without the need for mechanical cooling.

The material selection for the façade differed from the north to the south side, in part due to architectural aesthetics, but also due to the orientation of the building. On the southern façade, light colored materials help reflect some of the solar isolation, whereas on the northern façade, bricks were used as the facing material. Other design details that were incorporated into the prototype building include solar shading to reduce direct solar glare, and light shelves to allow the natural daylight to penetrate deeper into the office space. Through the use of the light shelves, the electric energy consumed by the general lighting can be reduced because the fixtures are outfitted with photo-sensors and are dimmable down to 10 percent. The building uses thermal mass to help temper the interior temperature by leaving small, upper windows open at night during the summer months to pre-cool ceiling soffits. The cross section of the ground floor of the prototype building with these design characteristics is shown in Figure 10.

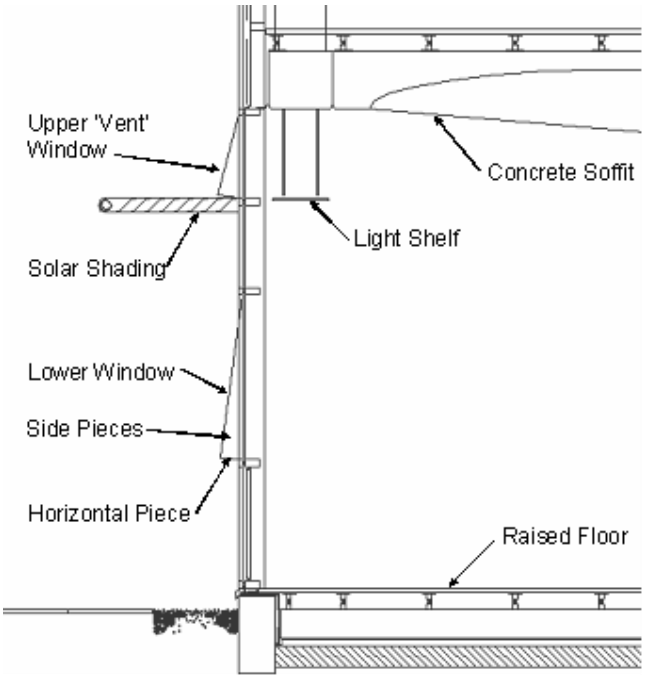

Figure 10. Prototype Building Design Characteristics

2.4 Building Performance Evaluation

A prototype building was selected to evaluate a scale modeling technique for naturally ventilated buildings. The building is a commercial office building, built and owned by the company that occupies the building. The company is an organization dedicated to providing housing and assistance to individuals and families in need, and thus desired a building that had relatively low construction and operational costs. The building is an example of the type of commercial office building currently being constructed that uses an open floor plan to allow for the greatest amount of flexibility, and incorporates much glazing into the building façade to take advantage of available natural daylight. The natural daylight throughout the building, particularly in those areas towards the center of the floor plan, provides an aesthetic of an open building, which is enhanced by the glass atrium included in the design. This feature is common to many commercial office buildings, both mechanically ventilated and naturally ventilated ones.

Several aspects of a building contribute to the overall building operation, such as thermal performance, ventilation performance, and energy performance. Each of these areas has an impact on specific systems of a building, yet they are interrelated, contributing not only to the overall performance of a building but also to the health and comfort of its occupants. Monitoring of buildings is not new, but applying the knowledge and assessing naturally ventilated buildings can pose some difficulties. A multi-pronged approach was taken to fully evaluate the naturally ventilated office building, including long-term and short-term monitoring, and surveying occupant behavior. This method provided adequate data on the overall building performance under a variety of conditions. Some aspects of these data were then used to determine how the building functioned relative to other buildings as well as compliance with building codes, as is the case with ventilation. Natural ventilation in particular has unique characteristics that must be

considered when determining how the building operates, including occupant controlled windows and environmental conditions that are available as resources to control building performance. The building data also were used to verify numerical simulations, using computational fluid dynamics software, scaled physical models and other design tools.

The methods used in evaluating the prototype building are described in the following sections.

2.4.1 Thermal Performance

Several factors contribute to the thermal performance of a building; building construction, interior loads and space temperature, and air movement. The building fabric can have significant impact on the thermal performance of a building in terms of both thermal conduction through exterior walls as well as passive heating and cooling strategies. Buildings that have more exposed thermal mass, i.e. are "thermally heavy", can retain heating or cooling energy better, and for longer periods, than ones that are thermally light, with less thermal mass. The overall temperature within a space and the amount of vertical temperature stratification within the space contribute to the thermal comfort and performance of a building.

Internal loads impact the interior temperature of a given space. People, equipment, and lighting are typical interior loads that contribute to the cooling load due to the heat that they emit. The density or number of units per floor area of these interior loads determines the heat load for the space. Office buildings typically have 10-15 square meters per occupant and 75-120 Watts per occupant. Lighting loads can vary between 12-20 Watts of energy use per square meter in a commercial office building. The ancillary equipment loads, including computers, monitors, printers, etc. typically contribute 10-18 Watts per square meter. These internal loads, and the heat that they generate, contribute to the increase in temperature in the interior environment, which then has to be removed through ventilation, natural or otherwise. Air movement, not ventilation specifically, contributes to thermal comfort of the occupants within a space. Comfort studies have found that the warmer the interior temperature, the higher the acceptable indoor air velocity for comfort of occupants (Daniels 2003).

2.4.2 Ventilation Performance

When evaluating ventilation effectiveness, the path of the air from entry to exit point must be considered. This is done on a macro and a micro scale; both global air flow into and out of the building and at a more detailed level, space by space. The method in which the air is introduced, travels through, and is exhausted from individual spaces and the building as a whole contribute to the ventilation performance and effectiveness of the building. For mechanically ventilated buildings, this evaluation generally means focusing on the heating, ventilation, and air-conditioning (HVAC) system. As the entry and often the exhaust of air both into and out of the building and individual spaces is controlled, this tends to be a straight forward procedure. Though there are often many components that make up the system that conditions the building, these components are often monitored and controlled by a building management system to ensure proper operation and occupant comfort.

Since the inlet and outlet points for a mechanical system are specifically designed and detailed, the methods to measure ventilation performance are well defined. Duct traverses, filter conditions, various system set points and dampers are some of the items assessed when determining ventilation effectiveness of a ventilation system and conditioned space. However,

airflow characteristics also play an important role in how effectively the fresh air is introduced to the occupied area. Some important ventilation characteristics for all buildings include air velocity, airflow patterns, and carbon dioxide levels.

The speed at which air enters into a space is part of what determines its impact on the conditions within the space. Air velocity can be measured in various ways, but one of the most common and accurate methods is using a hot-wire anemometer. This device measures the speed at which air is moving at a particular location. The hot-wire anemometer is useful for point measurements at specific locations, rather than for overall air velocity within a building. If the conditions are not steady state but change with time, then the point by point method of measuring air velocity can provide questionable results. Air velocity must be controlled within a space to avoid draft conditions, which can cause not only occupant discomfort due to increased evaporative cooling if the skin is exposed, but also disruption of papers and objects in the occupied space. Allowable levels of air velocity within an occupied space are normally below 2 meters per second. On the other end of the spectrum, stagnant air is also undesirable, as fresh air is important to the occupants' health and productivity.

Proper air movement in an occupied space as well as within the building as a whole can impact energy usage, indoor air quality, and thermal comfort. Airflow patterns include direction and movement through a space and throughout a building. Understanding how air flows within a space can be indicative of the effectiveness with which fresh air is reaching occupants and stale exhaust air is leaving the building. Smoke pencils are often used for local visualization of airflow patterns within occupied spaces. These devices provide a visible, neutrally buoyant stream of smoke that dissipates after several minutes and is harmless to occupants or furnishings.

Measurement and monitoring of carbon dioxide levels is another method of evaluating ventilation effectiveness. Through a series of measurements and calculations, the air exchange rate of a building can be determined. People exhale a certain amount of carbon dioxide, based primarily on their activity level, but also on their age and fitness. The determination of air exchange rate is based on the number of people within a building, along with the indoor and outdoor carbon dioxide level. The indoor carbon dioxide levels can also be compared to levels considered acceptable for indoor air quality and health, safety and environment standards.

2.4.3 Energy Performance

A key parameter contributing to a building's performance is energy consumption. Energy consumption analysis can be completed in different ways; using either a simple method or a more detailed means. The energy use of a building can be easily compared to other similar-type buildings. The more detailed the analysis of energy usage, the easier the ability to target areas for improving performance.

A very simple method, which looks at monthly energy, electric and natural gas, usage and cost bills provided by the respective utilities can provide some information on and trends in a building's energy usage. Although obtained only on a monthly basis, seasonal data can be extrapolated based on some known characteristics of the building. These characteristics include plug loads, such as number of computers, printers, and ancillary equipment, and lighting loads, such as number and type of lighting installed. Once the baseline consumption that remains constant over the course of the year is known, energy usage that is weather dependent can be determined. If the heating and cooling degree-day data or other measures of external

environmental conditions are examined, then the consumption by heating and/or cooling equipment can be determined. The degree-day data are readily available online from weather websites.

A more detailed method of determining the energy performance of a building includes sub-metering major energy using systems within a particular building. This method provides detailed information on the operation and consumption patterns of a building. Though requiring more investment in terms of time and equipment, understanding the energy usage for a specific system and for specific zones on an hourly or quarter-hourly basis can provide the more detailed data needed to improve the performance of a building. Common systems to monitor, as applicable, include the plug loads, lighting loads, chiller or other cooling system, air handling units, miscellaneous pumps, exhaust systems, and exterior lighting. These data can then be used to compare a building's performance to benchmark data.

2.4.4 Long Term Monitoring

Recording data over a twelve month period of time or longer can provide important insights into the overall operation of a building. The monitoring should be designed so that enough data to paint an accurate picture of the building performance are obtained. Fifteen-minute intervals are often used as they provide sufficient information for the partial hourly operation. Additionally, with commercial buildings, the thermal time response, occupancy patterns, and energy usage are slow enough to not require a shorter time interval. Long term monitoring includes energy usage, both by overall consumption and detailed by sub-system, internal conditions, including temperature and relative humidity, and external conditions.

Even in temperate climates, the external environment can impact the performance of a building. As a building goes through the seasons, the internal conditions and sometimes the schedule of occupants and equipment change. To best evaluate the performance of a given building, continuous monitoring for an entire year, through heating, cooling, and mild shoulder months provides the widest variety and most detailed data for analysis. The ability to record the outdoor conditions helps greatly in the analysis of the building. This includes the outdoor temperature, as well as the solar gain and wind.

With naturally ventilated buildings that often do not have cooling systems installed at all (or provisions to install them), data describing the summer conditions, and sometimes the shoulder months at the end of spring and beginning of fall, are important to ensure that there is a good internal environment for occupants. An understanding of the indoor environment can be ascertained by measuring internal temperatures throughout a building., During the winter months these buildings rely on infiltration to provide the required outside air since there is no forced air system in naturally ventilated buildings. This reliance can cause drafts and occupant discomfort if the infiltration is not purpose-provided and well controlled. One method for long-term evaluation of infiltration and ventilation is the use of carbon dioxide sensors. The interior levels can then be measured throughout the year, compared with the outside levels, and the air exchange rate of the building determined based on the number of occupants by measuring the levels of carbon dioxide in the external environment to provide a baseline.

2.4.5 Short-Term Measurements

Though long-term measurements are important for overall performance of a building, shorter term and spot measurements can enhance these data. The short-term measurements can be used to further explain the data collected over the long-term. Spot measurements at specific locations can help in determining what is occurring within a building for a given set of parameters. These insights can include the impact of solar gain on internal temperatures and airflow circulation on sunny days or impact of ventilation on internal conditions.

Short-term measurements include detailed vertical temperature distribution, air velocity measurements and visualization. The introduction of air into the space and exhaust out of the space is difficult to monitor over the long-term. Short-term measurements provide information that can be integrated into the long-term data to obtain the full picture of the building operation.

2.4.6 Building Benchmarks

Monitoring can provide important insight in to the operation of a building, and be used in comparing a building to other similar buildings. Often this technique can provide the impetus to fine-tune a building to further reduce its operating costs, or determine areas where there is room for improvement. Ventilation and thermal comfort requirements, and energy consumption, by either annual usage by fuel type or by sub-system, can be measured to establish several key performance indicators, standards and benchmarks for building comparisons. The relative performance of the subject building can be obtained by comparing these measurements to comfort scales. For both mechanically and naturally ventilated buildings, there are comfort scales, such as the American Society of Heating Refrigeration and Air-conditioning Engineers (ASHRAE) comfort charts; ASHRAE Standard 55 (ASHRAE 2004) provides separate comfort zones for mechanically and naturally ventilated buildings. Additionally for both ventilation types, carbon dioxide levels can be a key indicator for indoor environment and air quality. Health and safety organizations (Environmental Monitoring Services, Bureau of Environmental Health Assessment, ASHRAE) have published data for recommended exposure levels of carbon dioxide for the working environment.

Several factors should be quantified to determine a building's performance: occupancy and temperature schedules, mechanical systems, other equipment, building size, any control systems, building envelope, lighting systems, and weather data (MacDonald 1989). Comparisons of the energy used to condition the space (heating, cooling and ventilation) as well as lighting and equipment data (internal electric loads) can be used to determine relative performance in mechanically conditioned buildings, whereas for naturally ventilated buildings the primary comparisons are to internal electric loads and heating energy usage. The energy usage values are based more on the occupant and equipment density within the building, rather than its layout in mechanically ventilated buildings (air-conditioned standard and air-conditioned prestige), since there is a prescribed amount of ventilation that is delivered uniformly to all conditioned spaces of a building. For natural ventilation however, the amount of energy used can be dependent on the configuration of the building, whether the office layout is open floor or cellular, and the number of people within the space. For example, open floor plans tend to make better use of natural daylight throughout the space and have broader controls, whereas cellular offices restrict the penetration of daylight into the core of the building, and normally have controls for each individual space.

As natural ventilation is prevalent in the United Kingdom, standards have been developed for both mechanically and naturally ventilated buildings. Table 3 provides an example of typical standards. The Energy Consumption Guide 019 (ECG019) classifies both mechanically and naturally ventilated buildings into two categories; standard and prestige for mechanically ventilated buildings, and naturally ventilated cellular and naturally ventilated open-plan. Benchmarks like those in Table 4 also provide data as to standard practice (Std.), which does not employ energy saving equipment or technologies, and good practice (GP), which does.

Table 4. Energy Consumption Guide 019 Building Characteristic Data for UK[2]

Building Type	***Configuration***	***Floor Area***
Mechanically Ventilated (MV)		2,000-20,000m^2
Naturally Ventilated (NV)	Cellular	100-3,000m^2
	Open Plan	500-4,000m^2

Table 5. ECG 019 Benchmark Data for UK by Building Type[2]

Energy End Use	***MV Std.***	***MV GP***	***NV Std.***	***NV GP***
Lighting, W/m^2	20	12	15-18	12
Office Equip, W/m^2	16-18	14-15	12-14	10-12
Lighting, kWh/m^2	54-60	27-29	23-38	14-22
Office Equip., kWh/m^2	31-32	23	18-27	12-20
Heating, kWh/m^2	178-201	97-107	151	79

Table 5 shows the energy use, in watts per square meter and kilowatt-hours per square meter for the two building ventilation types and the range (Std. and GP) prescribed for UK office buildings by the ECG019. Energy use in kilowatt-hour per floor area is dependent on the number of hours that the energy using system operates. For the ECG 019, this varies by both building and ventilation type due to the configuration of the building and the incorporation of energy conserving technologies and practices. ECG019 purports that naturally ventilated buildings have a lower lighting, office equipment, and occupant density than mechanically ventilated buildings. This is in part due to limits with the amount of heating load that the natural ventilation scheme can successfully handle and the attention to detail in opportunities to reduce any additional heat loads within the occupied space to control the magnitude of the heat load. This leads to the slightly lower numbers when comparing the standard MV and NV energy end use numbers. The heating energy usage is slightly lower for the NV than MV buildings due to the design characteristics, such as thermal mass, that are incorporated into the design and the lower fresh air requirement with the reduced occupant load.

2.4.7 Characteristics Unique to Naturally Ventilated Buildings

There are several common configurations and methods for enhancing natural ventilation in buildings. The two main drivers for natural ventilation are buoyancy-driven and wind-driven flows. These are often both found working together in naturally ventilated buildings. Some of the concern with incorporating natural ventilation as the sole means for cooling the building is with still days, when only buoyancy driven ventilation is present. In this case, airflow through

[2] Energy Consumption Guide 019 2003

the building, carrying away the internal heat, is accomplished only through the difference in temperature over the building height. For this reason, often design characteristics are included that enhance this aspect of natural ventilation, incorporating stacks or solar chimneys or windows at multiple levels. When there is a significant wind present, consideration must be made to ensure that there is not too much or too high an air velocity entering into the buildings.

Purpose-provided openings, used to ensure adequate ventilation, are unique to naturally ventilated buildings and are usually in the form of windows, often at different heights for the inlets and outlets. Window type can have a significant impact on several aspects of the building performance, most importantly day-lighting and air movement control (Boutet, 1987). The effectiveness of the window in bringing in outside air can be affected by the type of window and how it opens. The effectiveness of a window includes evaluation of the airflow pattern and the effective opening area of the window. Some of the additional issues that arise when evaluating the use of operable windows for naturally ventilated buildings include noise control and security.

2.5 Summary

Natural ventilation can be used as a means to ventilate and passively cool spaces for occupant comfort. The dependence of this approach on a combination of buoyancy and wind-driven ventilation, along with thermal mass and window geometry presents unique issues when evaluating buildings. However techniques are evolving that allow these design characteristics work together, either enhancing or reducing the overall performance of the naturally ventilated office building. Benchmarks have been created with which these low energy buildings can be compared to one another; assessed for their lighting and equipment energy usage as well as their thermal performance.

Chapter 3.0

Evaluation of Prototype Building: Houghton Hall

3.1 Introduction

Using previous methods employed in monitoring and evaluating mechanically ventilated buildings as a baseline, adaptations were made to account for the challenges that arise in naturally ventilated buildings. The overall configuration and typical internal loads of the building were similar to a standard commercial office building and the energy consumption was readily measured, so the focus of the evaluation was shifted to temperature and airflow concerns. This chapter outlines the building design characteristics and method used to assess the prototype building in order to understand better the unique aspects of the naturally ventilated building and the resulting monitoring procedure.

3.2 Prototype Building: Houghton Hall

Houghton Hall, the naturally ventilated commercial office building assessed as the prototype building for developing and validating the model methodology, was located in Luton. This location is a temperate area of the United Kingdom that does not have a significant number of heating and cooling degree-days. Luton typically has 1902 heating degree-days (HDD), base 15.5ºC and 389 cooling degree-days (CDD) base 15.5ºC.

The three-story building is located in an office park with buildings of similar height, just outside of the city of Luton, 60 km north-northwest of central London. The buildings in the office park are well spaced, with approximately 20-30 meters between buildings. To the north of Houghton Hall is an open public access park. The surrounding office buildings located within the same office park are all mechanically ventilated and cooled. The building is owner-occupied by a housing assistance organization that made the decision to consolidate their operations into a central location and required that the building be low energy and best value-'Egan Compliance' (Egan, 1998), even if it was not the lowest in initial cost.

The prototype building is three stories in height, 2,600 square meters, with open plan office space on all three levels: south side of the first floor, both south and north sides of the second floor, and the north side of the third floor. A typical building floor plan and section through the central atrium are presented in Figure 11. The north side of the first floor is used as a large meeting room that is closed off from the rest of the building, and has the ability to be mechanically cooled due to the high internal heat gains for short periods of time that is used on a weekly basis. The south side of the third floor is closed off from the rest of the building and houses the mechanical room, printing room and file room. The occupied office spaces are completely open onto the central atrium that runs the length of the building along the east-west axis. The atrium extends a floor height above the third floor and is comprised of glass panels on both the east and west facades and along the roof, and houses five fan-powered ventilation stacks. Images from the exterior and interior of the building are presented in Figure 12 through 14. Figure 13 provides a detailed view of the atrium stack vent and fan.

The building envelope features several types of building constructions, as shown in Table 6. The light colored panels on the south façade reflect much of the solar radiation that might otherwise add to the cooling requirements of the building. The atrium has glazing on both façades and the roof section. There is a raised floor within the occupied space that contains all of the electrical conduit and networking equipment. The ceiling of each occupied space has a concrete soffit that serves several purposes. The concrete ceiling is a concave ellipse that not only acts as thermal mass tempering the internal temperatures, but also was designed to provide indirect lighting and to reduce noise due to its shape. The shape also was designed to direct airflow through the occupied space toward the atrium. Descriptions of the building constructions and their insulation properties are presented in Table 6 and Table 7 respectively.

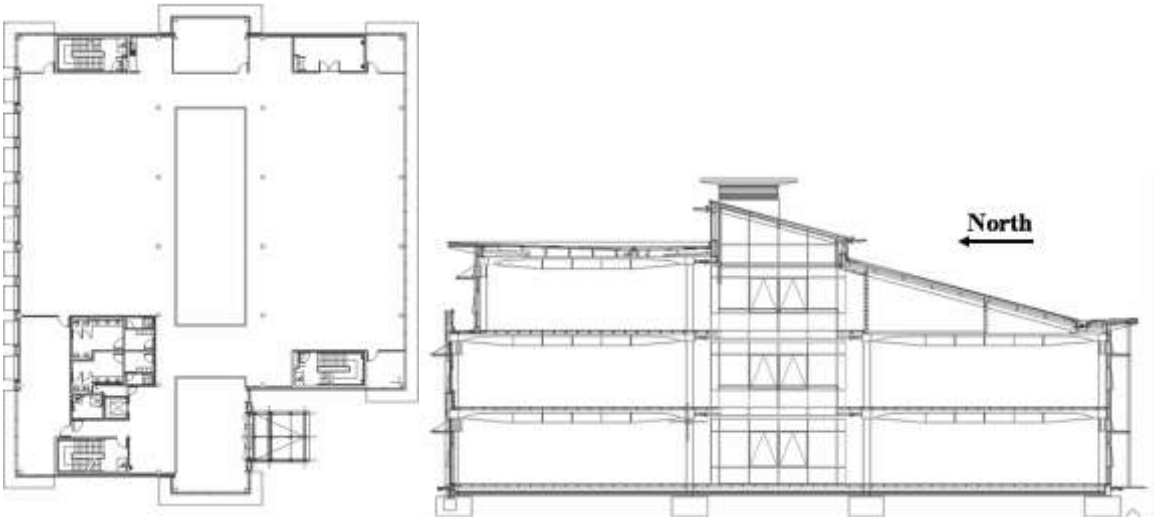

Figure 11. Building First Floor (a) Plan and (b) Section

Figure 12. Interior Atrium View

Figure 13. Atrium Stack Vent and Fan

Figure 14. Exterior View of Southern Facade of Prototype Building

Table 6. Prototype Building Construction Description

Construction	*Material*	*Thickness, mm*
Brick Façade	Masonry cavity wall, fill insulation, block work, plaster finish	400
Insulated Panels	Aluminum clad panels, board insulation, block work, plaster finish	210
Glazing	Argon-filled double pane glass window with tinted outer pane	28
South Roof	Aluminum decking over fiber insulation and aluminum panel	150
North Roof*	Membrane, roofing board, vapor membrane, aluminum panel	80

* has concrete slab below North Roof construction

Table 7. Prototype Construction by Orientation and U-value

Orientation	*Façade Type*	*Area, m^2*	*U-Value, W/m^2C*
North	Brick Façade	82	0.45
	Glazing	228	2.2
South	Insulated Panels	82	0.45
	Glazing	228	2.2
East	Brick Façade	260	0.45
	Glazing	100	2.2
West	Brick Façade	260	0.45
	Glazing	100	2.2

The ventilation of Houghton Hall is a combination of buoyancy-wind driven ventilation and fan-assisted ventilation stacks. There are seven sets of two windows, each containing a larger and a smaller window, at each floor level on both the north and south façades. Each larger, occupant-controlled window is located one meter above the floor, has a solar shading device located above it to reduce direct glare, and has a corresponding light shelf on the interior side of the window to direct sunlight further into the occupied space. All of the windows are overall 1.3 meters in width (without the frame, 1.2m), with the lower windows being 1.1 meter in height (0.9m without the frame) and the upper windows 0.45 meters in height (0.35m without the frame). The building manager controls the smaller upper window, determining when to open or shut it for the season. All of the windows are manually controlled to keep costs low without sacrificing function.

The building manager opens the upper windows in the spring when the internal temperature during an occupied day has risen above 22ºC. Ideally, the windows would be opened at intervals; beginning with every other vent initially and eventually having all of the upper windows open until the fall. The building operation philosophy (Rybka 2002) would have the building manager close these vents during the day in the springtime so as to not over cool the building and require additional heat. However, these windows are difficult to get to and are often opened all at once and left open, rather than as prescribed in the ideal operation. The occupant- windows are closed at night for security purposes.

Part of the building design included the installation of Venetian blinds to reduce the amount of solar glare throughout the year. These blinds are controlled by the occupants, and can be drawn up or down, as well as tilted to better control the amount of daylight entering the space. However, the blinds were installed on the upper portion of the frame of the upper window in each floor. When the blinds are all the way down, these blinds essentially cover the upper windows, restricting the amount of air that can enter (or exit) the building. Additionally, when these blinds are in the down position, they reduce the effectiveness of the light shelves, included in the building design to reduce the amount of fluorescent lighting required.

Table 8. Prototype Building Window Characteristics

	Width	*Height*	*Horizontal Opening*	*Location*
Single Window Opening	130 cm	90 cm	6.5 cm	South Half-Floors, Second North
Double Window Opening	2 x 90cm	90 cm	11.5 cm	First North
Single Vent Opening	130 cm	45 cm	5.0 cm	South Half-Floors, Second North
Double Vent Opening	2 x 90cm	45 cm	6.0 cm	First North

The stack vents have a series of louvers on each face of the stacks, which are controlled by orientation (e.g. all of the eastern louvers for all five stacks are either open or closed). The louvers do not modulate, and are therefore either fully open or fully closed. There also is a rain and wind sensor located on the roof that is tied into the simple control system for the fans in the stacks; if there is any rain indicated, then the louvers are closed, and likewise if the wind outside exceeds 4m/s the louvers are closed in the direction of the wind. The louvers are kept open if the fans located in the stacks are on. The fans are three-blade, 0.746kW fans that are unidirectional.

On still days, the airflow is driven by buoyancy flow, with the louvers open in the stack vents to enhance the stack effect. On windy days, the airflow can be more similar to single sided ventilation on the ground and second floors, with the potential for some cross ventilation on the first floor. In part this is dependent on the interior loads, number of windows open and solar radiation. In automated mode, the fans and louvers are controlled by a single temperature point located in the atrium just above the ceiling level of the second floor. If this thermocouple reaches 26ºC or more, the louvers are allowed to open and the fans are turned on. If the temperature drops below 26°C, then the fans turn off and below 22°C the louvers close.

The occupants are located on all three levels of the building: the south half of the ground floor, both north and south halves of the first floor, and the north half of the second floor. Within each half floor there are approximately 25 occupants, each with a computer and monitor, and a desktop printer for every three people. There are energy efficient T-8 fluorescent lamps located throughout the building, with the exception of the bathrooms and the 'street lighting' in the atrium. The lighting fixtures in the occupied space, each with two lamps, are connected in banks of two to a combined occupancy and photosensor control mechanism. This feature allows for the lighting to be shut off when the space is unoccupied, and continuous dimming from 100 percent on, down to 10 percent to achieve further reduction in energy usage when the space is occupied.

3.3 Monitoring Procedure

Long-term monitoring of Houghton Hall was conducted for internal temperature and relative humidity throughout the occupied spaces, energy consumption by sub-system, and external conditions. The equipment was installed at the beginning of the summer season and removed eighteen months later. This extended period provided time for troubleshooting equipment during the first summer prior to recording a complete data set for a twelve-month period. Problems that needed to be addressed included ensuring that data loggers were recording properly and thermocouples remained in position. Through some trial and error and data analysis after two months, the equipment was working properly. The measurements, both long term and short-term,

and experiments used in evaluating the performance of the prototype building and for evaluating the reduced-scale modeling technique are presented in the following sections.

3.3.1 Site Measurements and Experiments

The analysis of Houghton Hall was completed through a combination of long-term and short-term measurements, with some experimental work to focus on specific areas. Long-term monitoring of the building was meant to be unobtrusive and record building characteristics at fifteen-minute intervals over the period of twelve months. Short-term measurements were taken during site visits primarily during the spring, summer, and fall months. Short-term measurements were not taken during the winter months because the building was closed up, and natural ventilation system was not active during that period. However, data continued to be gathered as part of the whole building performance analysis.

3.3.1.1 Temperature Measurements

One of the more important things monitored was the interior temperature, as this is a first indication as to the performance of any building. If the internal temperature is outside of the comfort range, productivity can deteriorate. In addition to temperature, the data logging devices also recorded relative humidity levels, which can be another factor for naturally ventilated buildings, as they do not have means to either humidify or dehumidify the entering air. For long-term temperature and humidity monitoring, HOBO® H8 Series compact temperature and relative humidity data loggers were used throughout the building. Most of the data loggers were located at desk height, approximately 1.2 meters above the floor. An additional series of four data loggers was installed in each occupied floor area at four different heights, at the floor level, 0.76 m above the floor, 1.76 m above the floor, and 2.54 m above the floor, to obtain an initial determination of stratification within the occupied zone. Four other data loggers were placed around the atrium at each floor level to determine the amount of stratification that occurred within that space. The location of the HOBO® data loggers for a sample half-floor plate is shown in Figure 15. The data loggers were placed between windows, to avoid being in the direct airflow from the window. The data loggers located at the atrium were attached at the floor level at the ledge of the atrium.

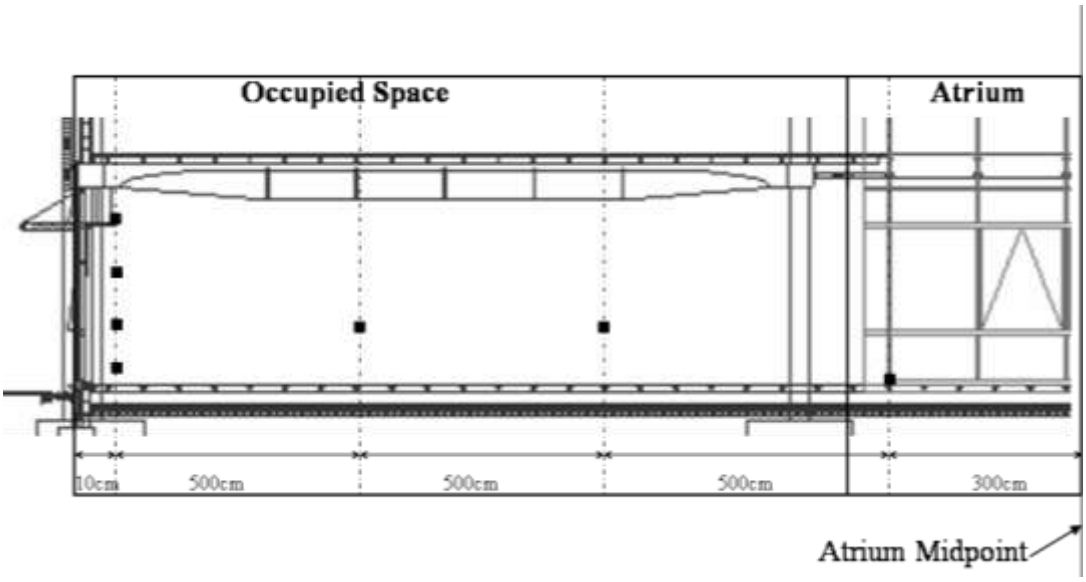

Figure 15. HOBO® H8 Series Temperature and Relative Humidity Data Logger Locations in a Sample Half Floor Area. The black squares represent the thermocouple locations. This layout is duplicated in each of the four half floor plates.

External conditions were recorded to provide data both on the conditions to which the building was exposed and on the entering air properties. As there was a substantial amount of glazing on the façades of the building (46 percent of the total façade area) solar radiation was an important condition to be monitored. Not only outside air temperature, but also humidity, barometric pressure, direct and diffuse solar radiation, and wind speed were recorded. A Campbell Scientific weather station using a CR10X data recorder was mounted on the roof of the prototype building. The weather station was located so that it would not be influenced by exhaust air from the stack vents, nor sheltered from the outside elements. The outside temperature gauge was housed in a white plastic device so that it was not subject to erroneous readings due to solar gain, rain or wind. The rotating vane cup anemometer was located 1 meter above the atrium roofline, approximately 1.5 meters away from any stack vent. The program used to record the data measured the gusting or peak wind speed over the fifteen-minute interval as well as the average value over the same interval. Both direct and diffuse solar radiation was measured using the weather station. The solar radiation data was recorded by using one pyranometer for the horizontal solar radiation, and another pyranometer along with a shadow-band device that recorded diffuse solar radiation. The shadow-band rotated to shade the direct solar radiation to the pyranometer, while recording the diffuse solar radiation.

3.3.1.2 Air Quality Measurements

Evaluating the ventilation performance of naturally ventilated buildings is more complex than the evaluation of a mechanically-conditioned building. The environment within the naturally ventilated building is affected not only by changes in the outside environment, e.g. wind speed and direction, but also by occupant behavior. In the prototype building, the main windows are occupant controlled and can be anywhere from cracked open to fully opened, 0.24 meters in the horizontal direction. The window geometry was an additional factor that had to be addressed in

evaluating the air exchange rate within the buildings. The methods used to measure the ventilation performance of the building are described in this section.

Building location and siting can influence the ventilation for a naturally ventilated building, but the focus of the assessment was on the building itself and the internal conditions. The window geometry proved to be a challenge. The effect of window geometry has been studied to a limited extent (Heiselberg 1999, 2001) but not specifically for the top hung awning-type windows that are used in the prototype building. The awning-type windows are hinged at the top, and are kept open by friction at the hinge. These window types are used both for the smaller, upper windows as well as for the lower, large occupant controlled windows. A method for determining the airflow rate of incoming air and exhaust air had to be developed because natural ventilation in buildings relies on external conditions to provide fresh air and remove internal heat gains, and wind speed and direction can change quickly. This characteristic increases the complexity of evaluating ventilation effectiveness. Part of the complexity lies in the effective opening area of the window; it has both a horizontal area, as well as two vertical pieces, that can all affect the total airflow rate. Initially velocity measurements were taken in the horizontal plane using hand-held hot-wire anemometers, as that dimension was determined to be the largest contributor to incoming and outgoing airflow for the window.

The stack vents were a key design characteristic that had to be considered when evaluating ventilation performance. The fans integrated in the stack vents were included in the assessment. Hot-wire anemometers were used to measure the air velocity just outside the louvers from the exterior and just below the fan in the interior. Measurements were taken under two conditions; with the fans on and off. In addition, smoke pencils were used when taking measurements at the exterior to determine the direction of the airflow.

Another method employed to determine the ventilation rate of the prototype building was the monitoring of carbon dioxide (CO_2) levels within the occupied spaces using a Tel-Aire carbon dioxide sensor, combined with a HOBO® H8 series data recorder. Measuring CO_2 can be used to determine air exchange rates, and to evaluate indoor air quality. Several groups have defined maximum acceptable levels of CO_2 for office spaces. Levels above 1,000 ppm can lead to lethargy and headaches (ems, 2004). However, both the United States OSHA (Occupational Safety and Health Association) and the United Kingdome BSRIA (Building Services Research and Information Association) have defined maximum exposure limits to be 800 ppm over an eight-hour period for office areas. The CO_2 level is dependent on the ventilation distribution, occupant density, and amount of outside air being introduced into the space (ASHRAE 2001). When evaluating the indoor environment with respect to occupant health, ASHRAE suggests that an indoor level of CO_2 650 ppm above the outside level is representative of an air exchange rate of 20 cubic feet per minute, with an occupant density of 100 ft^2 per person (ASHRAE 1997). Occupant comfort is also affected by higher CO_2 levels, with 20 percent of people dissatisfied at CO_2 concentrations of 650 ppm above the outdoor level (Liddament, 1996). In offices, carbon dioxide levels are primarily due to the respiration of the occupants. Initially the CO_2 and temperature monitor was place outside, away from the building in order to record the external conditions as a baseline. Then the CO_2 sensor was placed at desk level, away from direct exposure from an occupant, in the second floor office area and data recorded every fifteen minutes over the twelve-month monitoring period. On site visits, the number of people in each office area was logged over the period of the day and compared to the data recorded for that day.

Finally, airflow visualization was included as part of the assessment of the building to improve understanding of the characteristics of natural ventilation in the building design. Smoke pencils were used for localized flow patterns throughout the building. These experiments proved to be useful supplemental information in determining the airflow paths at the inlet conditions, within the occupied space and atrium, and at the exhaust, but cannot be quantified reliably outside of laboratory conditions. Another method with 'neutrally buoyant' helium balloons was used to track the airflow patterns within the building. The neutrally buoyant balloons were made neutral at a selected height, which corresponded with a specific temperature. When the balloon would move to an area of a different temperature, it would oscillate until reaching the neutral temperature again (Glicksman 2004). The balloons were then released near the inlet windows, and allowed to travel within the building. The balloons normally ended up near the roof of the atrium, the warmest location within the building. However, this method did not produce repeatable results for specific streamlines. The balloons were able to follow larger, macroscopic flow patterns within the space, but had difficulty with low velocity airflow and detailed flow patterns visible using the smoke pencils.

3.3.1.3 Energy Usage

The occupancy schedule and energy usage profile can be determined by monitoring the energy consumption and usage patterns within a building. The more detailed the metering of the electric energy using equipment, the more thorough is the understanding of the building energy performance. For the prototype building, not only the overall energy usage, but also a substantial amount of detailed monitoring was completed. This detailed monitoring included data collection on each floor level by orientation, miscellaneous building services, lifts, atrium fans and external/outside lights to determine their energy consumption. The energy usage for each floor could not be separated out in more detail, e.g. lights versus plug loads, due to problems with installation of the data loggers in the electrical closets. Current transducers (CTs) were also installed on the actuators for the boiler so that there was a measure of how often the boilers were in operation and their schedule of operation. Enernet K-20 electric energy data loggers were installed along with CTs of various sizes ranging from 50 amps to 500 amps to capture energy usage data. CTs were installed on each of the three phases for each sub-system. Though the data were recorded over the eighteen-month period, there was still a 10 percent margin of error between the monitored data and the monthly energy bills. Since there were a limited number of locations to install the K-20s, it is assumed that not every load was measured. Additionally, the total energy consumption was not recorded due to the limitation in size of CTs available and the location of the incoming power supply. As a validation for the recorded data, energy using equipment and systems were inventoried by a walk-through assessment of Houghton Hall for comparison.

3.4 Issues with Assessing a Naturally Ventilated Building

Overall naturally ventilated buildings are more difficult to assess than their mechanically ventilated counterparts, as they have more temperature variation, varying ventilation rates that are dependent on environmental conditions and window geometry and less controlled airflow patterns. This requires additional attention when determining air exchange rates, and in this case, the development and construction of a device to fit completely over the window to obtain more accurate volume flow rate measurements.

3.5 Window Airflow Rates

In naturally ventilated buildings, the type of window installed can impact the ventilation effectiveness and airflow entering and exiting the building. Operable windows are classified by their mechanism for opening and how they open. Common window types used in naturally ventilated buildings include casement windows, hung windows, and rotating windows. Understanding the benefits and drawbacks, and the geometry and its impact on effective opening area can assist in evaluating and designing naturally ventilated buildings.

The three main types of classification of windows were presented in the previous chapter. A device was built in order to better measure the volume of air entering through the awning-type window that existed in the prototype building. This was important primarily in being able to simplify the scale model window geometry, but also in determining an airflow balance in the prototype building. By having an effective opening area for the windows used in the prototype building, a rectangular opening could be used instead of the more complex awning, top hinged, geometry of the prototype building. The errors due to exact window geometry and angle of opening for the awning type window are then reduced. The measuring device had to be portable in order to test it at various sites and locations, and had to be capable of measuring varying airflow rates as seen with natural ventilation.

3.5.1 Window Airflow Device

A device was created that is similar to the hood or bag method often used in mechanically ventilated buildings to determine the supply airflow rate from a diffuser (Awbi 2003). The device used to measure airflow rates fits tightly over the supply diffuser and then one of two quantifying methods is employed. In the "hood" method, air is funneled using a rigid-walled device to a smaller exhaust cross-sectional area that is outfitted with multiple hot wire anemometers to measure the velocity across the exit point. In the simpler "bag" method, the time it takes to inflate a bag of known volume is recorded. For the awning windows and natural ventilation in the prototype building, a frame was constructed to fit over the large, occupant-controlled window. This frame had a bag made of thin, lightweight plastic film attached to it and supported by two rods extending from the frame. The bag began in the collapsed position at the start of the measurement, and the time it took to become fully inflated was recorded. Simultaneously velocity measurements in the same horizontal plane as before were recorded so that the airflow rate could be correlated to the air velocity measured. A diagram of the window bag device is shown in Figure 16.

The theory behind the device is derived from the bag method used to measure the airflow rates at diffusers in mechanically ventilated buildings. For mechanically ventilated buildings, the airflow rate is controlled, with either a constant volume or variable volume system. There are two measurement approaches; either a rigid device that measures air velocity, or a bag that inflates, measuring how long it takes to fill a known volume. For the former case, a rigid device fits over the supply diffuser, and hot wire anemometers, normally in grid form, are at the outlet of the device. This provides the velocity of air exiting the diffuser, and since the area of the outlet of the device is known, the airflow rate is easily calculated. With the timed bag method, a bag of known volume is placed over the supply diffuser, and the time it takes to inflate is recorded. However, with natural ventilation, neither the flow rate nor the wind direction is constant. Not

only is the airflow almost never at a constant velocity external to the building, but the direction of the wind and the resulting angle of the wind in relationship to the building façade can change quickly as well. Since windows in naturally ventilated buildings are subject to wind gusts, a device had to be built that would adjust to the varying flow rate of the air entering the window, rather than the static device that was used in mechanically ventilated buildings.

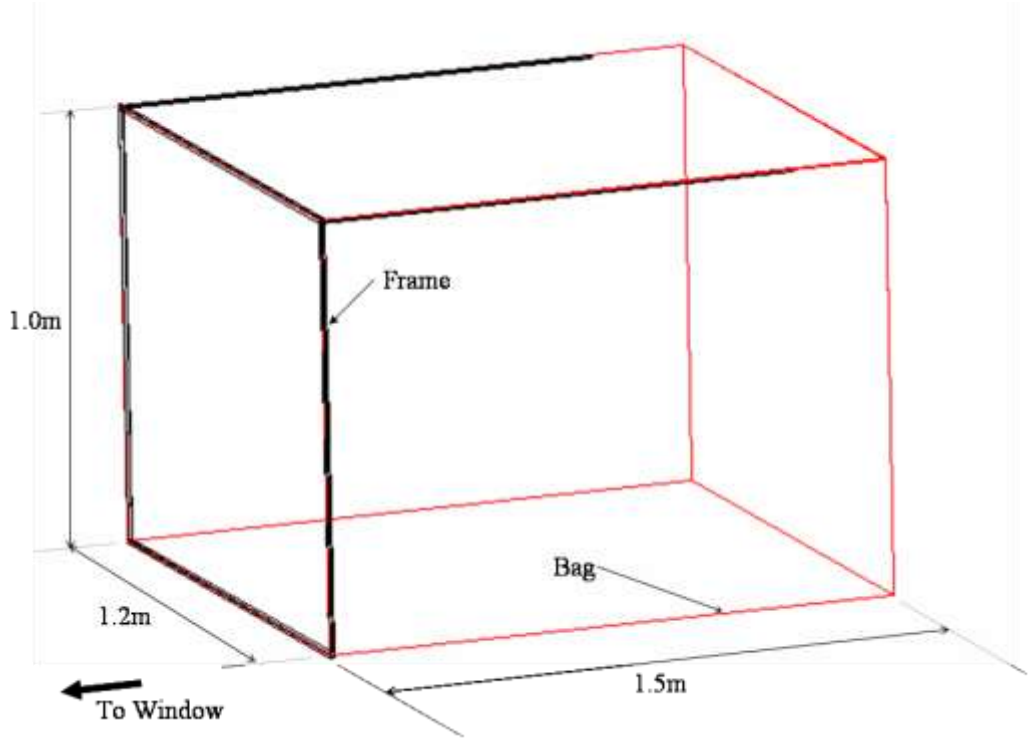

Figure 16. Window Bag Device for Measuring Airflow Through Awning-Type Window

Focusing on awning-type windows, it was unclear as to where to take an air velocity measurement in order to determine the flow rate of air entering through the window. Taking it in the vertical plane was difficult with a singular measurement point, either in the side opening pieces perpendicular to the façade or in the window plane inline with the façade. On the other hand, taking the velocity measurements in a horizontal plane could also provide an erroneous measurement, due to neglecting the side openings. Air velocity measurements alone would not be sufficient to determine airflow rates through windows.

In order to measure the volume of air entering through the awning-type window and determine its effectiveness, a device was constructed. This device was made to be portable and allow for varying wind speeds. Once built, it was tested on the prototype naturally ventilated building in Luton. The device was constructed of commercially available products; window plastic, 1x2 inch wood members, ¼ inch diameter dowel rods, and foam tape. The device had to be flexible so that it would be able to measure gusts of wind. First, a frame was made of 2 inch by 1-inch wood pieces, 40 inches (1.02 meters) wide and long. These measurements were used in order to fit the particular window-type of interest in the prototype building. It was desired that the frame would fit around the window, thereby collecting all of the air flowing through the window. Then a material had to be selected that was elastic enough to inflate with the slightest bit of wind.

Window plastic, or the material that is used to protect against cold drafts from leaky windows during the winter, was used. Several other thin, pliable plastic sheets were tried, but the window plastic was found to be durable, yet supple enough to use for the airflow device. The plastic was then taped together to form a rectangular volume that would fit the frame. A release flap was incorporated into the bag portion of the device, so that if there were sudden gusts of wind, the device could remain in place and not be destroyed by the sudden surge of air in the limited volume bag.

3.5.2 Airflow Device Measurements and Results

Once constructed, the airflow device was tested out on the awning-type windows at the prototype building. Previously, air velocity measurements had been recorded in the horizontal plane of the window, ignoring the vertical side pieces. With the bag device, velocity measurements were taken concurrently with air volume flow rates, so that the previously recorded air velocity measurements could be correlated to a volume flow rate. Measurements were taken during a low-wind day at the prototype building, with few gusts of wind.

Table 9. Window Bag Device Characteristics

Measured Dimension of Bag Device	*Value*
Length of Frame	1.0 meters
Width of Frame	1.2 meters
Horizontal Opening Area of Window	1.2 square meters
Depth of Bag	1.3 meters
Volume	1.5 m^3

The effective area was calculated by taking into account the volume flow rate Q (based on the window bag device measurements), recorded air velocity measurements V in the horizontal plane, and the total vertical cut-out area A of the awning window. This is represented by:

$$Q = V \times A \times Eff \tag{3.18}$$

where *Eff* is the effectiveness of the window opening. For the experiments, the time recorded was for the bag device to inflate 100 percent. The exception was Trial 8, in which the bag only inflated a third of the way. The resulting measurements for both the air velocity and time for the window bag device to inflate are presented in Table 10. This calculated effective area of 30 percent was then used in the modeling efforts presented in later chapters.

Table 10. Window Bag Device Measurements and Resulting Flow Rates and Effectiveness Calculations

	Time (sec)	*Air Velocity (m/s)*	*Volume of Air (m^3)*	*Volume flow rate (m^3/s)*	*Effective Opening (m^2)*	*Effectiveness of Window*
Trial 1	7	0.6	1.5	0.2143	0.3571	29.7%
Trial 2	10	0.4	1.5	0.1500	0.3750	31.2%
Trial 3	8	0.5	1.5	0.1875	0.3750	31.2%
Trial 4	6	0.7	1.5	0.2500	0.3571	29.7%
Trial 5	8	0.5	1.5	0.1875	0.3750	31.2%
Trial 6	7	0.6	1.5	0.2143	0.3571	29.7%
Trial 7	10	0.4	1.5	0.1500	0.3750	31.2%
Trial 8*	14	0.1	0.5	0.1071	0.3571	29.7%
Average	8.75	0.475	1.5	0.1826	0.3661	**30.5%**

*bag device inflated only 1/3 of the way

3.6 Prototype Building Monitoring Results

The data were analyzed to determine the seasonal and annual performance of the prototype building after the eighteen-month monitoring period from May 2003 to October 2004. This section presents the resulting data by area, internal environment and energy usage.

3.6.1 Indoor Environment

The data evaluating the indoor environment were collected and analyzed by season. The focus was on the shoulder months, spring and fall, and the summer months, as these periods had the most variation due to the operation of the building in response to the internal and external condition requirements. However, some winter data are presented for comparison of indoor conditions.

3.6.1.1 Temperatures

The average of all of the temperature data loggers at each fifteen minute interval was used to calculate an average internal building temperature for both a sample summer period and winter period. The summer data provide information on the ability of the building to keep the interior temperatures lower than the outside, even during extreme heat. The winter data show the fluctuation of internal temperatures during occupied hours, with the heaters in use primarily during occupied hours, but with a minimum set point to avoid frost.

Error! Reference source not found. Figure 17 and Figure 18 show the summer and winter internal building temperatures compared to the external temperatures. Through monitoring of the temperature within the office spaces in Houghton Hall, it was determined that the temperature varied little, between 1 and 2 degrees C, across each half floor, but more significantly between floor-levels. Sample data from occupied hours during a day in August 2003 are presented in Table 11 for two points on the ground floor (GF-1, GF-2), First Floor South (FFS-1, FFS-2), First Floor North (FFN-1, FFN-2), and Second Floor (SF-1, SF-2). For the most part the ground floor had the coolest temperatures, year-round. The second floor was observed to have the

warmest temperatures of all of the occupied office spaces. The stratification was most prevalent during the summer months, when the external conditions were relied upon for cooling. During the winter months, the internal temperature is controlled by thermostats for the perimeter (trench) heating system, and therefore tends to be uniform throughout the building (Figure 18). In some cases, the warm air left through the second floor occupied space, especially on days with high wind and/or rain, either of which would cause the louvers in the atrium stacks to close. Though impacted by the external environment, the internal conditions for the most part remained within comfort regions.

Table 11. Temperature Data at Two Locations per Floor: August Workday Occupied Hours

	GF-1	***GF-2***	***FFS-1***	***FFS-2***	***FFN-1***	***FFN-2***	***SF-1***	***SF-2***
10:00 AM	23.63	23.63	24.79	24.4	25.95	25.17	28.7	27.91
10:15 AM	24.01	23.63	24.79	24.79	26.34	25.56	29.1	29.1
10:30 AM	24.01	23.63	25.17	25.17	26.34	25.56	29.1	28.7
10:45 AM	24.01	24.01	25.17	25.17	26.73	25.95	29.1	28.7
11:00 AM	24.4	24.01	25.56	25.17	27.12	25.95	29.5	28.7
11:15 AM	24.79	24.4	25.56	25.56	27.12	26.34	29.5	28.7
11:30 AM	24.79	24.4	25.95	25.56	27.52	26.34	29.5	28.7
11:45 AM	25.17	24.79	25.95	25.95	27.91	26.73	29.5	28.7
12:00 PM	25.56	24.79	26.34	25.95	27.91	27.52	29.5	29.1
12:15 PM	25.56	25.17	26.34	26.34	28.31	27.52	29.9	29.1
12:30 PM	25.95	25.17	26.34	26.34	28.31	27.52	29.9	29.1
12:45 PM	25.95	25.56	26.73	26.73	28.31	27.52	29.9	29.1
1:00 PM	26.34	25.56	26.73	26.73	28.7	27.91	30.31	29.5
1:15 PM	26.34	25.56	27.12	26.73	28.7	27.91	30.31	29.5
1:30 PM	26.34	25.95	27.12	27.12	28.7	28.31	30.31	29.5
1:45 PM	26.73	25.95	27.12	27.12	28.7	30.31	30.31	29.9
2:00 PM	26.73	26.34	27.52	27.12	29.1	31.12	30.31	29.9
2:15 PM	27.12	26.34	27.91	27.52	29.1	33.59	30.31	29.9
2:30 PM	27.12	26.34	27.91	27.52	29.5	34.85	30.31	29.9
2:45 PM	27.52	26.34	27.91	27.52	29.5	33.59	30.31	29.9
3:00 PM	27.52	26.34	28.31	27.91	29.9	31.12	30.31	29.9

Neglecting the August 2003 data, which reflected record heat in the United Kingdom, the maximum temperatures within the building were on the second floor at 25.2ºC. Even during the record heat, when the external temperature reached 37ºC, the average internal temperature within the building was 30.7ºC, or almost 6ºC cooler than the outside. Sample data for the summer period, with the average occupied space temperature (Building Average Temperature) and outside air temperature are presented in Figure 17. One of the exceptions to this performance was on the weekends; when the heating was turned off during the winter months (except for frost protection) and the large occupant controlled windows were closed during spring, summer, and fall months. This led to cool interior temperatures in the wintertime and temperatures closer to or above the external temperature in the summertime.

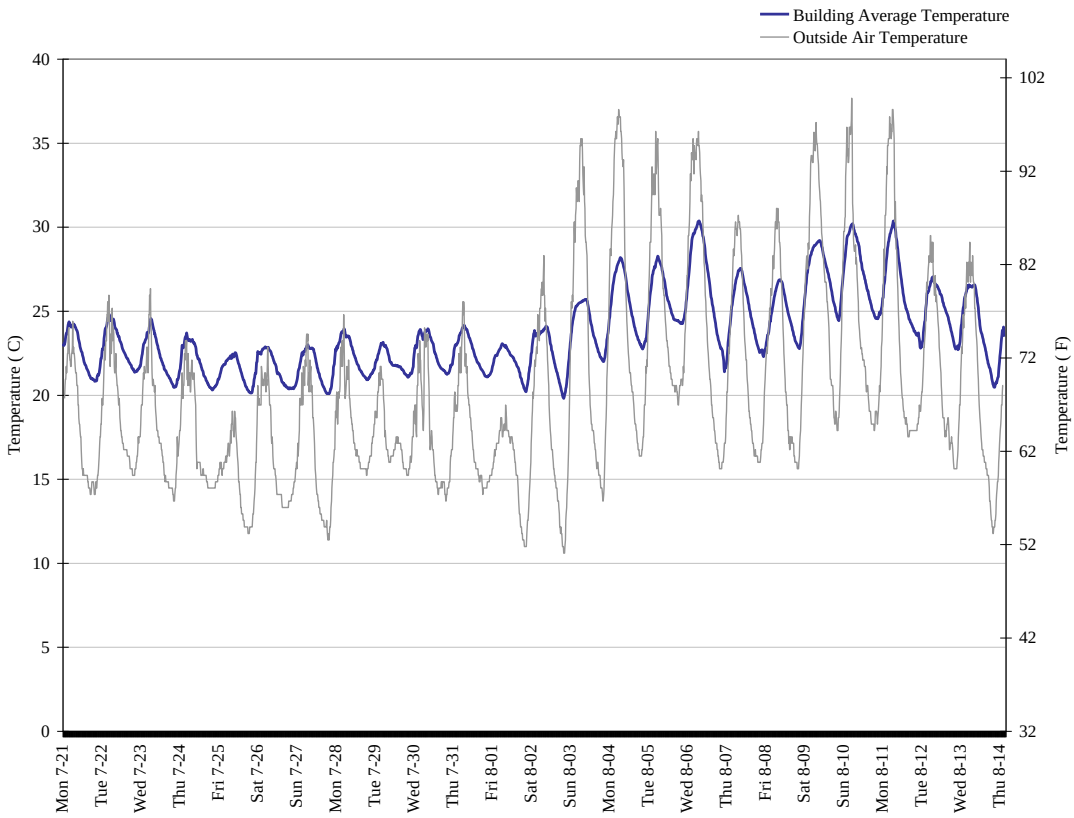

Figure 17. Building Average Internal and External Temperatures for Summer

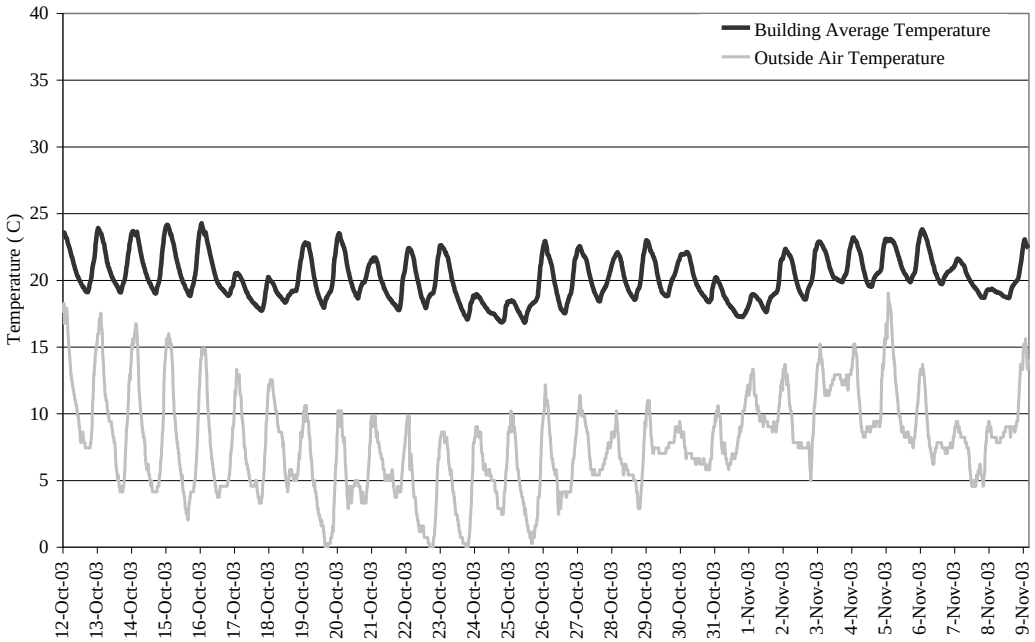

Figure 18. Building Average Internal and External Temperatures for Winter

Table 12 summarizes the range of internal and external conditions that were recorded for each season in the prototype building. The spring season is described as April through May when the external temperatures are still relatively cool and the occupant controlled windows are not necessarily open every day. The summer season is considered to be June through August, but the extreme heat of August 2003 was omitted from the table data set. The fall season is similar in operation of the windows to the spring season, while the winter season assumes that all of the windows and vents are fully closed. The building maximum temperatures occurred during mid-day periods, while the minimum temperatures occurred during nighttime periods. Sample data from a day of extreme heat during August, 2003 is presented in Figure 19.

Table 12. Internal and External Temperatures over 24-hours by Season

Temperature	*Spring, ºC*	*Summer, ºC*	*Fall, ºC*	*Winter, ºC*
Building Average	20.8	22.5	21.2	20.2
Building Minimum	18.5	16.9	16.0	13.6
Building Maximum	23.5	25.2	25.0	22.5
Outside Average	11.3	17.4	13.3	5.1
Outside Minimum	2.9	11.0	2.0	-2.8
Outside Maximum	24.4	28.3	27.4	11.8

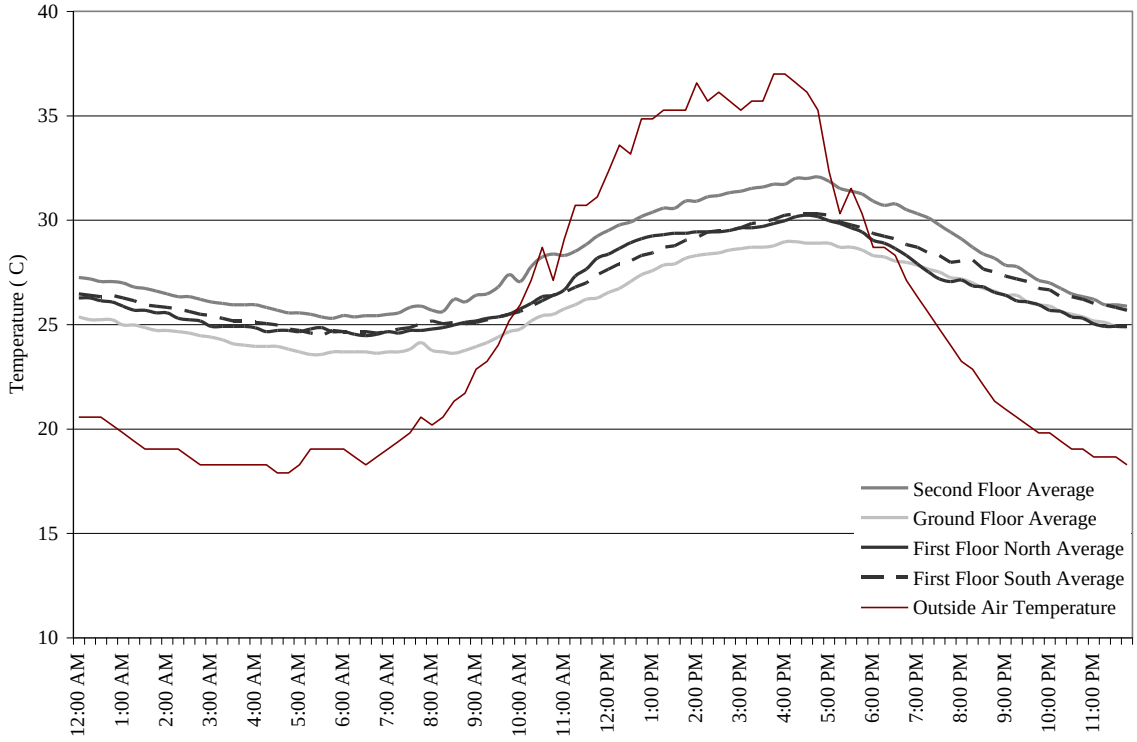

Figure 19. Internal Temperatures from Extreme Heat Summer Day: Summer 2003

Additionally, differences in temperature between the northern and southern halves of the building were observed. During the summer months, the maximum temperature difference between the north and south floors was 4ºC; while during the winter months the difference was as much as 8ºC. The maximum temperature difference for the summer period occurred during the nighttime hours, while the temperatures were similar for the north and south sides during the daytime hours. The south side of the building tends to remain warmer than the north side due to solar gains and thermal mass; it takes longer for the thermal mass to cool on the south side, since it is exposed to direct sunlight for more of the day than is the north side. This variation from north to south was present and more appreciable during the winter months, with the temperature difference between the north and south halves remaining relatively consistent throughout the day. The solar gains had a significant impact on the south half, particularly when the sun was lower in the horizon and the solar shading devices attached to the façade were less effective. The thermal mass retained the heat both from the solar gain and internal gains, and remained warmer during the wintertime. During the summer months, the windows were also open, allowing more air to flow through the building, causing a more even temperature throughout the building. The south half remained somewhat warmer during the summer nighttime hours when the thermal mass released the heat stored from both internal loads and solar gain during the daytime hours. The variation from north to south for a sample period of time (late July through early August) is shown in Figure 21 and for a sample cold period (late October through beginning of November) in Figure 20.

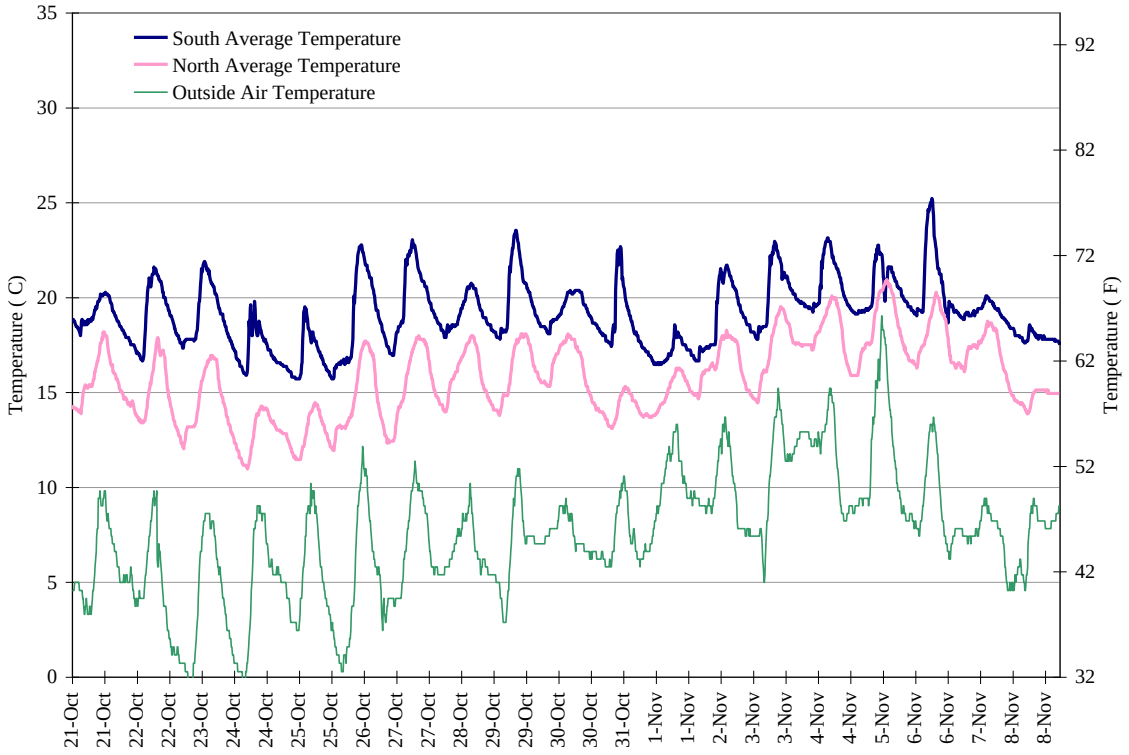

Figure 20. Fall Average Building Internal Temperature by Orientation: North versus South

Summer data were collected during the heat wave that occurred during the summer of 2003 in the UK, which provided data on the performance of this naturally ventilated building during extreme conditions. Though the external temperature reached over 36 ºC, the average internal temperature within the building was 30ºC, significantly lower than the outside. It was observed that when these high temperatures occurred during the workday, occupants wore lighter clothing and used personal fans to generate a breeze to improve their comfort. When comparing the internal and external temperatures to an adaptive standard for naturally ventilated buildings based on ASHRAE Standard 55 (Brager 2000, ASHRAE 2004), the internal temperatures fall within the 90 percent acceptability limits. Normally the temperate climate has approximately 30 hours when the outside air temperature is at or above 26ºC, whereas in 2003 there were over three times as many with 98 hours. As for internal conditions, there were 119 hours during the summer of 2003 when the average building internal temperature was at or above 26ºC; however thirty percent of this was during unoccupied hours.

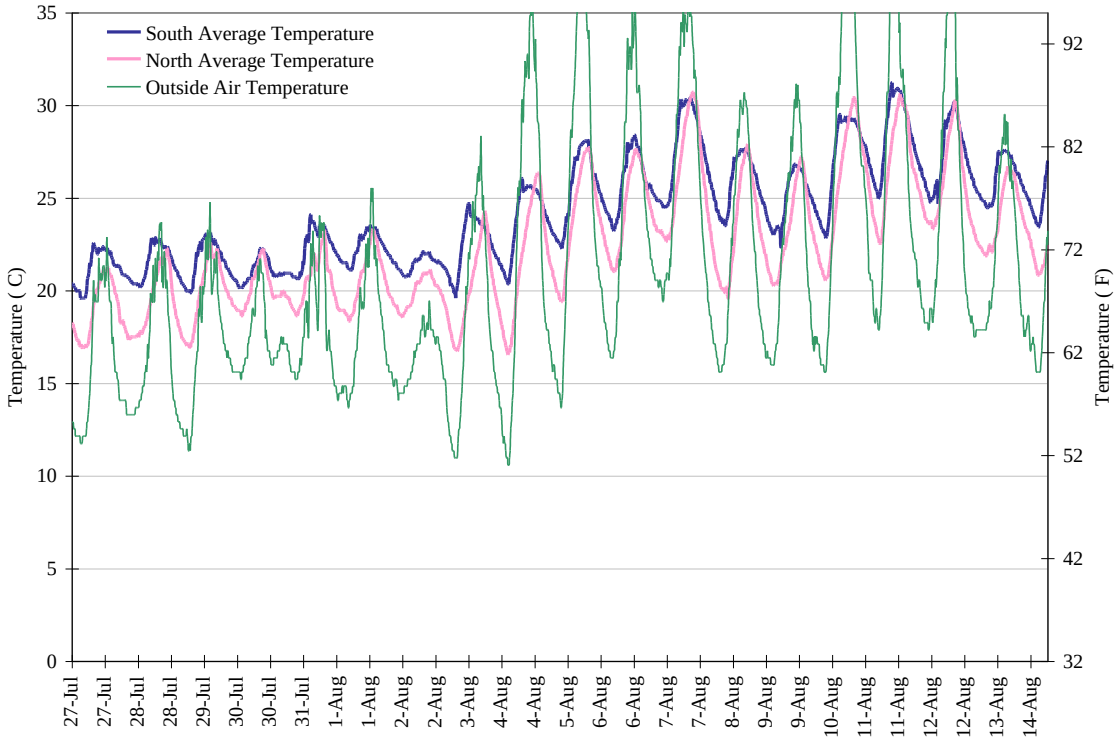

Figure 21. North versus South Average Building Temperature: Summer Conditions

The role of the ceiling soffits as thermal mass, designed to pre-cool the building during the summer night time was qualitatively assessed. The measured internal temperatures peaked approximately four hours after the outside temperature reached its maximum for the day (Walker 2004). This particular design aspect was not used to its fullest potential; during the nighttime hours, only the smaller, upper level vent windows were open. This does not allow for very high airflow rates needed to cool the concrete soffits. A recommendation was made to turn on the fans in the atrium vents to assist in drawing additional cool nighttime air into the building to further cool it, particularly during the summer months.

3.6.1.2 Ventilation

The ability of the naturally ventilated office building to provide adequate cooling and ventilation was evaluated during summer and fall site visits. A series of air velocity measurements at both the lower and upper windows for a variety of outside conditions were recorded, and the effective area, or percentage of the total vertical window area, for the awning-type window geometry was determined through measurement with a hot-wire anemometer and experiments using the bag device. The bag device that was created to determine the effective opening area for the awning-type window geometry was used in the late summer/early fall of 2004. With the awning-type window there are two triangular sidepieces and a horizontal piece that each can contribute to the volume of air entering (or leaving) through the window. Air velocity and air volume measurements were recorded so that a correlation between the previously recorded air velocity measurements and the volume of air entering and leaving the building could be determined. The

resulting data showed that the effective area of the awning-type window was approximately 30 percent of the total area of the window when the window was in the fully open position. This accounted for the contribution of the sidepieces and the horizontal opening for this window geometry. When the modified effective opening areas were applied to airflow balances previously attempted from summer measurements, it improved the overall airflow balance by up to 15 percent for the building. A sample set of data for a case without the stack vents is provided in Table 13. The effective window area improved the airflow balance calculation by 5 percent for the dataset presented. The original airflow balance included just the horizontal piece of the window as the effective area. Airflow balances for several days, both with and without the stack vents are presented in Table 14. The effective opening area was used in these calculations, providing an airflow balance within 2-25 percent.

Table 13. Comparison of Airflow with and without Effective/Corrected Area

		Air Velocity (m/s)	*Horizontal Area*	*Airflow (m3/s)*	*Corrected Area*	*Corrected Airflow (m3/s)*
Second Floor	Window	1.01	0.1413	0.1427	0.4039	0.4080
	Vent	0.34	0.1385	0.0471	0.1094	0.0372
First Floor North	Window	0.63	0.1413	0.0890	0.4039	0.2545
	Vent	0.24	0.1385	0.0331	0.1094	0.0261
First Floor South	Window	0.61	0.1413	0.0862	0.4039	0.2464
	Vent	0.14	0.1385	0.0200	0.1094	0.0158
Ground Floor	Window	0.00	0.1413	0.0000	0.4039	0.0000
	Vent	0.22	0.1385	0.0305	0.1094	0.0241
Airflow Balance				**26.7%**		**21.5%**

Table 14. Sample Site Measurements of Airflow at Each Floor Level and Airflow Balance using Effective Opening Area

	18 July -fan off		*19 July -fan on*		*20 July -fan on*	
	Airflow rate (m^3/s)	Direction	Airflow rate (m^3/s)	Direction	Airflow rate (m^3/s)	Direction
Second Floor	**0.71**		**2.06**		**1.23**	
Window	0.29	out	0.84	in	0.36	in
Vent	0.42	out	1.22	in	0.87	in
First Floor North	**0.50**		**1.31**		**1.64**	
Window	0.27	in	0.58	in	0.59	in
Vent	0.24	in	0.73	in	1.05	in
First Floor South	**0.29**		**1.41**		**0.94**	
Window	0.17	in	0.62	in	0.38	in
Vent	0.11	in	0.79	in	0.57	in
Ground Floor	**0.13**		**0.58**		**0.48**	
Window	0.00	in	0.55	in	0.45	in
Vent	0.13	in	0.04	in	0.03	in
Roof Vents			**5.20**	out	**4.21**	out
Airflow Balance	**22.7%**		**3.1%**		**2.0%**	

A range of air exchange rates was found and used to determine both when the façade heat loss dominated the energy balance and when airflow contributed an equal amount to heat loss. The low end of the air exchange rates was recorded on a day when only the upper vent windows on each floor were open. This was done because there were few, if any, days on site when there was little to no wind outside. The upper end of the air exchange rate was measured on a similar day, but with the occupant-controlled windows open. On extremely windy days, the occupant-controlled windows were often left closed, to prevent drafts that may disrupt papers on desks within the office area. The air exchange rates for the building ranged from 0.6 air changes per hour (ACH) to almost 1 ACH during a site visit in early fall when the windows were mostly closed. The results of ventilation rates using the three different techniques are presented in Table 15. The hot-wire data presented in Table 15 were determined using the effective opening area as calculated using the bag device presented in Chapter 3.5.1.

Table 15. Comparison of Hourly Air Change Rates (ACH) by Season and Method

	Hot-wire Anemometer	*Carbon Dioxide Data*	*Energy Balance*	*Inflated Bag Method**
Summer	3 ACH ($3.8\ m^3/s$)	2 ACH ($2.8\ m^3/s$)	-----	2 ACH ($2.6\ m^3/s$)
Fall	0.6 ACH ($0.85\ m^3/s$)	0.6 ACH ($0.87\ m^3/s$)	0.9 ACH ($1.2\ m^3/s$)	-----

*The inflated bag method is not directly comparable to the other measurements. It was done over a weekend with little internal loads, and is primarily wind-driven flow.

The measurements taken during site visits to understand the airflow patterns and ventilation effectiveness of Houghton Hall were also used in verifying air exchange rates calculated through both an energy balance for a snapshot in time and carbon dioxide measurements and corresponding calculations. For the energy balance, the solar radiation from the weather station was $200W/m^2$, recorded electric load was 16 kW, and the number of people, each at 100W, was 10. The outside air temperature was recorded at 14.9ºC and the exhaust temperature leaving the building was measured at 22.5ºC. In this snapshot the heat loss through the façade has an equal contribution to the heat loss due to airflow.

Carbon dioxide measurements were recorded throughout the year and used to corroborate the estimated airflow calculation. Using 0.3 L/min/person (McQuiston 2000), a measured outside CO_2 level of 464 parts per million (ppm), and a total of 120 people within the building, this provided an air exchange rate of 0.6 ACH with all of the windows closed. This is similar to the air velocity measurements that estimated 0.6 ACH with the windows closed. Several airflow balances based on air velocity measurements and flow rate calculations taken over the period of several days and several site visits, were determined to be within a 25 percent margin of error between the amount of air entering and leaving the building. The resulting carbon dioxide levels for the summer conditions when all of the windows were open, and the winter when all of the windows were closed is presented in Figure 22. The occupancy density that corresponds with these CO_2 levels is approximately $15m^2$ per person. This is on the low side for a commercial office building.

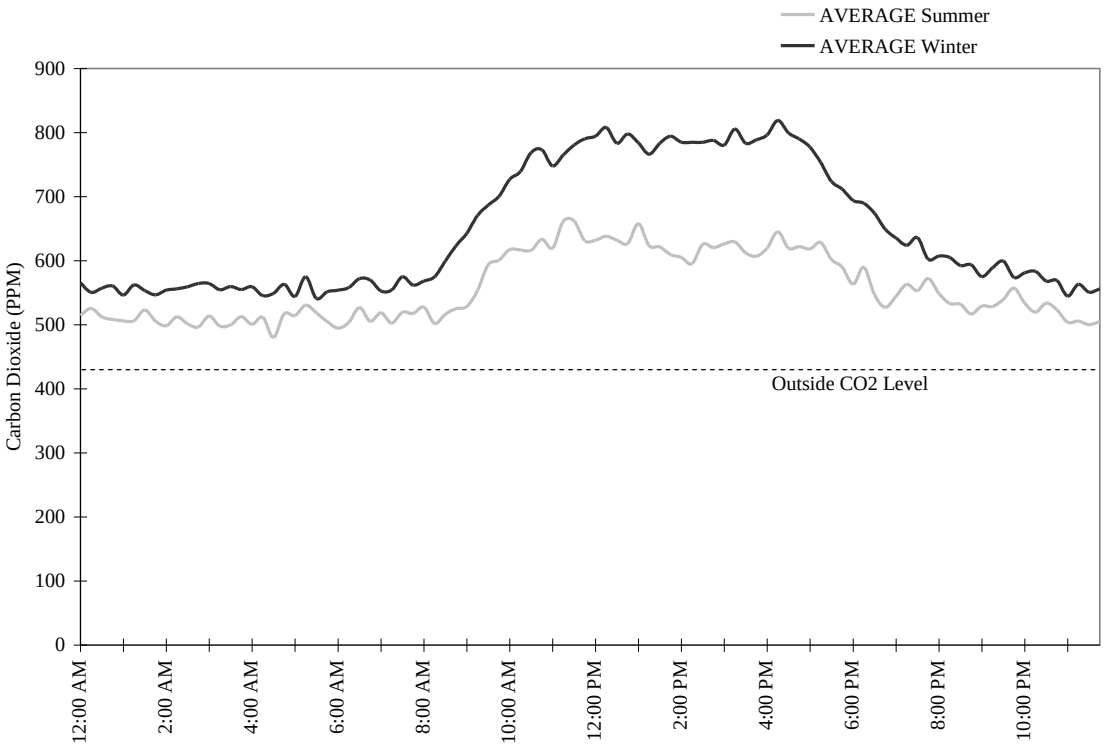

Figure 22. Internal Building Carbon Dioxide Levels: Summer versus Winter Conditions

Although, each method proved useful for comparison and for evaluating the air exchange rate, there was a certain amount of uncertainty in each of the methods used. The hot-wire anemometer measures air velocity in a single direction, and cannot account for flow that is not perpendicular to the wire. Additionally, the bag device had to be constructed to ensure that an accurate volume flow rate was being measured. The bag device was useful in providing a better idea of the volume of air entering the building, but could not be used for the upper windows, or the exhaust windows, due to restrictions in access to them. A single volume flow rate was measured, as there was only one bag device built for use in measuring volume flow rate. The carbon dioxide data had a degree of uncertainty due to the location of the device. There is some buoyancy flow in the building, and locating the carbon dioxide sensor on the upper floor could cause elevated measurements of the levels of carbon dioxide for the building. Finally, with the energy balance, data were used for a specific period of time, even though the building has transient effects due to the thermal mass, changes in the exterior environment such as clouds or wind gusts, and consistency of the state of the internal loads.

The airflow visualization techniques employed provided insight into the interaction of the occupied office spaces with the atrium. As the ground floor normally had the coolest temperature, warm air from the occupied zone on the ground floor slowly moved toward the atrium. However, on the first floor, the air in the atrium was cooler than the air in the occupied spaces on the first floor, so the air flowed from the atrium into the office space, and then exited at the ceiling level of the office space back into the atrium. At the second floor occupied zone, the airflow tended to either move from the atrium through the second floor space and then out of

the windows on the second floor, or from the second floor space into the atrium and then rise toward the stack vents where the air was exhausted to the outside. Figure 23 illustrates this airflow behavior. Smoke pencils verified the detailed flow patterns, particularly those at the connection of the atrium and office space. These airflow patterns did not seem intuitive when the experiments were carried out, but similar airflow patterns were observed when modeled using a computational fluid dynamics program.

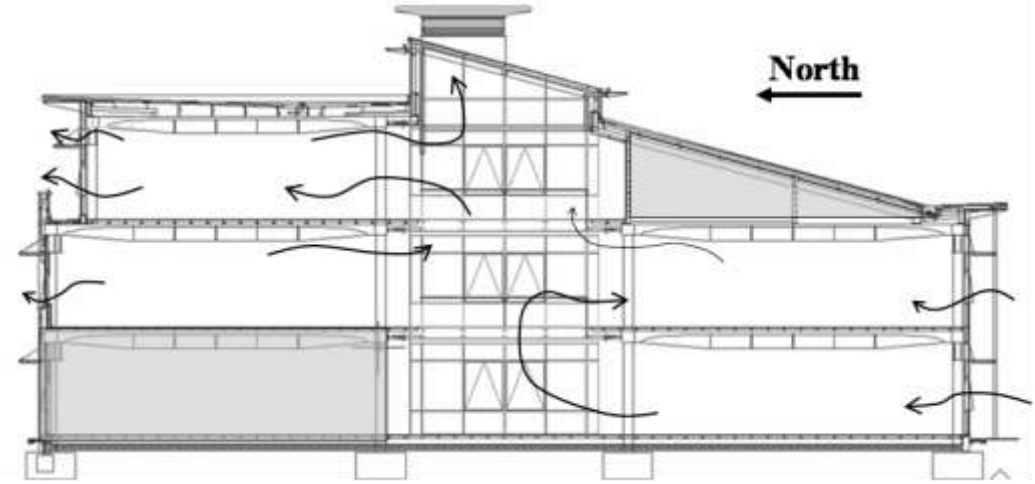

Figure 23. Airflow Patterns Observed in Prototype Building Field Measurements

3.6.1.3 Energy Usage

The energy usage analysis was divided by sub-systems into two separate day types; occupied (weekday) and unoccupied (weekend). Electric energy usage was also compared by season to determine if usage patterns changed due to internal and external environment. It was found that there was no significant change due to the season with the electric energy usage within the building. The occupant schedule was observed to stay regular throughout the year as people began arriving for the day at 8:00 am and for the most part left by 6:00 pm. From the usage trends and known information about the number of people within each office space, it was determined that the energy usage depended on occupant density; the more people in a half floor office area, the higher the energy usage. The number of occupants within an office space has a direct correlation to the number of computers, monitors, and printers within a given space, potentially explaining this trend. This is shown in Table 16. It should be noted that the Ground Floor South energy usage was determined by subtracting the computer server room energy consumption base load that it contributed to the measured power draw for the Ground Floor area. The second floor north had significantly more personal printers than either of the other zones, causing a higher peak energy usage per person.

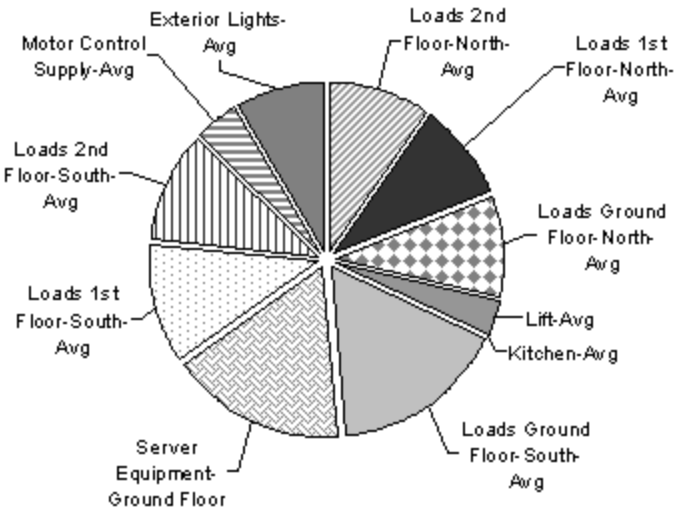

Figure 24. Annual Energy Usage Profile of Prototype Building by Category

Table 16. Comparison Energy Usage and Number of Occupants

	Ground Floor South	*1st Floor South*	*1st Floor North*	*2nd Floor North*
Peak Energy Usage (kW)	3.6 kW	3.1 kW	3.7 kW	2.7 kW
Number of Occupants	30	27	30	18

Also, it was determined through both analysis of data and observation of occupants during site visits that the energy usage does not decrease at all over the lunch period, as most of the occupants either brought their lunch or purchased items from an interior vending machine. The ground floor energy usage has a much higher base-load as compared to the other floors because it has additional equipment, such as the computer server room and several vending machines. These additional loads appear not only in the added energy consumption during the office hours, but also contribute to the base load, as they remain on all the time. The electric energy usage is broken down into sub-categories based on annual energy consumption and is presented in Figure 24. The daily electric energy usage for a typical weekend day, when the building is not usually occupied, has very small base loads for each of the office floor areas due to several light fixtures that are left on for safety and computers that are in stand-by mode.

3.7 Discussion

The analysis of Houghton Hall is useful to demonstrate how well it functions well as a naturally ventilated building. To further determine how this building is performing, the data are used to compare it to benchmark data. Here the comparisons are made between Houghton Hall, various standards for performance (Standard and Good Practice), and other low energy buildings, including one similar in climate and configuration that is mechanically ventilated and uses a chiller to provide cooling.

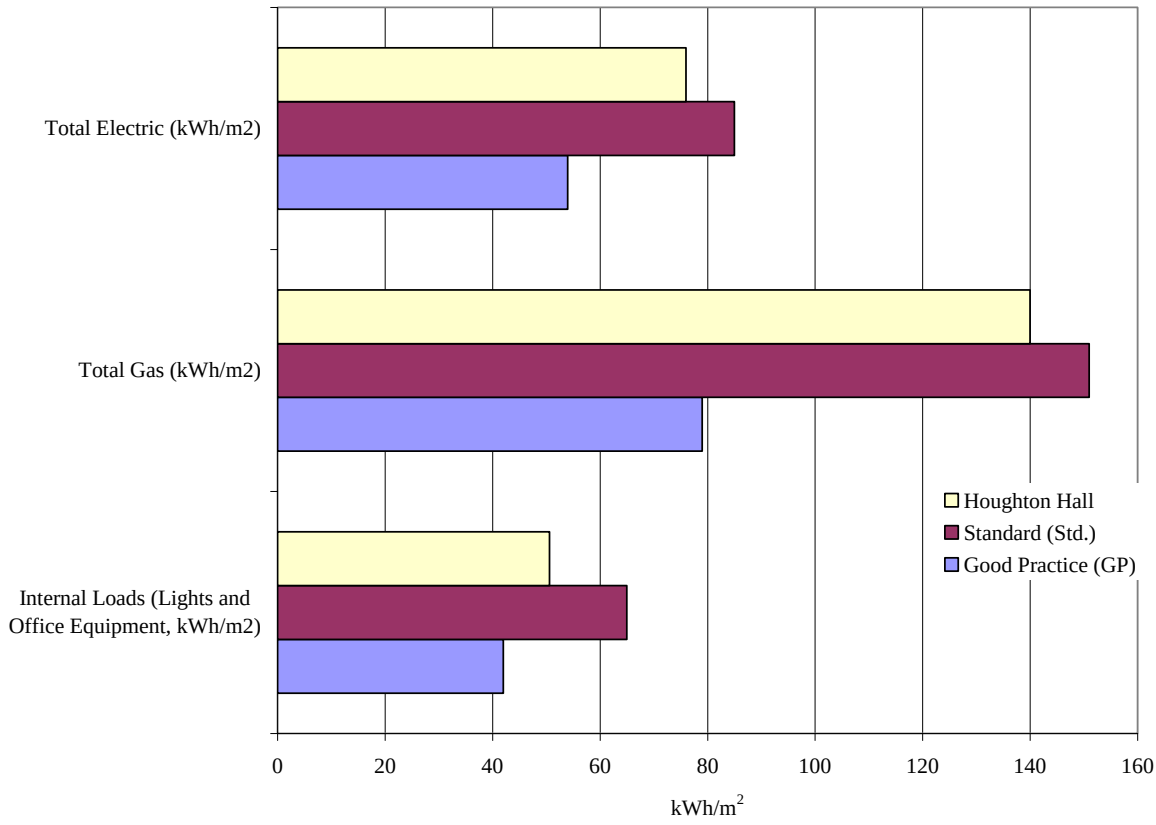

Figure 25. Comparison of Prototype to ECG019, Good Practice and Typical Natural Ventilated Buildings

The Energy Consumption Guide 019 (Action Energy, 2003) establishes a range of energy usage for buildings; Houghton Hall was compared to the Open Floor Plan Naturally Ventilated Office Building. Within this category, Houghton Hall overall fell in between Standard (Std) and Good Practice (GP), with the data leaning towards the Typical side of the range. This is shown graphically in Figure 25. The energy usage is the total annual consumption for each particular category, and for overall electric and natural gas energy usage. Since the internal loads could not be broken down into lighting and office equipment, these categories were combined and the results presented. It is thought that Houghton Hall is towards the 'Standard' side of lighting and office equipment due to the operation of the lighting and computer systems, inclusion of the computer server room in monitoring, and the energy usage of kitchenette areas located on each floor level. This inclusion increases the base line energy consumption, particularly during occupied and less so during unoccupied hours. It also contributes to the total annual electric energy consumption, as there is not much other electrical energy using within the building, with the exception of the lift. As for the natural gas consumption, the data presented was obtained from the first year of occupation of the building, when some issues with the control scheme and building tightness were being addressed. Originally, the louvers at the stack vents were not well sealed, and air from the building was leaking through the louvers, drawing in additional outside air during the winter months in other locations within the building. This caused the boilers to operate more frequently trying to keep the building warm. This issue was addressed, and rubber

seals installed, so it is believed that updated natural gas utility data, which were not available, would place Houghton Hall closer to the 'Good Practice' side of the scale.

In evaluating the indoor environment, the carbon dioxide levels that were measured throughout the year were found to vary by season. However, the levels within the building were not close to the levels at which there would be cause for concern or occupant dissatisfaction. Even during the winter months, the differential between the outside level and the interior level taken at the second floor was 360 ppm with the building fully occupied. During the summer months, there is definitely adequate airflow to meet indoor air quality levels without any potential health issues.

Table 17. Comparison of ECG 019 Benchmark, Mechanically Ventilated (MV) and Naturally Ventilated (NV) Buildings

	MV Std.	*MV GP*	*NV Std*	*NV GP*	*UFAD MV**	*Luton NV**
Total Energy Usage kWh/m^2	404	225	236	133	318	216
Total Natural Gas kWh/m^2	178	97	151	79	162	140
Total Electricity kWh/m^2	226	128	85	54	156	76
Lighting & Office kWh/m^2	85	50	65	42	55	51
Refrigeration kWh/m^2	31	14	0	0	29	0
Fans & Controls kWh/m^2	60	30	8	4	50	5

* Data from Experimental Measurements

The importance of incorporating natural ventilation into building design is further emphasized, including the benefit in energy conservation, through comparisons made between Houghton Hall (Luton) and another similarly laid-out office building located in Sunbury, within relatively close proximity. The main difference between the two buildings was the method of ventilation. Both buildings were located in office parks, and were three stories in height with an open office floor plan and central atrium. The mechanically ventilated building employed rooftop units and chillers to introduce and condition outside air for the building, rather than incorporating natural ventilation in the design. It had an all-glass façade but was a completely sealed building, with an under-floor air distribution (UFAD) mechanical system controlled by a building energy management system. This mechanically ventilated building was monitored in similar detail to the prototype building in Luton, including electrical energy detailed sub-metering, temperature distribution, and ventilation performance. Table 17 summarizes the range for both the mechanically ventilated office building and the naturally ventilated one, with the results for the two buildings.

The naturally ventilated prototype building used 13.6 percent less natural gas usage. Of more significance was the reduction of over 50 percent in electric energy usage per floor area. The mechanically ventilated building was an all-glass façade, with more surface area which may contribute to the higher natural gas usage. Both buildings were 'un-conditioned' on the weekends and both incorporated energy saving features on both lighting fixtures and office equipment. The overall energy consumption per floor area for lighting and office equipment is quite similar for the two buildings. However, the energy required for mechanical cooling or the refrigeration category makes a substantial difference. There is a substantial amount of additional energy usage required for using refrigeration, in the form of a chiller, within the office building in the temperate climate of the UK. By relying on the environment for not only cooling, but also air

movement, Houghton Hall has much less energy consumption for both refrigeration and fan energy usage. Overall the mechanically ventilated system used 354.5 kWh/m^2 compared to the naturally ventilated building with 216.1 kWh/m^2.

A factor that is often of some concern with buildings that do not have active cooling systems installed is temperature conditions within the occupied space, and the amount of variation within the occupied space. In the prototype building, there was temperature variation throughout the occupied hours, with personal fans used to provide additional breezes on particularly warm days. The vertical temperature within an occupied space could vary by as much as 3ºC, with further variation from floor to floor. On the other hand, in the building that had mechanical ventilation, the temperature never varied by more than 2ºC.

3.8 Challenges with Monitoring a Naturally Ventilated Building

From the analysis of Houghton Hall, there were several lessons learned, not only the methodology in assessing a naturally ventilated building, but also the thermal, ventilation, and energy performance of this type of building. It was determined that this naturally ventilated building generally met comfort conditions in the temperate climate of the UK, even in the extreme heat of 2003. The design characteristics incorporated into the building did seem to help in tempering the internal temperature, but more can be done to take further advantage of features such as thermal mass. There are strategies that are recommended for the operation of the fans in the atrium stacks. Running the fans at nighttime during the summer season would help to pre-cool the building further, enhancing the affect of the thermal mass. Having the fans operating when it is warm outside actually draws in the hot outside air, and reduces the effectiveness of the thermal mass.

Though infiltration is welcome in the summer months, there was some concern with possible leakage issues in wintertime that cause the boilers to engage. Since the windows are closed during the winter months, but outside air is still required, the only outside air seemed to enter the building when the main front door was open, allowing gusts of cold outside air to enter the building.

Occupants were surveyed in the spring, fall, and summer periods to evaluate comfort, using a 7 point scale. The goal of the surveys was to determine perceptions of comfort, indoor air quality, and personal control in the building. In general, the occupants were warm during the summer, neutral during the fall, and slightly cool during the spring (Walker 2004). The summer surveys were taken just after the heat wave in August 2003, and may be slightly skewed. The occupants did alter their perception of thermal comfort over the period of the day, corresponding with increased internal temperatures.

It was shown that Houghton Hall compared relatively well to open floor plan naturally ventilated buildings when compared to ECG019. When comparing this commercial office building to a similar mechanically ventilated office building, the energy consumption was significantly lower primarily due to the lack of mechanical cooling, or refrigeration equipment. This can have a distinct impact on energy consumption and the resulting carbon dioxide emissions.

Contrary to many mechanically ventilated buildings within a prescribed temperature range, there was no building management system to control the internal temperature of the naturally

ventilated building, which required additional analysis of temperature variation, both within each occupied space, by orientation, and by floor level.

Finally, there are areas for improvement in the overall performance of Houghton Hall, which can be applied to current and future naturally ventilated buildings. An important area for improved operation of the building is the development of controls for opening and closing of windows, fans, and louvers. For example, if the atrium stack fans were left on over night during the summertime, they would help to draw in additional cooler nighttime air through the smaller windows that remain open during the spring, summer, and fall. This would in turn make better use of the thermal mass, which would further help to temper the internal building temperature.

3.9 Summary

Houghton Hall works as a naturally ventilated commercial office building. Understanding the range of the internal building temperatures and the variation that occurs when there is no building energy management system precisely controlling the internal temperature is essential to making the argument that naturally ventilated buildings can be comfortable during warm summer months.

New techniques were developed to assess the ventilation rates of this naturally ventilated building. By using several methods and measurement techniques, a relatively complete data set were collected. The constantly changing external environment makes the process of evaluating a naturally ventilated building more challenging than a mechanically ventilated building. There were essentially no days without wind to evaluate a purely buoyancy driven ventilation scenario, but there were days with little wind and resulting lower air exchange rates to provide some insight into how the building would operate in terms of ventilation and carbon dioxide rates.

The design characteristics used in this building, while beneficial to the operation of the building, are not currently being used to their fullest extent. However, the in-depth assessment of this building provides important insight into the operation of a commercial office building that employs natural ventilation as a means to ventilate and cool the building. The data collected provided valuable information to use in evaluating the methodology of reduced-scale modeling as an approach to understand and simulate the internal conditions of a naturally ventilated building. The data will be non-dimensionalized, and then compared to the output from the experimental work to check for similarity in temperature distribution and airflow patterns. Through an appreciation of the complexities in assessing naturally ventilated buildings, the model methodology can be refined.

Chapter 4.0

Modeling and Visualization Techniques

Analysis of full-scale buildings can prove difficult for several reasons, including the vast amount of space to analyze, amount of instrumentation required to adequately monitor all important aspects, time requirement and cost. In the design stage, it is normally impractical to build a full-scale version of a building to test configurations to ensure adequate airflow and thermal comfort. For this reason, modeling techniques are employed for the prediction of performance in buildings. Several methods exist, including computer simulations, partial full-scale modeling, and reduced-scale modeling. Visualization techniques are incorporated into all of these methods in order to evaluate the flow patterns for various configurations and ventilation schemes within a single room or for an entire building.

This chapter covers both modeling techniques and visualization methods currently used for the above mentioned physical models. The focus will be primarily on the application of these methods on the analysis of airflow patterns with respect to buildings. Both airflow patterns within the building and exterior flow patterns around the building will be addressed, with a focus on internal airflow analyses. Techniques presented are currently used to evaluate both mechanical and natural ventilation schemes. However there is particular attention paid to those methods being used to evaluate airflow and temperature distributions in buildings and rooms using natural ventilation.

4.1 Overview of Modeling as a Method

Often it is not convenient to evaluate full-scale buildings in either the design or the occupancy phase of a building, so reduced-scale versions of the building are created to simulate the full-scale version. The goal of the reduced-scale modeling is to gather data at a more manageable, smaller size, then scale the data back to full-scale and apply it for use in the full-scale systems, using some sort of scale factor. Scale modeling has been used for a wide variety of systems, both to investigate flow around objects and within spaces and buildings. Details on the requirements for similarity between the full-scale prototype and reduced-scale counterpart are provided in Chapter 5.

Three types of models are currently used: mathematical models that provide an analytical solution, computational models that provide a numerical solution, and physical models used for experimental solutions. Analytical solutions are mathematical analyses that describe the phenomena under investigation through a series of equations. These mathematical models can provide a basis for the primary governing phenomena of a system. An analytical solution is assumed to have a closed-form solution, in that at least one solution can be expressed as a mathematical expression in terms of a finite number of well-known equations. If no closed-form solution exists, the equations must be solved numerically. The governing, analytical flow equations for buoyancy, wind, and combined flow were presented in Chapter 2. They are

applicable to simple configurations and geometries with well-mixed assumptions and a limited number of zones, such as a single room attached to an atrium.

The numerical solution is a more complex version of the mathematical model described above, in that it is a system of algebraic relationships that are solved simultaneously. The computational model provides point-like solutions, with unique values for a series of determined points. A common numerical solution in the area of ventilation is the use of computational fluid dynamics (CFD) software, such as PHOENICS, to quantitatively predict fluid flow in or around objects. CFD software packages have the ability to model the interactions of temperature, heat flow, buoyancy and air flow in and around buildings. A grid is used to solve the mechanical and thermodynamic relationships throughout the environment under analysis, taking into account the layout, ventilation opening(s), geometry and heat loads.

Experimental solutions are obtained through the use of physical models to examine the behavior and interaction of physical systems in a controlled environment. They are also used in determining the relationship among variables, as physical modeling allows for the adjusting and measuring of specific parameters of interest. Physical models are created at a variety of scales and normally using one of several working fluids for investigation. Scale modeling has been used extensively in the field of ventilation, at both small scales and large scales, on specific system components, such as flows in fume hoods and whole systems, such as buildings and surrounding sites. The size of these models varies from full scale to $1/200^{th}$ scale or smaller, particularly for wind tunnel investigations. In this work the focus will be on reduced scale models used for understanding the internal flow within spaces in buildings, rather than the flow around them. In this case, the scales range from full scale single rooms to $1/120^{th}$ scale models, though it is difficult to use models smaller than $1/50^{th}$ scale as there is not necessarily adequate space within which to make measurements (Szucs 1980).

The selection of the scale at which the model is created depends on several fators, including the working fluid used. The following sections present the methods used at full-scale and reduced-scale, focusing on the most common working fluids used and associated flow visualization techniques. Each of these areas has a significant contribution to the overall effectiveness of scale modeling as a method to assess the prototype counterparts. The application presented is on reduced-scale models that are used to investigate airflow patterns and behavior in internal, occupied spaces within buildings, specifically those that use natural ventilation.

4.1.1 Full-Scale Modeling

Full-scale models are created for specific, single room applications to predict and analyze the thermal environment of that space in the design phase. When designing a passively ventilated space, a mock-up of a portion of the space, at full-scale, can be useful to evaluate that space with the appropriate internal loads, including computers, people, and lighting. This method is time consuming and requires a lot of space, but may be useful for isolated spaces. However, this method only works if the space being analyzed is in isolation and does not interact with adjacent spaces or zones.

Existing buildings are often assessed in a post-occupancy evaluation of the design of a space and building at full-scale. Though this does not help in the design phase, it does provide information

for future design of similar type buildings. Full-scale modeling or evaluation of existing buildings is still time consuming and it can be expensive to purchase and install equipment to collect the relevant data required for analysis of the indoor environment. A description of the methodology used for the prototype building used to validate the method was provided in Chapter 3. Particularly with naturally or passively ventilated buildings, experimental analysis of these buildings and spaces is difficult not only in the preliminary design phase as described above, but also in the post-occupancy phase.

Additional considerations must be taken into account when using CFD software to analyze a single zone or full-building. It is important that specific details be included in order to accurately portray and model the space. An understanding of the boundary conditions is necessary to model the space under consideration correctly, which can be difficult if the design is in the schematic or preliminary phase. Additionally, the size of the grid will affect the amount of time and ability of the computer to run the simulation. Spaces that are open to adjacent zones must have a description of the interface between the two spaces, which can be difficult to define. Caution must be used when using CFD alone to predict the thermal environment of a whole building or individual space, as boundary conditions and turbulence models used can affect the results. The 2-equation κ-ε Re-normalization Group (RNG) turbulence models are often used due to their ability to provide a better prediction of separation and vortexes (Spalding 2002).

4.1.2 Reduced-Scale Modeling

Physical models at full-scale are not the only methods used in evaluating natural ventilation in buildings. Models at scales smaller than one-to-one are used extensively in the field of ventilation to predict air movement and temperature distribution. Reduced-scale modeling methods have been used to investigate a wide range of flows, such as internal and external flows, and flows through openings, both with and without heat sources. This method has benefits, such as the reduced need for space, however attention must be paid to maintain similarity between the reduced-scale model and the full-scale prototype.

Both physical modeling and CFD modeling have been used in the evaluation of airflow phenomena in and around buildings. The scales used in reduced-scale modeling can vary widely, from near full-scale to $1/250^{th}$ scale. With reduced-scale modeling, the scale of the model is often limited by one of two things: the amount of space and size of equipment available to conduct experiments, and the objective with respect to analysis of flow patterns. The smallest scaled models are normally used in wind tunnel experiments to evaluate the pressure differentials across the façades of a building. The surrounding environment is often modeled, to determine the impact of neighboring building heights on the effectiveness of airflow to the building in question. Due to the size of these models, it is difficult to ascertain the interior airflow patterns and velocities.

Models that range in size from virtually full-scale to $1/120^{th}$ scale are used to investigate the interior flows within a building. Not only the scale of the model, but also the fluids used impact the flow patterns obtained with these modeling techniques. The materials used in constructing the models to investigate airflow are important in making the flow patterns visible. One of the difficulties with smaller scale models is that a slight deviation from the prototype can cause significant changes in the resulting airflow data (Smith 1951). This effect is true both for

external and internal airflow patterns in wind tunnel and test chamber environments. In addition, the limits of achievable Reynolds numbers for models of small scale are of concern.

4.1.3 Experiment Fluids

In building ventilation modeling, several different fluids have been used in scale models to replicate fluid flow phenomena. Most work has been completed using water, salt water, or air as the working fluid. Each fluid has its own particular characteristics, which can influence the scale of the model used and the resulting flow patterns.

With water as the modeling fluid, smaller scale models are sufficient, often on the scale of $1/20^{th}$ to $1/120^{th}$. Water modeling techniques have been used extensively in experiments to understand fluid flow in naturally ventilated spaces. Water models are nearly always constructed of clear Plexiglas, which allows the flow patterns to be easily seen and captured on film. Two types of water models are used at present for evaluating buoyancy driven flow; heated water models and salt-water models. The heated water models require a heat source to drive the buoyancy flow, with the small-scale mock-up immersed in a large 'ambient' tank. The model is placed right side up in the tank, allowed to reach steady state, then measurements are taken. There is little to no heat loss through the walls of the model constructed of Plexiglas and with the relatively small (<10°C) temperature difference between the ambient and the internal space.

Salt-water modeling on the other hand uses saturated salt water on the small-scale model. These models are used at both steady state and under transient conditions, though the focus here is on their application at the former (Linden 1999). The scale of these models is similar to the heated water model experiments and with Plexiglas in their construction. The salt-water models rely on the density difference between the salt-water solution and the fresh water. Normally this technique is used in buoyancy-driven flow, with the salt water injected to create the buoyancy-driven flow. In this case, the density measurements are taken once the model has reached steady state at points of interest throughout the model. These measurements can then be used along with the ambient and source density measurements to evaluate the flow in the space.

Air modeling is the most common technique to visualize the flow in and around buildings. Small-scale wind tunnel experiments are carried out at $1/50^{th}$ to $1/250^{th}$ scales, often modeling much of the surrounding terrain to obtain the most accurate results. Wind tunnel experiments near the larger end of the scale have been able to measure and/or visualize flow within the building under investigation, while those models at the smaller end of the scale are often utilized for pressure distribution and airflow only on the exterior of the model. Air as the working fluid is also used at full-scale, replicating a specific room to gather detailed information on flow patterns and temperature distributions.

4.1.4 Buoyancy-Driven Natural Ventilation Modeling

Buoyancy-driven natural ventilation is more complex than mechanical ventilation due to the number of parameters that are dependent and interdependent on the driving forces in this type of ventilation. Andersen (1995, 1996, 2003) has developed analytical solutions for evaluating buoyancy-driven flow in buildings for various configurations, including a single space with

lower and upper openings and natural ventilation in atria. These provide the solutions to pure buoyancy-driven flow in simple building spaces with simplifying assumptions.

Full-scale modeling of buildings to analyze buoyancy-driven natural ventilation is preferable to mathematical models, reduced-scale models, and numerical models. CFD appears to be the preferred method of verifying experimental results when air is used as the fluid. Jiang and Chen (2002) compared the results from experiments using a single full-scale room with a single opening and then used CFD to determine the type of turbulent model that provided the most accurate results. Using the large eddy simulation (LES) models, they achieved better agreement with the full-scale experiments than with the Reynolds Averaged Navier Stokes models; however, they had limited success in then comparing the results to an empirical model. Other buoyancy flow experiments have compared full-scale flow of a multiple story stairwell (Peppes et al. 2002) to CFD models, using tracer gas to determine the airflow rate, and then comparing the results to a numerical model. Adequate agreement was achieved with the CFD models, as there was some difficulty in modeling infiltration, but good agreement was achieved between experimental results and analytical models.

However, with the water and salt-water modeling techniques for buoyancy-driven flow, the results from the experimental work have been compared to mathematical models or CFD models and not necessarily to full-scale prototype buildings or spaces. The type of heat sources used to drive the buoyancy flow varies for the models. Heated water models can use point source heaters (Lin and Linden 2002) or distributed heat sources (Gladstone and Woods 2001) depending on the goal of the modeling. With models that use heat sources, energy balances are calculated and the resulting temperature distributions are recorded.

Buoyancy-driven ventilation has been modeled using all of the above modeling methodologies, at a variety of scales. One variation is the source used to drive the buoyancy force, which varies depending on the fluid and goal of the investigation. The water and salt-water models use mathematical models based on simplified assumptions of temperature distribution to validate their results, while air models are more likely to use numerical models in verifying the results obtained. For buoyancy-driven ventilation, simple single room applications have been modeled and studied in depth. There has been only limited consideration for more complex spaces.

4.1.5 Wind-Driven Natural Ventilation Modeling

There are many examples of models constructed in order to evaluate wind driven ventilation. Since this type of natural ventilation is often seen in practice, there is reason for the wide range of investigations. While buoyancy-driven flow is intriguing, it is uncommon that pure buoyancy-driven flow exists in full-scale commercial office buildings. There are some examples of buildings using stacks to drive buoyancy ventilation, as in some of architect Alan Short's designed buildings; however, more common is combined wind-buoyancy driven flow. The wind-driven modeling occurs at three main areas; full-scale buildings, small scale (less than 1:1 but greater than 1:25) to investigate interior flows, and small scale (less than 1:25) to investigate pressure across façades and flow around buildings.

Full-scale models for the study of wind-driven ventilation are uncommon, but Sawachi (2002) investigated the flow of air through openings in a wind tunnel of a full-scale single room space.

It is more common to compare similar reduced-scale models with full-scale prototypes, as Chandra et al. (1983) did in investigating the natural wind on a $1/25^{th}$ scale clear plastic model with the full-scale prototype building next to it. Also common are wind tunnel investigations of airflow due to wind-driven ventilation.

Wind tunnel experiments examine the pressure fields on the façades and the internal flows. Ernest et al (1991) compared both internal and external measurements of a reduced-scale model in a wind tunnel to determine indoor air motion as a function of wind direction. Depending on the scale and the model construction materials, the determination of flow patterns can be done through flow visualization or measurements. When comparing the scaled wind models to the prototype, one common issue is the variation of the wind speed and direction that is experienced by the prototype building versus the normally constant wind speed controlled in the test chamber or wind tunnel. Depending on the frequency of the data measurements, some wind tunnels are outfitted with a turntable, so that the direction of approach of the wind speed can be varied, as done by Dutt et al (1992).

4.1.6 Combined Buoyancy-Wind Modeling

Closer to the actual building case, is the more complex combined wind and buoyancy driven flow. The wind direction in this case has a significant impact on the flow direction through the openings. The wind force can either work with or against the buoyancy force. Li and Delsante (2001) presented the analytical solutions to this complex natural ventilation case, and determined the stable solutions based on the strength of the heat source and wind. Salt-water models (Hunt and Linden 1996, 1997, 2001) have been used extensively to evaluate combined ventilation to provide quantitative results, including flow velocities and densities. Their model is for a simple single space configuration with multiple upper and lower openings. Additionally, some work has been completed using CFD simulations to evaluate the combined buoyancy and wind forces in a naturally ventilated building as a method for validating heated water models (Heiselberg et al. 2004). They furthered the analysis by investigating the effect of wind direction in enhancing or hampering the effectiveness of the flow through a simple space.

Combined buoyancy-wind driven natural ventilation is complex, with some concern over how best to model and analyze this complex case. As described in Chapter 2, it is often not as simple as adding the equations of each type of ventilation. Nevertheless, combined buoyancy-wind ventilation occurs most often in real world applications, and therefore is an important scenario to carefully model and understand for application to full-scale buildings.

4.2 Flow Visualization

Measuring airflow at inlet and outlet openings and temperature distribution is not enough to comprehend fully the airflow patterns within the space or interactions between spaces within a building. Flow visualization has historically been used to understand complex fluid flow patterns. In buildings, it plays an important role. In naturally ventilated buildings, this is particularly true in understanding how air will enter, flow through, and exit a space, floor, and building. These different scales of airflow require different characteristics in the media used to visualize the flow patterns. The application and scale of the space being evaluated and fluid used in scale modeling have a significant impact on the visualization technique used. Issues such as

the acceptable diffusion rate, or 'hang-time', are of importance and are influenced by both the amount of air movement in the space and the volume of the space. The fluid of the space being analyzed also will affect the selection of media used for flow visualization. This chapter will discuss current practices for applications used in analyzing buildings, and then describe the selection of media used in both the prototype building analysis and the reduced-scale air model.

4.2.1 Principles of Flow Visualization

There are three main aspects of flow visualization, application and scale, media selection and particle seeding, and visualization and imaging. Qualitative flow visualization experiments combined with quantitative measurements provide a more comprehensive analysis into the flow phenomena being investigated. The principles in selecting an appropriate flow visualization technique will be discussed, with an overview of the issues that can arise with using these methods, each of which was evaluated when the final flow visualization method was selected for application in the building and reduced-scale model.

Flow visualization is comprised of several important components necessary to not only visualize the flow, but also capture it for further analysis. This includes marking the fluid flow, illuminating the flow field, and imaging of the flow pattern. Marking the fluid occurs in a variety of ways, most commonly through the use of dyes in water models and smoke with air models. Important aspects arise when applying these techniques to either water or air models, such as diffusion of the marking material and neutral buoyancy. If either of these issues is not addressed, the results of the flow visualization can be inconclusive.

When a foreign substance is used, visualizing the movement of the substance rather than the fluid itself, it is considered an indirect method of flow visualization. It is assumed that if the tracer material is neutrally buoyant and its particle size small enough then it is accurately representing the fluid flow being studied. This method is applicable to the building fluid flow application under investigation, both at various scales and using different fluids. However, this method is only applicable to steady flows, because with unsteady flows the size of the particles becomes more of an influencing factor (Merzkirch 1987). Under steady flows, the particles are selected for visibility and weight neutrality for a particular condition; however with unsteady flows, the particles must be sized for the slowest velocities, while taking into account rate of diffusion to ensure visibility. The tracer material used will also vary depending on the fluid used in the modeling. In water, dyes are often used, providing high impact visualization of fluid flow patterns, while keeping the tracer material neutrally buoyant. This is assisted by the construction of the reduced-scale water models with Plexiglas.

The size of the individual particles in the media selected for use in airflow visualization is critical to its effectiveness in accurately portraying the flow under analysis. The media introduced is used to analyze the flow velocity based on the movement of the foreign particles in the flow media. In order to track the flow under investigation accurately, the particles must be sufficiently small so that the flow is not disrupted and the movement of the particles imitates the motion of the flow. The media can be introduced either at a single point or at multiple points simultaneously.

For airflow visualization, the particles must be highly reflective so that they are able to be captured on film for analysis. In general, for smoke and fog generating machines, the particle size is approximately 0.5μm (Smits and Lim 2000). The working fluid used to introduce the material for flow visualization should also be neutrally buoyant. For air, this requires that the material introduced be at the same temperature as the inlet air for the model. First order approximation of buoyancy effects due to particle size becomes negligible when the diameter is less than 1μm, and visibility of particles is possible when the particles are larger than 0.15μm (Merzkirch 1987). A system comprised of several outlets is often used in wind tunnels, providing a series of equally spaced lines of smoke, parallel to the main air stream.

In water bath models, flow visualization and imaging is more easily carried out than with air models. The use of clear Plexiglas for constructing the model allows light to penetrate through the model, easily projecting the flow visualization onto a screen behind the model. Often projectors are used as the light source, illuminating the entire water model setup and using a digital video camera to record flow patterns. Using water as the modeling fluid also enables a much wider range of tracer materials to be used for visualization of flow patterns. Typically colored dye, mixed with water at the same temperature as the ambient fluid is used. Multiple colors of dye can be used to help visualize more complex fluid flow patterns and the interaction between flows. However, with water models there are potentially problems with matching key dimensionless parameters, which will be discussed in Chapter 5.

Capturing the flow patterns created with the air modeling methods requires appropriate lighting and imaging equipment. Proper lighting can affect the visibility of the flow patterns and the ability to record them on film. Two main light sources are used for flow visualization: a) conventional light sources, such as spotlights, halogen lamps, mercury lamps, and b) lasers. Mirrors and lenses can be used with either type of light source in order to brighten, expand, and locate the desired shape of light. Using a combination of a mirror and cylindrical lens, a circular beam of light from a laser can be transformed into a light sheet to visualize the structure of flows. This is one of the more common techniques used in flow visualization when air is used as the fluid. Light sheets are created by aiming a beam from the light source at a cylindrical lens, which then, due to its geometry, creates a linear beam of light or a light sheet. The smaller the diameter of the cylinder, the larger the beam spread.

However, capturing these airflow patterns on film can prove to be a difficult task. Camera and light source position can affect which cross-section is observed and the image quality. The availability of higher speed 35mm and digital cameras has improved the ability to capture flow visualization images. Often the exposure or shutter time, resolution, aperture size can affect the quality of the resulting image. High-speed cameras are of some concern with reduced-scale modeling using air as the fluid, as they require increased illumination, which often leads to additional heat dissipation.

4.2.2 Application to Buildings

Effective ventilation is important to thermal and occupant comfort when evaluating and designing spaces for use. Indoor air quality is also influenced by airflow. It is difficult to predict these flow patterns without the use of visualization techniques. A variety of methods have been developed for a wide range of application types (Merzkirch 1987), but here the focus is on

applications involving full-scale buildings, scaled models using water or air, and wind tunnels. These are the three areas that are currently used to evaluate building design, and each has its own unique requirements for flow visualization. There are three methods of flow visualization defined by Merzkirch: one which introduces foreign material into a flow (indirect method), one which records the varying density (optical method), and one which introduces energy into a flow. The latter two normally apply to compressible fluids, and are therefore not presented here. The former is applied to incompressible fluids, including air, and does not release further energy into the flow, which may influence the initial flow.

Flow visualization is commonly used to evaluate mechanical systems to ensure that air is being introduced and exhausted properly, and that the occupants have a healthy and comfortable environment in which to work. Several studies, including one sponsored by the USDOE Building Technologies Program (McWilliams 2002) cover the types of airflow measurement techniques used in evaluating indoor environments. Fogging machines and smoke pencils have been used extensively in evaluating such systems as displacement ventilation and under-floor systems. The airflow rate is controlled, with high enough velocities so that media can be introduced and flow patterns traced and captured on film.

When air is the fluid used in the experimental procedure at both small and full scale, issues of visualization and neutral buoyancy are important, in addition to the dissipation rate, or 'hang time', of the tracer material. This is of note particularly in full-scale buildings when large volumes of air and turbulent mixing quickly dilute the tracer material and make visualization of airflow patterns on a large scale difficult. Localized flow patterns in full-scale buildings can make use of methods such as smoke pencils; if the local air velocities are relatively slow (less than 0.5 m/s).

In evaluating fluid flow patterns in air models, in full-scale spaces and reduced-scale models, the ability of a tracer material to visibly follow the airflow, without effecting or changing it, is important. This requires the tracer material to be neutrally buoyant, be visible, and not disperse too quickly. For air models, these requirements leave only a few alternatives that were evaluated for use in both the full-scale prototype building and the reduced-scale air model. They included Draeger smoke pencils, fog generating machine, and helium bubbles. In developing the methodology for evaluating and designing naturally ventilated buildings, the ability not only to analyze the temperature profile throughout the occupied space, but also to visualize the flow patterns within the space provides a stronger impetus for using the methodology. With the capability to map the path of outside air as it is introduced, move through the space being ventilated, and finally be exhausted, the methodology combined with flow visualization techniques can further the understanding and improve the ventilation effectiveness, thereby improving the design of naturally ventilated buildings.

4.2.3 Methods Used

For use in the MIT test chamber with the reduced-scale air model, a marker was needed that would be neutrally buoyant, non-toxic, and highly visible. Neutrally buoyant helium bubbles were initially used for both a full-scale and reduced-scale room test case. This method involved a single-head Sage Action Helium Bubble Generator, which connected a tank of helium gas to a reservoir of bubble fluid and an air compressor. Through trial and error, neutrally buoyant

helium-air bubbles were created using this generator. This media proved useful in its long hang time; the bubbles disappeared when they burst when colliding with a surface. However, the generation rate of the small (2-3 mm diameter) bubbles was approximately 5-10 per second. For a large volume room, this rate was insufficient to track airflow patterns accurately within the space. In the reduced-scale models, the small volume of space did not allow the bubbles to travel a great distance before bursting on impact with a surface, particularly with the buoyancy-driven flow.

Draeger smoke pencils were used for much of the localized airflow within the prototype building, but these were found to dissipate too quickly within the model. They were able to show localized airflow patterns within the occupied space, as the measured air velocities were well below 0.5 m/s. Since they were being used for localized flow, the flow visualization experiments could be carried out during occupied hours, when heat loads due to the occupants, lights, and office equipment were present. This provided realistic airflow patterns for an occupied commercial office building. By determining localized airflow patterns at various height and locations throughout the prototype building, an understanding of the overall airflow patterns was obtained. Though useful for localized flow patterns within the prototype building, the smoke pencils dissipated more quickly in the reduced-scale air model. The velocities that were recorded for the scale model were 0.2-0.8 m/s, causing a much faster dissipation of the smoke pencils. In the prototype building, the smoke dissipated quickly at the windows, but was visible enough to show the flow direction. In the occupied space of the prototype building the measured air velocities ranged from still to 0.5 m/s within 1 meter of an open window. Therefore, another approach was created, to try to produce a relatively steady stream of 'smoke', at multiple inlet locations. This was done using a fogger machine that initially uses heat to produce fog, which was then attached to a series of tubes to decrease the inlet velocity and cool down the fog media.

The fogging machine has its own benefits and drawbacks. One of the problems with fogging machines is the difficulty in controlling the amount of media that is being generated by the fogger. Too much smoke can obscure airflow patterns, thereby making them indistinguishable. The fog machine produces a visible fog by heating up a glycerin-based solution, which exits the fog machine at 45°C. An apparatus was created in order to cool down the fog that was produced to the inlet air temperature of the model and then introduce the fog in through the window openings. A series of small nozzles was attached to a long tube that extended the length of the façade of the model. The nozzles were spaced so that each one supplied fog to each window. This apparatus worked for the single and two-zone cases, but was removed for the full-model experiments, as it did not allow adequate amounts of fog into the model. The use of a remote control device to provide small spurts of fog, rather than one constant stream also helped in controlling the amount of fog being introduced. Care was taken to ensure that the intermittent fog being introduced into the model was not introduced with significant velocity, which would disrupt or alter the airflow patterns.

Three independently controlled 9-watt compact fluorescent lamps were used in the reduced-scale air model to provide some amount of illumination used to capture the airflow patterns. These lamps were chosen for their lumen output and their low heat output. It was important to limit the amount of additional heat added to the model, as additional heat sources would influence the flow patterns within the model. The compact fluorescent lamps combined with a Canon S40

digital camera with both manually operated shutter speed and aperture size and video capture, provided adequate imaging of the airflow visualization. A Sony® digital video camera captured movies of the airflow movement through the model. The setup used with the fogging machine, with the box required to cool-down the fog, and the flexible tubing to introduce the fog into the model is shown in Figure 26. The specific details used for capturing the flow patterns are outlined in Table 18. The automatic flash was turned off for all cases.

Table 18. Flow Visualization Imaging Settings

Airflow	*Lighting*	*Camera Setting*	*Shutter Speed*	*Camera Type*
Simplified model	Fluorescent	Manual	2 second	Digital
Buoyancy Driven	Fluorescent	Manual	2 second	Digital
Buoyancy Driven	Laser	Manual	4 second	Digital
Wind-driven	Fluorescent tube (T-5)	Back lighting	---	Digital/Video

A laser sheet was also created as an alternative flow visualization technique, using a 630-680nm wavelength laser diode with attached cylindrical lens, creating a light sheet. The laser could be kept outside of the model, and due to its size did not produce much heat. The laser light sheet proved to be difficult to capture on film due to the red color of the laser and the lower intensity of the light produced, but did provide some amount of 2-dimensional flow visualization within the sheet. The view window created as part of the construction of the reduced-scale model was used for much of the imaging of the flow patterns. The laser was useful for a single zone test box, but was did not penetrate deep enough into the model for flow visualization of the reduced-scale model.

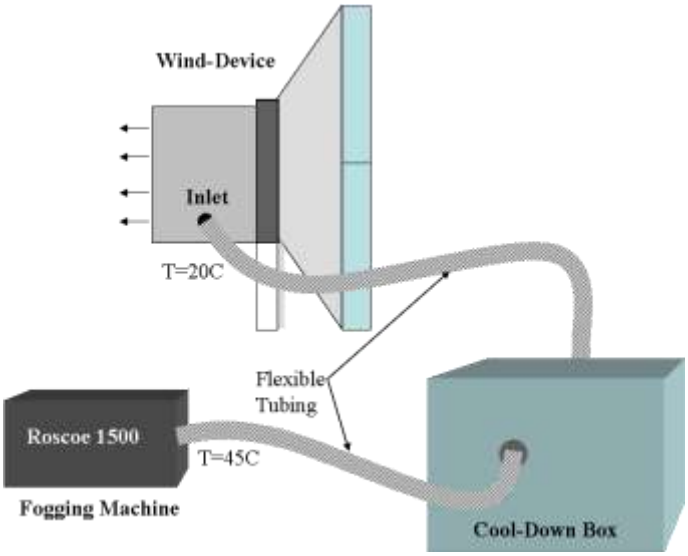

Figure 26. Fogging Machine and Set-up For Airflow Visualization

4.3 Summary

Many modeling and flow visualization methods are currently in use. The methods presented have been used to evaluate various cases of natural ventilation and to better understand the

phenomena of airflow patterns and in some cases temperature and pressure distributions. Depending on the case of natural ventilation being modeled, there are influencing factors such as the fluid used, scale and model type that affect the decision as to the method to use. Each of these factors can influence the resulting data, as will be discussed in the next chapter, Dimensional Analysis and Similitude. The modeling methodology developed for this research investigates each of the natural ventilation cases, using air as the fluid and comparing the experimental results to numerical models.

The use of flow visualization in both the prototype and reduced-scale model proved useful in verifying flow patterns predicted by theory and computational fluid dynamic modeling. Though several techniques were tried before determining that smoke pencils and fogging machines were the most useful, the influence of relatively small heat sources on the airflow was observed. This observation affected the selection of media used in tracing the flow patterns as well as the visualization technique employed. Investigating airflow patterns in both the prototype building and reduced-scale model was difficult due to the hang time of the media used. Capturing the flow patterns also proved to be a complex task, with hand sketches for various locations within the prototype recorded and photo imaging along with hand sketches used in the reduced-scale air model. These methods suited the scale of each application, and provided necessary data for comparison to computer-simulated models.

Chapter 5.0

Dimensional Analysis and Similitude

Certain scaling issues need to be resolved before any conclusions can be drawn from the comparison of reduced-scale modeling of any kind and the full-scale application. When evaluating models at scales smaller than the prototype, the goal is to replicate the behavior of full-scale prototype. This comparison is done by measuring the relevant parameters in the reduced-scale model and by obtaining the values for the prototype using a known scale factor. Both dimensional analysis and similitude must be established for this comparison, as one cannot define the other alone. Two systems are said to be similar if their features can be mapped point-by-point, from one region to another region. These regions do not have to be of the same size, and often one is many times smaller. By making the equations that describe the flow dimensionless, the outcome will result in key dimensionless parameters that provide solutions that are similar, if the resulting dimensionless parameters are equal. Dimensionless relationships are validated through the analysis of equations, while similitude describes the similarity of behavior or phenomena. There are some limitations to this approach in meeting all similarity requirements, as an exact match is virtually impossible at anything other than the same scale as the prototype, which will be addressed later in this chapter.

Experiments are carried out with models for a variety of reasons. Model studies can provide data while avoiding costly mistakes and can be used to obtain information that will assist in the design of the prototype. Models are relatively inexpensive to build and to modify both in layout and in construction as compared to full-scale versions. But it is important to first understand the theory of the phenomenon being studied before attempting to build and evaluate a model for a given problem statement. It is not useful, and in fact wasteful, to resort to a model study if the results can be accurately predicted by theory. Often models are used to assess spaces that are difficult to evaluate, such as spaces in which there is not enough control in the prototype or in cases where it is too expensive to outfit the space with the required instrumentation (Szirtes 1998). Once the relevant dimensionless products are found from an analysis of the governing equations used in describing the phenomena, then a series of experiments can then be performed to find the functional relationship between the dimensionless parameters. This relationship can then be used over a much wider range of conditions than those employed for the experiments. It is crucial that the relevant dimensionless parameters are identified, in addition to the range in which they can be used if an exact match is not possible. There are many variables involved and some means must be used to eliminate those of lesser importance.

5.1 Governing Equations

For both the full scale and the reduced scale physical models and the CFD simulation, there are equations that can be used to describe the flow of the fluid as well as the heat transfer. These equations are the conservation of mass, or continuity equation, the conservation of momentum, or Navier-Stokes equation, and the conservation of energy. The models were evaluated for conditions at steady state.

The equations of mass, momentum, and energy must be non-dimensionalized in order to evaluate them for reduced-scale models (Rolloos 1977). The conservation of mass equation is given by:

$$\frac{\partial u_i}{\partial x_i} = 0 \tag{5.1}$$

where u is the velocity component in the direction x.
The Navier Stokes equations describe flow in an enclosure, and are applicable to ventilation within a building. The Navier Stokes equations represent the sum of the inertia, viscous, pressure and buoyancy forces acting on the fluid. The Navier-Stokes equation for steady, incompressible and turbulent flow is given by (ibid):

$$\frac{\partial u_i}{\partial x_k}\left(\rho U_k\right) = -\frac{\partial p}{\partial x_i} + \mu \frac{\partial}{\partial x_k}\left(\frac{\partial u_i}{\partial u_k}\right) - \rho g \beta \Delta T \tag{5.2}$$

Where ρ is the density at some reference temperature, ΔT is the difference from a given reference temperature, and μ is the dynamic viscosity. The Navier Stokes equation must also be made dimensionless, normalizing the variables with respect to characteristic values of length, velocity and temperature.
Finally the energy equation is given by (ibid):

$$\rho c_p u_k \frac{\partial \theta}{\partial x_k} = \lambda \frac{\partial}{\partial x_k}\left(\frac{\partial T}{\partial x_k}\right) \tag{5.3}$$

Where c_p is the specific heat and λ the thermal conductivity.

5.1.1 Dimensionless Equations and Resulting Parameters

Knowing the governing equations and which dimensionless numbers are relevant when describing them in their non-dimensionalized form, the analysis can be performed to determine which of the dimensionless numbers are most important to retain when analyzing the scaled model for the buoyancy driven case.

Since the temperature and velocity distribution within the model must adequately represent those in the prototype building, these and related values must be normalized with respect to a characteristic value. The above three governing equations are non-dimesionalized by using $x^*=x/H$, $u^*=u/u_o$, $P^*=P/\rho u_o^2$, and $\theta^*= (T-T_\infty)/\Delta T_{ref}$. The subscript o represents a characteristic value. The governing equations then become:

$$\frac{\partial u^*}{\partial x^*} = 0 \tag{5.4}$$

$$\frac{\partial u^*}{\partial x^*}\left(u^*\right) = -\frac{\partial p^*}{\partial x^*} + \frac{\mu}{\rho_o u_o H}\frac{\partial}{\partial x^*}\left(\frac{\partial u^*}{\partial u^*}\right) - \frac{gH\beta\Delta T}{u_o^2}\theta^* \tag{5.5}$$

$$u^* \frac{\partial \theta^*}{\partial x^*} = \frac{\lambda}{\rho c_p u_o H}\frac{\partial}{\partial x^*}\left(\frac{\partial \theta^*}{\partial x^*}\right) \tag{5.6}$$

From equations 5.5 and 5.6, several dimensionless parameters are evident. These are the Reynolds number (Re), the Archimedes number (Ar), and the Prandtl number (Pr). These are:

$$\frac{\mu}{\rho u_o H} = \frac{1}{\mathrm{Re}} \tag{5.7}$$

$$\frac{gH\beta\Delta T}{u_o^2} = Ar \tag{5.8}$$

$$\frac{\lambda}{\rho c_p u_o H} = \frac{1}{\mathrm{Re}\,\mathrm{Pr}} \tag{5.9}$$

The reference temperature, ΔT_{ref}, used in non-dimensionalizing the temperature data is obtained through an energy balance on the reduce-scale air model. This was done by ensuring the conservation of energy around the model. The heat input was made to be equal to the heat loss through advection, neglecting heat loss through the envelope. The flowrate, Q, is equal to the mass flowrate, $\dot{m} = \rho UA$, times the specific heat and temperature difference between the interior and ambient:

$$Q = \rho A c_p U \Delta T \tag{5.10}$$

For the buoyancy case, a buoyant velocity is derived, using the Boussinesq approximation for ideal gas and a characteristic length of the height difference, H, between inlet and outlet: The buoyancy velocity, u_B, is substituted into the equation, resulting in:

$$Q = \rho A c_p \sqrt{g\beta H\Delta T}\,\Delta T \tag{5.11}$$

Then, solving for the reference temperature, ΔT_{ref}, this equation becomes:

$$\Delta T_{ref} = \left[\frac{Q/A}{\rho c_p \sqrt{g\beta H}} \right]^{2/3} \tag{5.12}$$

The reference temperature is calculated for each model case where the number of heaters is altered and for the full-scale prototype building.

5.2 Parameters for Buoyancy-Driven Ventilation

For the buoyancy-dominated natural ventilation case, the Reynolds number, the Prandtl number, and the Grashof number (Gr) become the key dimensionless parameters to consider. The buoyancy velocity needs to be derived, since the motion of the air is due only to temperature differences, rather than a forced airflow. The reference velocity is not an independent parameter, and resultant from other influencing factors. This derivation is achieved by beginning with a force balance on a unit volume of air with temperature T and density ρ, surrounded by a fluid at temperature T_∞ and density ρ_∞. Air is approximated as an ideal gas when evaluated at normal pressures and temperatures. The buoyancy velocity is calculated to be:

$$u_B = \sqrt{g\beta H\Delta T} \tag{5.13}$$

This buoyant velocity can then be substituted for the velocity term in the Reynolds number. When the Reynolds number is squared, using buoyant velocity term, it is equal to the Grashof number. For the buoyancy-driven ventilation, the Archimedes number, which relates buoyancy to inertial forces, is equal to one, when u_B is substituted in as the reference velocity.

$$\frac{\partial u^*}{\partial x^*}\left(u^*\right) = -\frac{\partial p^*}{\partial x^*} + \frac{1}{\mathrm{Re}_B}\frac{\partial}{\partial x^*}\left(\frac{\partial u^*}{\partial u^*}\right) - Gr\theta^* \tag{5.14}$$

$$u^* \frac{\partial \theta^*}{\partial x^*} = \frac{1}{\mathrm{Re}_B \,\mathrm{Pr}}\frac{\partial}{\partial x^*}\left(\frac{\partial \theta^*}{\partial x^*}\right) \tag{5.15}$$

In the reduced-scale model, the fluid used is air so the Prandtl number remains the same as for the prototype building. This leaves the Reynolds number and Grashof number to be calculated. Several papers have addressed the question of which of these parameters is more important to match in reduced-scale models (Awbi and Nemri, 1990, Rolloos, 1977, Awbi, 2003). They have concluded that if the Reynolds number for both the prototype and model falls within the turbulent region, i.e. Re>2.3x10^3, then the Grashof number is the key parameter to match. Hagstrom (2002) cites a critical Rayleigh (Ra=PrxGr) number of 2x10^7 when natural convection of a plume is modeled under (mechanical) ventilation conditions, resulting in turbulent convection flows.

5.3 Similarity Requirements

There are specific similarity conditions that are required for the results from the scaled model to be transferable to the full-scale prototype. To validate the model for application in buildings, there must be similarity in the velocity distribution, airflow patterns, and temperature distributions between the prototype building and the model. The three main criteria required for similarity between a reduced-scale model and prototype are geometric, kinematic or dynamic, and thermal similarity.

5.3.1 Geometric Similarity

Geometric similarity is one of the basic criteria used to obtain similarity between a prototype and scaled model. Geometric similarity is also the easiest of these criteria to meet by simply scaling down the linear dimensions of the full-scale building. This must be done at least in the depth (distance from the exterior wall to the atrium to the exterior wall) and height of the model, while providing some amount of width to prevent constriction of the airflow since natural ventilation in buildings is not a two-dimensional problem. This scaling must ensure that the linear dimensions of the prototype are reduced proportionately in the three dimensions, x, y, and z. The linear dimensions must use the same scaling factor in all three directions in order to meet this criterion. This pertains to all surfaces and openings within the model, including walls, floors, and windows. The depth of the space can affect the airflow patterns and ability of the air to mix within the occupied zone; this variable is important, as naturally ventilated buildings are often designed using a guideline for determining the maximum depth and ratio of depth to floor-to-ceiling height that will still allow for adequate penetration of outdoor air into the space. Lack of geometric similarity can influence the flow patterns and temperature distribution within the space under analysis. In natural ventilation, the ratio of the depth of the space to the height of the space often limits the effectiveness with which air can be introduced into the space. The ratio of height of the space, H, to the depth of the space, X, should remain equal for geometric similarity to exist. This is represented in equation 5.1, where the subscript M indicates the model values, and P the prototype.

$$\left(\frac{X}{H}\right)_M = \left(\frac{X}{H}\right)_P \tag{5.16}$$

5.3.2 Kinematic Similarity

For kinematic similarity, the ratios of the fluid velocities and accelerations must be equal. This will ensure that the streamlines and flow patterns will be similar. This requirement is tied closely to the dynamic similarity which necessitates that the ratio of all of the forces that cause motion in the operating fluid be equal between the model and prototype. From similarity theory, a scale model will replicate the kinematic boundary conditions of the prototype if the Prandtl, Reynolds, and Archimedes numbers are identical for both cases.

The Reynolds number, Re, is the dimensionless ratio between inertial and viscous forces, used in dynamic similarity for evaluating the magnitude of these forces.

$$\mathrm{Re} = \frac{\rho U L}{\mu} \tag{5.17}$$

With a low Reynolds number, flow rate has a strong dependence on the viscosity, whereas with a high Reynolds number the viscous forces can often be neglected. To meet similarity requirements:

$$\mathrm{Re}_M = \mathrm{Re}_P \tag{5.18}$$

$$\left(\frac{\rho U L}{\mu}\right)_M = \left(\frac{\rho U L}{\mu}\right)_P \tag{5.19}$$

When air is used and the density of air between the model and prototype does not vary substantially, equation 5.19 can be simplified to:

$$(UL)_M = (UL)_P \tag{5.20}$$

The Prandtl number describes the ratio of molecular momentum to thermal diffusivity. When evaluating kinematic similarity in the case of buildings, if air is used as the fluid for the model, the Prandlt number is then matched at 0.71. This assumes that the operating temperatures for the building and model fall between 0°C and 100°C. For a Prandtl number less than one, the thermal diffusivity or speed of heat propagation is larger than the momentum diffusivity. If a fluid other than air is used, the Prandtl number must be evaluated and compared to the prototype value.

$$\mathrm{Pr} = \frac{\mu c_P}{k} \tag{5.21}$$

Finally, the Archimedes number, or the measure of the relative magnitude of buoyancy forces to inertial forces acting on a fluid, is used to evaluate the motion of fluid due to density differences. For ventilation purposes, it provides the ratio of pressure difference associated with buoyancy driven flow to the pressure difference associated with wind driven flow. Recalling equation 2.7 for the pressure difference due to buoyancy, and equation 2.9 for the pressure difference due to wind, the ratio of buoyancy force to inertial, or wind force is:

$$\frac{\Delta P_B}{\Delta P_W} = \frac{\rho g \beta H \Delta T}{\rho U^2} = \frac{g \beta H \Delta T}{U^2} \tag{5.22}$$

For similar wind pressure differences, Δp_w can be simplified to U^2. The dimensionless ratio then becomes the Archimedes number, Ar:

$$Ar = \sqrt{\frac{g\beta L\Delta T}{U^2}} \tag{5.23}$$

When the flow is driven purely by buoyancy, the reference velocity in the denominator is the buoyancy velocity, making the Archimedes number equal to 1.

It is impossible to match all of the dimensionless parameters that are the result of making the governing equations dimensionless. Reducing the scale by a factor of ten will result in an increased velocity by a factor of 10 to keep the Reynolds number, and a temperature difference factor of 1,000 to retain the Archimedes number. However, literature states that this can be resolved if the flow is fully developed turbulent flow (Etheridge and Sandberg, 1996). Then the Archimedes number becomes the most relevant to match between the prototype and scale model.

When evaluating the dimensionless parameters, the characteristic length selected will have an impact on the Reynolds and Archimedes numbers and therefore influence how the flow regime is described within the model. Popiolek et al (1998) studied the effect of the Reynolds number on similarity for models at small (1:10), medium (1:5) and large (1:1.175) scales for a mechanically ventilated room. They found a critical threshold Reynolds number of 10,000 to 20,000. Similarity is improved when the Reynolds number exceeds 20,000, but doesn't substantially degrade until the Reynolds number is approximately 2,000. At that point, any discrepancies between the model and prototype become evident.

5.3.3 Thermal Similarity

The requirement of thermal similarity is met when the temperature differences and patterns are comparable. Thermal similarity is achieved with similar heat flows and distribution through the modeled space. The model and prototype temperatures are compared using the reference temperature difference calculated using equation 5.12. Using the non-dimensionalized temperature of the model and the appropriate reference temperature for the prototype, the corresponding prototype temperature difference for a specific location can be determined, and vice versa.

$$\left[\frac{(T - T_\infty)}{\Delta T_{ref}}\right]_M = \left[\frac{(T - T_\infty)}{\Delta T_{ref}}\right]_P \tag{5.24}$$

5.4 Other Issues for Similarity

The same similarity requirements discussed above also apply to the boundary conditions. The geometric boundary conditions are achieved if overall geometric similarity is satisfied. The inlet air velocity and flow pattern will be similar if the inlet opening and surface roughness are similar in the model and prototype, achieving kinematic similarity at the boundary. Thermal similarity is the most difficult of the three to achieve at the boundary conditions. At the boundary, the heat flux, distribution of surface temperatures and radiation all must be considered and evaluated between the model and prototype. If the Ar, Re, and Pr numbers are not matched, it is impossible to match the surface temperature distributions between the prototype and model.

Radiation was found to have an impact in the case with lower airflow rates through the model in the buoyancy-driven flows. This effect contributes to the difficulties in meeting similarity requirements at the model surfaces. When forced convection dominates in the wind-driven ventilation cases, the boundary condition similarity requirements are less critical due to the internal airflow motion, and radiation contributions are less significant.

5.5 Characteristic Values

The selection of a characteristic length for use in evaluating the dimensionless parameters is not straightforward. There is some question in ventilation, particularly natural ventilation, as to which characteristic length to use when evaluating the dimensionless parameters. When investigating buoyancy driven ventilation, the height difference between the inlet and outlet should be used as that difference in pressure, combined with the temperature difference between the interior and exterior that drives the flow through the building. However, when determining the flow regime to verify that the flow falls within the turbulent conditions, the height difference will not represent an appropriate characteristic length. Therefore, several characteristic lengths are used in evaluating the model for similitude with the prototype.

Etheridge (2002) defines the window diameter as the characteristic length for flow at the windows, and the height of the building for determining the Reynolds number for use in a wind tunnel. Using the window opening as the characteristic length is common in evaluating natural ventilation in buildings (Awbi 2003, Nielsen 1995, Yu 2002).

5.6 Application of Dimensional Analysis and Similitude

The goal of the reduced scale model was to predict accurately the temperature distribution and velocity patterns for the prototype building. The reduced-scale air model met the geometric similarity requirements by creating the model as twelfth-scale replica of the prototype building. The physical scaled model is one-twelfth of the size of the prototype building, in overall geometry and in effective opening sizes. The effective opening area was calculated through simulation and experiment, and the equivalent vertical opening determined as 30 percent of the full window size. The aspect ratio for the prototype building and reduced-scale air model was maintained as 3.6, further ensuring similarity.

The hydraulic room diameter was used in evaluating the Reynolds number for both the prototype and reduced-scale air model, while the height of the atrium was the characteristic length for the Grashof number. When comparing the reduced-scale air model and water model to the prototype building, the Peclet number and Rayleigh number must be evaluated, to account for differences in the Prandtl number between the working fluids. If evaluating buoyancy-driven flow, with the motion of the fluid only generated by temperature, then the Grashof number is a key parameter, as discussed previously. However, when fluids other than air are used, the Prandtl number is included in the evaluation, through the Rayleigh number, $Ra=GrPr$, for water bath modeling (Etheridge and Sandberg 1996).

Table 19. Summary of Values and Dimensionless Parameters for Full-Scale Building, Scaled Air and Scaled Water Models

	Air-Building	*Air-Model*	*Water Model*	*Water Model*
Scale	1	12	12	100
g (m/s^2)	9.8	9.8	9.8	9.8
β (1/°K)	0.0033	0.0034	0.0002	0.0002
ΔT (°K)	5	30	6	6
g'=gβΔT	0.1655	0.9800	0.0118	0.0118
H=height of Atrium (m)	15	1.2	1.2	0.75
α (m^2/s)	$2.16x10^{-5}$	$2.40 x10^{-5}$	$1.44 x10^{-7}$	$1.44x10^{-7}$
ν (m^2/s)	$1.477 x10^{-5}$	$1.60 x10^{-5}$	$1.01 x10^{-6}$	$1.01 x10^{-6}$
A_{CS} (m^2)	6.32	0.522	0.559	0.037
Pr	0.7	0.7	7.0	7.0
Re	$6.74x10^5$	$3.54 x10^4$	$1.10 x10^4$	$1.70 x10^4$
Pe=PrRe	$4.72 x10^5$	$2.47 x10^4$	$7.68 x10^4$	$1.19 x10^5$
Gr	$3.84 x10^{13}$	$7.94 x10^9$	$2.05 x10^8$	$3.65 x10^9$
Ra=PrGr	$2.69 x10^{13}$	$5.56 x10^9$	$1.43 x10^9$	$2.55 x10^{10}$

For the reduced scale air model, the primary characteristic length used in evaluating the occupied zones is the hydraulic diameter of the cross section of a single floor. This parameter accurately describes the main flow through the model and provides a characteristic length of 0.52m. However, the height of the atrium is used in evaluating the buoyancy velocity, since it is the height difference between the inlet and the outlet, at the top of the stack, which drives the air flow. The Reynolds number for the model was approximately $3.54x10^4$, using the hydraulic diameter of a single heated zone. This falls in the turbulent regime. The Grashof number for the scale model is on the order of $1.2x10^8$. When comparing both the Reynolds number and Grashof number to those calculated for the prototype building for buoyancy-driven flow, the prototype building is also in the turbulent regime ($Re=7.1x10^5$) and buoyancy dominated flow ($Gr=9.1x10^{10}$). Finally, for thermal similarity the temperature differences and heat flow must remain proportional. The internal heat load per square meter (W/m^2) is scaled using the same 12^{th} scale to provide the similar buoyancy effect. The temperatures recorded from the reduced-scale air model are non-dimensionalized using the ΔT_{ref} to obtain the resulting full-scale building temperatures for analysis.

From Table 19, the critical Reynolds number, $2.3x10^3$ is achieved for all models and the full-scale prototype building. The air model achieves a slightly closer value of Reynolds number than either of the water models, but is still off by a factor of 10. When the Prandtl number is accounted for using the Peclet number, Pe, the small-scale water model achieves a closer match to the full-scale prototype than either of the other models. It is assumed that each of the models, as well as the prototype building, is operating in a turbulent regime for the airflow in the heated zone. For the buoyancy-driven case, equality of Grashof number is required after meeting the critical Reynolds number condition. The twelfth-scale air model and 100^{th} scale water model more closely match the Grashof number, but none of the models matches it exactly. Some research (Etheridge and Sandberg 1996) that indicates that for buoyancy-driven flow it is sufficient to achieve critical values of Grashof number when using air as the working fluid. They propose a critical value of Grashof number in the range of 10^6 to 10^9 based on some experimental work, and using the height of a room as the characteristic length. When the room

height is used for the full-scale building and air model, the Grashof number is $4.5x10^{10}$ and $1.1x10^{8}$ respectively.

Larger models may reflect better the full-scale prototype building. However, space limitations limit the use of larger scale models. At the scales presented, both water and air models are able to achieve turbulent flow regimes within the heated zones, which is critical for the analysis of the flow and makes the models comparable to the full-scale prototype. There are limited sources in determining the critical values that must be reached for natural ventilation. Critical Reynolds numbers found in the literature often use the supply diffuser area, rather than the cross-section of the space for their characteristic length. This is appropriate for mechanically ventilated spaces, when the supply jets are of concern, however with natural ventilation; the airflow within the occupied space is of importance.

5.7 Summary

The governing equations were identified and made dimensionless to use them in comparing the full-scale prototype to the reduced-scale model through the resulting dimensionless parameters. The key dimensionless parameters identified in the non-dimensionalized governing equations were the Reynolds number, the Archimedes number, and the Prandtl number. For the buoyancy-driven case, the Grashof number was identified as the critical parameter to match between the prototype and model cases. There are no guidelines in the selection of the characteristic length, but based on the goals for analysis of the flow, characteristic lengths were selected for defining the Reynolds and the Grashof numbers.

Chapter 6.0

Reduced-Scale Model Methodology and Experiments

6.1 Introduction

The previous chapters laid the foundations for both the types of natural ventilation and the methodology behind the development of the reduced-scale air model described. This chapter will focus on the experiments performed using a reduced-scale air model. Experiments were conducted on a reduced-scale air model and those results used in the development of a numerical model. The buoyancy, wind, and combined ventilation experiments are explained along with the description of the physical and numerical modeling methods used. Both the physical model and the numerical model developments are presented, along with the experiments for all three natural ventilation cases.

6.2 Model Development

A reduced-scale air model methodology has been developed to evaluate natural ventilation in buildings using a reduced scale air model. The reduced-scale air model was modeled after the naturally ventilated prototype building described in Chapter 3. The geometry and layout of the prototype building were created at one-twelfth linear scale for use in the experiments. Given that the model was created to approximate the performance of a full-scale naturally ventilated building, several factors had to be compared to determine the validity of the newly developed approach. This included scaling not only the physical geometry of the building, but also the internal thermal loads. The models used in evaluating the method were:

- a one-twelfth scale physical model with air as the fluid
- a numerical model using the PHOENICS CFD software package.

Experiments were carried out on the reduced-scale model; those measured parameters and boundary conditions were then used in creating the CFD model. The physical model served as the base case, with the geometry, internal loads, temperature and air velocity data from the experimental work used as the input parameters and boundary conditions for the computational model. This approach allowed the differences between the modeling techniques to be identified, and the limitations of using CFD software in modeling natural ventilation in buildings understood. In the following sections, both the physical and computational models are described.

The reduced scale model that was based on the prototype building was created with the ability to adjust the number of heated zones, as well as inlet and outlet openings in the model. This flexibility allowed for a gradual increase in the complexity of the model, and the development of understanding of the issues as they arose that was particular to the reduced-scale air model. The scaled air model constructed in the development of this methodology to evaluate natural ventilation in buildings thus was used as the framework. In some tests, sections of the model were isolated using insulation board in order to achieve the desired model geometry.

6.3 Model Descriptions

6.3.1 Physical Model

A scale model of the naturally ventilated prototype building was created at one-twelfth scale, and evaluated using air as the fluid. The central section of the building was modeled, encompassing two floors of open floor office plan and the central atrium. The model neglected the stairwells at the east and west ends of the building and the service core. The building is three stories in height on the north half of the building, and two on the south half of the building. The north half of the ground level of the building was excluded because it consisted of meeting rooms that are closed off from the rest of the building and can be mechanically ventilated when in use.

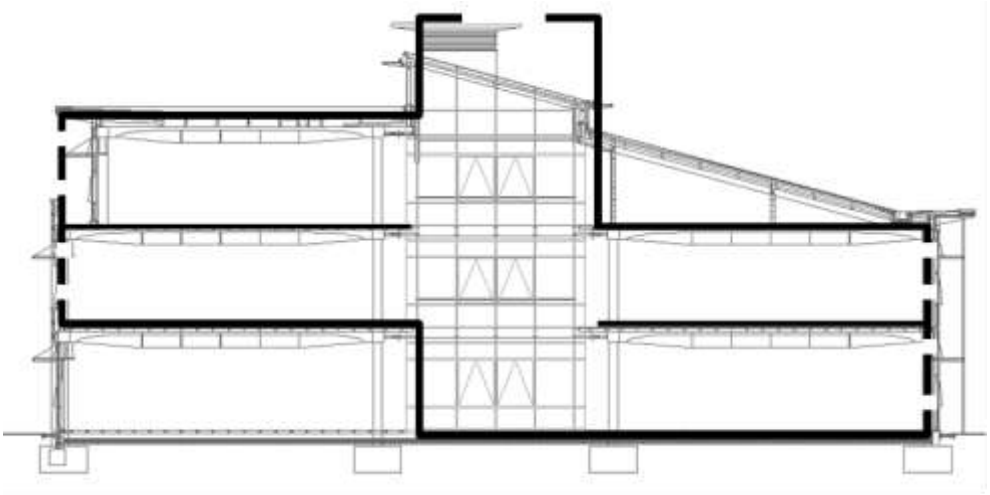

Figure 27. Section of the Prototype Building with Outline of Area Modeled

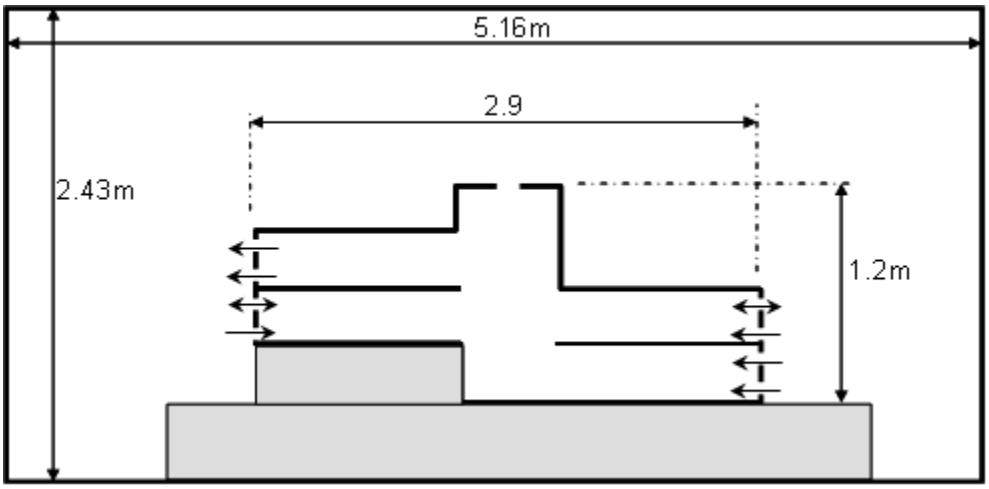

Figure 28. Reduced-Scale Model and Test Chamber Section View and Dimensions

The model is located in an insulated test chamber that is 5.16 meters in length, 3.65 meters in width, and 2.43 meters in height. The dimensions of the test chamber along with the overall model dimensions are presented in Figure 28 and Figure 29. All of the surrounding walls have

an insulating value of R-30, or 5.3 Km^2/W. The test chamber has its own heating, ventilating, and air-conditioning unit and controls. The control interface allows the operator to control set points of the system, including supply air temperature and airflow rate.

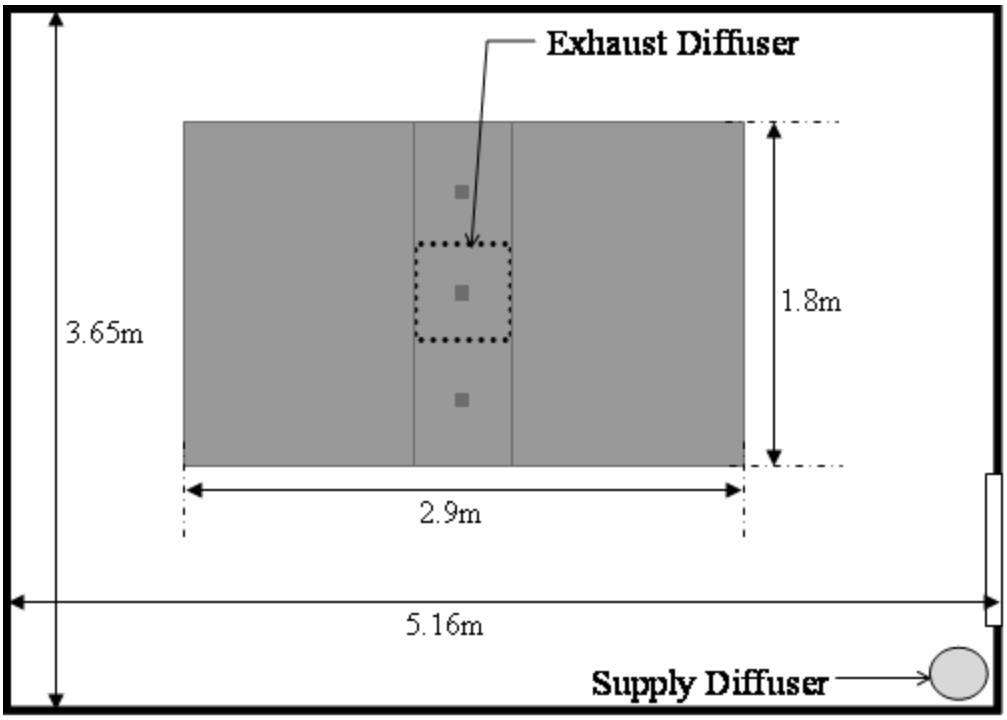

Figure 29. Test Chamber Plan View with Dimensions

The dimensions of the scale model developed are 2.9 meters in overall length, 1.8 meters in width, and 1.2 meters in total height. The model has two 1.2 meter by 1.8 meter by 0.3 meter occupied zones on each side of the atrium, which is 0.5 meters by 1.8 meters. The half floors are located on the ground and first floors on the south half of the model and the first and second floor on the north half of the model. All of the occupied zones are completely open to the central atrium. The atrium extends above the roof of the second floor and includes openings that represent the stack vents used to assist in ventilation of the building. The geometry of the atrium roof was simplified in the model construction, and does not include the slight slope of the prototype building. Instead, the atrium in the model is a rectangular shape. Railings were added around the perimeter of the atrium for the combined wind-buoyancy modeling.

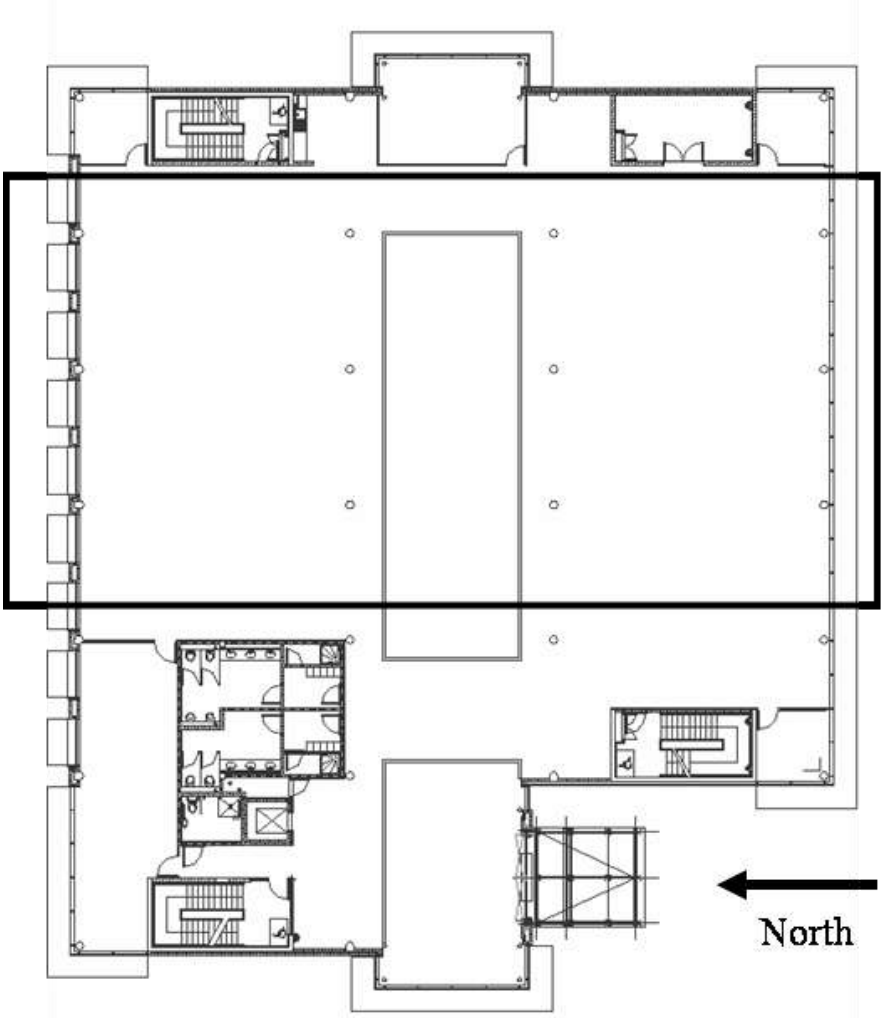

Figure 30. Floor Plan of the Prototype Building with Outline of Area Modeled

The scale model was constructed of several readily available materials, medium density fiberboard (MDF), plywood, and insulation board. All of the walls were constructed of single layer of ½ inch MDF and 1 ½ inch, R-6.5 insulation board. MDF was selected for its strength, rigidity and relative ease with which it can be cut. This was needed to create the multiple window openings at each floor level and its ability to carry loads. The window openings were cut from a single large sheet of MDF for both the northern and southern façades. The eastern façade was constructed completely of MDF; with two Plexiglas view windows installed in the western façade to assist in airflow visualization, one at the atrium and one at the north half of the building. The atrium section window covered the full height and width of the atrium. The window in the northern portion of the western façade was installed in proximity to the joint with the northern façade. Plexiglas that was one eighth inch thick was selected for the view windows since it was strong enough and had enough rigidity to provide structural support in the large atrium window. These Plexiglas windows were covered with a layer of insulation board during experiments in order to obtain a more uniform temperature distribution and to reduce the heat loss through these view-windows.

Table 20. Model Surface Characteristics by Orientation

	Primary Material	*Number of Openings*	*Size of Opening*	*Surface Area*	*Overall U-Value*
North Wall	MDF	28 (2 levels of 7 per floor)	17.1 cm x 2 cm		
East Wall	MDF	None	---		
South Wall	MDF	28 (2 levels of 7 per floor)	12 cm x 2 cm		
West Wall	MDF	2 View Windows	50 cm x 120 cm 10 cm x 60 cm		
Roof	Plywood	3 (along atrium roof)	7.5 cm x 7.5 cm		
Floors	Plywood	None	None		

Due to the complex geometry of the awning-type windows found in the prototype, the openings were simplified to a vertical, rectangular cut-out in the façade. The windows were sized based on the effective opening area defined in Chapter 3 experiments. Two sets of seven windows were modeled for each floor level of the model; an upper vent and lower window opening. The upper opening is located near the ceiling (24 cm from the floor to the sill), while the lower opening is located near the floor (5 cm above the floor). The locations and heights of the windows relative to the floor remain constant for both upper and lower openings, on both sides of the building (north and south) at all floor levels. Though the height remained the same, 2 cm, the width of the windows on the north façade is larger than those on the south façade. The window in the prototype building had wider window openings on the northern façade than the southern façade. The windows for the scale model on the southern façade are 12 cm in width shown in Figure 32, while those on the northern façade are 17.1 cm wide shown in Figure 31. The stack vents, used to assist ventilation in the prototype building and located along the roof of the atrium were created in the reduced-scale model. These three openings are located along the center of the roof of the atrium. Each measures 7.5 cm by 7.5 cm, and they are located approximately 0.40 cm apart. These openings can be either open or closed depending on the case being modeled. They are evenly spaced and centered across the 1.8 meters of the atrium, as shown in Figure 33.

The floors within the model, including the ceilings/roofs, were constructed of a layer of 1/8th inch plywood and a layer of R-6.5 insulation board. The insulation was required to reduce heat loss to the test chamber (external environment) and heat transfer between floors. There are columns in the model along the atrium similar to those in the prototype building. These inch-thick, dowel-rod columns allow for the unrestrictive opening between the occupied spaces and the atrium, and provide support to the floors of the model. A combination of More-Tite® rope caulk and duct tape was used to seal up joints within the model to reduce and control air leakage between floors and to the ambient.

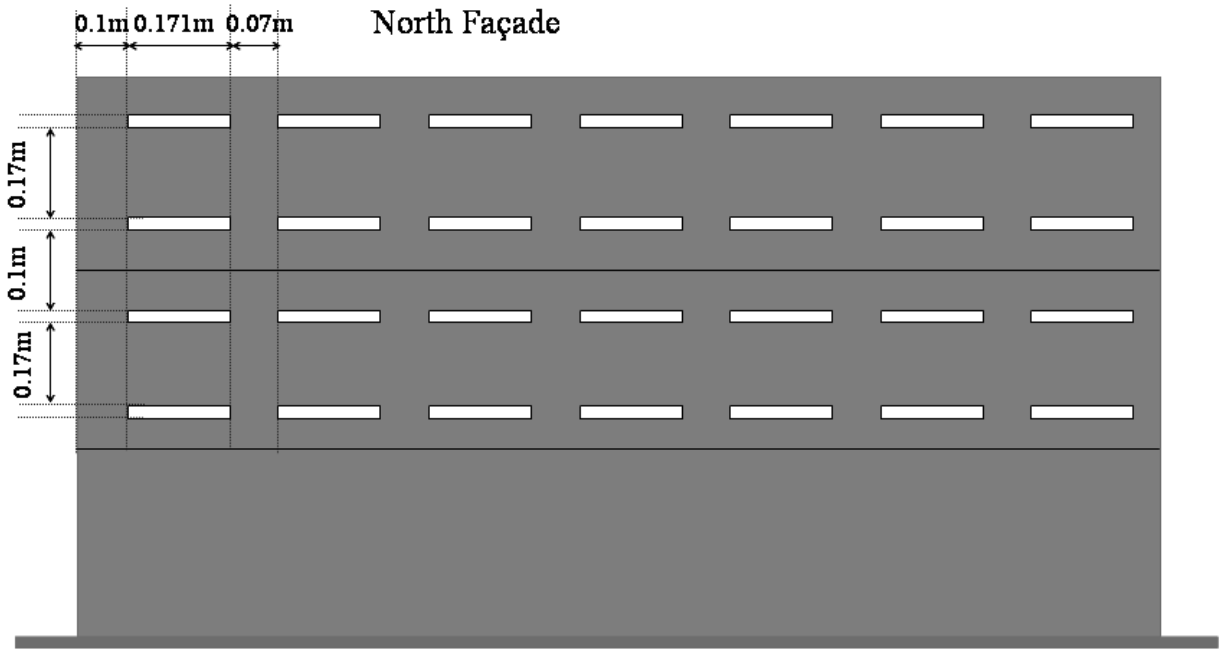

Figure 31. North Facade of Model with Dimensions and Spacing

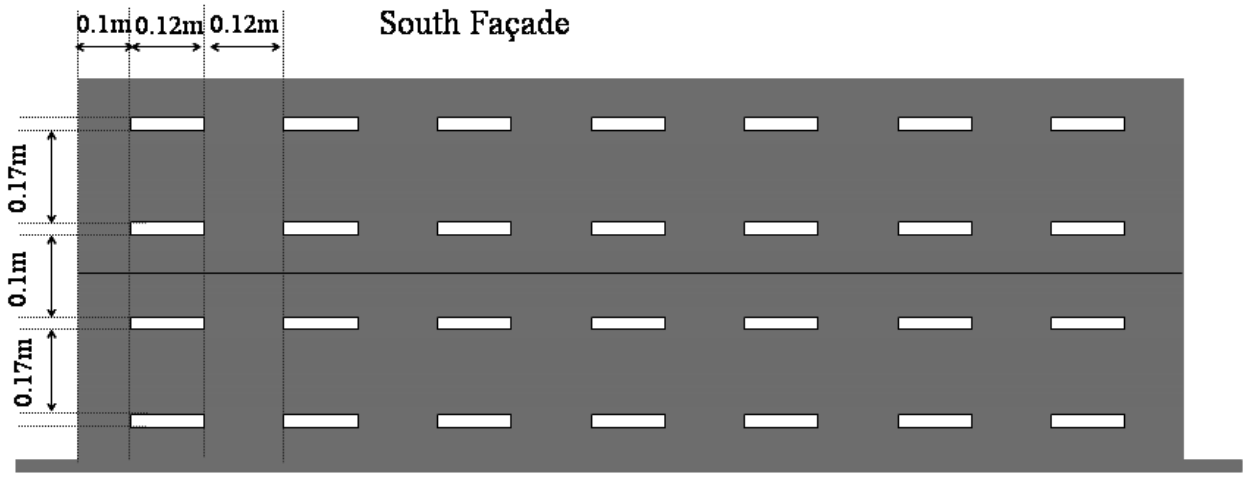

Figure 32. South Facade of Model with Dimensions and Spacing

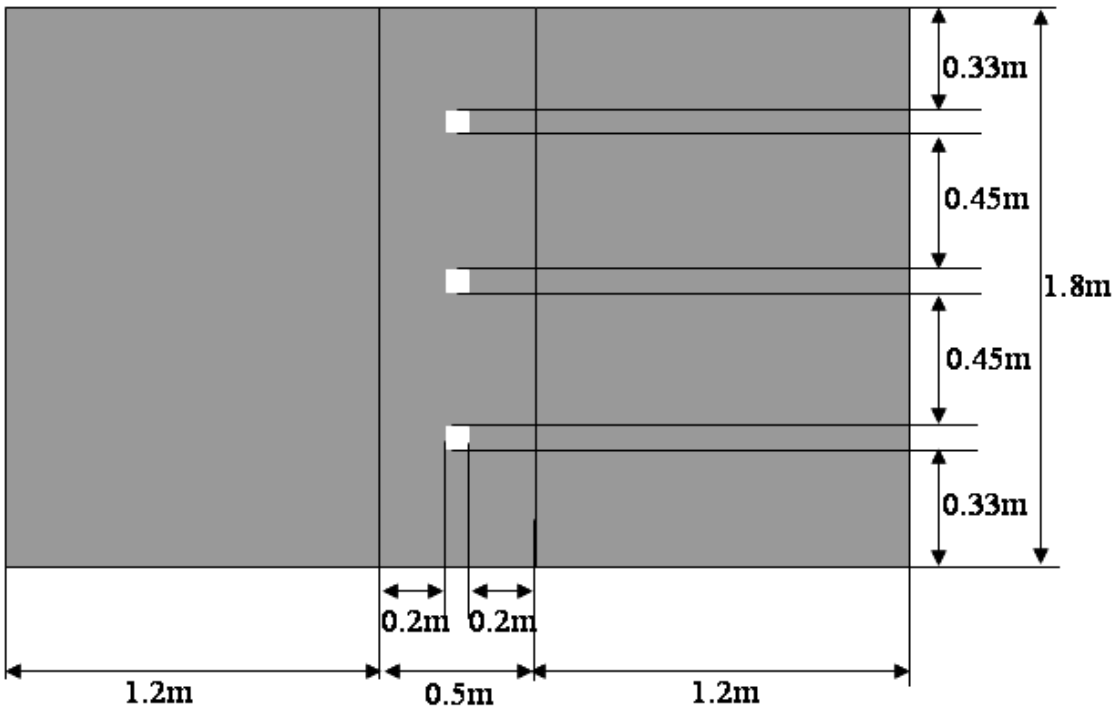

Figure 33. Plan View of Top of Reduced-Scale Air Model with Stack Vents

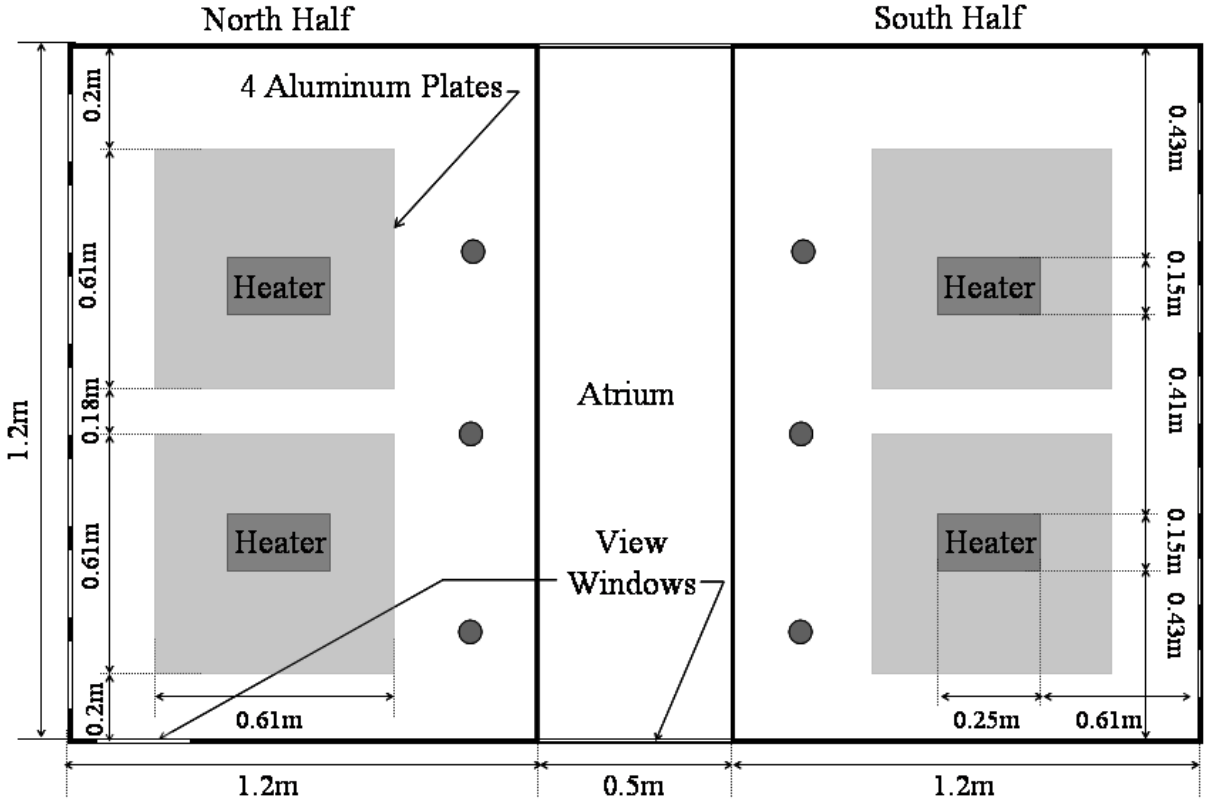

Figure 34. Floor Plan and Dimensions of Model, Aluminum Plates, and Heaters

Monitoring data collected from the prototype building were used to calculate the needed size of resistance heaters that were then inserted into the model to simulate the building internal loads due to people and plug loads. The plug loads included in the model were electric lighting, computers, and miscellaneous office equipment. Based on the average 20 W/m^2 measured in the prototype building as a typical occupied workday period, the heaters were sized at 240 W/m^2, or twelve times that for the prototype building to result in the same buoyant driving force. This was calculated by assuming equal Grashof (Gr) numbers between the reduced-scale model and the prototype. Simplifying the expression for the Grashof number, and equating the reduced-scale model Gr to the prototype Gr:

$$(H\Delta T)_M = (H\Delta T)_P \qquad (6.1)$$

In order to obtain a temperature difference in the reduced-scale model that is 12 times that of the prototype building, the heaters need to provide 12 times the heat input into the space. Two 0.25 meter by 0.15 meter heaters that were rated to generate 7,750 watts per square meter, 295.3 watts total, were installed for each half-floor plate. However, the heaters were actually delivering less than the rated value, or 7,440 watts per square meter, 283.5 watts. The resulting total internal load was 2,000 watts for the building, or approximately 240 W/m^2, which is proportional to the prototype building occupied conditions.

The heaters used to represent the internal loads were relatively small in physical size, measuring 0.15 meters by 0.25 meters, compared to the floor area of a half floor plate, 1.2 meters by 1.8 meters. Originally, there was an aluminum plate of one-quarter inch thickness (0.006 mm) on the ground floor only. The heaters were placed on top of the aluminum plate, representing a uniformly distributed internal load. In refining the model, a three-quarter inch ledge was installed underneath the perimeter of each floor, to provide additional support and to reduce the amount of sagging from the weight of the plywood. This added perimeter support made it possible to accommodate aluminum plates on the other floors as well to ensure that the interior heat load approximated a distributed load rather than two large point heat sources. This refinement resulted in a configuration that more accurately represented the prototype-building situation. Two 0.6m x 0.6m x 0.003m aluminum sheets were added to each heated zone, other than the ground floor, underneath each heater, to provide a more distributed heat load. This is shown in Figure 34. The temperatures measured of the aluminum plate varied from 75°C at the heater to 65°C at the furthest distance from the heaters.

Light sources were installed inside the model to provide illumination to assist with flow visualization. Compact fluorescent lamps were selected due to their thermal efficiency, and provided adequate light levels within the model without the addition of large amounts of excess heat. There were three compact fluorescent light bulbs, 9 watts each, that were located in the central atrium; one at each floor level. When airflow visualization was not in process, these lamps were turned off so that they did not contribute to the heat load within the model. Even when all three lamps were on, they contributed less than 2 percent additional heat load in the model.

6.3.2 CFD Model

PHOENICS (CHAM 2002) is a general-purpose software package which predicts quantitatively how fluids (air, water, oil, etc) flow in and around engines, process equipment, buildings,

natural-environment features, the associated changes of chemical and physical composition, and the associated stresses in the immersed solids.

A model with the same geometry and dimensions as the scaled physical model was created using the PHOENICS program. The surrounding conditions were made to simulate the test chamber conditions, including the dimensions, wall temperature and location within the chamber. As with the scaled physical model, there are cutouts for the window and stack vent openings with the same size as those elements in the physical model. The CFD model however did not use columns in the simulation, as in the scaled physical model the columns have a negligible effect on both the airflow patterns and temperature. A cross-section of the CFD model is shown in Figure 35.

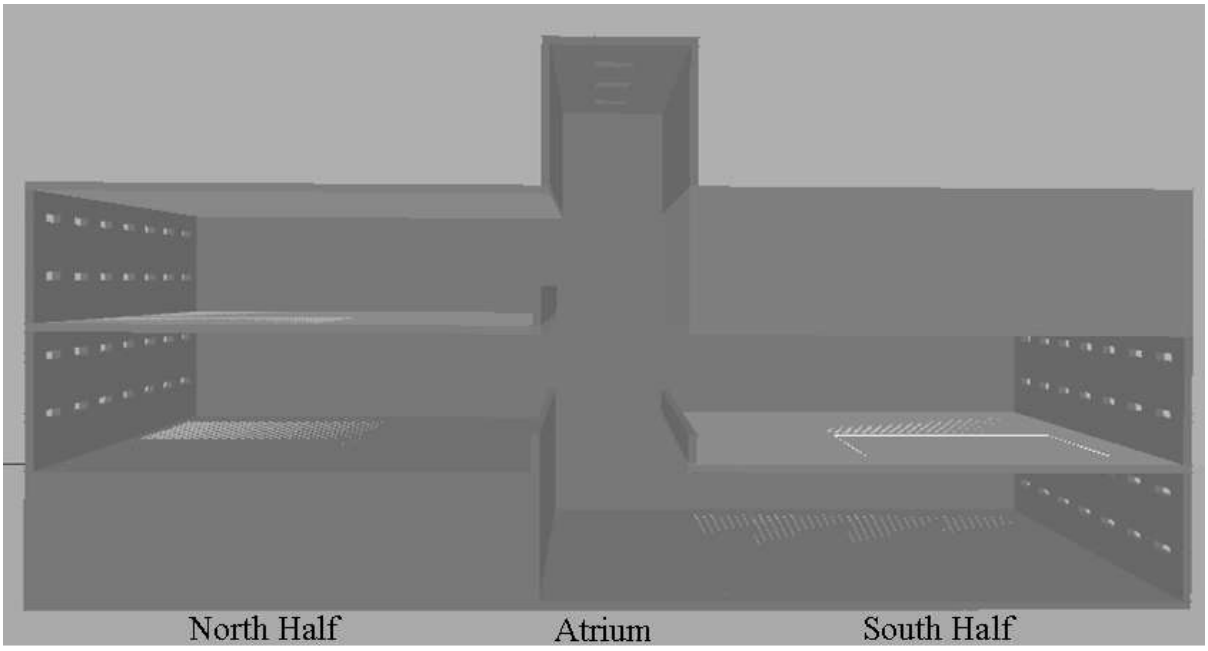

Figure 35. PHOENICS Scale Model Geometry

The CFD software was found to have limitations for use in simulations of the reduced scale air model. Surfaces such as walls and floors are considered adiabatic in CFD simulations. There was no easy way to simulate the thermal properties associated with heat loss through the envelope or between floor constructions. The surfaces of the experimental case, the reduced-scale air model, were not adiabatic and had some amount of heat loss through the envelope. Results from the reduced scale air model with heat loss for each experiment provided data for comparison with each corresponding CFD simulation with adiabatic walls. The strength of heat source used in the reduced-scale air model were also described in the CFD model. The prescribed heat sources in the CFD model were 283W each, to simulate the heaters in the physical scaled model, and therefore the internal loads for the prototype building. The heat source, sited in approximately the same location as in the scaled physical model, was distributed over the entire size of the aluminum plates. In the single zone model, heat loss through the walls was modeled in the atrium portion, as is described in Section 6.5.1.1 Single Heated Zone Experiments.

By default, there was no accounting for any effects due to radiation in the CFD model. Through measurements in the reduced-scale air model, it was determined that there was a measurable amount of radiation to the ceiling in each heated zone. The CFD model was modified in order to account for the radiation that occurred in these zones. Additional simulations were carried out to obtain the percent of the heat input that was radiated to the ceiling of the model. By measuring the temperatures of the surfaces within the physical model, approximations for the heat transfer due to radiation were made using grey body assumptions for two parallel plates (Incropera and DeWitt 1996). Using the measured surface temperatures of 70 °C at the aluminum plate and 55°C at the ceiling, and an emissivity of 0.7 for aluminum and 0.89 for wood, it was determined that 30 percent of the heat was radiated to the ceiling.

6.4 Experimental Equipment and Measurements

The equipment used in evaluating and monitoring the reduced-scale air model are presented in this section, along with a description of the facility in which the physical model was located through the duration of the experimental procedure. The flow patterns, temperature distributions, and heat transfer issues within the model were evaluated using a variety of instrumentation and equipment. These pieces of equipment helped to quantify the temperature distribution and air velocities within the model.

Table 21. Summary of Equipment Used in Experiments

Equipment	*Type*	*Experimental Use*
Test Chamber	Controlled Environment	
CR10X	Data Acquisition System	Thermocouples
Keithley	Data Acquisition System	Thermocouples
	Hot-wire Anemometer	Air Velocity
Draeger	Smoke Pencils	Flow Visualization
	Fogging Machine	Flow Visualization
	Infrared Temperature Gun	Surface Temperatures
Omega®	Heaters, 5W/in^2, 500W each	Internal Loads

6.4.1 Equipment

A well-insolated test chamber was used as the control environment in which the scaled-model was placed. Therefore the ambient conditions around the model and the fluctuations normally seen in typical building environments could be controlled. The MIT test chamber in its entirety consisted of a well-insulated enclosure separated into two rooms by a partition wall with a large, double-glazed window. The scale model was located in the main room, a well-insulated single room that had a dedicated ventilation and control system to manage the conditions within the test chamber. All walls had an insulating value of R-30, or 5.3 Km^2/W. The test chamber was outfitted with a combination of permanent monitoring equipment and portable measuring devices.

The supply air entered the test chamber through a single duct opening in the corner, and air was exhausted through a grill ceiling exhaust. Care was taken to ensure that there were no significant drafts from the supply diffuser blowing on the model that might have affected the measurements. The heating, ventilation, and air-conditioning (HVAC) system that conditioned the test chamber

had a dedicated supply and return fan with a variable-speed drive incorporated into the control scheme for each. A computer software package allowed for a more refined control over the HVAC system. The computer interface, shown in Figure 36, allowed the operator to control various system set points, including supply airflow rates, temperature, and relative humidity. The control system also allowed recording for all data points in the control system at a time interval specified by the operator. The supply air temperature and the supply fan airflow were adjusted during experiments to have the test chamber positively pressurized so that warmer air from the space surrounding the test chamber was not drawn into the test chamber itself. The set points used for the experiments are presented in Table 22.

Table 22. Test Chamber HVAC System Set Points

Variable	*Set Point*
Supply Flowrate	165 l/s (350 CFM)
Supply Fan Variable Frequency Drive	97.5%
Return Fan Variable Frequency Drive	95.5%
Supply Air Temperature	6°C (±2°C)

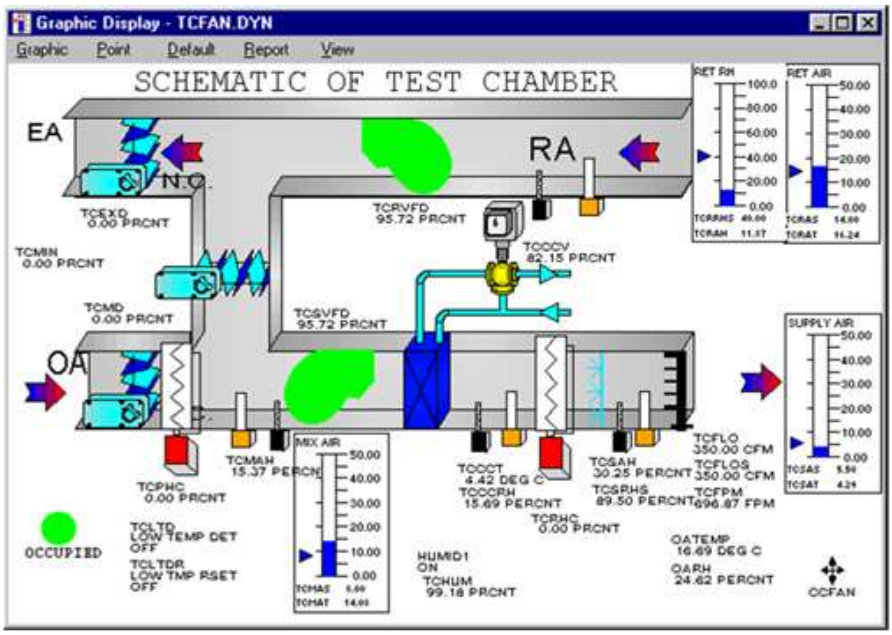

Figure 36. Test Chamber HVAC Computer Interface Control Panel

A separate computer controlled and recorded data from a Campbell Scientific CR10X data acquisition system. The CR10X was outfitted with two sets of ports having a total of 50 monitoring locations available. These locations were equipped with Type K thermocouple wires that had been painted with silver paint to reduce any error in measurement due to radiation. An RS-232 cable connected these locations to the desktop computer. The computer software package, TComm®, was used to monitor and record data from the CR10X data acquisition system. The CR10X was used for long-term data recording at minute intervals, as long as the data logger was turned on and connected to the computer. The setup file for the CR10X data acquisition system is provided in Appendix A. A second, more portable, data acquisition system monitored additional temperature locations throughout the model. The Keithley® 2700 had a

40-location card inserted into the data-recording device. Data could be measured and downloaded to a computer in real time or to a designated file location on the computer. The channels, or locations, on the card were configured for recording temperature measurements, using Type K thermocouple wire, and an internal reference temperature. When the channels were set up to record data with an internal reference temperature, rather than the external or simulated, the measurements were all relative to one another, rather than relative to a prescribed reference temperature or ambient reference temperature. By using the internal reference temperature, the data collected using the Keithley® could be directly compared to the temperature data recorded using the CR10X. The Keithley® data acquisition system was set up to record data every 0.16 seconds. Since there were 40 locations that were monitored at any given time, it took 6.4 seconds for each data set to be recorded. The average temperature over 15 measurements was used as the temperature for data analysis purposes. The setup files for the Keithley® data recorder are provided in Appendix A.

Thermocouples were used to measure temperatures not monitored within the HVAC system. Type K thermocouples were used throughout the test chamber to record temperature measurements both inside and outside the scale model. The thermocouples were then placed on the interior of the scaled model, often using a highly heat resistant duct tape to ensure that the thermocouple would remain in place even when exposed to high temperatures (>70°C). In each heated zone, six thermocouples attached to the CR10X were placed at mid-height in each heated zone of the model, and a thermocouple was placed on each of the three sides of the atrium at the first floor level, and on the two sides of the second floor level. All thermocouples were 2mm in diameter, and the junctions were coated with aluminum paint to reduce the effect of radiation on air temperature measurements. These thermocouples remained in place for the duration of the experiments. The thermocouples attached to the Keithley® system were moved as needed among different experiment configurations. These thermocouples were primarily used to record more detailed temperature stratification measurements for specific areas of the model under investigation.

Several globe anemometers were placed on the interior of the model in order to measure the interior air velocity. The globe anemometers provide an air velocity measurement, but not the direction of airflow. The globe anemometers had silvered tips and were connected to a data acquisition system located on the same computer as the CR10X thermocouples. The software package allows for instantaneous readings using the globe anemometers.

Several pieces of hand-held equipment were used to gather data that are more detailed on the reduced-scale model and the surrounding conditions. Hot-wire anemometers were used to take air velocity measurements at inlet and outlet openings. Due to the geometry of the openings, an average velocity was taken over the opening area. The hot-wire anemometer, with a probe size of 1mm diameter, had precision of 0.1 m/s. An infrared temperature sensor was used to gather data on the surface temperatures within the model and surrounding the model to assure that thermal radiation effects either between surfaces within the model or between the exterior surfaces of the model and the test chamber did not distort experimental results.

Additionally, flow visualization equipment was used to determine the airflow patterns within the model qualitatively and to ensure that there were no significant leaks in the model. Draeger

smoke pencils were used for localized airflow visualization and to determine the direction of the airflow at inlets and outlets. It was found, however, that the smoke they gave off dissipated when there were large amounts of air flowing at a particular location in the model and due to turbulent flow within the model. A fogging machine was used when the smoke given off by the pencils did not perform satisfactorily. The fogging machine was found to produce a neutrally buoyant, white fog that could be used to trace the flow within the model. The fogging machine uses heat to generate the fog, so a long flexible tube was used from the outlet of the fogging machine to the outlet nozzle that introduced the fog into the space to ensure that the fog was at the ambient temperature when it entered the model. This technique minimized the potential for thermal effects that potentially could be introduced in experiments by the use of fog as a visualization tool.

6.4.2 Measurements

Air velocity measurements were taken at both the inlet and outlet openings for each experiment in order to calculate the heat loss due to airflow, or advection. The heat loss through conduction could be determined from the total heat input into the model by the heaters and the heat loss due to air flowing through the model. Air velocity measurements were taken at each window and stack that was open during a particular experiment to ensure uniformity in airflow across a given façade. The measurements were taken at the center of each window, at the exterior face of the window opening on each façade. The average of the measurements for a particular set of windows or stacks in each experiment was used in calculating the airflow balance and heat loss due to advection. In cases where there was only a single opening, only one measurement was taken. Mass flow balances were conducted to ensure that there was not significant air leakage.

The power output of the heaters was measured to make certain that the internal load input was constant and known. Using a clamp-on ammeter and a multi-meter, both the current and voltage for the heaters were measured, and the power output of the heaters calculated. The single-phase heaters were wired in parallel. The heaters are rated at 300 Watts; however, through the measurements described above, it was determined that the heaters were only providing 88 percent of their rated output.

The accurate measurements of ambient conditions were important both to determine if any vertical temperature stratification existed, and to identify the best parameters to use as inputs to the CFD model. The supply air temperature was kept constant, set to 13°C, but the ambient temperatures varied from a value of 16 to 18°C due to the number of heaters used in a given experiment for the buoyancy-driven ventilation cases. With the wind-driven experiments, the ambient temperature reached 24°C. The increase in ambient temperature of the test chamber was less the fewer heaters used in a given experiment. This not only provided insight into the impact on ambient conditions on the model, but also contributed to the understanding of heat loss due to temperature difference. For both cases, the ambient temperature was carefully monitored to ensure that it did not vary over the course of the experiments. The measurement locations for the ambient temperature recordings occurred at 0.5m intervals from the floor to the ceiling of the test chamber in the corner facing the supply diffuser.

6.5 Experiments

To evaluate the model under the different cases of natural ventilation, experiments were conducted. This was completed for buoyancy, wind, and combined buoyancy-wind driven natural ventilation experiments using the reduced-scale air model. The summary of model variables that were altered is listed in Table 23. These experiments were carried out at steady state conditions, and did not account for variations in external or ambient temperature or wind conditions that might occur in the prototype building, but were run multiple times to ensure repeatability. This section describes the sets of buoyancy and wind-driven experiments that were completed during the process of developing and evaluating this modeling methodology.

Table 23. Matrix of Model Variables

Variable	*Option 1*	*Option 2*	*Option 3*
Number of Heated Zones	1	2	4
Status of Heaters	On	Off	----
Location of Open Windows Used	Lower	Upper	Lower and Upper
Stack Status	All Closed	All Open	Some Open

6.5.1 Buoyancy

Using natural ventilation alone to passively cool and ventilate a building under the buoyancy driven case is the critical design situation for applying this ventilation strategy in buildings. The highest internal temperatures occur on hot summer days when there is no wind driving the airflow. The analysis of the buoyancy driven case is complicated by the need to consider multiple and interdependent design parameters including the size of inlets and outlets, the height of the space, the strength of the heat sources driving the airflow, and the resulting temperature difference between the interior and exterior spaces. It is this complexity and the lack of understanding of the physical mechanisms involved in buoyancy driven natural ventilation that reduce the effective use of natural ventilation in building design. Much research has been completed in the theoretical aspects of buoyancy driven natural ventilation, using a variety of methods, including physical and computer modeling of single story and multiple story spaces. Analyses are most often done under steady-state conditions to simplify otherwise complex phenomena and investigate the impact of the above parameters on the airflow through the space of interest.

Assumptions found in many buoyancy driven natural ventilation models should be understood before using the modeling method. Among the issues that arise, include the assumption of a well mixed, or uniform interior temperature and uniform velocity across inlet and outlet openings. The restrictiveness of the zones under consideration affects the effectiveness and behavior of the airflow for a building, which in turn helps to determine the location of and number of neutral planes within the building or space under investigation. Li investigated natural ventilation in buildings with large openings and defined internal pressures for each zone, relative to the outside pressure. This method created neutral planes for each internal zone (Li 2000). However, in experimental modeling, measuring the internal and external pressures can be difficult, so mass flow balances were used in determining the neutral plane in the reduced-scale model.

With the reduced-scale model, experiments were carried out where the driving force for the airflow through the building was the temperature difference between the ambient conditions in the test chamber and the higher interior temperature due to the modeled interior loads. Of all of the types of natural ventilation, buoyancy driven airflow is better understood in scale modeling, as long as the interior loads causing the temperature increase inside the model are known. The theoretical airflow rate can then be compared to the measured values obtained through experiment.

In this case, three configurations were carried out for the buoyancy-driven ventilation case: a single heated zone connected to the atrium, two heated zones connected to the atrium, and the full model with four heated zones connected to the atrium. These experiments were carried out on the main model, with modifications. The full model with the isolation for the single heated zone case is shown in Figure 37. The grey areas represent zones that do not have any heaters on, and are sealed off from the areas under investigation. Each of these models builds on the previous model in the understanding of the complex heat transfer issues surrounding reduced-scale air modeling of buildings. These three physical models are described along with the corresponding CFD simulations in the following sections.

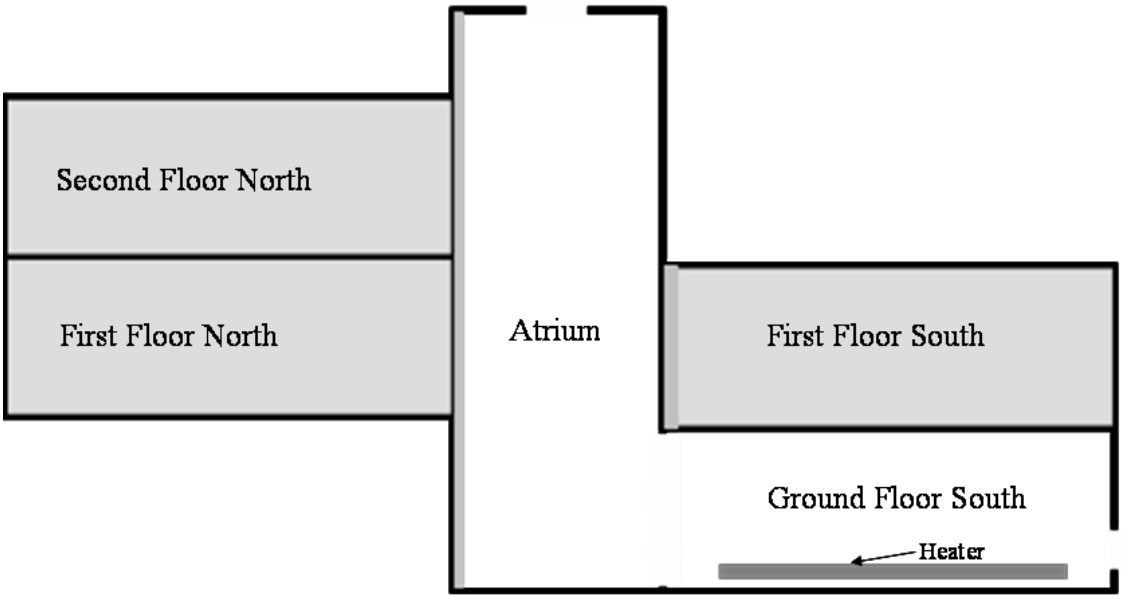

Figure 37. Full Model with Isolation of Single Heated Zone, with Blocked-Off Zones Shaded

6.5.1.1 Single-Zone Model

A simple model with a single heated zone connected to an atrium to compel buoyancy-driven flow was created by modifying the main full building model. This simplified geometry was constructed in order to better understand heat transfer issues, building characteristics, and airflow patterns related to the air model. Only a single set of windows, either upper or lower ones, was used so that the inlet conditions could be accurately modeled and controlled, reducing the variability in the model. Experiments were carried out using the upper windows in isolation, and then repeated using only the lower windows. For both cases, the number of stack vents open was

modified to determine the impact of the effective area ratio of inlet to outlet areas on the temperature and airflow. The ground floor south half-floor was used as the single heated zone connected to the atrium. This was the zone most readily isolated and provided the maximum height differential between the inlet and outlet openings to drive the buoyancy-driven ventilation. This configuration, along with the location of the thermocouples used in measuring the temperature variation throughout the single-zone model, is shown in Figure 38.

One-inch thick insulation board was used to isolate the heated zone and atrium from the rest of the model. The insulation board was placed on the north side of the atrium and the connection of the south first floor to the atrium. The surface area of the modified model is 12 square meters. All surfaces have a layer of insulation board on the external surface in order to reduce the heat losses to the ambient. Foil tape and duct tape were used at major junctions in order to provide a seal, such as to prevent uncontrolled infiltration, exfiltration, and heat loss. The overall heat transfer coefficient was calculated both by measured data and through calculations using material data properties. Thermocouples were located throughout the model; measuring horizontal and vertical temperature variation in both the heated zone and atrium. Airflow visualization techniques, using the smoke pencils, were incorporated into the experiment to understand the flow patterns and determine if they varied with the location of the windows.

The CFD simulation of the single heated zone model kept the same geometry as the reduce-scale model construction. A large plate heater was located on the floor in the heated zone with a prescribed heat flux that was uniform over the plate surface. The ambient conditions for the computational model were derived from measured experimental data. The CFD model was refined in a second step by adding an additional heater plate on the ceiling to replicate the radiation heat transfer that was observed between the heaters on the floor and the ceiling in the experimental case. All other surfaces were originally kept as adiabatic in the computational model. In a third and final step, prescribed heat loss at key surfaces, particularly those in the atrium, were inserted into the CFD model to more accurately simulate the experimental conditions.

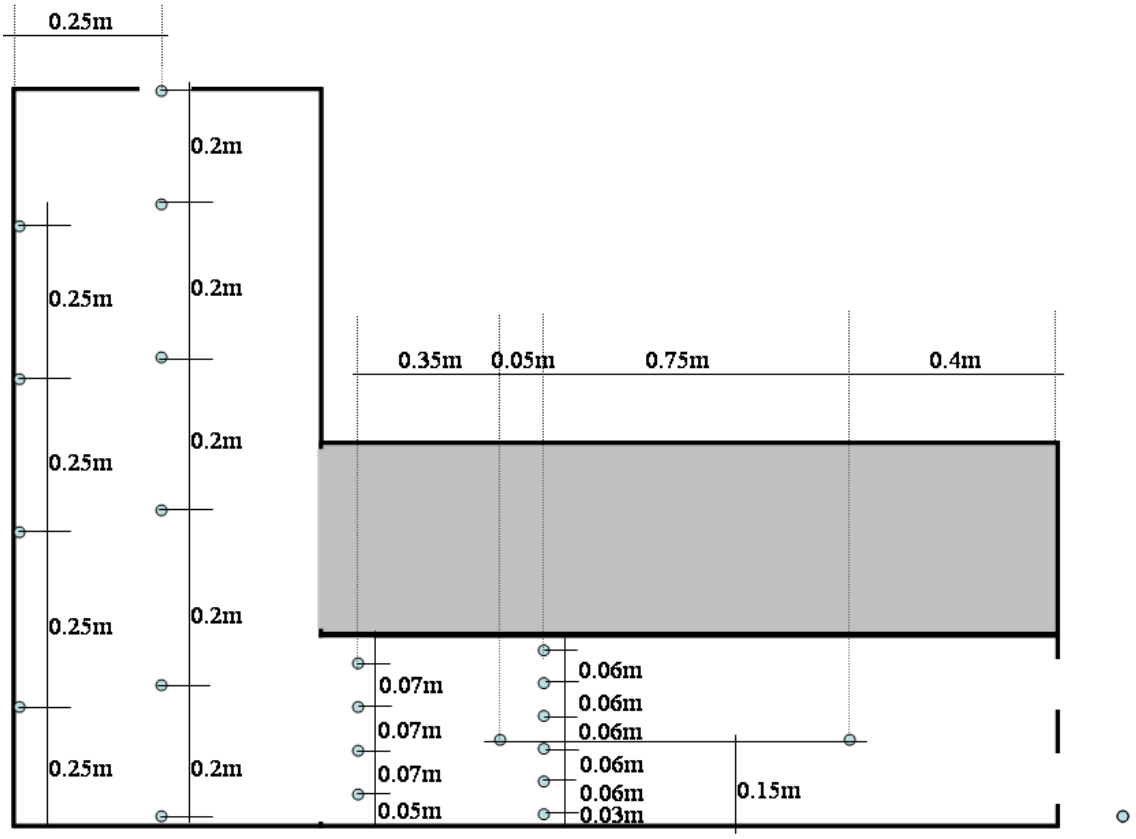

Figure 38. Single Heated Zone Model Cross-Section with Thermocouple Locations

6.5.1.2 Two-Zone Model

The single zone model configuration was revised, and a second heated zone above the first was created. The model was again revised and a second heated zone opened up to the atrium, increasing the complexity of the model. The insulation board divider that was used in the single zone case was removed from the first floor south zone. Thermocouples to measure the vertical temperature stratification within the heated zone and at the connection with the atrium were placed in approximately the same location as were used in the single-heated zone case.

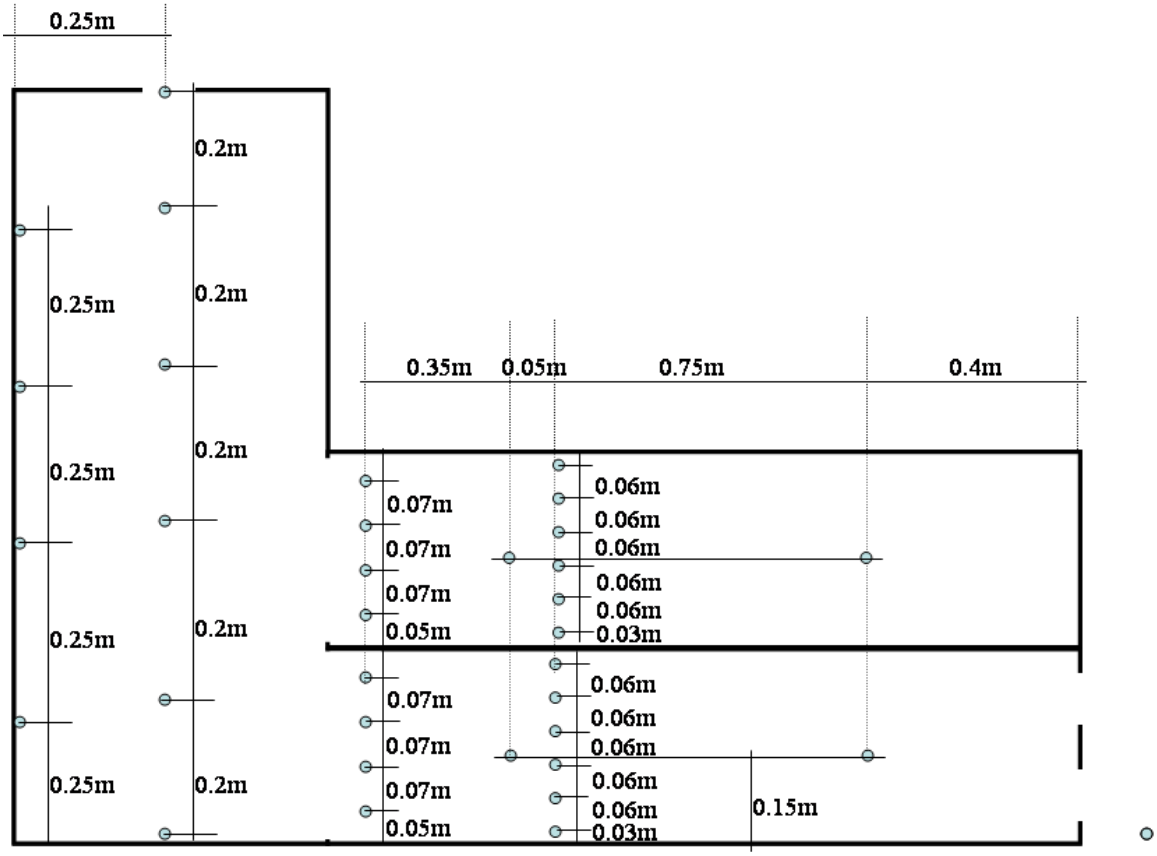

Figure 39. Two Heated Zone Model

With two heated zones, one above the other, both the effects due to radiation from the heaters in each heated zone and any heat transfer between the zones due to conduction from the ceiling of the ground floor zone through the floor of the first floor zone had to be accounted for. Experiments were carried out with for two cases, one with the stacks open and one the stacks closed. The window location was kept constant for these cases, with only a single set of lower windows in each heated zone was left open.

A CFD model was created to compare the results of the experimental model with a numerical model. As with the single-heated zone case, the total heat input was equal to the combined heater output. In the two-zone case, however, not only the radiation from floor to ceiling, but also the heat transfer between the ground floor and first floor zones had to be accounted for in the model. This modification was done in a similar manner to the way it was done in the single-zone case. Plates were located on the ceiling to account for the radiation to the ceiling for each zone, and a plate was added to the floor of the first floor zone with a low-level heat flux of 15 Watts per square meter to account for the heat transfer from the ground floor zone to the first floor zone.

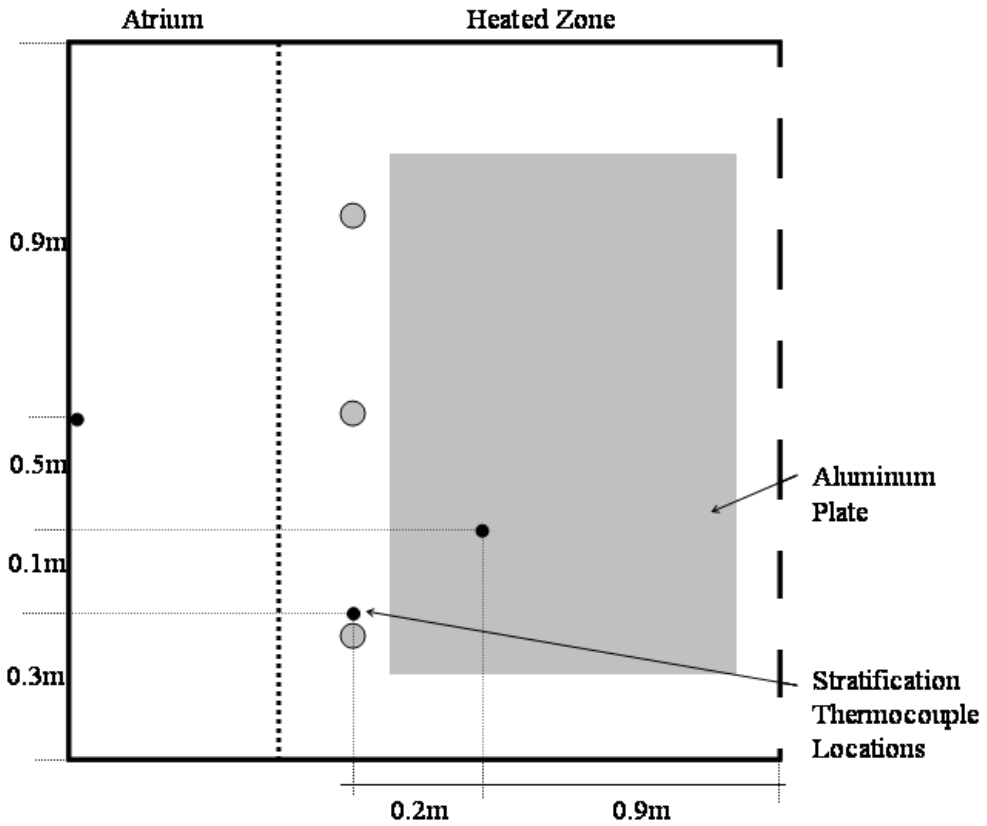

Figure 40. Plan View of Floor with Stratification Thermocouple Locations

6.5.1.3 Full Model

The full model case most closely represents the prototype building, with two heated zones on either side of a central atrium. Both upper and lower windows were modeled as open during the buoyancy driven full model cases, with all of the atrium stack vents open in one case and with them all closed in the other. An additional case was run with one stack vent open for comparison with the stacks closed case. This experimental design provided further information regarding the operation of the model and defined the effect of stack vents status as a design characteristic.

The insulation board divider used to isolate the northern portion of the model for the single and two zone cases was removed, and additional thermocouples were placed in locations similar to those in the other heated zones. The additional thermocouples allowed temperature stratification measurements to be recorded for the two cases modeled. Care was taken to insulate the underside of the first floor north side to ensure that there was no additional heat loss due to the void beneath this heated zone. The same types of heaters used in the first two experiments were used in the full model scenario. This provided a total heat input into the model of 2,000W. Aluminum plates were installed in the rest of the heated zones to model a more distributed load, rather than point heat sources in the zones.

The model was allowed to run while being monitored to ensure that it reached steady state conditions. Once the temperature measurements inside the model remained consistent over a 15-

minute interval, the model was assumed to have reached steady state. During operation air velocity and temperature measurements were taken at the entry and exit points of airflow and throughout the internal space. Air velocity measurements were taken using a hand-held hot-wire anemometer at the window face, and data obtained were used to calculate an airflow balance. Smoke pencils were used to view airflow patterns of air throughout the internal space.

The CFD model was created for the full-model case. As with the previous computational models, the effects of both radiation and heat loss were considered in the simulation. All of the windows were modeled, seven upper and seven lower per half floor plate. The two experimental cases were considered; stacks open and stacks closed. In the full-model case the heat transfer between floors had less of an impact than the effect of radiation to the ceiling. The any additional heat transfer between floors was considered to be negligible. The model was simulated using a fine grid size to ensure that there were adequate points to evaluate the model correctly. This was of particular concern near the heaters, both the heaters representing the internal loads and those representing the radiative effects within the heated zone. The grid size was 63x59x72, for a total of over 267,000 points. A κ-ε RNG turbulence model was used for all of the CFD simulations.

6.5.2 Wind-Assisted

Wind effects were found when monitoring of the prototype building, and there were rarely days when pure buoyancy-driven ventilation occurred. Therefore as an additional refinement, research focused on the modeling of a more realistic but more complex wind-assisted natural ventilation situation.

Although wind velocities varied with time in the prototype building, and mean wind speeds over a specific period of time, often years or decades (Awbi 2003), a design wind speed was used for the model experiments.

It was decided that in order to model the wind caused by the natural environment, a device would be built that would allow a constant, uniform wind speed. This device was created to provide a constant air velocity on the south side of the reduced-scale model, as this was the predominant direction of the wind for the prototype building during the summer months, as seen in Figure 41.

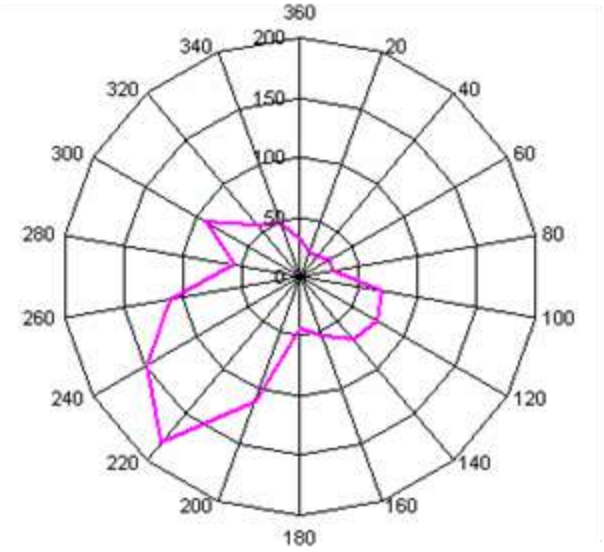

Figure 41. Wind Direction Data for Summer: Luton, UK (US DOE, 2004)

The wind-generating device had to be relatively compact, due to the space limitation in the MIT test chamber. It was decided to use a series of 6 box window fans organized into two rows of three fans each. The fans were plugged into a single power strip so that they could all be turned on and off together. A nozzle was then built that contained a flow straightener. Because the window fans are three bladed fans, there is a possibility that the airflow would not be approaching at an angle perpendicular to the façade of the model. The flow straightener helped in making the flow more uniform and better controlled. It was found that the flow straightener was not adequate in providing a uniform velocity across the entire face of the façade. Techniques used in the development of wind tunnels were used to resolve this; namely, plastic screens wrapped around a wood frame were constructed at decreasing mesh sizes to help make the flow uniform. A 1" by 3" piece of wood was used as the frame, and the fine plastic screens were placed on each face of the wood structure. With the addition of two screens and a collar to force the air directly to the south façade of the model, uniform velocities were achieved across the entire façade of the model (Figure 42).

The fans in the wind-generating device have three levels, low (1), medium (2), and high (3). These fan settings corresponded to air velocities entering the windows at 3 m/s, 4 m/s, and 5 m/s. These entering air velocities caused strong jets of air on the interior of the model, and made the buoyancy flow negligible. It was determined that lower air velocities were needed at the inlet openings. A Variac® was inserted in between the power strip in to which the six fans were plugged and the electrical outlet. The Variac® had the ability to reduce the voltage supplied to the fan, thereby reducing the speed of the fans. With use of the Variac®, the speed of the fans was able to be further reduced, providing air velocity measurements at the window face of 1 m/s at 57% of the full voltage and 2 m/s at 83% of the full voltage. Measurements were taken to ensure that the entering air velocity remained at a constant speed throughout the set of experiments, and was uniform across the façade.

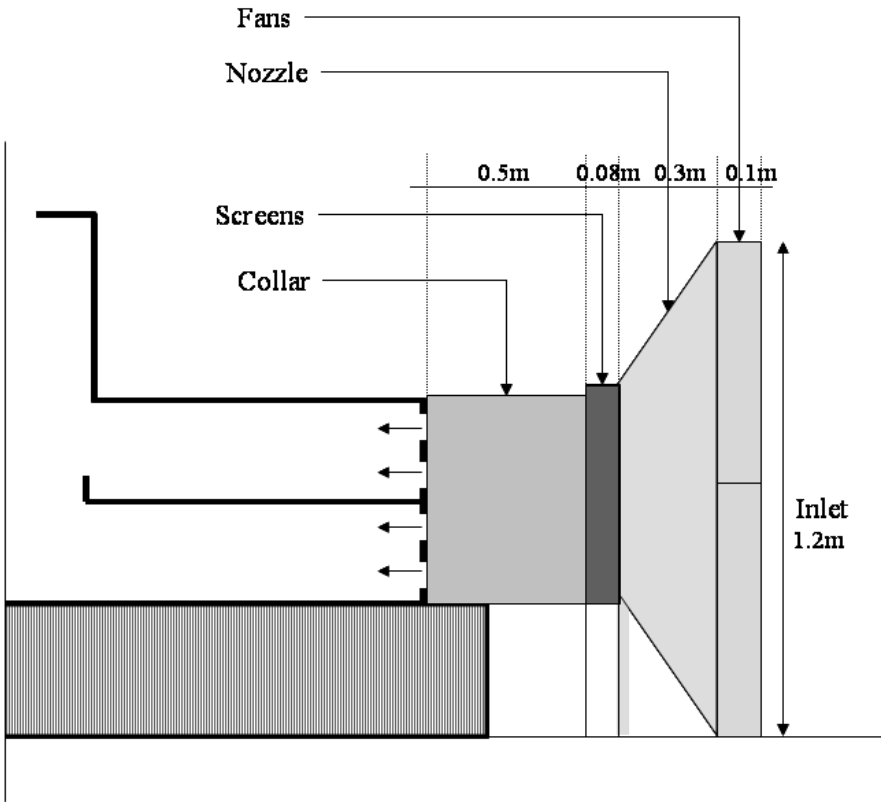

Figure 42. Cross-Section of Wind-Generating Device

Experiments with the full model were carried out using the wind-generating device. First the experiments were run without the heaters on, in order to determine the wind-driven ventilation alone, without any effects of buoyancy. The fans were left on for a period of two hours so that the model was allowed to reach steady state. Once those data were collected, then the heaters were turned on. The model was again allowed to reach a new steady state, and the data collected. Both the stacks open and stacks closed cases were modeled.

Air velocity and temperature measurements were recorded for all of the fan settings, from 0.5 m/s up to 5 m/s in 1 m/s intervals. Temperature measurements were recorded using thermocouples located within the model and the ambient surroundings, attached to both the CR10X and Keithley® data acquisition systems for the buoyancy-wind cases. Air velocity measurements were recorded at the inlet and outlet openings of the model using the hot-wire anemometer for both the wind-only and the wind-buoyancy cases.

A numerical model using CFD was also completed (Figure 43) using the internal loads, ambient temperature, and measured window velocity as boundary conditions. Initially the reduced-scale model created for use with the buoyancy-driven ventilation was modified, and a uniform velocity equal to that measured in the experiments applied. The ambient temperature was set at 24°C for the combined wind-buoyancy experiments, with an applied fan object placed at the south façade windows to describe the inlet velocities. The resulting interior temperatures, flow patterns, and velocities were then compared to the experimental results. The same model characteristics that

were developed and used in the buoyancy-driven CFD model were also used in the wind-buoyancy model. That includes particularly the radiation from the floor to the ceiling.

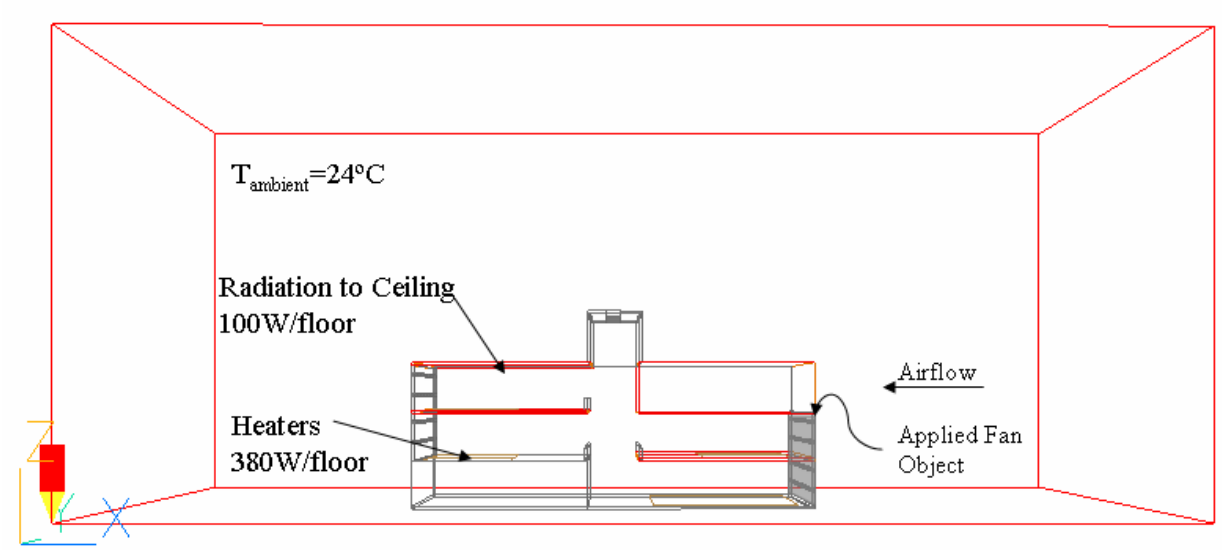

Figure 43. PHOENICS Model with Boundary Conditions for Combined Wind-Buoyancy

6.6 Summary

Three natural ventilation scenarios were modeled using both the reduced-scale air model and the corresponding CFD simulation. Care was taken in recording pertinent data to be able to fully compare temperature distribution, airflow patterns and air velocities for the models and simulations. The buoyancy-driven flow experiments provided pertinent information in understanding heat transfer issues in reduced-scale air modeling methodology. They also illustrated areas of improvement to increase the accuracy of CFD simulations to better model experimental results. By slowly building the complexity of the buoyancy-driven reduced-scale air model, the influence of design characteristics, such as window location and stack openings was better comprehended. A summary of the buoyancy-driven experiments is presented in Table 24. In the wind-driven and combined wind-buoyancy cases, a wide range of wind speeds was tested both with and without heat sources. The focus was more on the impact of exterior conditions, using the various wind speeds and its impact on the internal conditions. However, the influence of the stack vents on temperature distribution and air velocities was recorded. The wind driven flow experiments are summarized in Table 25. The results and comparisons of these results are presented in the next chapter.

Table 24. Summary of Buoyancy-Driven Ventilation Experiments

Number of Heated Zones	*Windows Used*	*Stacks Status*
1	Lower	All open
1	Upper	All open
2	Lower	All open
2	Lower	All closed
4	Lower and Upper	All open
4	Lower and Upper	All closed

Table 25. Wind-Assisted Ventilation Experiment Summary

Case	*Heaters Status*	*Case 1*	*Case 2*
1 m/s at inlet	Off	Stack Open	Stack Closed
2 m/s at inlet	Off	Stack Open	Stack Closed
3 m/s at inlet	Off	Stack Open	Stack Closed
4 m/s at inlet	Off	Stack Open	Stack Closed
5 m/s at inlet	Off	Stack Open	Stack Closed

Table 26. Combined Wind-Buoyancy Ventilation Experiment Summary

Case	*Heaters Status*	*Case 1*	*Case 2*
0.5 m/s at inlet	On	Stack Open	Stack Closed
0.7 m/s at inlet	On	Stack Open	Stack Closed
1 m/s at inlet	On	Stack Open	Stack Closed
1.5 m/s at inlet	On	Stack Open	Stack Closed
2 m/s at inlet	On	Stack Open	Stack Closed
3 m/s at inlet	On	Stack Open	Stack Closed
4 m/s at inlet	On	Stack Open	Stack Closed
5 m/s at inlet	On	Stack Open	Stack Closed

Chapter 7.0

Experimental Results

Experiments were carried out on the reduced-scale air model described in Chapter 6. The results of those experiments are presented here, categorized by the type of ventilation: buoyancy-driven, wind-driven and combined buoyancy-wind driven flows. The airflow rates and temperature distributions are used to assess the ventilation scheme and then compare the reduced-scale air model to the prototype building that was monitored. The temperature data are presented as predicted temperatures for a full-scale building, using the dimensionless methods presented in Chapter 5. The data recorded using the reduced scale model require the use of the reference temperatures to scale the recorded data for use in predicting full-scale building temperature distributions. This was completed using the reference temperature equation presented in Chapter 5. The reference temperature was based on the heat flux, W/m^2, the properties of the working fluid used, and the height of the model.

For the single zone case (a), there was only one heated zone with two heaters that had a measured output of 500 watts. The two heated zone case (b) had twice the number of heaters and therefore twice the amount of heat at 1,000 watts. The full model experiments (c) had a total of 2,000 watts of heat input. Diagrams for each of the configurations with the heaters are shown in Figure 44 a, b, and c. The reference temperatures were calculated using equation 7.1. The resulting reference temperature differences are provided in Table 27.

$$\Delta T_{ref} = \left[\frac{\left(Q / A \right)^2}{\left(\rho c_p \right)^2 g \beta H} \right]^{1/3} \tag{7.1}$$

If the model accurately simulates the building, then:

$$\left[\frac{\left(T - T_\infty \right)}{\Delta T_{ref}} \right]_M = \left[\frac{\left(T - T_\infty \right)}{\Delta T_{ref}} \right]_P \tag{7.2}$$

$$\Delta T_P = \frac{\left(\Delta T_{ref} \right)_P}{\left(\Delta T_{ref} \right)_M} \Delta T_M \tag{7.3}$$

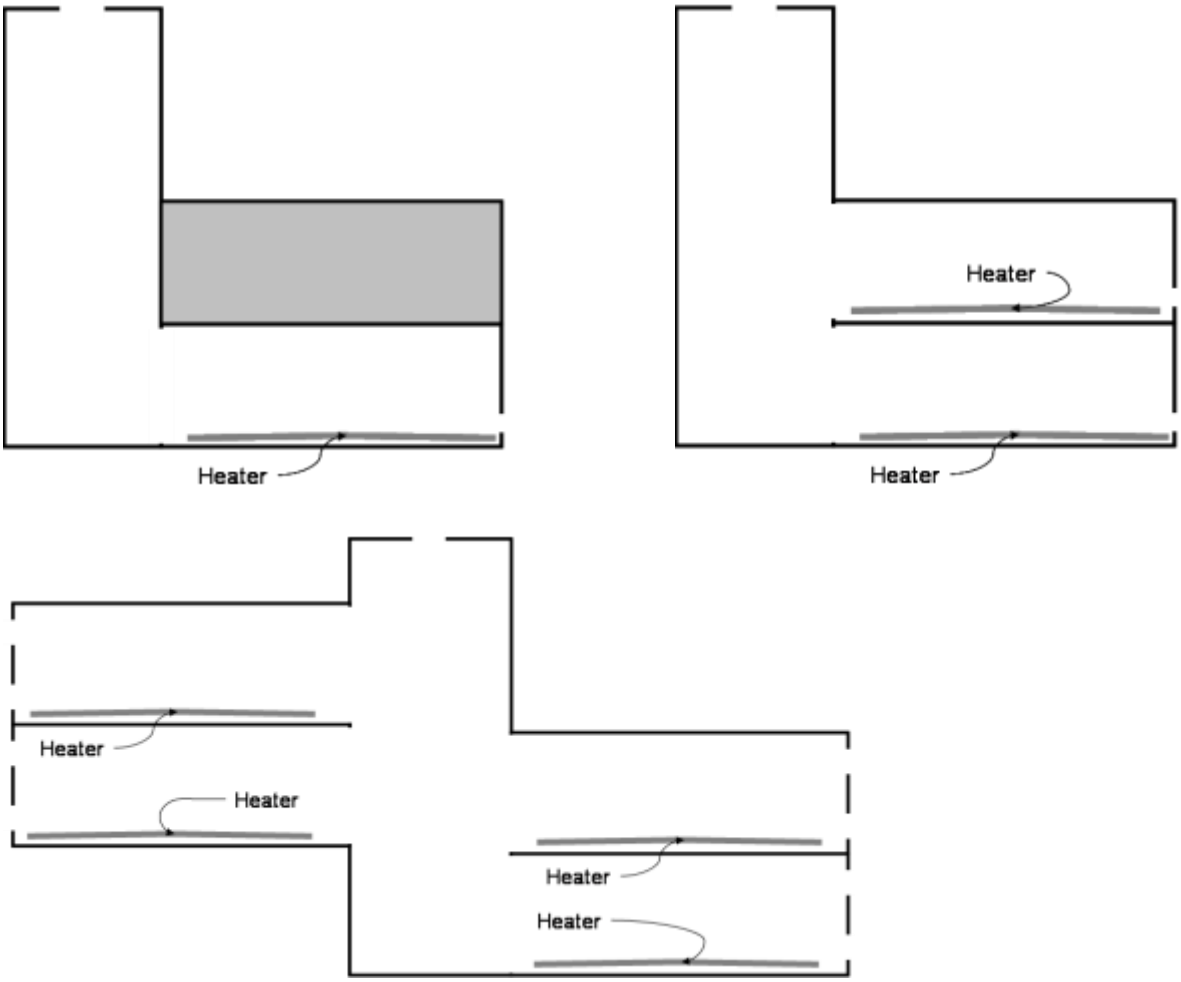

Figure 44. Heaters and Zones for a) single zone case, b) two zone case, and c) full model

In order to scale the data for application in the full-scale model predictions, the reference temperature differences for both the scale model and the full-scale prototype had to be ascertained. Once the reference temperature differences were known, then the full-scale temperature difference, inlet to outlet, for the prototype building was determined. By selecting an ambient temperature, the resulting internal temperature distributions were obtained.

Table 27. Variables and Calculated Reference Temperature Difference for Model Case and Full-Scale Building

	Full-Scale Building	*Single Zone Air Model*	*Two-Zone Air Model*	*Full Air Model*
Q (Watts)	35,000	500	1,000	2,000
A (m^2)	1,800	2.16	4.32	8.64
rho (kg/m^3)	1.2	1.2	1.2	1.2
c_p	1007	1007	1007	1007
g	9.8	9.8	9.8	9.8
Beta (1/K)	0.0033	0.00314	0.00314	0.00314
H (m)	15	1.2	1.2	1.2
ΔTref (°C)	**0.083**	**0.997**	**0.997**	**0.997**

7.1 Buoyancy-Driven Ventilation Results

The results for the three buoyancy-driven ventilation experiments, single zone, two zone and full model, are presented along with the comparisons to the numerical simulations.

7.1.1 Single Heated Zone Case

The simplified model with a single heated zone connected to the atrium was investigated using only the lower windows initially, and then using only the upper windows. This allowed viewing the effect of window location on the flow patterns and resulting temperature distribution within the heated zone. The physical model was then created as a CFD simulation using PHOENICS. The single heated zone model was evaluated for temperature distribution, air flow rate through the model, and heat loss through the envelope. The temperature distribution was evaluated in both the heated zone and within the atrium space. Additional temperature measurements were recorded at the inlet and outlet conditions.

The measured temperature data within the physical model provided insight into the influence of window location on the internal temperature distribution. The data for the upper windows open case and lower windows open case were compared using the situation with seven windows and three stacks open for each case in Figure 45 through 47 below. The data recorded from the physical model were non-dimensionalized and scaled for use in predicting the full building temperatures. The full building temperatures and corresponding height within the space are presented, using 20°C as the ambient conditions for the full building case. At the column, located at the edge of the heated zone where it connects to the atrium, the temperature distribution was similar for both the upper and lower window case (Figure 45). This was similar to the atrium temperature distribution, shown in Figure 47, where the location of inlet windows did not significantly affect the temperature stratification. The maximum temperature difference between the upper and lower window measurements for both the scaled column and atrium measurements was 0.13°C.

In the heated zone, the temperature patterns were somewhat different between the upper and lower window locations. When the upper windows were used, the temperature measurement closest to the floor and ceiling were higher than for the lower window case at the mid-point of the heated zone, where the vertical temperature measurements were taken. For the lower window experiments, the temperatures within the heated zone were very similar for the upper four points, and then increased closer to the floor, which was located 3 cm above the heated aluminum plate. The maximum temperature difference of 0.45°C occurred at a height of 1.1m (9.5cm as measured in the model) from the floor.

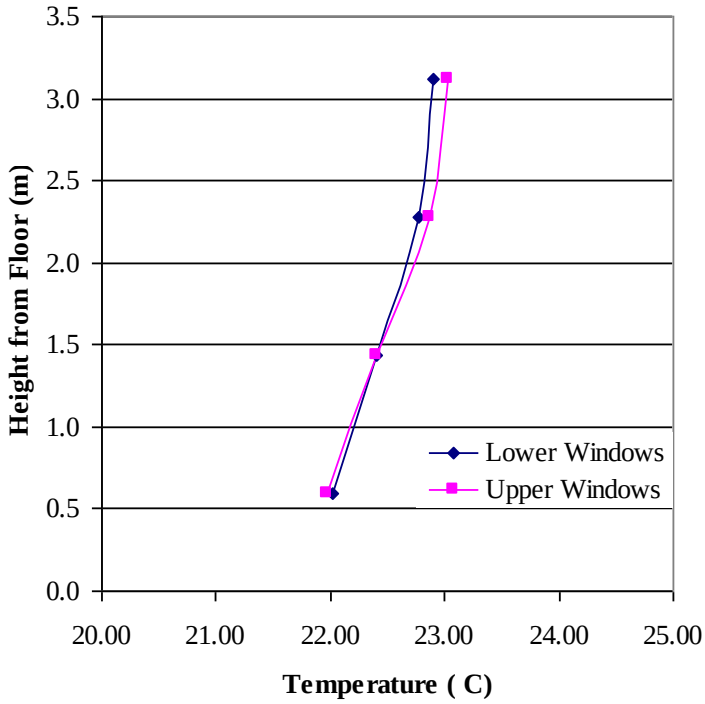

Figure 45. Single Zone Scaled Temperature Distribution Scaled for Full Building, Seven Window, Three Stack Open Case: At Column

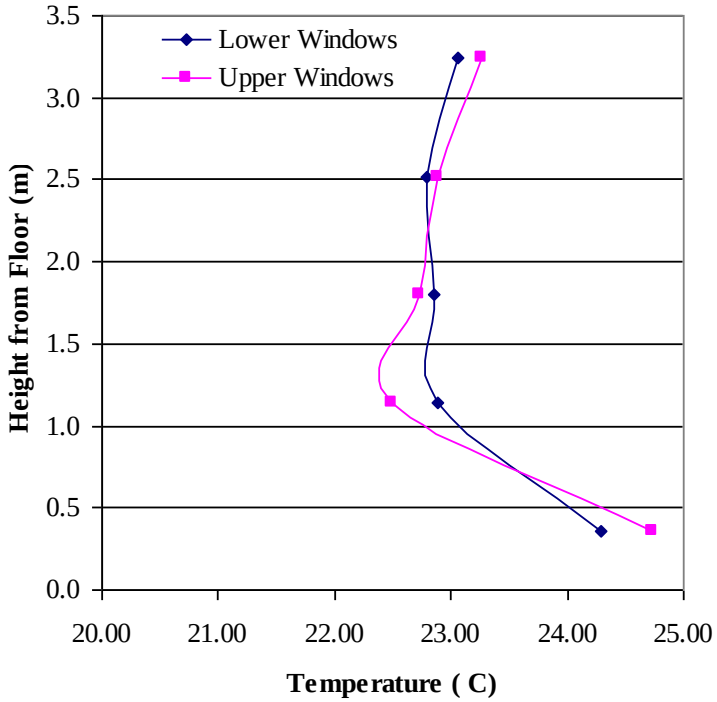

Figure 46. Single Zone Scaled Temperature Stratification Scaled for Full Building, Seven Window, Three Stack Open Case: In the Middle of the Heated Zone

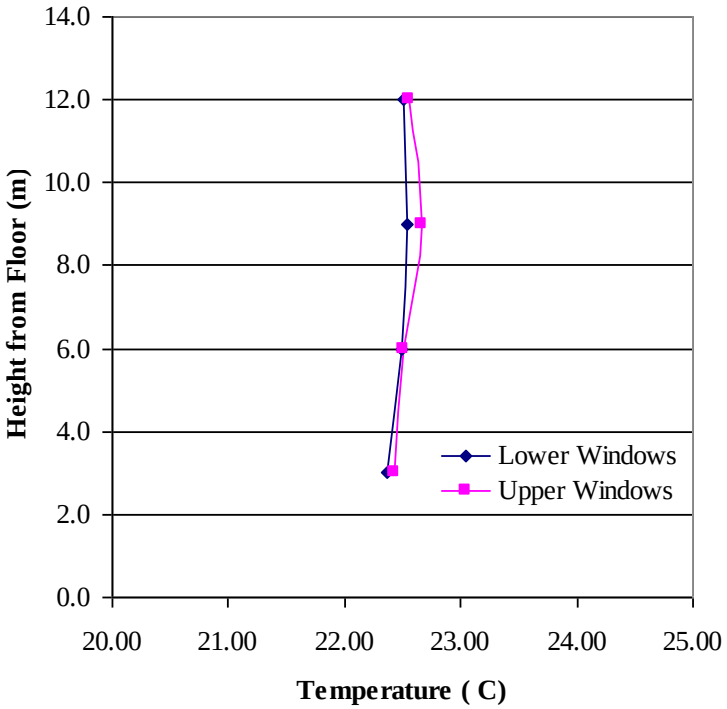

Figure 47. Single Zone Scaled Temperature Stratification Scaled for Full Building, Seven Window, Three Stack Open Case: In Atrium

Additional data for the single zone temperature measurements are provided in Appendix B. Experiments were carried out for a variety of cases where the number of windows and stacks open was changed. In general, as the number of windows and stacks decreased, the internal temperatures increased, but the temperature distribution remained similar at the column and within the atrium. However, in the heated zone the temperature stratification changed, in part due to the reduced airflow through the heated zone and in part due to the location of the vertical temperature measurements. The thermocouples were located in between two windows, and mid way between the window façade and the atrium, not fully within a jet from the window inlet. With decreased window openings, if the thermocouple location was not near the incoming air jet, then the temperatures were higher and not influenced by the incoming air stream.

Inlet and outlet velocity measurements were recorded for the single heated zone case. The measured velocity did not vary significantly between the experiments with the upper windows or lower windows. The velocity measured was due to buoyancy-driven flow, and as there was little height difference between the two windows, little variation in velocity measurements was expected. The variation between the two measurements is less than 15 percent, and may be associated with error due to the sensitivity of the hot-wire anemometer used.

With the inlet and outlet velocity measurements along with the inlet and outlet temperature measurements, the heat loss due to advection, or airflow through the model, was calculated. An energy balance around the model is written as:

$$Q_{input} = \rho V A_O \Delta T + U A_S \Delta T \qquad (7.4)$$

Where V is the outlet velocity, A_o is the area of the outlet, A_S is the total surface area of the model, U is the weighted average overall heat transfer coefficient of the model materials, and ΔT is the temperature difference between the outlet or exhaust temperature and the inlet temperature. The heat input, Q_{input}, equals the heat loss due to advection ($\rho V A_o \Delta T$) plus the heat loss due to conduction through the envelope ($UA_S\Delta T$). The heat loss due to advection uses the velocity and properties of air at either the inlet or the outlet measurement locations, and the temperature difference in both parts of the equation is the inlet minus the ambient temperature. For the seven windows, three-stack case, the values needed for the calculation are provided in Table 28.

Table 28. Data from the 7 Window, 3 Stack Single Heated Zone Model

	7 Windows, 3 Stacks	
	Lower Windows	Upper Windows
V_{inlet}	0.6 m/s	0.75 m/s
V_{outlet}	0.7 m/s	0.8 m/s
A_{inlet}	0.0168 m^2	0.0168 m^2
A_{outlet}	0.016875 m^2	0.016875 m^2
T_{inlet}	13°C	13°C
T_{outlet}	36.3°C	36.9°C

The theoretical flow rate, Q, was calculated and compared to the measured velocities and airflow rates for the single heated zone experiment. The theoretical flow rate was calculated using an equation for two resistances in series for a simple model:

$$Q = c_d A_1 \sqrt{\frac{gH\left(1 - T_o / T_i\right)}{\left[\frac{A_1}{A_2}\right]^2 + 1}} \qquad (7.5)$$

where A_1 is the inlet area, A_2 is the outlet area, and c_d is the discharge coefficient, 0.6 for sharp edged orifices. The comparison of measured flow rates, Q, and theoretical flow rates, Theory Q, that do not account for the heat loss through the envelope, are presented in Table 29.

Table 29. Air Velocities and Flow rates for Several Cases

	7 Windows			*5 Windows*			*2 Windows*		
# of Stacks	3	2	1	3	2	1	3	2	1
V_{inlet} (m/s)	0.6	0.7	0.9	0.4	0.5	0.8	0.4	0.5	0.6
V_{outlet} (m/s)	0.7	0.8	1	0.4	0.6	0.7	0.3	0.4	0.5
Measured Q (m^3/s)	0.0101	0.0118	0.0151	0.0068	0.0068	0.0039	0.0051	0.0045	0.0028
Theory Q (m^3/s)	0.0096	0.0079	0.0042	0.0066	0.0057	0.0037	0.0033	0.0030	0.0026

For the 7 window, 3 stack case, two-thirds of the heat loss was due to advection, while the remaining one-third was due to heat conduction through the envelope of the model. As the number of openings decreased, the interior temperature in the model increased, and the percentage of heat loss through the envelope increased.

Table 30. Percentage of Heat Loss through Advection for Various Window and Stack Configurations for Single Zone Model

	7 windows (0.0168 m^2)	*5 windows (0.012 m^2)*	*2 windows (0.0048 m^2)*
3 stacks (0.016875 m^2)	74.57%	73.45%	71.98%
2 stacks (0.01125 m^2)	59.84%	67.05%	63.08%
1 stack (0.005625 m^2)	39.02%	44.04%	41.71%

In the three stacks case, the outlet area was always greater than the inlet area, causing the inlet area to restrict the airflow. In the single stack case, it was the outlet area that restricted the flow for the 3 window through 7 window cases. Only when one opening area was significantly smaller than the other was a reduction in airflow apparent, as in the 7 windows, 1 stack case.

The numerical models created to simulate the experimental case for the single heated zone model provided information on some of the limitations with the PHOENICS software package. Initial runs of the simulation modeled the reduced-scale air model, using the exact dimensions and interior heat loads (heaters) as the physical model. However, as discussed in Chapter 4, there is no conduction through the envelope of the model in PHOENICS. This was apparent in the initial run when the resulting numerical model had much higher internal temperatures than observed in the experimental model. Surface temperature measurements were recorded for the single zone model, and the resulting heat loss through the main surfaces of the model determined. It was found that the main heat loss was through the atrium walls, as much as 69 percent of the total heat loss in some cases. The heat losses due to conduction through the model envelope for the physical model are presented in Table 32.

The heat losses were calculated using the surface temperatures measured on the exterior of the model, the floor and ceiling temperatures on the interior of the model, and air temperatures in each interior zone and the air surrounding the model (the ambient air). The material properties obtained from ASHRAE 2001 Fundamentals were used to calculate an overall heat transfer coefficient for each separate wall construction. Two wall constructions were identified and the heat transfer coefficient and surface area determined (Table 31). From the heat transfer coefficient, surface area and temperature measurements, the relative heat loss for each surface was calculated.

Table 31. Material Properties and Surface Areas for Heat Loss Calculation

Materials	*U-Value (W/m^2K)*	*Total Surface Area (m^2)*	*Location*
1-layer Insulation board, MDF	0.38	7.2	All Walls, and Atrium
1-layer Insulation board, MDF, batt-insulation	0.37	5.2	Ceiling and Floor

The atrium had the most surface area, primarily due to the north wall, and accounted for 34 percent of the total surface area. However, the floors and ceilings of the heated zone were better insulated, and so contributed less to the overall heat loss for the model.

Table 32. Conduction Heat Loss for Single Heated Zone Model for Various Cases

	Heat Loss W/m^2	*Total Heat Loss* *W*	*Atrium Heat Loss*	*Percent Heat Loss thru Atrium*
7Window 1Stack	23.36	290.93	90.78	31.2%
7Window 2Stack	14.66	182.65	80.18	43.9%
7Window 3Stack	8.62	107.39	69.16	64.4%
5 Window 1Stack	21.28	265.10	92.83	35.0%
5 Window 2Stack	11.81	147.12	80.39	54.6%
5 Window 3Stack	8.62	107.40	73.12	68.1%
2 Window 1Stack	22.11	275.34	98.64	35.8%
2 Window 2Stack	13.30	165.66	85.26	51.5%
2 Window 3Stack	9.81	122.17	80.02	65.5%

The heat loss due to conduction through the envelope had to be accounted for in the CFD simulations, since as much as 60 percent of the heat loss was due to conduction in the 7 window, 1 stack case. As it was determined that most of the heat loss occurred in the atrium, the CFD model was modified to account for heat loss through the atrium walls as a negative heat flux. By adjusting the CFD model to account for the conduction issues found in the single heated zone model, the resulting data for the numerical models were comparable to the experimental ones.

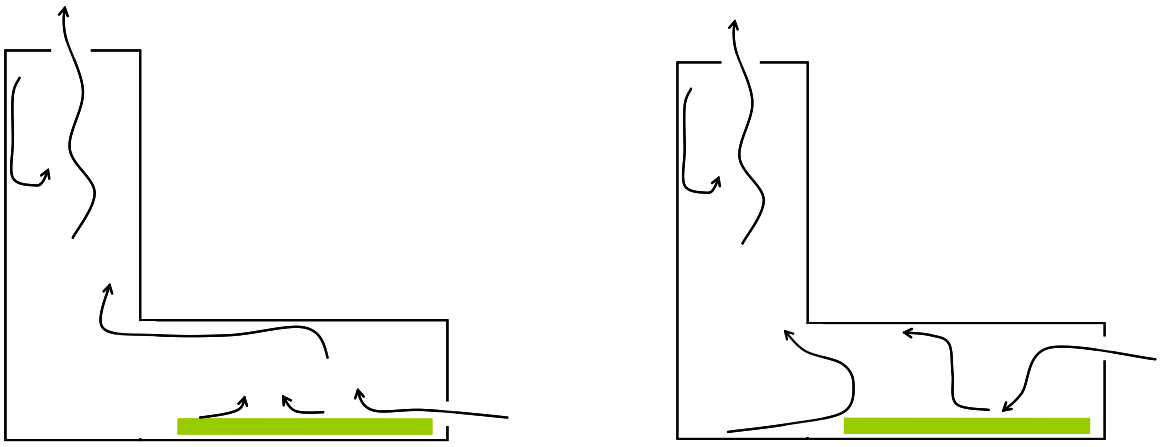

Figure 48. Airflow Patterns for Single Heated Zone Case from Airflow Visualization in the Model: a) Lower Windows, b) Upper Windows

The location of the windows influences the temperature distribution in the heated zone, as was shown in the experimental and CFD models. The airflow, as measured by inlet and outlet velocities, is not impacted significantly by the small height difference between the lower and upper windows. However, the total size of the inlet and outlet openings does affect the interior temperature and airflow; restrictive openings caused a higher internal temperature, leading to reduced heat loss due to airflow and increased heat loss due to conduction through the envelope. The heat loss modeled using PHOENICS (Figure 49) showed the impact of the prescribed heat loss at the atrium walls. The overall temperature was reduced by a scaled full building temperature of approximately 0.5°C.

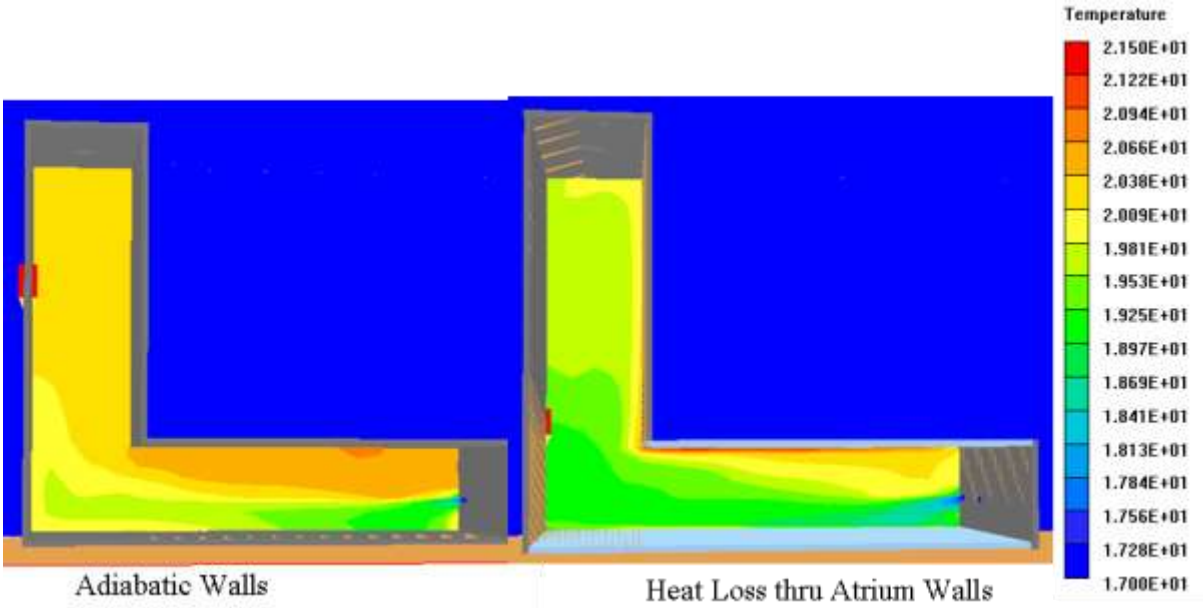

Figure 49. Comparison of Single Zone CFD Model without and with Heat Loss through Atrium Walls

A CFD simulation was also created to evaluate the influence of the working fluid used on the resulting flow pattern. The single zone case was used due to its simplicity and the ability to calibrate the CFD model with existing data. Data were provided for a single-zone, reduced-scale water model of a similar configuration of a single heated zone connected to an atrium. However, the reduced-scale water model was not geometrically similar to the reduced-scale air model. These data were used to validate a CFD model with the geometry of the original water model, and then the CFD model was modified to be geometrically similar to the reduced-scale air model. The ideal air model simulation was used, with no heat loss through the envelope. The resulting temperature distribution is provided in Figure 50. The temperatures have been scaled using the reference temperatures, so that they are comparable. The inlet jet at the window dissipated quite differently for the two fluids. The jet in the air model spreads along the floor of the heated zone, reaching the far end of the atrium wall, while the inlet jet in the water model just reaches the junction between the heated zone and the atrium. The temperature stratification patterns within the heated space also differ with the working fluid used. The warm fluid in the heated space permeates lower into the heated zone in the air model than in the water model, due to the differences in thermal properties of each fluid.

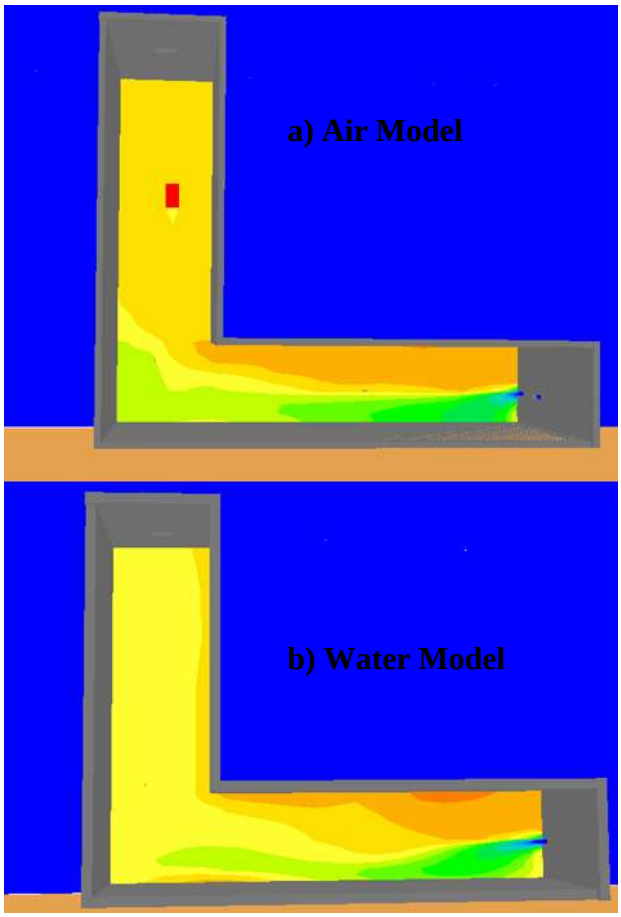

Figure 50. Comparison of Reduced-Scale a) Air Model and b) Water Model[3] at a Window Opening

7.1.2 Two Heated Zone Case

As described in Chapter 6, with the two heated zone case, temperature and velocity measurements were recorded for experiments with the stacks open and with the stacks closed. The temperature stratification in each heated zone, at the column for each level where the heated zone connected to the atrium, and within the atrium were measured for comparison.

In the two heated zone experiments, the lower windows were used for both the ground floor and first floor heated zones. The number of stacks open was varied, from three stacks open to all three stacks closed. This affected the entering and exiting air velocities and resulting temperature distribution in both the heated zones and within the atrium. The air velocity measured using the hot-wire anemometer and resulting airflow through the inlet and outlet openings are presented in Table 33. The air velocities presented are the average of all the velocities measured at each window for a given floor level. A schematic of the airflow patterns for the stacks open case is shown in Figure 51.

[3] Data provided by S. Livermore, BP Institute, Cambridge University. December 2004.

Table 33. Two Heated Zone Velocity and Airflow Data Summary

	ground floor windows	*first floor windows*	*stacks*	*airflow in*	*airflow out*
1 Stack Open	0.5 m/s	0.15 m/s	-0.9 m/s	0.00932 kg/s	0.00806 kg/s
2 Stacks Open	0.6 m/s	0 m/s	-0.8 m/s	0.01119 kg/s	0.00978 kg/s
3 Stacks Open	0.7 m/s	0.15 m/s	-0.7 m/s	0.01585 kg/s	0.01305 kg/s
Stacks Closed	1.0 m/s	-1.0 m/s	---	0.02060 kg/s	0.01680 kg/s

* negative values indicate outflow

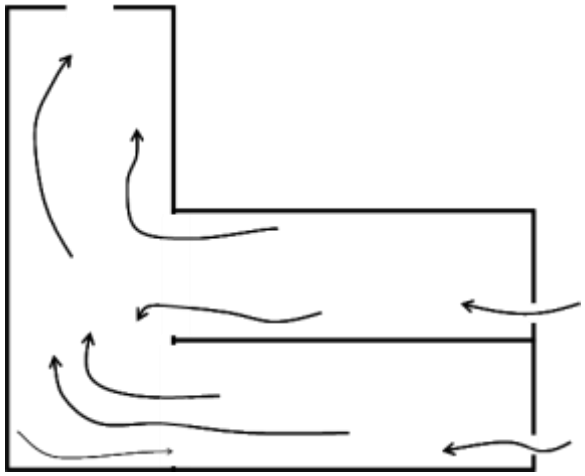

Figure 51. Two-Zone Stacks Open Airflow Patterns

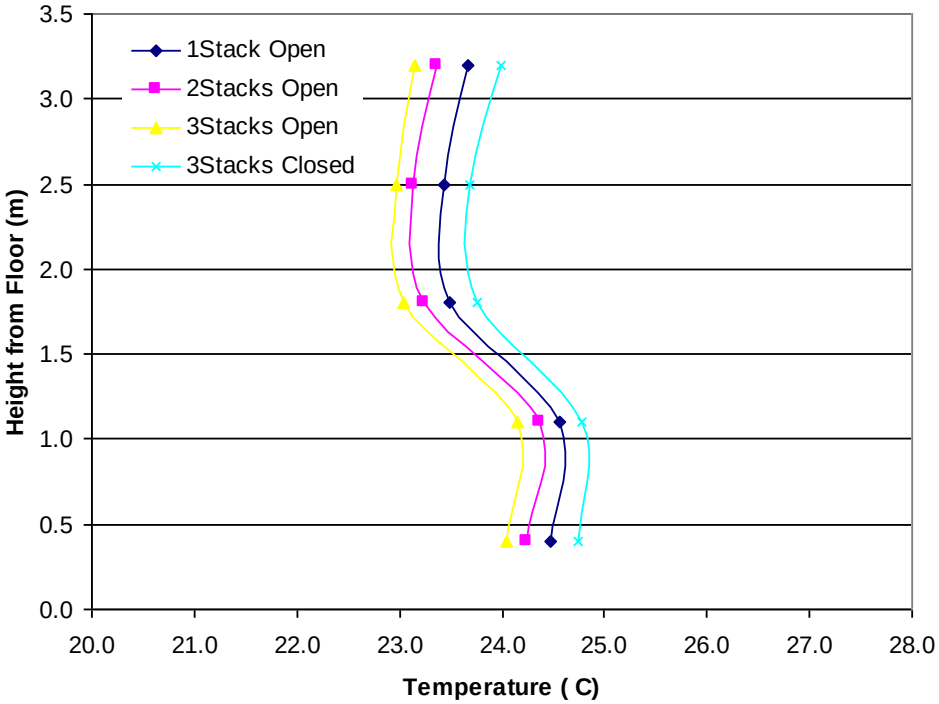

Figure 52. Two Zone Scaled Temperature Stratification for Full-Scale Building: Ground Floor Heated Zone

The temperatures measured in the heated zone of the ground floor exhibited similar temperature patterns, though the smaller the outlet opening sizes the higher the overall temperatures in the heated zone (Figure 52). As seen in Table 33, the air entered through the windows at the ground floor level in all four cases investigated. The thermocouple locations closest to the heated aluminum plate had the highest temperatures for each case. There was some amount of radiation at the ceiling, as seen by the slightly increased temperatures at the upper-most thermocouple location.

At the column measuring locations for the ground level, the temperature pattern for each case was more linear than was seen in the heated zone (Figure 53). The thermocouple closest to the floor recorded the lowest temperature for all four cases. As mentioned previously, the most significant heat loss occurred in the atrium, as was evident in the thermocouple reading near the floor. The cooler air from the atrium was drawn into the edge of the heated zone closest to the atrium at the floor level. The atrium floor and exposed walls also have the largest heat loss, which contributes to the slightly cooler temperatures of the air that is in close proximity. The temperature closest to the ceiling for all four cases was the highest and caused by a hot plume of air from the ceiling of the ground floor. In the stacks closed case, this was slightly more prominent as all of the incoming air from the ground floor air exited at the first floor level. This caused the hot plume of air from the ground floor zone to exit the ground floor zone at the ceiling and then proceeded to enter the first floor zone at the floor level.

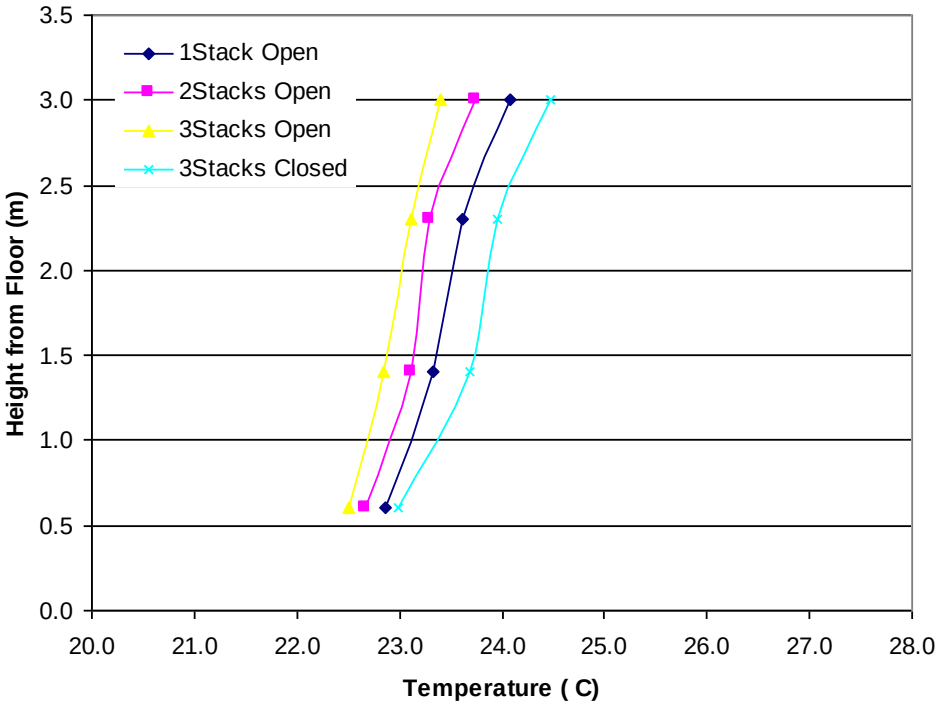

Figure 53. Two Zone Scaled Temperature Stratification for Full-Scale Building: Ground Floor Column

For the first floor heated zone (Figure 54), the temperature distribution pattern was similar for the three cases. Again, as the number of stacks open decreased, the internal temperature

distribution remained the same, but the overall temperature increased. The thermocouples closest to the floor recorded the coolest temperature for all four cases. For the two and three stacks open cases this was due to the incoming ambient air at 13°C. However, for the one stack open case there was essentially no incoming or outgoing flow through the first floor windows. The temperature stratification was then due to warm, still air at the ceiling level in addition to some amount of radiation from the heaters. The warm temperatures near the floor were not seen in the first floor case, as the two-heated zone model was carried out before the installation of aluminum sheets in the upper floor areas. The thermocouples were located 12cm from the heaters, which acted more like large point sources rather than a distributed load in the heated zone. The thermocouples were therefore not as affected by any radiation from the heaters. With the stacks closed case, the air exited the model at the first floor level and the temperature at the lowest thermocouple location in Figure 53 was almost equal to the temperature of the exiting temperature from the ground floor at the ceiling.

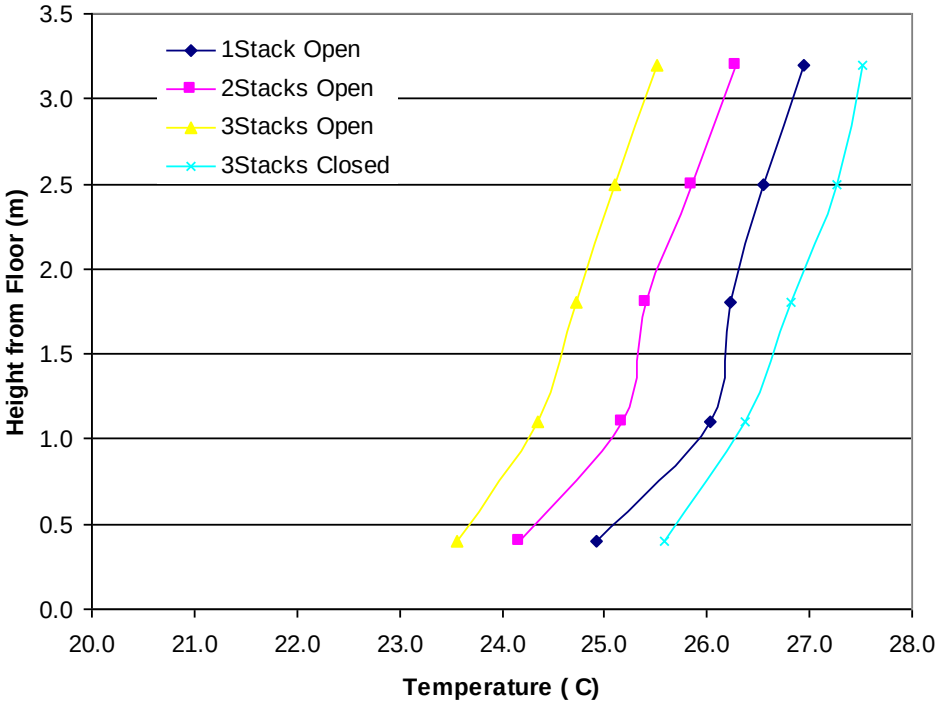

Figure 54. Two Zone Scaled Temperature Stratification for Full-Scale Building: First Floor Heated Zone

As seen in Table 33 and discussed above, for the 2 and 3 stacks open cases the air entered at the first floor level. All of the air from the first floor for these cases exited the first floor, mixed with air from the ground floor in the atrium, and was exhausted through the stacks. By the time the air reached the column, it was well mixed for the three stacks open case, and less so for the two stacks open case (Figure 55). Similar to the ground floor, the top thermocouple for the first floor column consistently recorded a higher temperature, due to a hot air plume in the 2 and 3 stacks open cases. For the 1 stack open and stacks closed cases, the temperature distribution at the column was essentially linear, as there was no inflow at the first floor windows.

In the atrium of the two heated zone model, there were definite temperature stratification patterns caused by the number of stacks open (Figure 56). With the three stacks open case, the atrium temperatures in the lower half of the atrium (where the heated zones connect to the atrium) were similar, only varying by approximately 0.25°C. However, the upper half of the atrium was well mixed at a higher temperature than the lower half. As the number of open stacks decreased, the well-mixed portion of the atrium extended lower into the atrium. With no inlet or outlet airflow for the 1 stack open case at the first floor, it was assumed that the neutral plane occurred approximately at the height of the window in the first floor within the model. This corroborated with the atrium temperature measurements, as the temperatures at and above the second floor level did not vary. With the stacks closed case, when the airflow was out of the first floor windows, the neutral plane occurred approximately at the floor level of the first floor and then the temperature was uniform above that point.

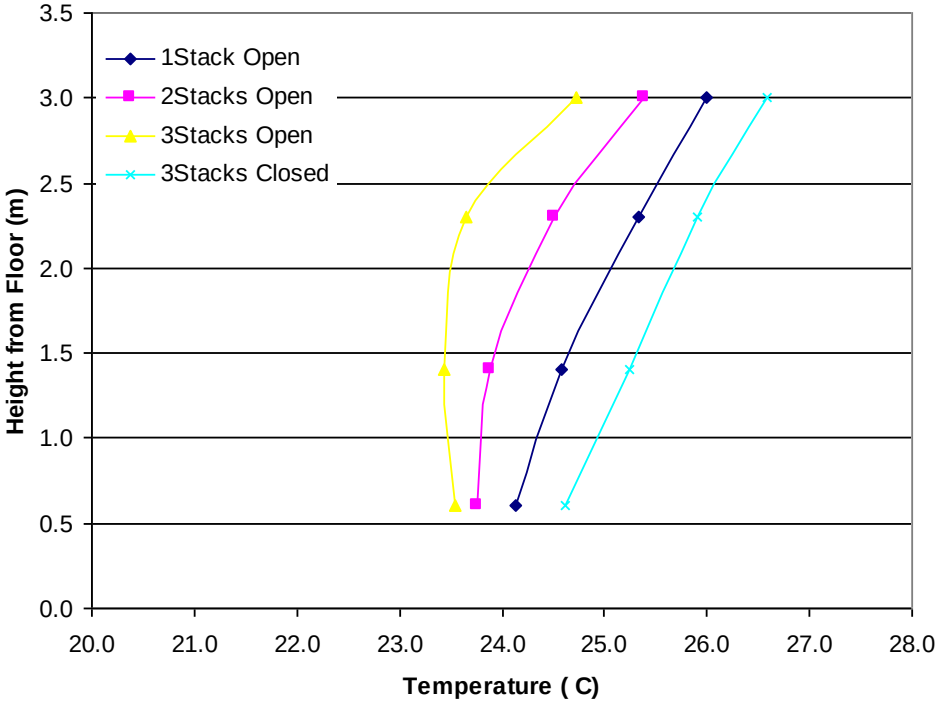

Figure 55. Two Zone Scaled Temperature Stratification for Full-Scale Building: First Floor at Column

The experimental results from the physical model provided information into the behavior of airflow patterns and temperature distributions when the number of outlet openings was decreased, thereby decreasing the overall outlet area. By limiting the number of variables, using only the lower windows for the ground floor and first floor, the influence of the stack openings was determined to be significant in the airflow at the first floor windows. When the stacks were closed, the air exited at the first floor windows; when one stack was open there was virtually no airflow in or out of the first floor windows; with 2 or 3 stacks open there was inflow of ambient air.

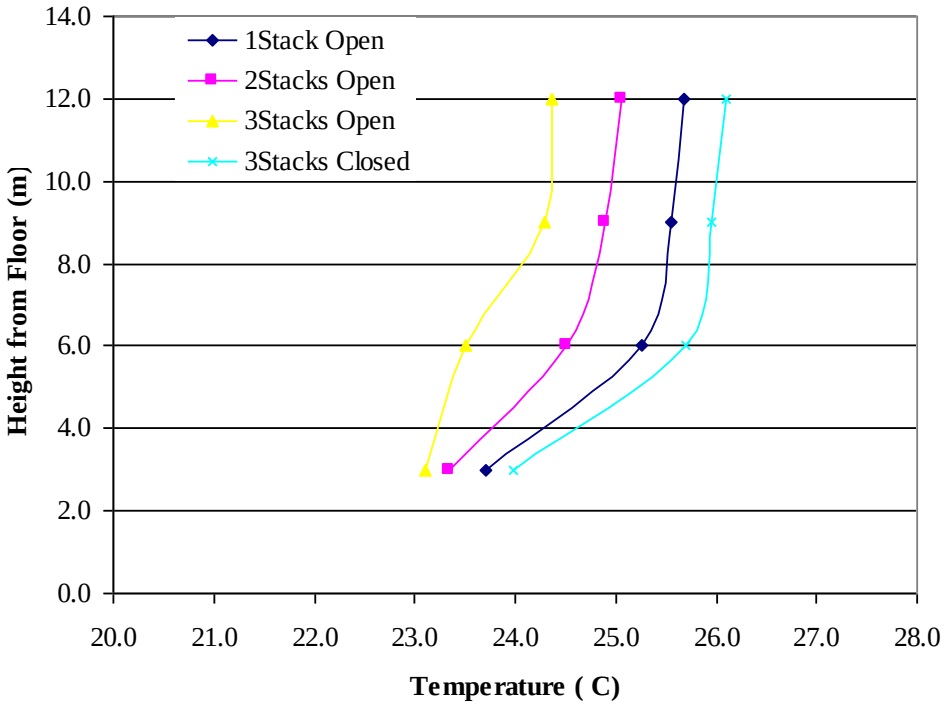

Figure 56. Two Zone Scaled Temperature Stratification for Full-Scale Building: In Atrium

7.1.3 Full Model Case

With the full model case using four heated zones, the interactions between the zones for cases with all of the stacks open, one stack open, and all of the stacks closed were investigated using both the physical model and numerical simulations.

The thermocouples were located at the columns for each level and within each heated zone. For the buoyancy-driven case, whether or not the stacks were open or closed influenced the location of the neutral plane within the model. This in turn affected the airflow patterns and direction of airflow at the first floor upper windows. When any of the stacks were open, the air flowed in both sets of windows at the ground floor level, and in both sets of windows at the first floor level for both the north and south façades. Air exited through both sets of windows at the second floor level and through the stacks at the roof of the atrium, as shown in Figure 57. In the case where all three stacks were closed, air still entered both sets of windows at the ground floor level, and exited both sets of windows at the second floor level. However, at the first floor level, the air entered the lower set of windows at both the north and south façades and exited the upper set of windows at both façades.

Table 34. Measured Air Velocities for Full-Model Stacks Open and Stacks Closed Cases

		Stacks Open Velocity	*Stacks Closed Velocity*
Ground	Upper Window	0.69 m/s	0.54 m/s
	Lower Window	0.74 m/s	0.67 m/s
First South	Upper Window	0.13 m/s	-0.18 m/s
	Lower Window	0.42 m/s	0.32 m/s

First North	Upper Window	0.17 m/s	-0.15 m/s
	Lower Window	0.42 m/s	0.42 m/s
Second	Upper Window	-0.31 m/s	-0.5 m/s
	Lower Window	-0.23m/s	-0.40 m/s
Stacks		-0.70 m/s	---

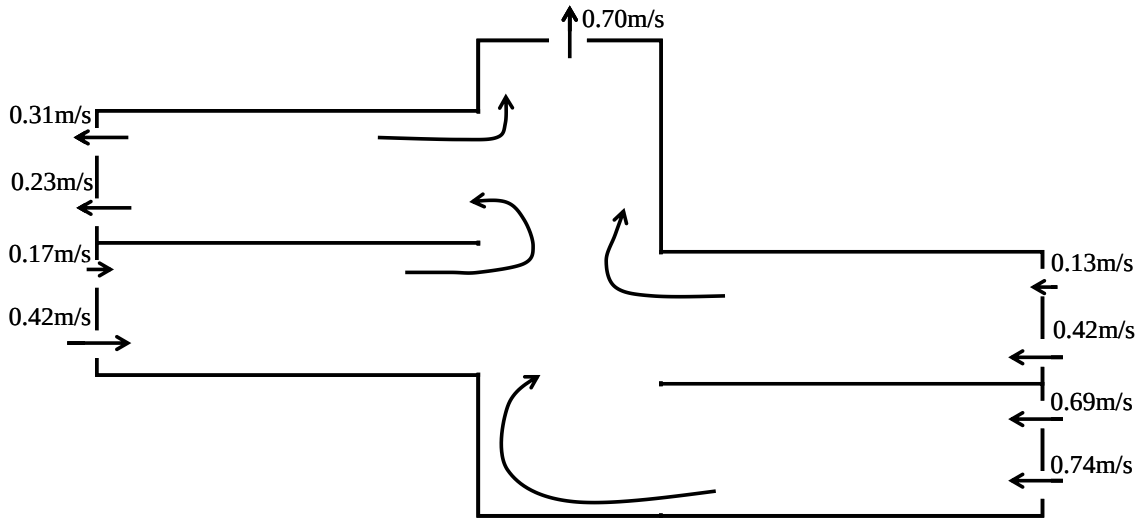

Figure 57. Airflow Patterns and Velocities for Stacks Open Case

At the ground floor level, the thermocouple closest to the floor in the heated zone (Figure 58) recorded the warmest temperature since it is within 2cm of the heated aluminum plate. The temperatures were slightly cooler in the mid-height of the heated zone and then warmer at the ceiling level. The cooler temperatures at mid-height were due to the inflow of ambient air at approximately 17°C, while the warmer temperature at the ceiling were caused in part by radiation to the ceiling and subsequent convection to the air near the ceiling . The maximum temperature differential from floor to ceiling measured in the heated zone for the ground floor level was 1.7°C. The difference in temperatures for the same location between the stacks open and stacks closed case at the same location was 0.1°C. At the column, the temperature stratification pattern was similar for the three cases presented (Figure 59). The lower three thermocouples were at virtually the same temperature, while the upper-most thermocouple had a 0.5°C temperature increase as compared to the lower thermocouples. The air from the ground floor heated zone rose in the space and exited at the ceiling level into the atrium, in close proximity to the top thermocouple location at this point.

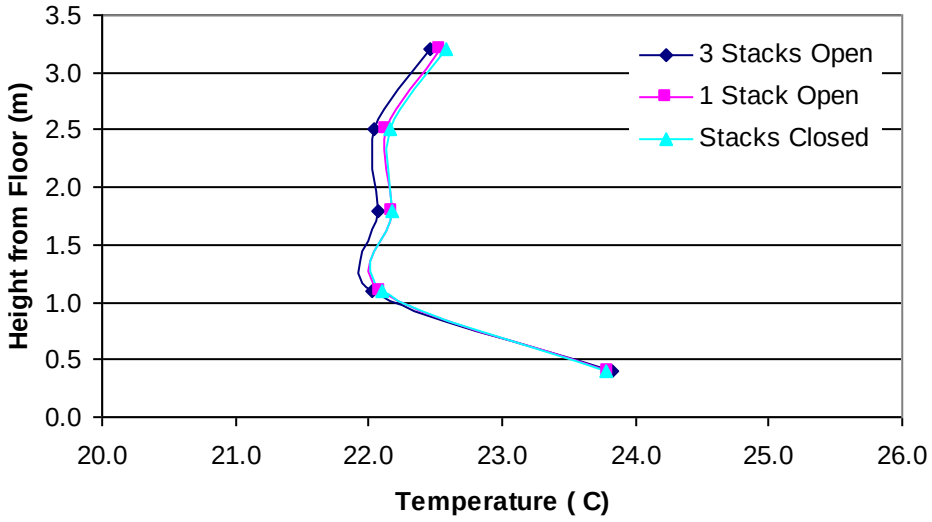

Figure 58. Full Model Scaled Temperature Stratification for Full-Scale Building: Ground Floor Heated Zone

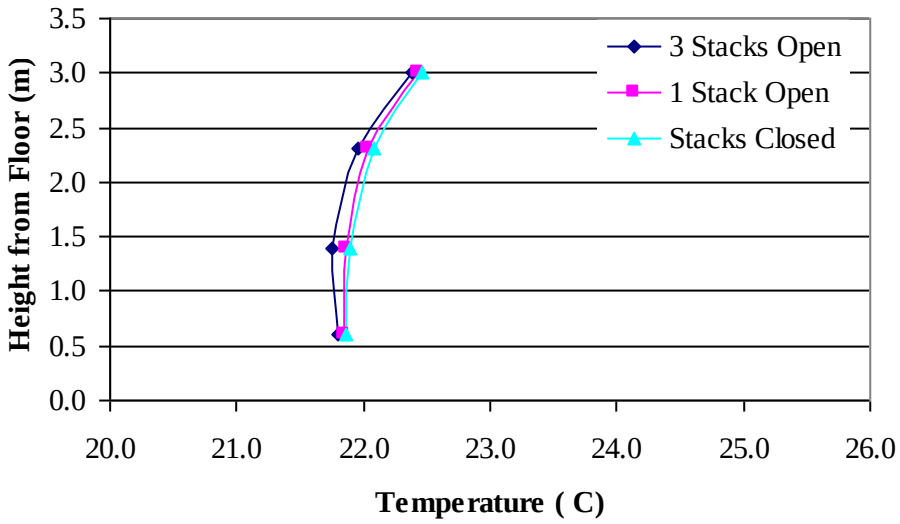

Figure 59. Full Model Scaled Temperature Stratification for Full-Scale Building: Ground Floor at Column

At the first floor level, there was variation between the north and south sides of the building, both at the column measurement locations and within each heated zone. Some differences between the north and south halves of the first floor were expected because the two zones on each side of the model were not exactly opposite from one another. The first floor south side has a heated zone below, with a small amount of heat transfer through the floor from the ground level. Additionally, there is a warm plume that exited the ground floor heated zone at the ceiling and partially entered the first floor heated zone. The temperature of the air at the air at the top of the ground floor column, 22.5°C, was equal to the measured temperature at the floor location of

the column at the first floor south. On the other hand, the first floor north side had insulation and ambient air below the floor level. On the south side, the lower two thermocouples at the column were at essentially the same temperature, but the upper two thermocouples were almost 1°C higher (Figure 60). This was caused by the warm air rising within the heated zone and some of the warmer air leaving at the ceiling level. Within the heated zone, the cooler air entered near the floor level and was slowly heated as it traversed the heated zone. The same heated floor as seen in the ground floor level was not apparent in the first floor heated zones (Figure 61) because of the location of the thermocouples with respect to the heaters and aluminum plates. At the ground floor there was an aluminum plate that covered 90 percent of the floor of the heated zone. However, on the first floor, there were two plates that were located toward the edges due to their weight, and the thermocouples measuring the temperature stratification within the heated zone on the first floor south side was located at the edge of one of the aluminum plates, and not directly above it as with the ground floor.

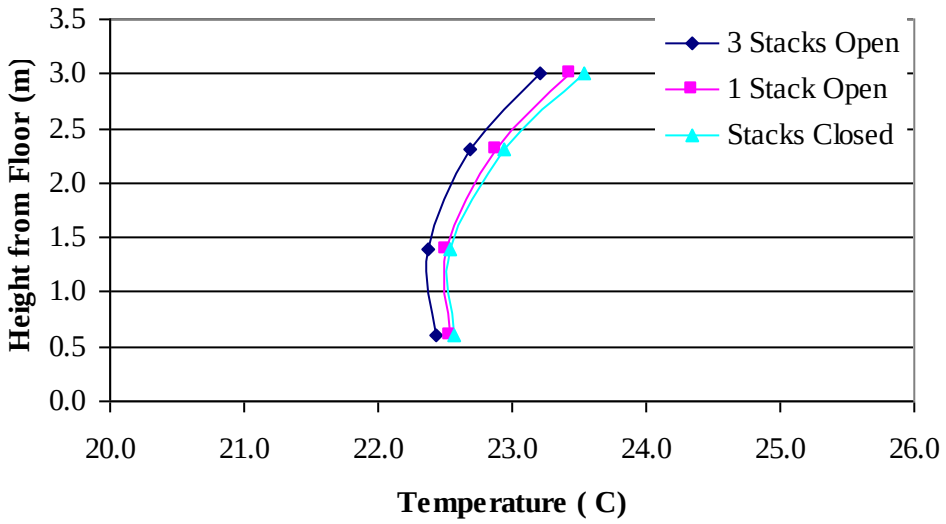

Figure 60. Full Model Scaled Temperature Stratification for Full-Scale Building: First Floor South at Column

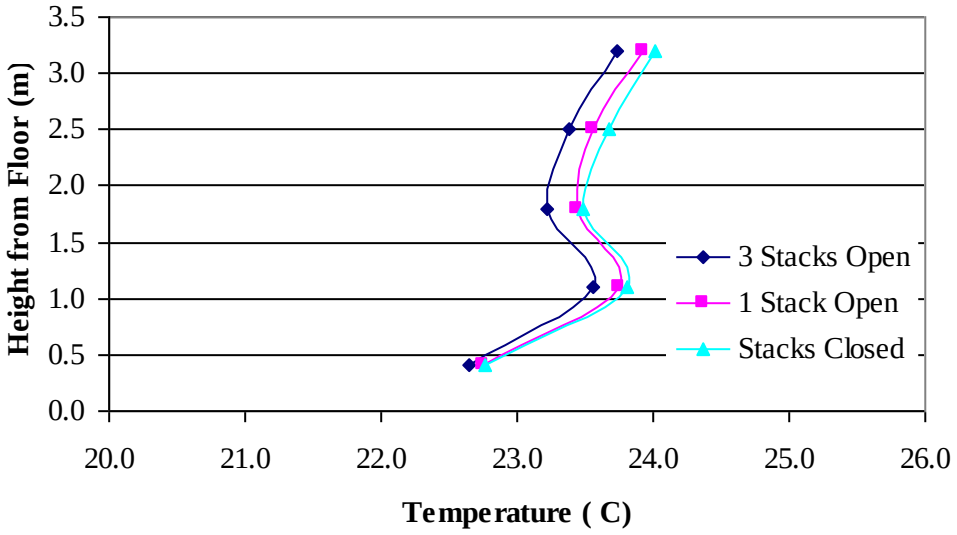

Figure 61. Full Model Scaled Temperature Stratification for Full-Scale Building: First Floor South Heated Zone

At the north side of the first floor, the temperature measurements at the column were slightly different than those for the south first floor level. The lower three thermocouple measurements were very similar in all three cases presented, while the upper-most thermocouple had a 1.2°C temperature increase above the other three points (Figure 62). The same pattern followed for all of the cases presented. The warm temperature at the ceiling was due to airflow from the first floor north that rose and exited either through the stacks (in the stacks-open cases) or through the second floor windows (in the stacks closed cases). The small amount of airflow that exited the upper window at the first floor level in the stacks closed case did not influence the warm air at the first floor north near the atrium. In the heated zone at the first floor in the north half of the model the measured temperatures were cooler near the floor due to incoming air, as was seen on the south side of the first floor. However, on the north side at mid-height in the heated zone the temperatures were higher due to the airflow patterns in the space. Some air entered from the atrium into the first floor north zone and was warmed by the heaters in the space (Figure 63).

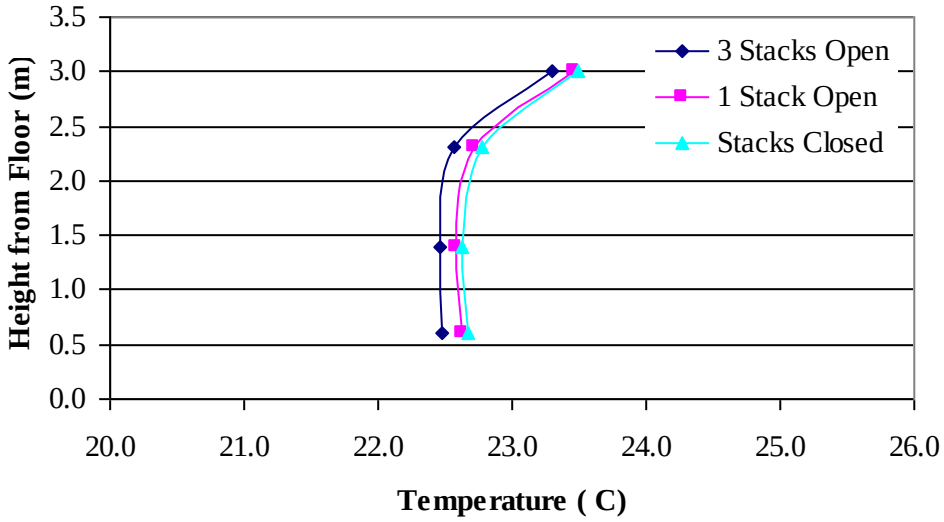

Figure 62. Full Model Scaled Temperature Stratification for Full-Scale Building: First Floor North at Column

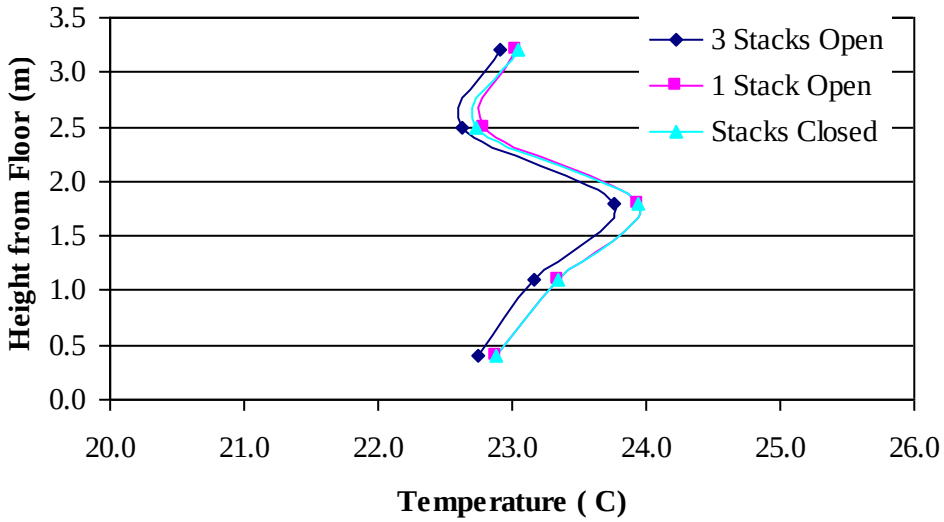

Figure 63. Full Model Scaled Temperature Stratification for Full-Scale Building: First Floor North Heated Zone

Though attempts were made to locate the thermocouples in the same location relative to windows, the longer windows in the north façade made it difficult to locate the vertical temperature measurements between two windows. On the south half, the thermocouples measuring the vertical temperature stratification were located at the edge of the incoming jet flows from the windows, whereas on the north half the thermocouples were located more towards the center of the window jet. This affected the temperature measurements for the north half of the model, but was unavoidable due to the size and location of the windows.

The second floor was always the warmest location during the experiments, as air exited through both sets of windows at the second floor level in the three cases presented. The measurements recorded at the second floor also had the largest variation between the stacks open and stacks closed cases, of 0.4°C. Overall, the temperature varied 1.5°C from floor to ceiling in the second floor-heated zone. At the second floor column, the highest temperatures occurred at the ceiling, due to air exiting through the stacks in the stacks open case and due to the warmer air in the top section of the atrium entering the heated zone at the second floor and influencing the top thermocouple in the stacks closed case (Figure 64). In the heated zone (Figure 65), warm air from lower floors spilled into the second floor level at the floor. Additionally, even with the stacks open case, some warm air from the atrium entered into the second floor-heated zone, causing more warm air to enter just below the ceiling level. The complex airflow patterns and interactions of the second floor-heated zone with the atrium affected the temperature distribution in that space (Figure 66 and Figure 67).

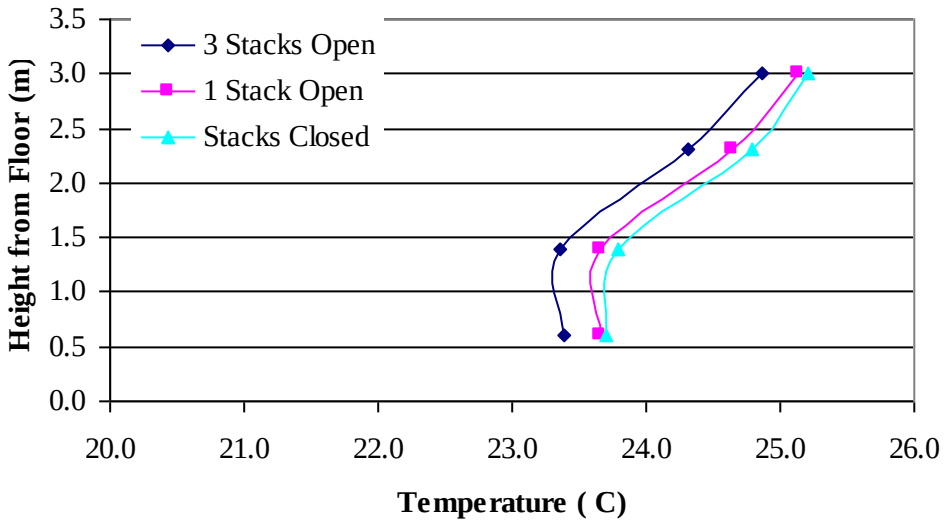

Figure 64. Full Model Scaled Temperature Stratification for Full-Scale Building: Second Floor at Column

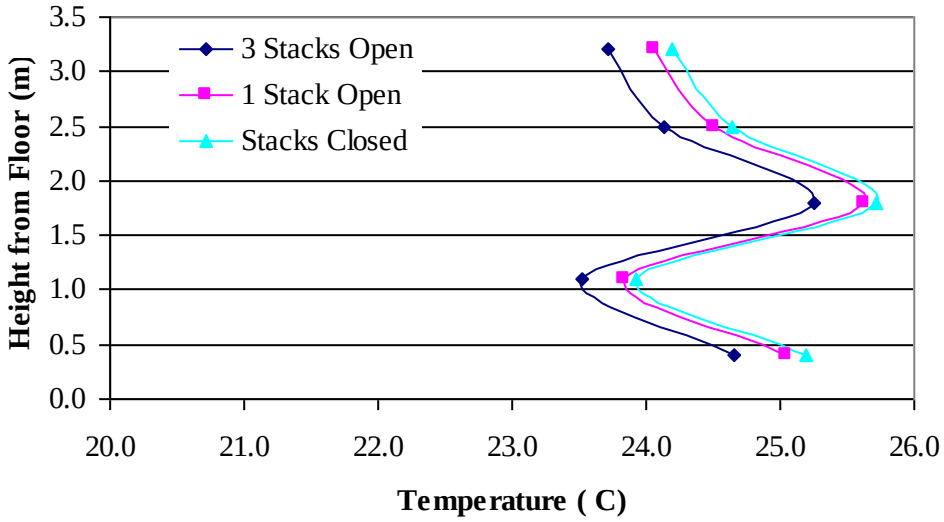

Figure 65. Full Model Scaled Temperature Stratification for Full-Scale Building: Second Floor Heated Zone

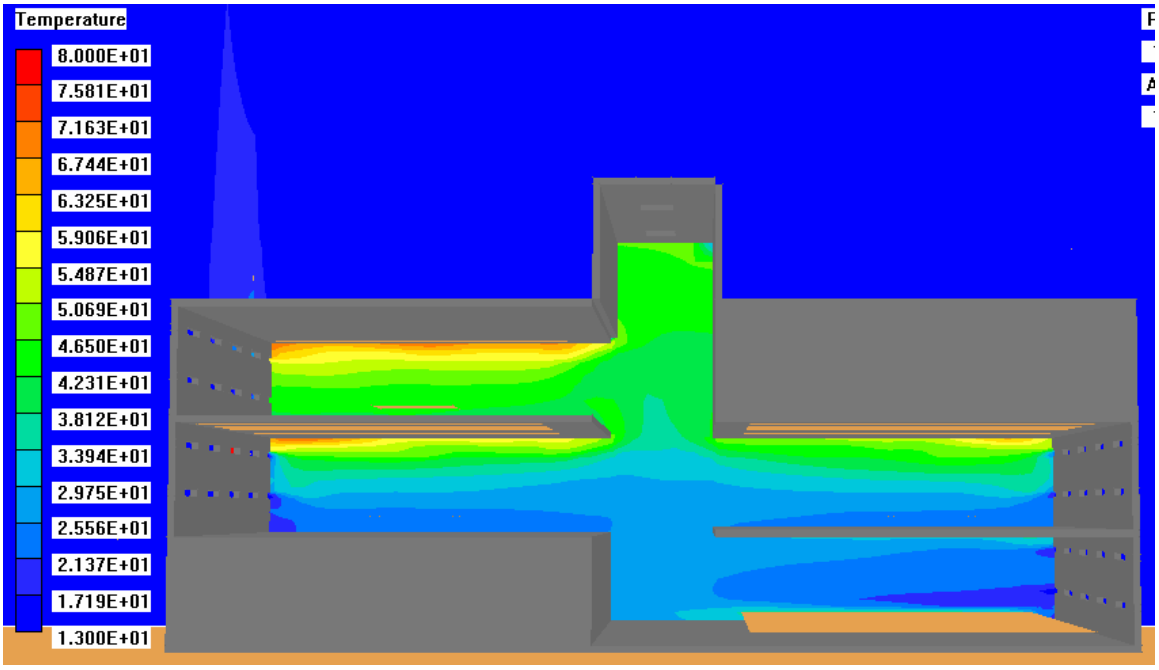

Figure 66. Temperature Distribution for Buoyancy Case: Full Model with Stacks Open

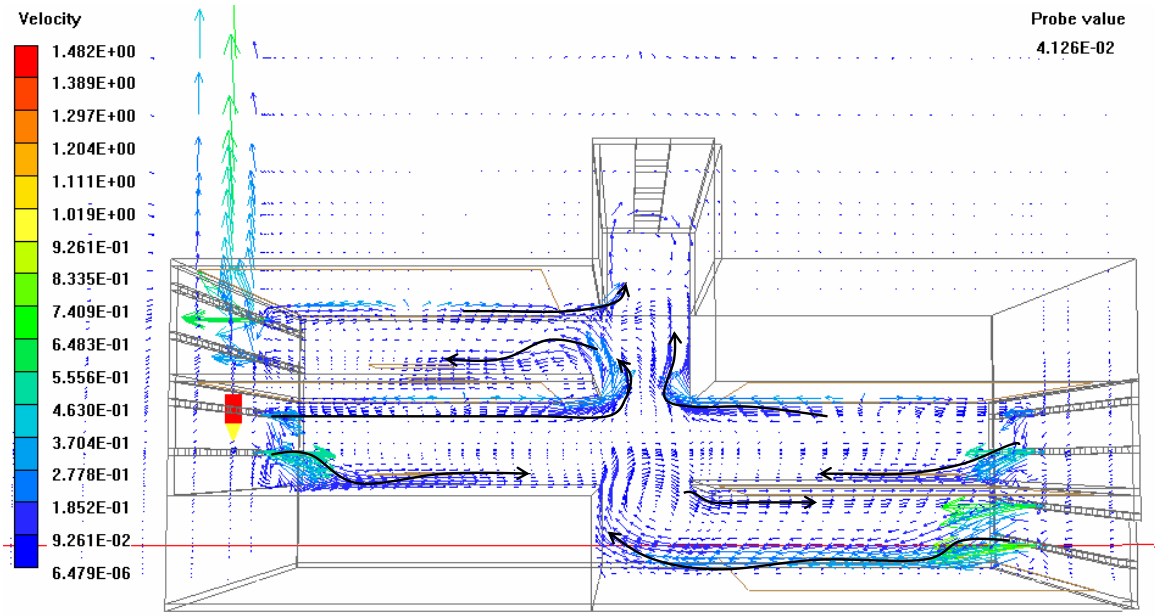

Figure 67. Airflow Patterns for the Buoyancy Case: Full Model with Stacks Open

7.2 Wind-Driven Ventilation Results

The experiments on the physical and CFD models were carried out for a range of wind speeds, both with and without the use of the heaters for the internal loads. The wind-only cases are presented first for the full-model configuration with either all of the stacks open or all closed. The inlet velocities and outlet velocities were measured and airflow balance calculated.

7.2.1 Wind-Only Case

Conducting the wind-only cases before the addition of internal heat loads assisted in the understanding the air velocities caused by wind alone. Experiments were carried out using a variety of fan speeds, simulating external wind conditions. The stacks were set to either all open or all closed for each of the fan speeds to determine how much wind exited through the stack vents when they were open.

The focus of the wind-only experiments was determining the inlet velocity at the windows on the south façade and the resulting outlet velocities on the north façade and at the stacks for the stacks open scenarios. Using the wind device described in Chapter 6, the model was evaluated at five different wind speeds. The inlet velocities were recorded at 5 m/s at fan setting 3, 4 m/s at fan setting 2, and 3 m/s at fan setting one. Further experiments were carried out at lower fan settings using a Variac® that reduced the voltage provided to the fans. Measurements were recorded at two additional points, at fan setting 1 with the Variac® at 83% and at fan setting 1 and the Variac ® set at 57%. This provided air velocities of 2 m/s and 1 m/s respectively. The inlet velocities were uniform across the south façade of the model as measured at the face of the window, and at all of the inlet windows. The measurements between windows deviated by ±0.1m/s, which was the measurement error of the hot-wire anemometer used. The airflow balance was determined by calculating the inflow volume of air, minus the outflow volume of air, divided by the inflow volume of air. The maximum percentage error in the airflow balance

was less than 12 percent. These values, along with the measured velocities for the wind-driven flow experiments are presented for the stacks closed case in Table 35 and for the stacks open case in Table 36. When the stacks were closed, the only location of outflow of air was at the northern façade. The inlet windows on the south façade were smaller in size than the outlet windows on the north façade. The inlet windows were 2 cm tall by 12 cm long, whereas the outlet windows were 2 cm tall by 17 cm long. There were an equal number of windows on the north and south façades.

Table 35. Average Inlet and Outlet Velocities for Wind-Driven Case: Stacks Closed

	Setting 3	*Setting 2*	*Setting 1*	*Setting 1-83%*	*Setting 1-57%*
Window Inlet	5.1 m/s	4.0 m/s	2.9 m/s	2.0 m/s	1.0 m/s
Window Outlet	3.2 m/s	2.6 m/s	1.8 m/s	1.3 m/s	0.7 m/s
Airflow Balance	10.6%	7.4%	11.6%	7.4%	0.2%

Table 36. Average Inlet and Outlet Velocities for Wind-Driven Case: Stacks Open

	Setting 3	*Setting 2*	*Setting 1*	*Setting 1-83%*	*Setting 1-57%*
Window Inlet	5.1 m/s	4.1 m/s	3.0 m/s	2.0 m/s	1.0 m/s
Window Outlet	2.8 m/s	2.3 m/s	1.7 m/s	1.1 m/s	0.6 m/s
Stack Outlet	3.1 m/s	2.2 m/s	1.9 m/s	1.0 m/s	0.5 m/s
Airflow Balance	6.5%	6.6%	3.3%	9.1%	1.9%

The air entered through all of the window openings on the south façade at the same velocity, and exited the north façade with uniform velocity. In the stacks open scenario, approximately 85 percent of the air exited at the north façade and the remaining 15 percent of the air exited through the stack openings. This was consistent over the range of wind velocities used for the wind-only case.

7.2.2 Combined Wind-Buoyancy Driven Case

The addition of heaters to mimic the internal loads to the wind cases resulted in a combined wind-buoyancy airflow. The heaters were left on at full strength, while the speed of the fans was adjusted, from 5 m/s down to 0.5 m/s. Both temperature measurements and inlet and outlet velocity measurements were recorded and an airflow balance calculated.

The wind speeds that were utilized in the wind-only cases were used in the combined wind-buoyancy case. However, with these inlet velocities the wind-driving force dominated the airflow. So reduced fan speeds were used to achieve wind speeds at the inlet windows on the south façade of 2 m/s, 1 m/s, 0.7 m/s and 0.5 m/s. The measured inlet and outlet air velocities for the stacks open case are presented in Table 37. As the inlet air velocity decreased, the percentage of air exiting through the stacks increased. This is shown graphically in Figure 68, where the dashed lines represent the buoyancy case for reference. For the stacks closed case, all of the entering air from the south façade where the wind device is located exited through windows located on the north façade. When there is no wind present, under pure buoyancy-driven flow, a greater percentage of the outflow exits through the stacks. As the applied wind speed increases, the percentage of outflow that exits through the stacks decreases.

Table 38 lists the average exit velocity for the range of inlet velocities for the stacks closed experiments. As the wind speed at the south façade decreased, the distribution of exiting air velocities on the north façade displayed distinct variations from first floor to second floor, and even between the two sets of windows (upper and lower) at each floor level. This occurred for both the stacks open and the stacks closed cases, as presented in Table 39.

Table 37. Air Measurements: Combined Wind-Buoyancy Stacks Open Case

		5 m/s	*4 m/s*	*3 m/s*	*2 m/s*	*1.5 m/s*	*1 m/s*	*0.7 m/s*	*0.5 m/s*
Inlet		5.1	4.1	3.1	2.0	1.5	1.1	0.7	0.5
Outlet	Windows	2.9	2.3	1.6	0.9	0.7	0.5	0.3	0.2
	Stacks	2.7	2.2	1.7	1.0	0.9	0.6	0.5	0.5
Airflow In (m^3/s)		0.343	0.275	0.208	0.134	0.101	0.074	0.047	0.033
Airflow Out (m^3/s)		0.323	0.257	0.182	0.115	0.083	0.060	0.038	0.028
Airflow Balance		5.7%	6.6%	12.7%	14.9%	18%	20%	20%	17%

Table 38. Air Measurements: Combined Wind-Buoyancy Stacks Closed Case

	5 m/s	*4 m/s*	*3 m/s*	*2 m/s*	*1.5 m/s*	*1 m/s*	*0.7 m/s*	*0.5 m/s*
Window Inlet	5.0	4.0	3.0	2.0	1.5	1.1	0.7	0.5
Window Outlet	3.2	2.6	1.9	1.1	0.8	0.6	0.4	0.3
Airflow In (m^3/s)	0.336	0.269	0.201	0.134	0.101	0.074	0.047	0.034
Airflow Out (m^3/s)	0.307	0.249	0.182	0.110	0.077	0.058	0.038	0.029
Airflow Balance	8.8%	7.4%	9.7%	17%	22%	22%	19%	14%

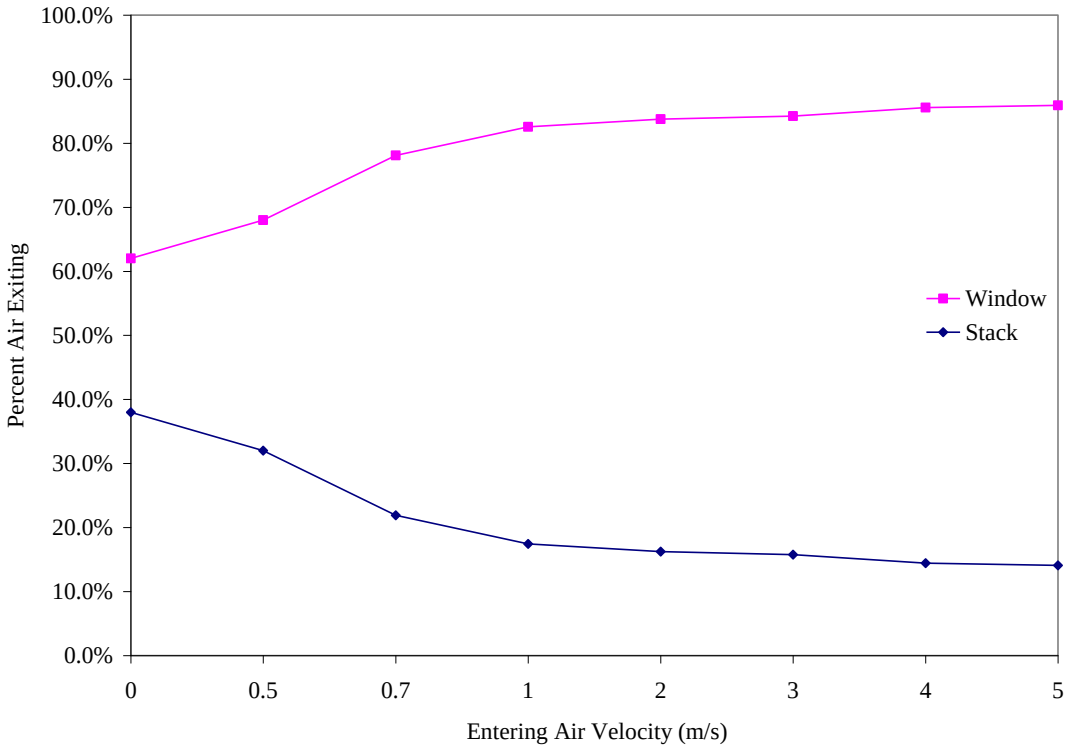

Figure 68. Percent of Air Exiting Through Stacks versus Windows for Range of Applied Wind Velocities for Combined Wind-Buoyancy Case

Table 39. Variation of Outlet Wind Velocity by Floor Level: Combined Wind-Buoyancy Cases

		Stacks Open			*Stacks Closed*		
		1 m/s	0.7 m/s	0.5 m/s	1 m/s	0.7 m/s	0.5 m/s
Window Inlet		1.1	0.7	0.5	1.1	0.7	0.5
Second Floor	Upper	0.5	0.4	0.3	0.5	0.4	0.4
	Lower	0.4	0.3	0.1	0.5	0.3	0.2
First Floor	Upper	0.5	0.3	0.1	0.5	0.4	0.3
	Lower	0.3	0.1	0.1	0.4	0.2	0.1

The three smallest wind velocities for the stacks open and stacks closed cases along with the exiting velocities at each window level showed that the exiting air velocity increased with height. This did not occur in the wind-only case, where the exiting velocities were uniform at all window heights. This difference was due to the effect of buoyancy combined with the wind flow in the model. Though not a substantial difference, only varying by 0.1-0.2 m/s per floor level, and as much as 0.3 m/s from the second floor to the first floor, the change in exiting velocity was repeatable and distinct. The simulation results illustrating the temperature distribution for the 0.5 m/s wind case are provided in Figure 69, while the airflow patterns for the same wind speed are shown schematically in Figure 70 and the CFD in Figure 71.

The scaled temperature variation was calculated using the reference temperature difference for the reduced-scale air model and full-scale prototype building, as shown in equation 7.3. The temperature stratification for the experiments showed that the stratification pattern changed based on the inlet air velocity. As shown in Figure 72 and Figure 73 for the ground floor, at the column and in the heated zone, the temperature distribution was distinct for those cases with entering air velocities above 1-1.5 m/s and those with entering air velocities below 1-1.5 m/s. At the column, there was a linear temperature variation that increased with height for the entering air velocities below 1 m/s, and was virtually constant in the 1 m/s case. For all of the other cases, at 1.5 m/s and above, the temperature variation caused a reduction in overall temperature and a decrease in the temperature difference from floor to ceiling. This demonstrated the influence of higher, wind-dominated flow on the interior temperature stratification. Within the heated zone of the ground floor, there was a reduction in overall temperature, and the temperature became increasingly uniform for a larger portion of the space as the wind velocity was increased.

At the first floor level, the cooler ambient air initially entered the model at the south façade, increased in temperature due to the heaters, and entered into the atrium space. Figure 74 and Figure 75 graphically present the temperature distribution for the south half of the first floor at the column and within the heated space. In the heated space, the temperature measurements had some minimal variation in the lower half of the space and then were consistent in the upper half of the heated zone. The similar temperatures for each case in the upper half of the heated zone indicated that the air was well-mixed within this portion of the space. The lower temperature points were due to the airflow patterns, with some amount of cooler air reaching the thermocouples at the mid-point within the heated zone remaining at the floor level. The air was slowly heated by a small but measurable amount at a location 9.5 centimeters above the floor. At the column location, the temperatures were virtually uniform from floor to ceiling, indicating a well-mixed condition. This well-mixed condition occurred for all of the wind speeds used in

the experiments. The variation at the column between the ground floor and first floor on the south side resulted from to two main factors; the addition of a railing at the first floor level and some amount of heat transfer between the ground floor and the first floor.

On the north half of the first floor, air exited at both the lower and upper windows for all of the wind speeds used in the wind-buoyancy cases. At the column, a distinct pattern between entering air velocities above 3 m/s, between 1 and 3 m/s and below 1 m/s was found (Figure 76). At the higher wind speeds, the temperatures at the column had less variation from floor to ceiling; however, for the mid-range of wind velocities the temperature measured near the ceiling was distinctly warmer than that of the lower measurement locations. At the mid-range of wind speeds, the warm air from the atrium entered the north half of the first floor, was further heated by the interior loads, and then some of the air exited back into the atrium. At the mid-way point between the atrium and the north façade, the air either moved toward the windows at the north façade and exited, or flowed toward the atrium and exited at the ceiling level of the first floor north. At the lowest wind velocities, the cooler air from the atrium entered into the first floor north zone and then was heated due to the interior loads and exited back into the atrium, as with the mid-range air velocities. However, since there was less airflow with the lower wind speeds, the air reached higher temperatures. In the heated zone of the north half of the first floor a distinct temperature pattern arose with wind velocities less than 4 m/s (Figure 77). There was some amount of heat loss through the floor of this zone, though a layer of insulation board and additional R-13 batt-insulation was installed. The temperature of the air increases due to the heaters and rises toward the ceiling. The warm air that exited back into the atrium at ceiling level was seen in the temperature measurements from the heated zone.

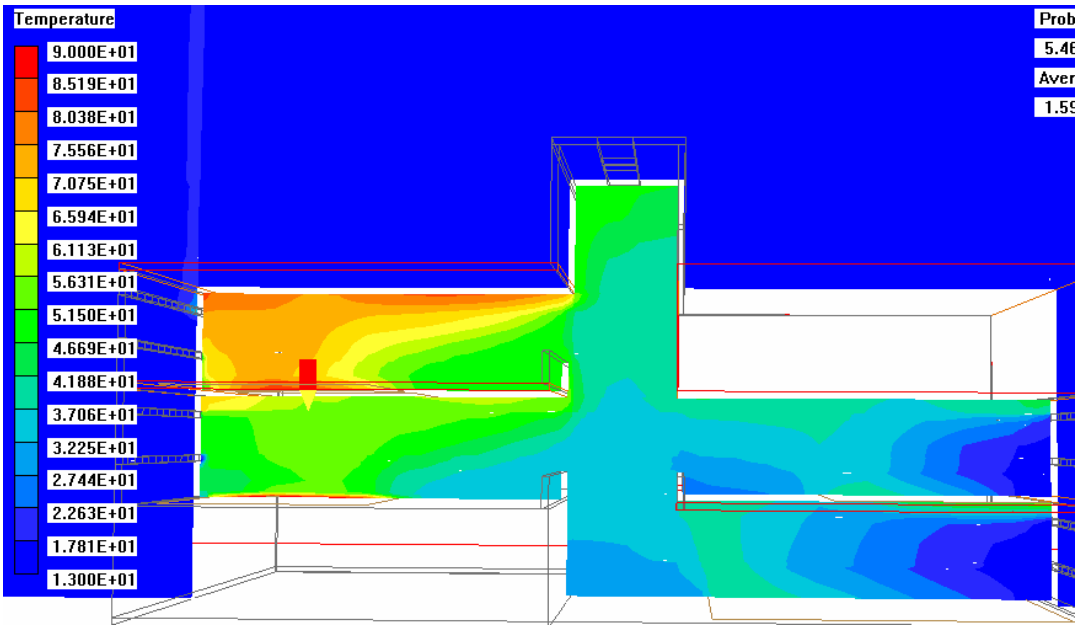

Figure 69. Temperature Distribution for Combined Wind-Buoyancy Driven Flow at 0.5 m/s

In the second floor, the temperature distribution varied noticeably with the inlet wind speeds at the column (Figure 78). At higher wind speeds, 4-5 m/s, the temperature was uniform from floor to ceiling. However, at velocities less than 4 m/s, the temperature close to the ceiling rose considerably. For the lower two measurement locations at wind speeds at or below 1.5 m/s, the

temperature of the air was the same as the temperature leaving the south half of the model. This implied that some of the air from the atrium entered the second floor and warmer air exited at the ceiling level. The data presented are for the stacks open case, which explains why there was significantly warmer air at the ceiling measurement point. In the heated zone, the temperature pattern was similar for all of the wind speeds used (Figure 79). For each case, cooler temperatures were recorded at the mid-height of the heated zone. The actual temperature corresponded to the temperature of the exiting air from the ground and first floor south zones. Since there were no heating loads in the atrium space, the air exiting the south zones was driven into the two zones on the north half of the model by the wind force. The air from the atrium spilled over the railing into the heated zones on the north half of the building, while warmer air exited at the ceiling level for both floors (Figure 69). Airflow visualization carried out for several different wind speeds verified this explanation for the temperature variation in the heated zone (Figure 70) as did the CFD simulations (Figure 71). In Figure 77 and Figure 79, the coolest air temperatures correspond to the exiting air temperatures from the south half of the model, where the wind-driven air is entering the model. However, the heat sources at the floor and some amount of radiation to the ceiling causes the thermocouples near the floor and ceiling to record higher temperatures. Some of the cooler air enters into the first floor north half of the model over the railing, causing cooler temperature measurements near the floor. There is some amount of jet flow, introducing the cooler air at the mid-height of the space. These flow patterns were visible with the airflow visualization technique and also provided with the CFD simulations.

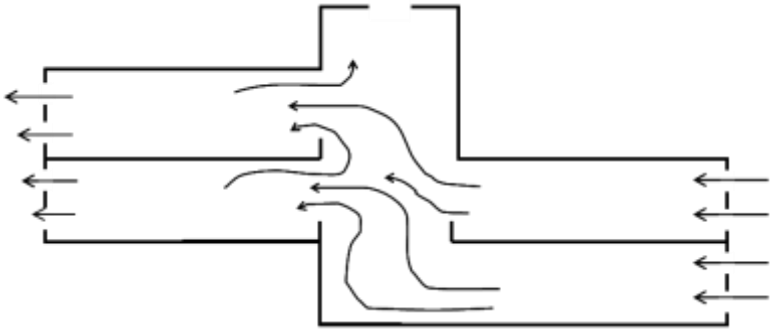

Figure 70. Airflow Patterns for Reduced-Scale Air Model with Stacks Open: Combined Wind-Buoyancy Case

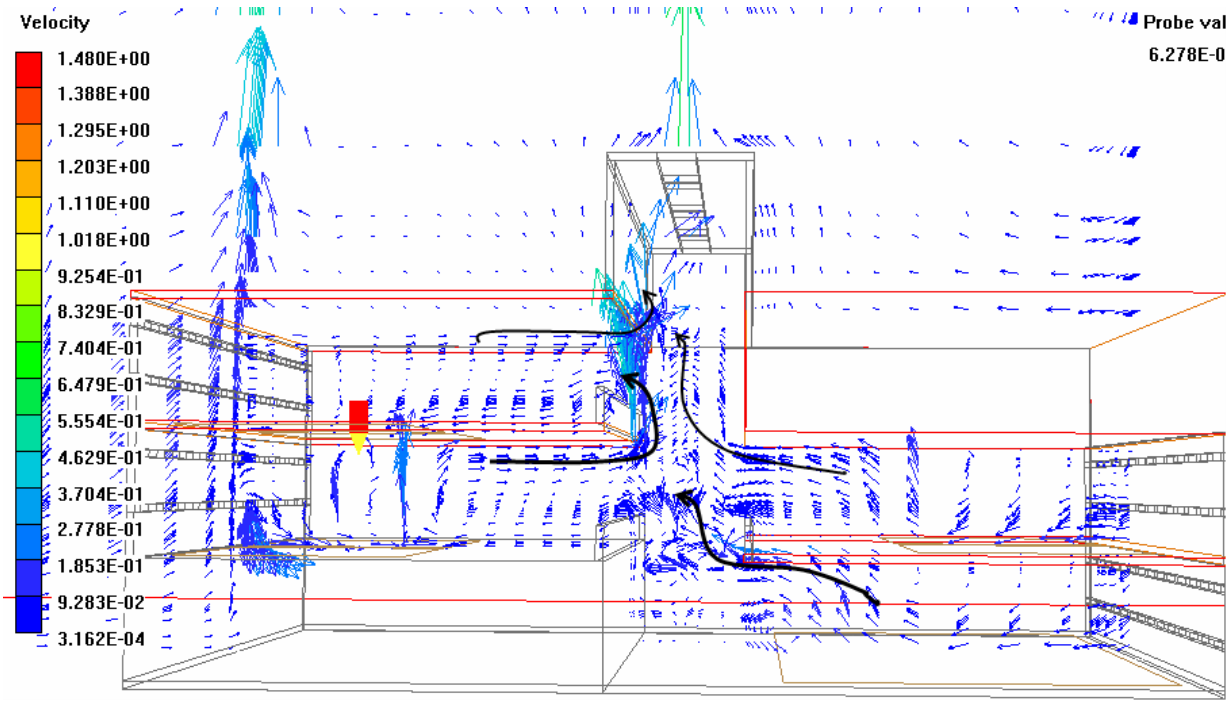

Figure 71. Airflow Patterns for Combined Wind-Buoyancy Driven Flow at 0.5 m/s

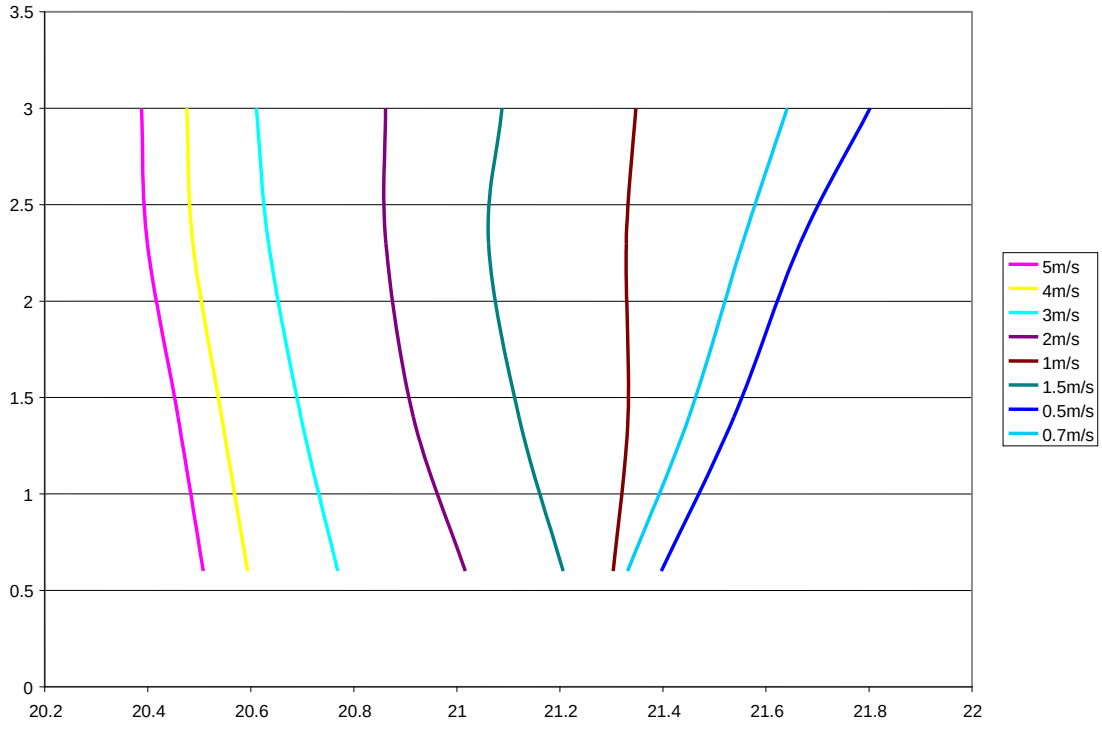

Figure 72. Combined Wind-Buoyancy Full Model Ground Floor Scaled Temperature Stratification at Column

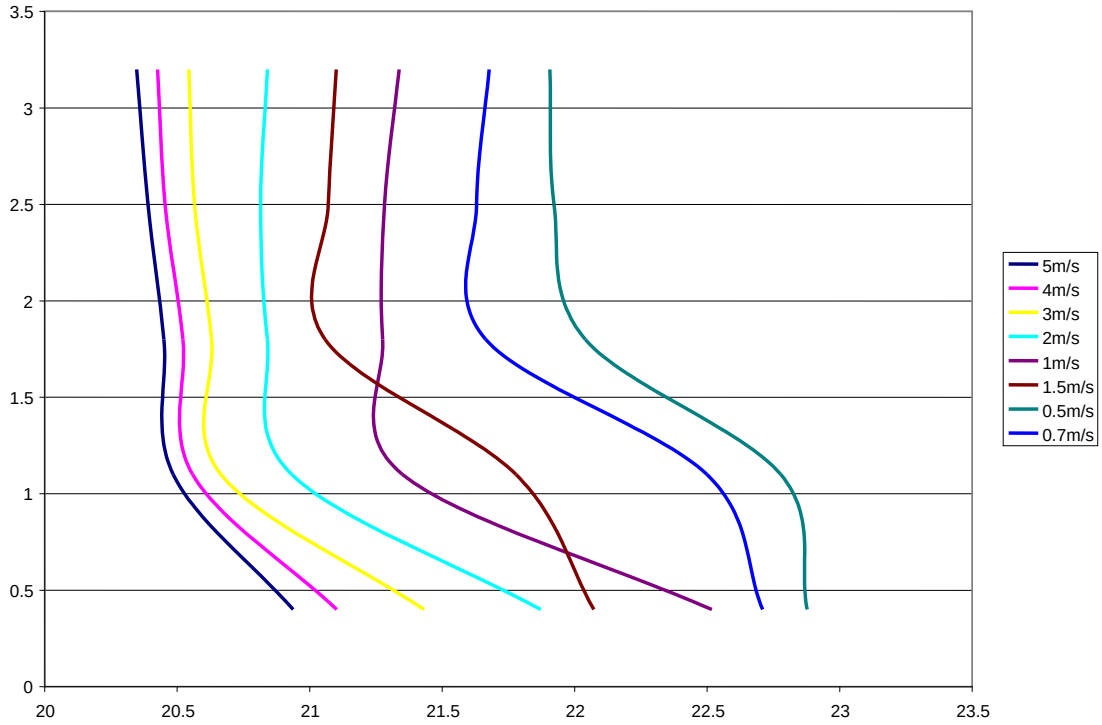

Figure 73. Combined Wind-Buoyancy Full Model Ground Floor Heated Zone Scaled Temperature Stratification

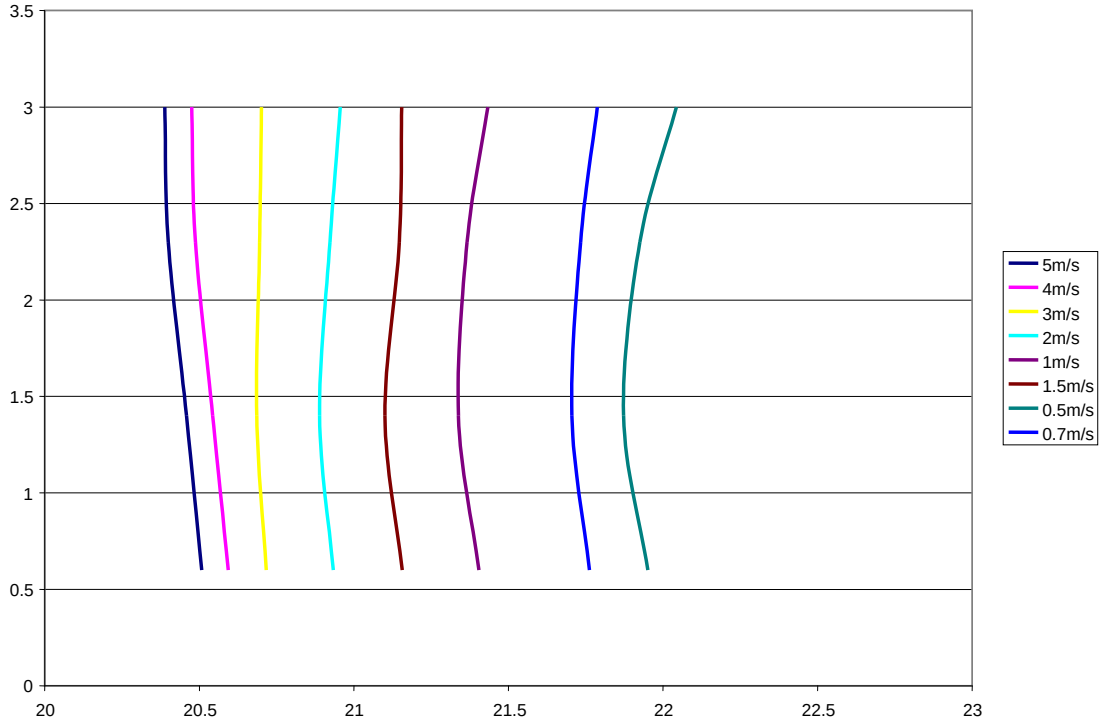

Figure 74. Combined Wind-Buoyancy Full Model First Floor South Scaled Temperature Stratification at Column

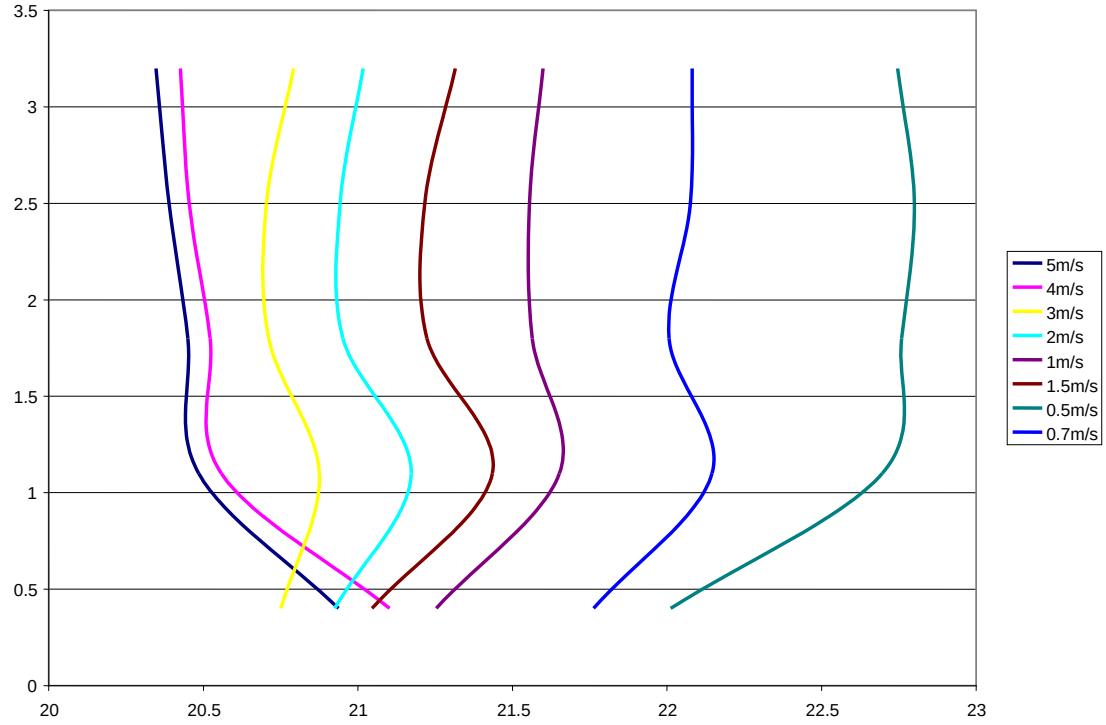

Figure 75. Combined Wind-Buoyancy Full Model First Floor South Heated Zone Scaled Temperature Stratification

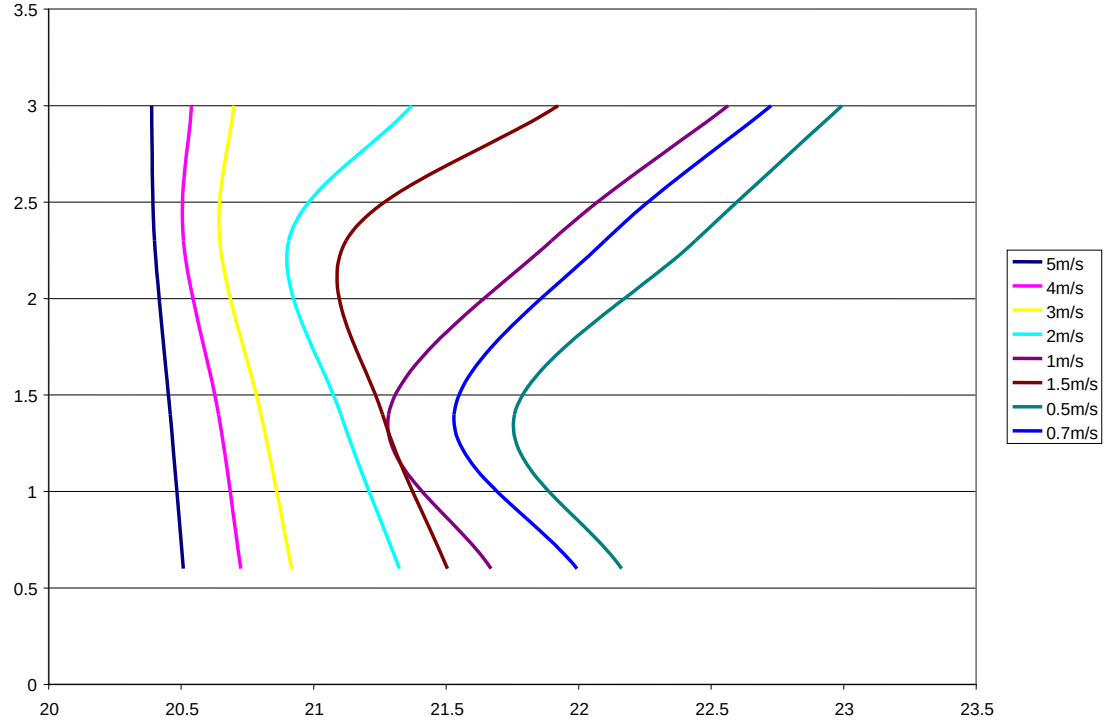

Figure 76. Combined Wind-Buoyancy Full Model First Floor North Scale Temperature Stratification at Column

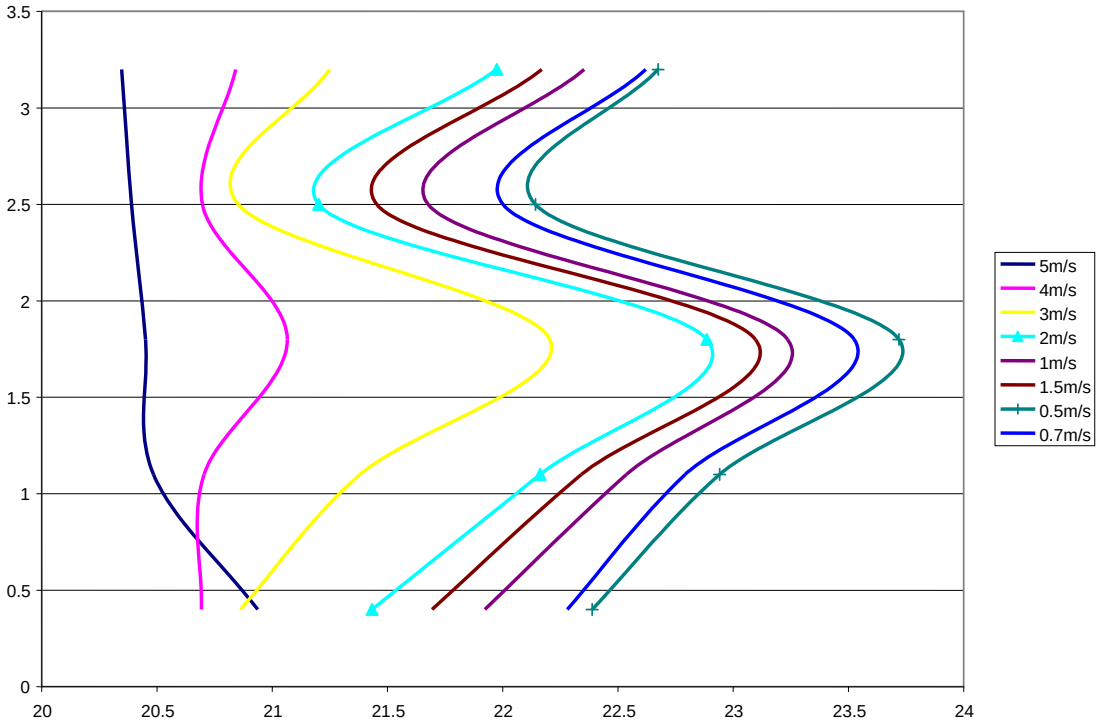

Figure 77. Combined Wind-Buoyancy Full Model First Floor North Heated Zone Scaled Temperature Stratification

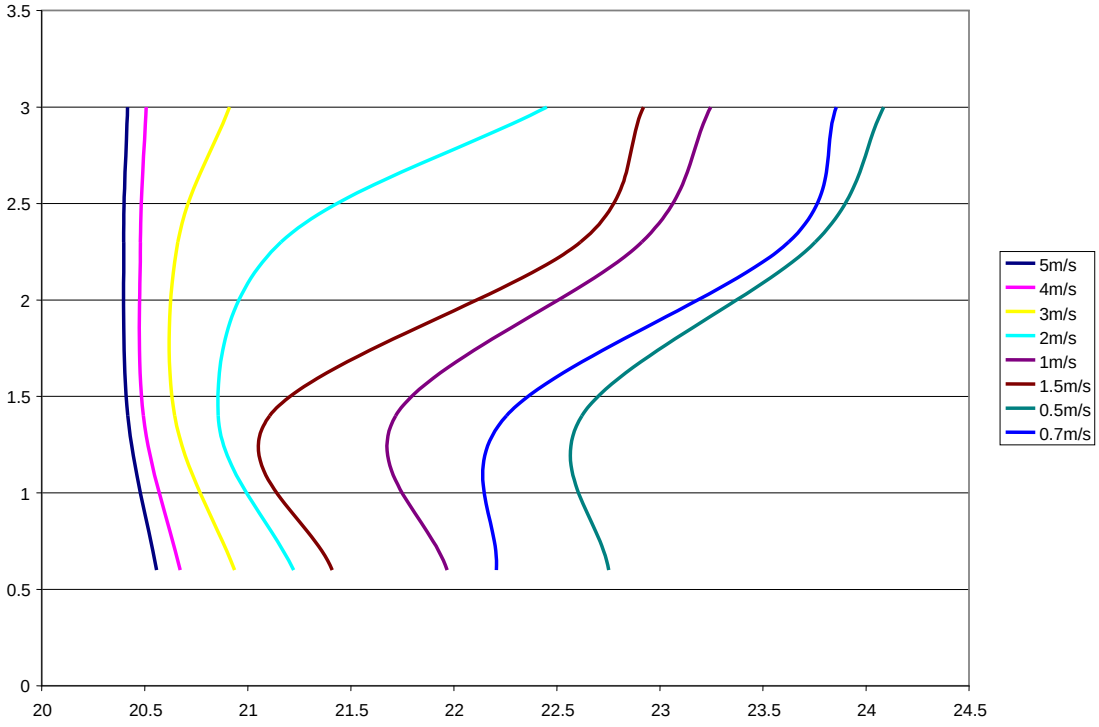

Figure 78. Combined Wind-Buoyancy Full Model Second Floor Scaled Temperature Stratification at Column

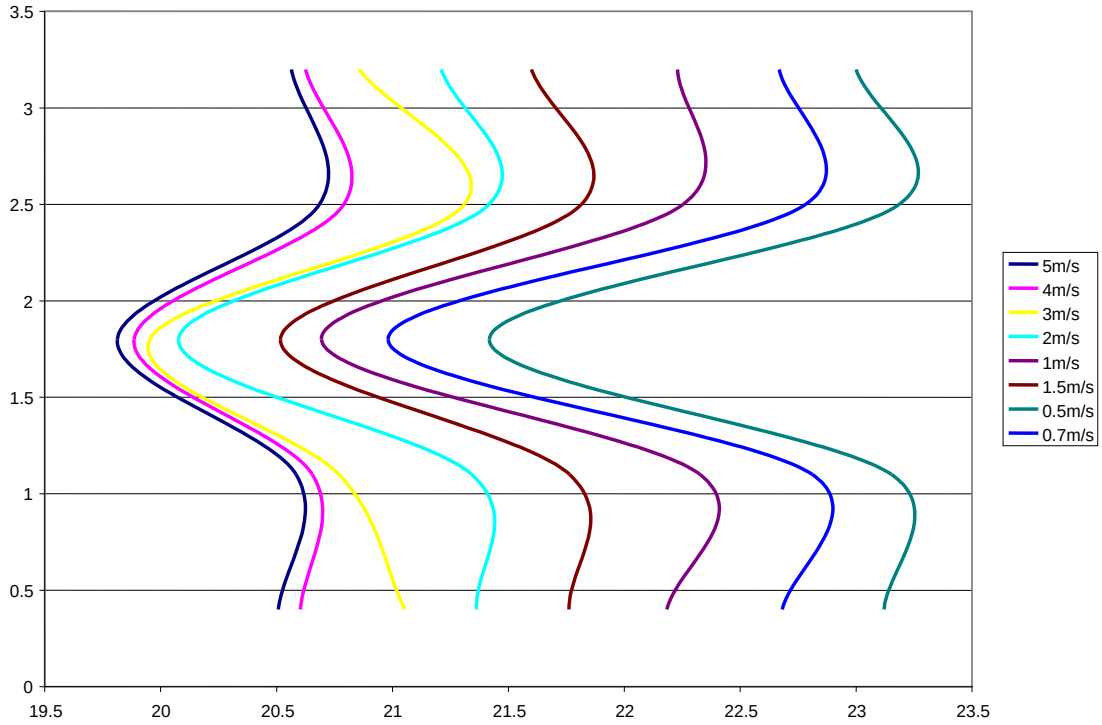

Figure 79. Combined Wind-Buoyancy Full Model Second Floor Heated Zone Scaled Temperature Stratification

7.2.3 Summary of Wind Experiments

The wind device was created to ensure that the inlet air velocity was uniform at all of the south façade openings for a wide range of wind speeds. In the wind-only case the wind speeds ranged from 1 m/s to 5 m/s, and the exiting velocities were uniform at the north façade for the stacks closed case. For the stacks open case, it was determined that 15 percent of the air exited the stacks for any given wind speed. With the combined wind-buoyancy case, the inlet air velocities were still kept constant, though at velocities between 0.5 m/s and 5 m/s. Attention was focused on the wind speeds at or below 1 m/s, because at these wind velocities the wind-driving force did not clearly dominate. The temperature distributions, along with airflow patterns from the airflow visualization techniques in the reduced-scale model, verified by the CFD simulations provided critical detail to determine how the air was moving throughout the model.

7.2.4 Calculating Archimedes Number (Ar)

The Archimedes number is the ratio of buoyancy to inertial forces, used in ventilation calculations and in determining the diffusion of non-isothermal jets. Normally the Archimedes number is presented as:

$$Ar = \frac{g\beta H\Delta T}{U_O^2} \qquad (7.6)$$

where Uo is some reference velocity, and $g\beta H\Delta T$ equals the square of the buoyant velocity .

The average and exhaust internal building temperatures were known for both the prototype building and the reduced-scale air model. The ambient temperature was known for each case as well. The height in the buoyancy force calculation used was the overall building/model height, 15m for the building and 1.2 meters for the model.

In the prototype building field measurements, the air velocity for the surrounding environment was known from recorded data at the weather station. The entering air velocity at the awning-type window was known for several site visits, and was measured in the horizontal plane of the window (neglecting the side/vertical pieces and their contribution). For the reduced-scale air model, the entering air velocity was known at the window face, which was a vertical, rectangular opening in the façade. Since the velocities were at different locations and for different window configurations, the pressures due to wind and buoyancy were used rather than the buoyant and reference velocities. The Archimedes number then could be calculated as:

$$Ar = \frac{\Delta P_B}{\Delta P_W} \quad \textbf{(}7.7)$$

From Chapter 2, the pressure due to buoyancy, or the stack effect, was given as:

$$\Delta P_B = \rho_O g H \left(\frac{T_I - T_O}{T_I} \right) \quad (7.8)$$

The pressure due to wind was given as:

$$\Delta P_w = C_P \rho_O \, U_O^2 / 2 \quad (7.9)$$

with C_p equal to the ($C_{p\ upwind}$-$C_{p\ downwind}$) The pressure due to wind could also be calculated using the power law equation:

$$Q = c_d A \sqrt{2 \frac{\Delta P}{\rho}} \quad (7.10)$$

The pressure difference could be calculated based on the flow rate through the model. After this, re-arranging, equation 7.10 becomes:

$$\Delta P_W = \frac{1}{2} \rho \left(\frac{Q / A}{C_d} \right)^2 \quad (7.11)$$

Where Q is the flow rate, A is the area of the inlet opening, and C_d is the discharge coefficient, normally estimated as 0.6 for windows.

7.3 Measurements and Results for the Prototype Building

The goal of the reduced-scale air model is to predict the ventilation performance of a full-scale building, using temperature distributions and airflow patterns. Data from the reduced-scale air model, reduced-scale CFD model, and full-scale CFD model were compared to the prototype building. The models predicted steady-state conditions for a given ambient temperature and internal load, while the prototype building was operating under transient conditions. The reduced-scale model was created based on a typical temperature differential between interior and exterior temperature of 5-8°C.

Data from four building-occupied days during a site visit to the prototype building were applied, using temperature measurements from the mid-day period, when the temperature difference between the interior and exterior fall within the above range. The building internal temperature used in calculating the temperature difference was determined by taking the average temperature over all three floors. The temperature differences for the four days are presented in Table 40. The variables used in calculating the pressure differences due to stack and wind are listed in Table 41.

Table 40. Measured Temperature Difference for Prototype Building

	Temperature Difference	*Outside Velocity (m/s)*
Site-1	3.50	6.7
Site-2	3.69	3.7
Site-3	1.06	4.3
Site-4	1.69	4.1
Site-5	0.75	3.4

Table 41. Variables Used in Calculating Pressure Differences

variable	*value*
ρ	1.2
g	9.8
H	15.0
C_p	0.6
C_d	0.6

Using the above equations, the pressure difference due to wind and buoyancy each were calculated for the prototype building on the days of the site visits. Calculations were made using both data sets available, the ambient wind conditions with the pressure coefficient, and the window velocity measurements with the coefficient of discharge. The method that used the window velocity measurements were adjusted for the total airflow through the window, rather than just the flow through the horizontal section of the window opening. It was estimated that an additional 70 percent of airflow would be present when the sidepieces were accounted for. This was based on the bag device measurements for determining the volume of air entering a window and the relative areas of the horizontal and vertical pieces. The resulting wind and buoyancy pressure differences for each method are presented in Table 42 and Table 43.

Table 42. Calculated Wind and Buoyancy Pressure Differences and Resulting Archimedes Number Using Ambient Wind Conditions and Equation 7.8

	Pw	*Pb*	*Ar*
Site-1	16.2	27.4	1.7
Site-2	4.9	26.6	5.4
Site-3	6.7	7.4	1.1
Site-4	6.1	12.4	2.0
Site-5	4.2	5.2	1.2

Table 43. Calculated Wind and Buoyancy Pressure Differences and Resulting Archimedes Number Using Measured/Corrected Entering Window Velocities and Equation 7.8

	Pw	*Pb*	*Ar*
Site-1	16.1	27.4	1.7
Site-2	4.6	26.6	5.8
Site-3	5.3	7.4	1.4
Site-4	5.7	12.4	2.4
Site-5*	---	---	---

*Site-5 window velocity measurements were not recorded

Using both of the above-described methods, the Archimedes number was calculated for each set of measurements. For the site visits with low wind velocity, buoyancy force dominated the flow. At high wind velocity, buoyancy and wind forces were comparable. Both methods provided similar results.

7.4 Comparison to Full-Scale and Prototype Building

It was important to compare the dimensionless parameters identified in Chapter 5 for the reduced-scale model and the prototype building. The predicted full-scale building temperature distributions have been presented in the previous sections, and now the comparison of the Reynolds numbers, the Grashof numbers and the Archimedes numbers are provided to ensure that the magnitude of these parameters is similar for the two scales. The Grashof number is presented for the buoyancy driven case and the Archimedes number for the wind-driven case. For the buoyancy driven ventilation case, the Reynolds numbers were calculated using the hydraulic diameter of a heated zone, rather than the inlet window, as it was the flow in the building space that was of concern. The measured air velocity at the window was used for the wind driven case.

Table 44. Key Dimensionless Parameters and Variables: Buoyancy-Driven Case

	Prototype Building	*Reduced-Scale Air-Model*
Scale	1	12
g	9.8	9.8
β	0.0034	0.0033
ΔT	8	30
H	15	1.2
A_{CS}	6.61	0.522
Pr	0.7	0.7
Re	$8.9x10^5$	$3.5x10^4$
Gr	$4.1x10^{12}$	$6.6x10^9$

Although the Reynolds numbers for the prototype and reduced-scale model in the buoyancy-driven case, Table 44, were not equal, they were well above the critical Reynolds number required for turbulent flow. They were calculated using the cross sectional area (A_{CS}) of the heated room.

Using data from the reduced-scale air model under a variety of wind conditions, the Archimedes number was calculated. The variables used in the calculations are presented in Table 45, where

H is the height of from the ground floor to the top of the atrium, which drives the buoyancy force. A discharge coefficient of 0.6 was assumed for a sharp edged orifice. The density of air was assumed relatively constant over the operating temperatures in the model. The measured temperature differences and the full-scale building temperatures scaled from the non-dimensional equation 7.3 for wind speeds measured at the face of the inlet windows are presented in Table 46. The measured velocities range from 5 m/s down to 0.5 m/s.

Table 45. Variables Used in Calculating Pressure Differences

variable	*value*
rho	1.2
g	9.8
H	1.2
Cd	0.6

Table 46. Measured Temperature Difference for Reduced-Scale Air Model and Corresponding Full-Scale Building for Combined Wind-Buoyancy Case

Measured Velocity	*Stacks Open ΔT*	*Stacks Closed ΔT*	*Dimensionless Stacks Open ΔT*	*Dimensionless Stacks Closed ΔT*
5 m/s	4.3	4.3	0.5	0.5
4 m/s	5.0	5.1	0.6	0.6
3 m/s	6.7	6.7	0.7	0.7
2 m/s	10.1	10.3	1.1	1.1
1.5 m/s	13.0	12.2	1.4	1.3
1 m/s	15.8	16.8	1.7	1.8
0.7 m/s	18.8	19.5	2.1	2.1
0.5 m/s	20.8	21.4	2.3	2.4

The resulting pressure differences due to wind and buoyancy forces are presented along with the calculated Archimedes number for the reduced-scale model cases in Table 47. Data are presented for both the stacks open and stacks closed cases, though there is little variation between the two. From Table 47, wind dominated all of the cases when the inlet air velocity was above 1 m/s in the scaled model tests. It was difficult to have the wind generating device produce uniform velocities below 0.5 m/s at the face of the inlet windows.

Table 47. Calculated Wind and Buoyancy Pressure Differences and Resulting Archimedes Number Using Measured Entering Window Velocities and Equation 7.8

		Stacks Open	*Stacks Closed*	*Stacks Open*	*Stacks Closed*
m/s	P_w	P_b	P_b	Ar	Ar
5	41.7	0.2	0.2	0.005	0.005
4	26.7	0.2	0.2	0.009	0.009
3	15.0	0.3	0.3	0.02	0.02
2	6.7	0.5	0.5	0.07	0.07
1.5	3.75	0.6	0.6	0.2	0.2
1	1.7	0.7	0.8	0.4	0.4
0.7	0.8	0.9	0.9	1.1	1.1
0.5	0.4	1.0	1.0	2.3	2.4

In the last two lines, for both the stacks open and the stacks closed cases, an Archimedes number was found to be similar to three cases from the prototype building, site-3, 4, and 5. A comparison of the Archimedes number for all cases considered is presented in Table 48. The reduced-scale model yielded scaled temperature differences around 2.8 °C, while in the prototype building, the temperatures for the selected cases range from 0.5 to 3.1°C. This was in part due to the operation of the stack fans, which increased the velocity and therefore airflow through the prototype building, reducing the temperature difference between interior and exterior environments. The reduced-scale model scaled temperatures follow the same trend as the prototype building, with the ground floor as the coolest (least temperature difference between interior and exterior) and temperatures increasing with higher floor levels. Since similar interior loads and exterior wind conditions existed for the three site cases, the same CFD simulation was used in comparing all three. The inlet air velocities for the site measurements were similar, at an average of 1.5 m/s inlet conditions. When determining the airflow and relating the air velocity to the simplified opening, the vertical cut out rather than the awning-type window, the inlet air velocity could be approximated as 0.5 m/s.

Table 48. Comparison of Archimedes Number for Cases Assessed

	Wind speed (m/s)	*Ar*
Scale Model (Stacks Open)	0.5	2.4
CFD Model (Stacks Open)	0.5	2.4
Site-3	4.3	2.4
Site-4	4.1	1.7
Site-5	3.4	1.4

Table 49. Comparison of Average Temperature Difference ($T-T_{ambient}$) by Zone for Combined Wind-Buoyancy Case: Prototype Building and Reduced-Scale Air Model Measurements

	Ground Floor Temp (°C)	*First Floor South Temp (°C)*	*First Floor North Temp (°C)*	*Second Floor Temp (°C)*
Site-3	0.5	0.9	0.5	2.4
Site-4	1.5	2.1	0.7	3.1
Site-5	-0.1	0.6	1.2	1.3
Physical Model	1.9	2.7	2.7	3.9
CFD Model	1.2	2.0	1.9	2.7

Not only the building average temperature, but also detailed temperatures for each occupied zone were evaluated to validate the methodology. For more detailed temperature comparisons, the thermocouples in the reduced-scale model were compared to similar temperature measurement locations in the prototype building. Both the thermocouples and the HOBO® data loggers were located at mid-height of the occupied zone for the reduced-scale model and prototype building respectively. The detailed temperature differences, $T-T_{ambient}$, by floor level are presented in Table 50 for the ground floor,
Table 51 for the first floor (north and south halves), and Table 52 for the second floor.

Table 50. Ground Floor Detailed Temperature Difference ($T-T_{ambient}$) Comparison, 0.5 m/s Inlet Velocity

	west		*mid-space*		*east*		*atrium*
Location	#1	#2	#3	#4	#5	#6	#7

Reduced-Scale Model	1.17	1.24	1.44	1.10	1.02	1.02	1.09
Prototype Building Site-3	1.15	1.54	1.92	1.54	1.15	1.54	1.15
Prototype Building Site-4	1.53	1.53	1.92	1.53	1.15	0.77	1.15
Prototype Building Site-5	1.15	1.53	1.92	1.53	1.53	1.15	1.92
CFD Reduced-Scale Model	1.1	1.3	1.6	1.5	1.08	1.07	1.08

Table 51. First Floor Detailed Temperature Difference ($T-T_{ambient}$) Comparison, 0.5 m/s Inlet Velocity

	South-West		*South Middle*		*South-East*		*Atrium*	*North-West*		*North Middle*		*North-East*	
	#1	#2	#3	#4	#5	#6	#7	#8	#9	#10	#11	#12	#13
Model	1.55	1.58	1.73	1.62	1.74	1.84	1.65	1.92	1.82	1.88	1.74	1.80	1.72
Site-3	1.53	1.53	1.92	1.53	1.15	1.15	2.3	0.77	3.46	0.77	3.46	0.38	3.46
Site-4	1.92	1.92	1.92	1.53	1.15	1.53	2.69	1.15	2.3	0.77	2.3	0.38	2.3
Site-5	2.3	2.3	2.3	2.3	1.91	1.91	3.07	1.53	2.68	1.15	2.68	1.15	2.68
CFD	1.8	1.8	1.9	1.9	1.9	1.9	1.65	1.8	1.75	1.7	1.6	1.8	1.7

Table 52. Second Floor Detailed Temperature Difference ($T-T_{ambient}$) Comparison, 0.5 m/s Inlet Velocity

	atrium		*North-West*		*North Middle*		*North-East*	
	#1	#2	#3	#4	#5	#6	#7	#8
Model	2.09	2.47	2.71	2.51	2.83	3.12	2.77	2.66
Site-3	4.68	2.71	0.77	1.93	0.77	1.93	0.77	2.32
Site-4	5.03	4.25	1.92	3.47	1.92	3.08	1.92	3.47
Site-5	3.87	3.48	1.54	2.31	1.54	2.31	1.15	2.31
CFD	2.1	2.6	2.8	2.6	2.9	3.1	2.8	2.7

The temperature comparison between the reduced-scale model and the prototype building on a point-by-point basis identify some of the simplifications and assumptions made in the development of the reduced-scale air model and the issues involved in building monitoring. The temperatures in the atrium for the upper two floors were higher in the prototype building than predicted in the reduced-scale model due to solar gains that occur through the atrium and influence some of the measurements on the second floor occupied zone. Again, the reduced-scale air model follows the same trend as the prototype building in general, though there are some anomalies with the data. There were some locations, such as on the second floor, that there was a small temperature difference. This was due to the operation of the large windows and the fluctuation of the wind, which did not always come from the south direction. At points in or along close to the atrium, the temperatures in the prototype were recorded as warmer than surrounding temperatures because of solar gains due to the glass atrium. This caused significantly higher temperatures at points 1 and 2 on the second floor.

There were similarities between the full-scale building and the reduced-scale air model when comparing the temperature distributions and airflow patterns. The overall temperature stratification was similar in both cases (Figure 80 and Figure 81). The airflow patterns had some general similarities in overall flow, but there were differences at the edge of the floor at the atrium (Figure 82and Figure 83). This was caused by the lack of railings in the reduced-scale CFD simulation.

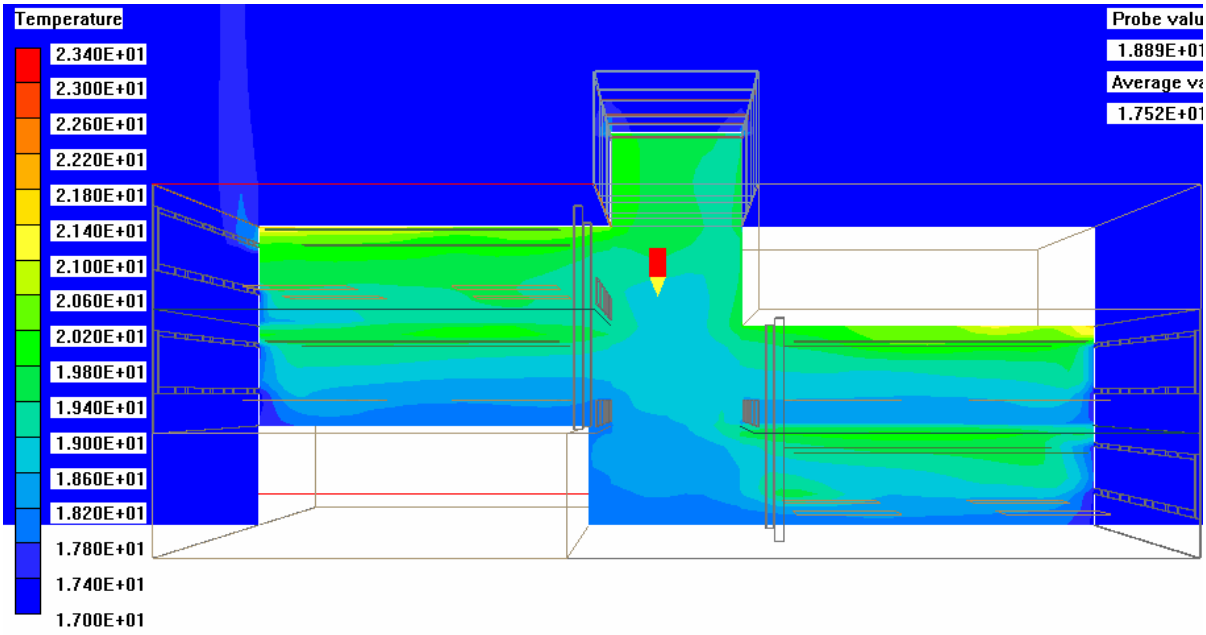

Figure 80. CFD Simulation of the Temperature Distributions for Full-Scale Model: Buoyancy Driven Flow with Stacks Open

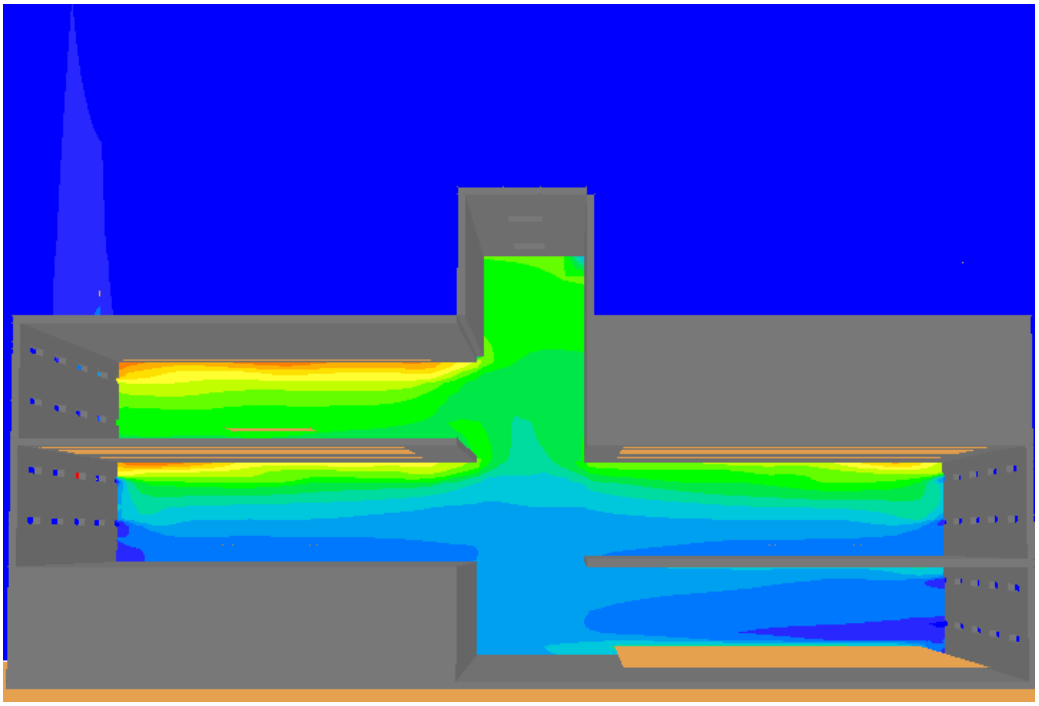

Figure 81. CFD Simulation of Temperature Distribution for Reduced-Scale Air Model: Buoyancy Driven Flow with Stacks Open

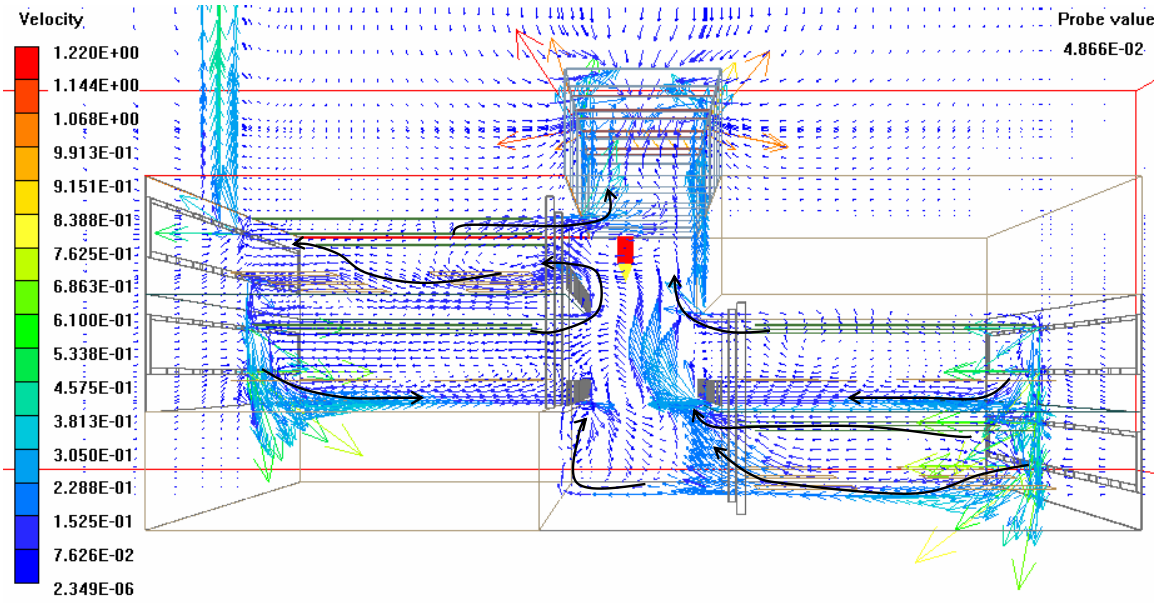

Figure 82. CFD Simulation of the Airflow Patterns for Full-Scale Building: Buoyancy Driven Flow with Stacks Open

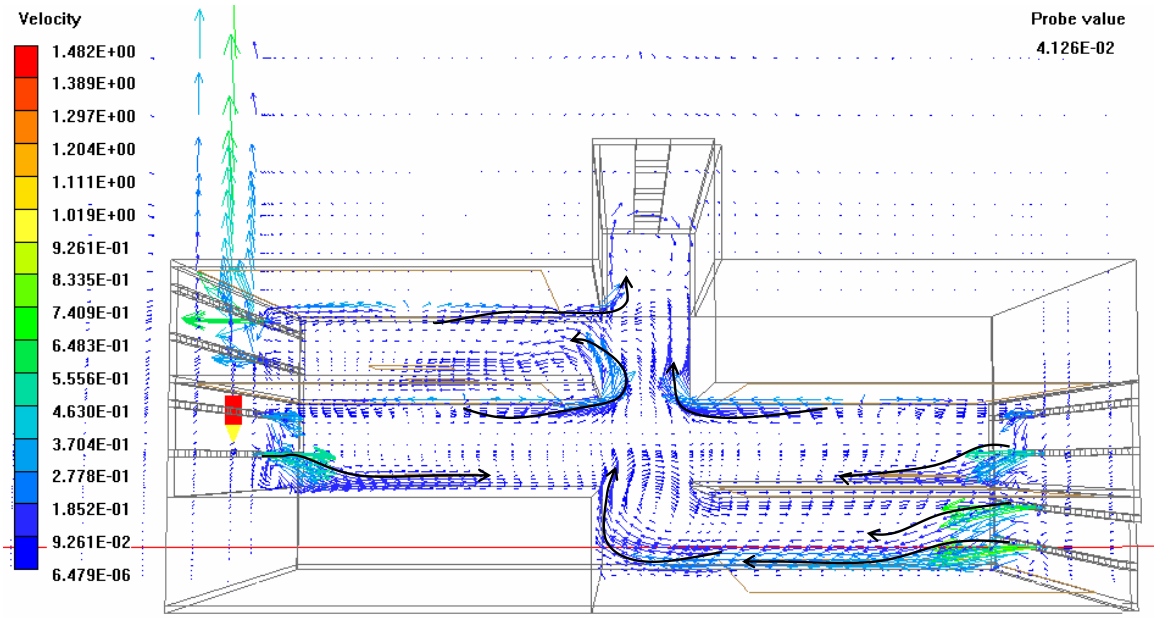

Figure 83. CFD Simulation of Airflow Patterns for Reduced-Scale Air Model: Buoyancy Driven Flow with Stacks Open

7.5 Model Details

Models aim to reproduce phenomena that occur at full scale. In the evaluation of the reduced-scale air methodology, the influence of modeling details on the airflow patterns was of interest. CFD simulations were carried out both with and without a significant detail in terms of airflow, the railing around the atrium. The airflow pattern changed between the two cases; for the

buoyancy case the air from the ground floor rose in the atrium and 'fell' over the solid railing into the heated zone of the first floor zone above. This also occurred between the first and second floors on the north side of the model, the physical reduced-scale air model, reduced-scale CFD model and full-scale CFD simulation. Having the railings in the models allowed cooler air to collect at the base of the railing near the column in the pure buoyancy-driven case, whereas in the case without railings, the cooler air mixed with the warmer air in the atrium. Figure 84 shows the temperature distribution with and without railings for the reduced-scale CFD simulations.

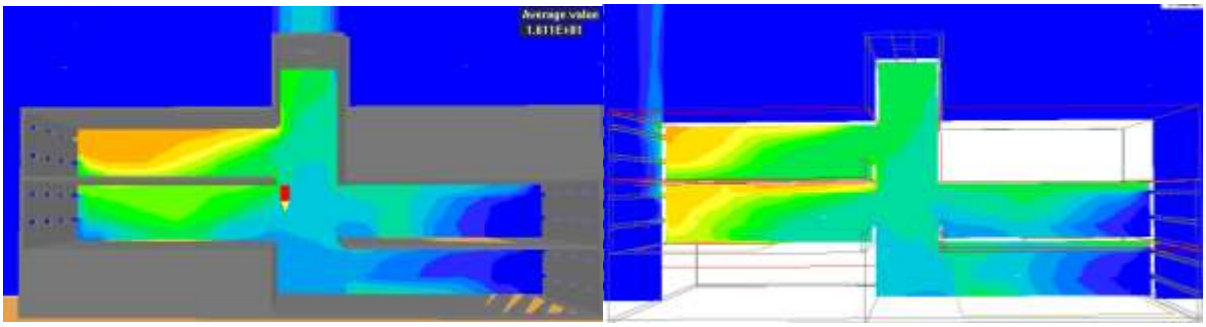

Figure 84. Influence of Railings on Temperature Distribution for Reduced-Scale CFD Simulation; a) without railings, b) with railings.

Field measurements from the prototype building provided unusual airflow patterns on a day with relatively low ambient wind velocity. At the first floor south zone, a flow reversal was observed using the smoke pencils for airflow visualization. A full-scale CFD simulation was completed by G. Tan, for the specific space within the building, and included details such as desks, computers and individual people, rather than a uniform distributed load, as was used in the reduced-scale air model. An image from the simulation, with the curved lines indicating airflow streamlines predicted by CFD and arrows indicating flow direction from field measurements is shown in Figure 85.

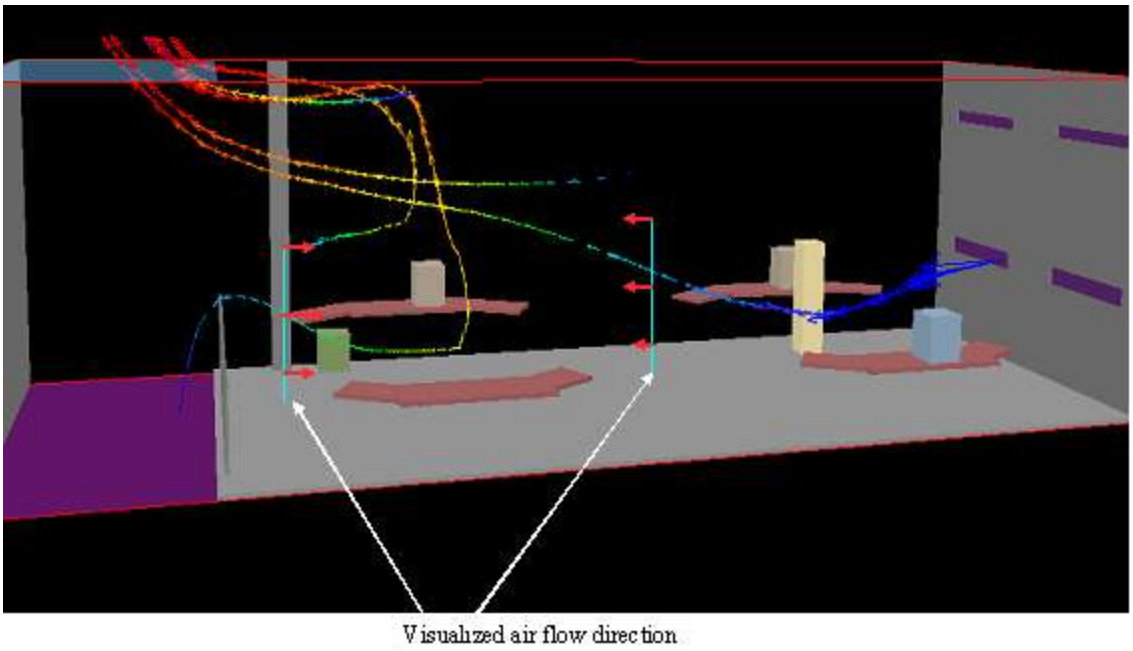

Figure 85. Detailed Full-Scale CFD Simulation of Flow Reversal on First Floor South-Buoyancy-Driven Flow[4]

A similar flow pattern was observed using flow visualization techniques discussed in Chapter 4. For the buoyancy-driven full model case, the air from the ground floor entered the atrium, slowly rising over the railing and then entered the first floor south zone. The air from the atrium was heated and mixed with the heated air in the first floor south zone and then exited at the ceiling. This corroboration of the field measurements, with the full-scale CFD, reduced-scale CFD and reduced-scale air model validates the reduced-scale air model as a method to model even unusual flow patterns observed in the full-scale building. The simplification of the internal loads as a uniformly distributed load is adequate in assessing the airflow patterns within the space.

The temperatures measured in the reduced-scale air model, when scaled for full-scale buildings, were validated based on the measured building site data for several summer days. The addition of the atrium fans and thermal mass influenced the resulting internal temperatures in the prototype building, but were of less significance in the reduced-scale air model. Had the thermal mass in the prototype building been better used with night cooling, the reduced-scale air model still may prove as valid a methodology, however further research is required. The airflow patterns within the model were validated by both field measurements and observations, and through CFD simulations, though additional field tests would need to be completed under other conditions.

[4] G. Tan. CFD Simulations of Houghton Hall, Luton, 2004.

Chapter 8.0

Summary, Conclusions and Future Research Work

8.1 Summary

Natural ventilation offers many benefits for the performance and comfort of office buildings. Among the advantages of passive ventilation are (Martin and Fitzsimmons 2002):

- Reduced operating costs
- Lower first (construction) costs
- Decreased impact on the environment
- Increased occupant comfort
- Improved indoor environment

However, before natural ventilation can be widely adopted as a passive cooling and ventilation strategy, the underlying phenomena that govern the flow patterns and temperature distribution must be understood. Though modeling tools are available, there has been limited validation between design phase and post-occupancy phase performance of these passive buildings. This research developed an innovative modeling methodology for evaluating natural ventilation in a commercial office building for a commonly used office plan. This was completed using a 1:12 scale model and CFD simulations. This research also incorporated a novel means to assess window airflow through the creation of a bag device. Through monitoring, modeling and simulation, the methodology was able to predict the temperature distribution and airflow patterns in the prototype naturally ventilated office building. Further research using additional site data would be needed to fully validate the method. Monitoring methods currently in use for evaluating mechanically ventilated buildings were adapted for use in assessing a naturally ventilated commercial office building which was used as the prototype for validating the reduced-scale air model method. Numerical modeling techniques were refined and guidelines developed for the use of these methods in evaluating naturally ventilated buildings. The guidelines are presented in this section.

The main types of natural ventilation, buoyancy, wind, and combined wind-buoyancy, were described and presented in chapter two along with simple analytical analyses. Design characteristics that often are incorporated into passively ventilated buildings, including atrium stacks to enhance buoyancy-driven flow and window locations, were identified as they pertain to the prototype building and scaled model. Additionally, methods for evaluating building performance, with a focus on those required for evaluating naturally ventilated buildings, were presented. These methods were implemented in evaluating the prototype building described in chapter three. The monitoring and measuring methodology used and problems encountered in assessing a naturally ventilated building were identified, along with the resulting data from the monitoring period. The variation in performance due to seasonal conditions was described, and the performance compared to existing benchmarks for typical and good practice naturally ventilated buildings. The challenge of determining an effective window opening area was addressed through the design and use of a device to measure the volume flow rate of air through

windows of naturally ventilated building. Though designed specifically for the prototype main windows, the design could be adapted for application for other window geometries and other buildings.

There were additional factors that influenced the modeling methods along with the challenges addressed in monitoring and evaluating the full-scale prototype building. The range of modeling methods available, at scales ranging from full-sized to $1/250^{th}$ scale, and their characteristics were presented. Two of the more common techniques for modeling, using either water or air, and their respective flow visualization techniques, were described. Flow visualization has been shown to be a powerful technique to determine flow patterns within a model but there have been concerns raised regarding the neutral buoyancy of the material selected to introduce into the fluid stream. The use of fog, at the same temperature as the entering air, proved useful for use in the reduced-scale model airflow pattern visualization. Modeling techniques were described for a range of applications, including how each method incorporated flow visualization into the evaluation of fluid flow for the model. The requirements for tracing flow patterns included not only neutral buoyancy, but also effective visualization and low diffusion rate. The benefits and problems were identified for both water and air as the working fluids in modeling. Finally, the methods of flow visualization used for the reduced-scale model were presented, including imaging techniques. Based on the above requirements, a fogging machine as the neutrally buoyant tracer, a digital video camera to capture the flow visualization and fluorescent lamps to provide illumination proved a useful combination.

Critical to the use of scale modeling as a method for predicting fluid flow in full-scale buildings has been the similarity of calculated or monitored parameters. Dimensional analysis and similitude were presented as means to ensure similarity between the prototype and scale model. The governing equations, in their full and dimensionless forms, were presented in chapter five. The resulting dimensionless parameters, the Reynolds, the Archimedes or the Grashof, and the Prandtl numbers, were identified, and determination of characteristic length was discussed. The selection of characteristic length affected the regime used to describe the flow, and results in the use of several characteristic lengths, depending on the field under evaluation. Comparisons between the full-scale prototype, reduced-scale air, and reduced-scale water for the key parameters including the Reynolds number, the Prandtl number, and the Grashof number were presented. All of the models and the prototype were found to fall in the turbulent regime when using the hydraulic diameter of a single zone as the characteristic length.

The reduced-scale air model constructed to meet the geometric similarity requirement was presented in chapter six. Descriptions of the test chamber, control system and equipment used in carrying out the experiments were discussed, along with descriptions of the experiments. Each of the experiments for buoyancy, wind, and combined wind-buoyancy cases was described in detail. The influence of window location on the flow pattern in the occupied space was identified using the single zone model. Though there was little change in the overall airflow rate through the building, the temperature distribution within the heated zone was affected by the location of the windows. The two-zone model demonstrated the effect of the stack vents on the airflow and resulting temperature distribution within the two zones. In poorly designed naturally ventilated buildings, the upper floor can become the only location for outflow from the building, causing warm, stale air to traverse the occupied space before exiting the building. The full-

model case using CFD simulations was completed with the stacks open and stacks closed, to determine the resulting airflow patterns and temperature distributions. The stack openings were a design characteristic that affected the airflow in the building, reducing the temperatures in the upper-most floor. The wind and wind-buoyancy driven cases were carried out over a wide-range of wind speeds. The wind-driven cases were used to determine the percentage of air that exited through the stack without any buoyancy effects. A uniform velocity was achieved at the south façade for each of the wind speeds from 1 to 5m/s for the wind-driven case and the exiting air velocities at the north façade were uniform as well. A wide range of wind speeds were used, from 0.5 m/s to 5.0 m/s, to determine when the flow was dominated by wind versus a more equal balance between wind and buoyancy flows through analysis using the Archimedes number.

The key results from the experiments were presented in chapter seven. Temperature distributions, both measured from the physical model and the numerical simulation were compared. The data were presented for all of the experimental cases as the scaled building temperatures, using calculated reference temperatures. The temperature distributions and air velocities for each case were shown, along with descriptions of the flow phenomena. Comparisons of the resulting reduced-scale air model and selected data from the full-scale prototype were discussed. The reduced-scale model showed comparable results for conditions with stacks open when evaluated with data recorded from the prototype building for the summer case. The comparisons of the experimental data to the numerical simulations provided insight into some of the modeling attributes of computational fluid dynamics simulations.

8.2 Conclusions

The validation of this reduced-scale air model through comparisons with data obtained from the prototype building and numerical simulations provides an additional tool for the prediction of airflow and temperature distribution in naturally ventilated buildings. With careful attention to requirements of similitude to ensure scalability between the results recorded in the reduced-scale model and the prototype building, this experimental reduced-scale model was able to predict average temperatures in each zone.

Modeling airflow and temperature distribution in buildings is a complex problem that researchers continue to pursue. The variety of techniques available has applicability to the design of passively ventilated buildings, but the user must be aware of limitations of each technique.

There are several key factors to address when modeling airflow in buildings:

- Clearly identify the problem
- Identify the governing phenomena
- Determine the desired detail of the results
- Understand limitations of the method used

First, the problem must be clearly identified. Whether the goal is to model in detail a specific space or an entire building the purpose chosen can affect the selection of modeling technique. If an entire building is to be modeled, then there are limitations in terms of complexity of the model that can be used regarding analytical methods, space required for physical models, and time required for numerical models. Important values for modeling, both physical modeling and numerical modeling, were identified including the boundary conditions and level of detail. It is

difficult to select the boundary conditions for modeling buildings, as was found in the analyses here. With the experimental modeling, the ambient conditions were constantly measured to ensure that the assumptions of consistency and steady state conditions could be used. If any number of variables changed, it affected the ambient temperature surrounding the model. Decreasing the number of inlet windows or outlets (windows or stacks) increased the temperature inside the model and increased the heat loss to the test chamber. The geometry of the window and measurement location influenced the recorded inlet and outlet velocity.

Water models aim to meet dynamic similarity requirements, but not necessarily thermal or geometric requirements. Both heated and salt-water models demonstrate macroscopic flows for spaces, focusing on the restrictions between spaces and replicating the general phenomena for natural ventilation, but not necessarily specifically for a building. They are constructed at small scale to obviate the requirement for a large amount of space. However, they do require the equipment and apparatus to run the experiments. Water models do not have abundant amounts of detail, focusing rather on the connection of spaces and the restrictiveness between zones. One large benefit of water bath models is the ability to incorporate flow visualization easily in the experimental techniques. Dyed water, at the same temperature as the ambient, is easily injected at the inlets and light shining through the model is easily projected on to a screen behind the model. Water bath models have less than 1 percent of the heat input lost through the model walls (Gladstone and Woods 2001).

With air models, the heat loss through the walls is significantly higher as described in chapter seven. The heat loss can be controlled to a certain extent, particularly with the exterior walls; however, heat transfer between floors is also a concern. The reduced-scale air model developed in this methodology allows for a certain amount of detail, which contributes to the success of modeling a prototype building. For example having the railings around the atrium in the combined wind-buoyancy driven flow influenced the flow patterns in the atrium and in the northern half of the model. In general, with reduced-scale modeling, a small variation, as little as 3 mm, can influence the resulting flow patterns. In the twelfth-scale air model, there is more detail than most reduced-scale models. Therefore, there must be an increased attention to detail with respect to major obstacles that might influence the flow. Airflow visualization is more difficult with the twelfth-scale air model than the water models, but can demonstrate the flow patterns more distinctly than the water models, which show whether a space is well mixed or not, and not specific flow patterns within an enclosed space.

Numerical solutions are complicated in the modeling technique and require an experienced user to obtain meaningful results. If the boundary conditions are not known, describing the model in the domain becomes much more difficult. With CFD simulations, complex mathematical models are solved iteratively until the solution converges. The selection of turbulence models will influence the results and the computing time required for the solution to converge. There is limited interaction between the surfaces and the working fluid, requiring assumptions of adiabatic walls and no radiation between surfaces. However, CFD does provide detailed temperature distributions, air velocities and flow patterns when modeled correctly. These simulations can help explain experimental results both at the reduced and full-scale.

This novel reduced-scale air modeling method developed for use in evaluating natural ventilation in buildings provides more detail than current water modeling techniques and can enhance numerical simulations. This methodology shows detailed temperature distribution and the main airflow patterns while behaving more like a typical building with radiation and heat loss. Although there can be difficulties with the monitoring equipment and initial boundary conditions, modeling using air as the fluid provides accurate results. This is due to the thermal properties that are conserved when using air, such as radiation and thermal diffusivity. Using real fluids in physical models allows the flow to re-circulate and separate. The conservation equations are automatically included in the analysis with physical modeling with air because there are no approximations or missing terms. The experimental work can not be adjusted to try and match theory, whereas with simulation methods, a slight change in a variable can be sued to obtain a better match of results. Reduced-scale air models may not be fast or flexible enough for sensitivity analyses, but they can enhance the tools that are used to do so. There was good agreement between the full-scale CFD simulations in terms of temperature distribution and airflow patterns when compared to the full-scale prototype. Additionally there was good agreement when comparing the reduced-scale air model to the reduced-scale CFD simulation. The two CFD simulations provided good correlation between the full- and reduced-scale versions as well.

8.3 Future Research Work

This research provides the foundations for reduced-scale air modeling as a means to predict the temperature and airflow in naturally ventilated buildings. It is by no means exhaustive. There are areas for further work, both with the current configuration to understand better the prototype passive design, and with other configurations of passively ventilated buildings that could benefit from additional analyses using the reduced-scale model technique.

For the current configuration, experiments with fan-assisted airflow through the stacks would help not only in improving the building performance, but also in better understanding atrium fans as a design characteristic. Understanding the effectiveness of the atrium fans will reduce the occurrence of uncomfortably warm temperatures in the upper floors, which is a common problem in naturally ventilated buildings. Altering the height of the atrium stack and thereby increasing the buoyancy effect, is an additional design strategy that could be implemented in the reduced-scale model.

The open floor plan connected to a central atrium is a common commercial building layout, but is not the only one in use. Testing configurations other than that used for the reduced-scale model, the prototype potentially could improve building design configurations as well. This modeling technique is a method for evaluating different configurations and design characteristics to understand the flow patterns and temperature distributions in full-scale buildings through dimensional analysis and similitude. The results can then be used in formulating tools and enhancing numerical simulations to predict more accurately natural ventilation in commercial buildings.

Finally, the airflow visualization methods could be improved. The techniques developed as part of this methodology were useful in determining airflow movement from one zone to another as well as how the zone interacted with the atrium. Tracing the streamlines, akin to what CFD

simulations are able to do would allow further analysis of detailed flow patterns within the zone. Better controlling the media used to trace the fluid patterns would be of great help.

There is much research yet to complete in the field of passive ventilation techniques, particularly in the area of modeling airflow and temperature distribution in buildings. Through a combined approach, using field measurements, modeling efforts, and simulation techniques, tools can be enhanced in order to better predict the performance of buildings, while maintaining comfort conditions and reducing energy consumption and life cycle cost.

References

Action Energy. 2003. Energy Consumption Guide-ECG019: Energy Use in Offices. Best Practices Programme. Crown. March 2003.

Allard, F. ed. 2002. Natural Ventilation in Buildings: A Design Handbook. James & James, London.

Allocca, C. Q. Chen, and L. Glicksman. 2003. Design Analysis of Single-Sided Natural Ventilation. Energy and Buildings, v. 25, pp. 785-795. 2003.

Andersen, K.T. 1995. Theoretical Considerations on Natural Ventilation by Thermal Buoyancy. ASHRAE Transactions, v.101, Pt.2. 1995.

Andersen, K.T. 2003. Theory for Natural Ventilation by Thermal Buoyancy in One Zone with Uniform Temperature. Building and Environment, v. 38. 2003.

Andersen, K.T. 2002. Friction and Contraction by Ventilation Openings with Movable Flaps. Eighth International Conference on Air Distribution in Rooms, RoomVent2002. Copenhagen, Denmark. September 2002.

Andersen, K.T. 1996. Design of Natural Ventilation by Thermal Buoyancy: Theory, Possibilities, and Limitations. 5th International Conference on Air Distribution in Rooms, RoomVent ;96. July 1996.

Andersen, K.T. 1996. Design of Natural Ventilation by Thermal Buoyancy. 5th International Conference on Air Distribution in Rooms, RoomVent '96, v.3. 1996.

Andersen, K.T. 1995. Natural Ventilation in Atria. ASHRAE Transactions: Symposia. V.101, Pt. 2. 1995.

ASHRAE. 2004. ASHRAE Standard 55-2004 Thermal Environmental Conditions for Human Occupancy. Atlanta: American Society of Heating, Refrigerating and Air-Conditioning Engineers, Inc.

ASHRAE. 2001. 2001 ASHRAE handbook—Fundamentals, Chapters 12, 9. Atlanta: American Society of Heating, Refrigerating and Air-Conditioning Engineers, Inc.

ASHRAE. 1997. 1997 ASHRAE handbook—Fundamentals, Chapter 9. Atlanta: American Society of Heating, Refrigerating and Air-Conditioning Engineers, Inc.

Awbi, H. Ventilation of Buildings, Second Edition, Chapters 6, 7, 9. Spon Press. London. 2003.

Bordass, W.T., A.K.R. Bromley and A.J. Leaman. 1993. User and Occupant Controls in Office Buildings. ASHRAE Conference Proceedings—Building Deisng, Technology, and Occupant Well-Being in Temperate Climate. Brussels, Belgium. P. 12-17.

Boutet, T.S. 1987. Controlling Air Movement: A Manual for Architects and Builders. McGraw-Hill. New York. 1987.

Brager, G.S, R. de Dear. 2000. A Standard for Natural Ventilation. ASHRAE Journal. October 2000.

Chandra, S., P.W. Fairey III, and M.M. Houston. 1986. Cooling with Ventilation. Florida Solar Energy Center, Solar Technical Information Program. SERI/SP-273-2966.

Chandra, S., K. Ruberg, and A. Kerestecioglu. 1983. Outdoor Testing of Small Scale Naturally Ventilated Models. Building and Environment, v. 18, No. 1/2. 1983.

Daniels, Klaus. 2003. Advanced Building Systems: A Technical Guide for Architects and Engineers. Translated by Elizabeth Schwaiger. Boston. Birkhauser-Publishers for Architecture. 2003.

Dean, B.N. 2000. Naturally Ventilated Buildings in Europe: August 2000 Trip Report. Massachusetts Institute of Technology. http://cmiserver.mit.edu/natvent/

Department of Trade and Industry (DTI). 2004. The Digest of the United Kingdom Energy Statistics 2004. The Stationary Office, Norwich. 2004.

Dutt, A.J., R.J. de Dear, and P. Krishnan. 1992. Full Scale and Model Investigation of Natural Ventilation and Thermal Comfort in a Building. Journal of Wind Engineering and Industrial Aerodynamics, v. 41-44. 1992.

Egan, J. 1998. Rethinking Construction.

Emmerich, S.J., W.SW. Dols, and J.W. Axley. 2001. Natural Ventilation Review and Plan for Design and Analysis Tools. National Institute of Standards and Technology. August 2001.

Environmental Monitoring Services. 2004. www.ems-online.co.uk.

Etheridge, D.W. 2002. Nondimensional Methods for Natural Ventilation Design. Building and Environment:33. p. 1057-1072.

Etheridge, D, M. Sandberg. 1996. Building Ventilation-Theory and Measurement, Chapter 14. New York. John Wiley & Sons. 1996.

Fisk, W.J., M.J. Mendell, J.M. Daisey, D. Faulkner, A.T. Hodgson, M. Nematollahi, and J.M. Macher. 1993. Phase 1 of the California Healthy Building Study: A Summary. Indoor Air. V. 3 p.246-254.

Flourentzou, F., J. Van der Maas, and C.-A. Roulet. 1998. Natural Ventilation for Passive Cooling: Measurements of Discharge Coefficients. Energy and Buildings. V. 27, pp. 283-292.

Fracastoro, G.V., G. Mutani, and M. Perino. 2002. Experimental and Theoretical Analysis of Natural Ventilation by Windows Opening. Energy and Buildings. V.34, pp. 817-827.

Gladstone, C. and A. W.Woods. 2001. On Buoyancy-Driven Natural Ventilation of a Room with a Heated Floor. Journal of Fluid Mechanics: 441. p 293-314.

Hagstrom, K. 2002. Influence of Kinetic Energy Sources and Internal Obstructions on Room Air Conditioning Strategy, Efficiency of Ventilation and Room Velocity Conditions. PhD Dissertation, Helsinki University of Technology.

Heiselberg, P. 1998. International Energy Agency Annex 35 HybVent. Hybrid Ventilation in New and Retrofitted Office Buildings. 44th IEA BCS Executive Committee Meeting, Brussels, Belgium. 1998.

Heiselberg, P., H. Dam, L.C. Sorensen, P.V. Nielsen, K. Svidt. 1999. Characteristics of Air Flow through Windows. HybVent Forum '99. September 1999.

Heiselberg, P., K. Svidt, P.V. Nielsen. 2001. Characteristics of Airflow from Open Windows. Building and Environment, v.36, pp. 859-869. 2001.

Housing Transfer Manual 2003 Programme. Office of Deputy Prime Minister: London. March 2003.

Incropera, F.P. and D.P. DeWitt. 1996. Introduction to Heat Transfer, 3rd Ed. Chapters 12 and 13. John Wiley & Sons, New York. 1996.

Jiang, Y. and Q. Chen. 2002. Buoyancy-Driven Natural Ventilation in Buildings: Experimental and Numerical Studies. 8th International Conference on Air Distribution in Rooms, RoomVent 2002.

Jones, J. and A.W. West. 2001. Natural Ventilation and Collaborative Design. ASHRAE Journal. P. 46-51. November 2001.

Karava, P., T. Stathopoulos, and A.K Athienitis. 2004. Wind Driven Flow through Openings-A Review of Discharge Coefficients. The International Journal of Ventilation. V.3, No. 3. pp. 255-266. December 2004.

Lechner, N. 1991. Heating, Cooling, Lighting: Design Methods for Architects. John Wiley & Sons, New York.

Levermore, G.J. 2000. Building Energy Management Systems: Applications to low-energy HVAC and natural ventilation control. Spon Press. 2000.

Li, Y., A. Delsante, and J. Symons. 2000. Prediction of Natural Ventilation in Buildings with Large Openings. Building and Environment, v. 35, pp. 191-206. 2000.

Linddament, M. 1996. Why CO2? Air Infiltration Review, v. 18. December 1996.

Linden, P.F. 1999. The Fluid Mechanics of Natural Ventilation. Annual Review of Fluid Mechanics. Vol. 31: 201-238.

Merzkirch, W. 1987. Flow visualization. Orlando : Academic Press, 1987.

MacDonald, J.M., D.M. Wasserman. 1989. Investigation of Metered Data Analysis Methods for Commercial and Related Buildings. Oak Ridge National Laboratory, US Department of Energy. ORNL/CON-279. May 1989.

Martin, A. and J. Fitzsimmons. 2000. Making Natural Ventilation Work. Guidance Note GN 7/2000. BSRIA.

McQuiston, F.C., J.D. Parker, J.D. Spitler. 2000. Heating, Ventilating, and Air Conditioning: Analysis and Design. Chapter 4. Wiley & Sons, New York. 2000.

Nielsen, P.V. 1995. Airfow in a World Exposition Pavilion Studied by Scale-Model Experiments and Computational Fluid Dynamics. ASHRAE Transactions:100v2. p. 1118-1126.

Orme, M. 1999. Applicable Models for Air Infiltration and Ventilation Calculations. International Energy Agency, Air Infiltration and Ventilation Center. AIC-TN-51-1999.

Orme, M. and N. Leksmono. 2002. AIVC Guide 5: Ventilation Modeling Data Guide. International Energy Agency, Air Infiltration Ventilation Center. AIC-GUI 05.

Peppes, A.A., M. Santamouris, and D.N. Asimakopoulos. Experimental and Numerical Study of Buoyancy-Driven Stairwell Flow in a Three Story Building. Building and Environment, v. 37. 2002.

Popiolek, Z. et al. 1998. Airflow Characteristic in Scale Models of Room Ventilation. 6th International Conference on Air Distribution in Rooms, RoomVent 1998.

Rolloos, M. 1977. Possibilities and Limitations for the Prediction of Air Flow Patterns, Temperatures, and Velocities in Large Halls Using Scale Models. Heat Exchangers, Air Conditioning – Heat Pumps. Refrigeration Science and Technology. International Institute of Refrigeration. Yugoslavia, 1977.

Rybka. 2002. Aldwyck Housing Association: Building Operational Philosophy. October 2002.

Sawachi, T. 2002. Detailed Observation of Cross Ventilation and Airflow through Large Openings by Full Scale Building Model in Wind Tunnel. 8th International Conference on Air Distribution in Rooms, RoomVent 2002.

Seppanen, O. and W.J. Fisk. 2002. Association of Ventilation System Type with SBS Symptoms in Office Workers. Indoor Air. v. 12. p.98-112.

Smith, E.G. 1951. The Feasibility of Using Models for Predetermining Natural Ventilation. Research Report No. 26. Texas Engineering Experiment Station. College Station, TX, 1951.

Spalding, D.B. 2002. PHOENICS User Manual. CHAM, London.

Szucs, E. 1980. Similitude and Modeling. Fundamental Studies in Engineering 2. Elsevier Scientific Publishing Co. New York, 1980.

Szirtes, T. 1998. Applied Dimensional Analysis and Modeling. Chapter 17: Dimensional Modeling. McGraw-Hill Co. New York, 1998.

TelAire 7000 Series Operation Instructions. April, 2002.

U.S. Department of Energy. 2004. Real-Time Weather Data. Energy Efficiency and Renewable Energy Building Technologies Program. May-July 2004.

Walker, C.E., S. Manchanda, H.C. Spindler, L.K. Norford. 2004. Building Performance: Analysis of Naturally Ventilated UK Office Building. International Conference on Air Distribution in Rooms: RoomVent 2004 Conference Proceedings. September 2004.

William Bordass Associates. 1996. Mixed Mode Ventilation and Cooling Systems in Buildings. June 1996.

Yu, H., C-H. Hou, and C-M Lao. 2002. Scale Model Analysis of Opening Effectiveness for Wind-Induced Natural Ventilation Openings. Biosystems Engineering: 82(2). P. 199-207.

Appendix A: Data Logger Parameter Files

K-20 Data Logger Files

```
RECORDER_TYPE
DESCRIP: Main Panel-Luton
  MODEL: K20-8
 SERIAL: 10045
RECORDER_INFO
   PSID: 1
    MIN: 15
 PSDESC:
  RINGS: 2
 CUTOFF: 0
OPTIONA: 0
OPTIONB: 0

K20_CT_TABLE
|CH|DESCRIP        |AMPS |VH|VL|VMULT |VLT|AMP|DLT|PW|
-------------------------------------------------------
 0  MainA          500.0 C1 N1 1.0    ON  ON  OFF 0
 1  MainB          500.0 C1 N1 1.0    ON  ON  OFF 1
 2  MainC          500.0 C1 N1 1.0    ON  ON  OFF 2
 3  ExtLightA       200.0 C1 N1 1.0    ON  ON  OFF 3
 4  ExtLightB       200.0 C1 N1 1.0    ON  ON  OFF 4
 5  ExtLightC       200.0 C1 N1 1.0    ON  ON  OFF 5
 6               0.0   A1 N1 1.0    OFF OFF OFF 6
 7               0.0   A1 N1 1.0    OFF OFF OFF 7

K20_PW_TABLE
|PW|DESCRIP        |KW |KWH|KVA|KVH|
-------------------------------------
 0  MainA          ON  OFF OFF OFF
 1  MainB          ON  OFF OFF OFF
 2  MainC          ON  OFF OFF OFF
 3  ExtLightA       ON  OFF OFF OFF
 4  ExtLightB       ON  OFF OFF OFF
 5  ExtLightC       ON  OFF OFF OFF
 6               OFF OFF OFF OFF
 7               OFF OFF OFF OFF


RECORDER_TYPE
DESCRIP: Main Panel4-Luton
```

MODEL: K20-8
SERIAL: 10047
RECORDER_INFO
PSID: 1
MIN: 15
PSDESC:
RINGS: 2
CUTOFF: 0
OPTIONA: 0
OPTIONB: 0

K20_CT_TABLE

CH	DESCRIP	AMPS	VH	VL	VMULT	VLT	AMP	DLT	PW
0	SecondFl-2A	70.00	C1	N1	1.0	ON	ON	OFF	0
1	SecondFl-2B	70.00	C1	N1	1.0	ON	ON	OFF	1
2	SecondFl-2C	70.00	C1	N1	1.0	ON	ON	OFF	2
3	MCC-SupplyA	400.0	C1	N1	1.0	ON	ON	OFF	3
4	MCC-SupplyB	400.0	C1	N1	1.0	ON	ON	OFF	4
5	MCC-SupplyC	400.0	C1	N1	1.0	ON	ON	OFF	5
6		0.0	A1	N1	1.0	OFF	OFF	OFF	6
7		0.0	A1	N1	1.0	OFF	OFF	OFF	7

K20_PW_TABLE

PW	DESCRIP	KW	KWH	KVA	KVH
0	SecondFl-2A	ON	OFF	OFF	OFF
1	SecondFl-2B	ON	OFF	OFF	OFF
2	SecondFl-2C	ON	OFF	OFF	OFF
3	MCC-SupplyA	ON	OFF	OFF	OFF
4	MCC-SupplyB	ON	OFF	OFF	OFF
5	MCC-SupplyC	ON	OFF	OFF	OFF
6		OFF	OFF	OFF	OFF
7		OFF	OFF	OFF	OFF

RECORDER_TYPE
DESCRIP: Main Panel5-Luton
MODEL: K20-8
SERIAL: 10048
RECORDER_INFO
PSID: 1
MIN: 15
PSDESC:
RINGS: 2
CUTOFF: 0

OPTIONA: 0
OPTIONB: 0

K20_CT_TABLE

CH	DESCRIP	AMPS	VH	VL	VMULT	VLT	AMP	DLT	PW
0	SecondFl-3A	70.00	C1	N1	1.0	ON	ON	OFF	0
1	SecondFl-3B	70.00	C1	N1	1.0	ON	ON	OFF	1
2	SecondFl-3C	70.00	C1	N1	1.0	ON	ON	OFF	2
3		0.0	A1	N1	1.0	OFF	OFF	OFF	3
4		0.0	A1	N1	1.0	OFF	OFF	OFF	4
5		0.0	A1	N1	1.0	OFF	OFF	OFF	5
6		0.0	A1	N1	1.0	OFF	OFF	OFF	6
7		0.0	A1	N1	1.0	OFF	OFF	OFF	7

K20_PW_TABLE

PW	DESCRIP	KW	KWH	KVA	KVH
0	SecondFl-3A	ON	OFF	OFF	OFF
1	SecondFl-3B	ON	OFF	OFF	OFF
2	SecondFl-3C	ON	OFF	OFF	OFF
3		OFF	OFF	OFF	OFF
4		OFF	OFF	OFF	OFF
5		OFF	OFF	OFF	OFF
6		OFF	OFF	OFF	OFF
7		OFF	OFF	OFF	OFF

RECORDER_TYPE
DESCRIP: BoilerRm-Luton
MODEL: K20-8
SERIAL: 10049
RECORDER_INFO
PSID: 1
MIN: 15
PSDESC:
RINGS: 2
CUTOFF: 0
OPTIONA: 0
OPTIONB: 0

K20_CT_TABLE

CH	DESCRIP	AMPS	VH	VL	VMULT	VLT	AMP	DLT	PW
0	Boiler-1	50.00	C1	N1	1.0	ON	ON	OFF	0
1	Boiler-2	50.00	C1	N1	1.0	ON	ON	OFF	1

```
 2  Boiler-3        50.00 C1 N1 1.0    ON  ON  OFF 2
 3  Atrium Fans     50.00 C1 N1 1.0    ON  ON  OFF 3
 4                  0.0   A1 N1 1.0    OFF OFF OFF 4
 5                  0.0   A1 N1 1.0    OFF OFF OFF 5
 6                  0.0   A1 N1 1.0    OFF OFF OFF 6
 7                  0.0   A1 N1 1.0    OFF OFF OFF 7

K20_PW_TABLE
|PW|DESCRIP        |KW |KWH|KVA|KVH|
-------------------------------------
 0  Boiler-1        ON  OFF OFF OFF
 1  Boiler-2        ON  OFF OFF OFF
 2  Boiler-3        ON  OFF OFF OFF
 3  Atrium Fans     ON  OFF OFF OFF
 4                  OFF OFF OFF OFF
 5                  OFF OFF OFF OFF
 6                  OFF OFF OFF OFF
 7                  OFF OFF OFF OFF


RECORDER_TYPE
DESCRIP: Main Panel2-Luton
  MODEL: K20-8
 SERIAL: 10050
RECORDER_INFO
   PSID: 1
    MIN: 15
 PSDESC:
  RINGS: 2
 CUTOFF: 0
OPTIONA: 0
OPTIONB: 0

K20_CT_TABLE
|CH|DESCRIP        |AMPS |VH|VL|VMULT |VLT|AMP|DLT|PW|
-------------------------------------------------------
 0  GroundFl-2A     200.0 C1 N1 1.0    ON  ON  OFF 0
 1  GroundFl-2B     200.0 C1 N1 1.0    ON  ON  OFF 1
 2  GroundFl-2C     200.0 C1 N1 1.0    ON  ON  OFF 2
 3  FirstFl-2A      70.00 C1 N1 1.0    ON  ON  OFF 3
 4  FirstFl-2B      70.00 C1 N1 1.0    ON  ON  OFF 4
 5  FirstFl-2C      70.00 C1 N1 1.0    ON  ON  OFF 5
 6                  0.0   A1 N1 1.0    OFF OFF OFF 6
 7                  0.0   A1 N1 1.0    OFF OFF OFF 7

K20_PW_TABLE
```

```
|PW|DESCRIP        |KW |KWH|KVA|KVH|
-------------------------------------
 0  GroundFl-2A      ON  OFF OFF OFF
 1  GroundFl-2B      ON  OFF OFF OFF
 2  GroundFl-2C      ON  OFF OFF OFF
 3  FirstFl-2A       ON  OFF OFF OFF
 4  FirstFl-2B       ON  OFF OFF OFF
 5  FirstFl-2C       ON  OFF OFF OFF
 6                OFF OFF OFF OFF
 7                OFF OFF OFF OFF


RECORDER_TYPE
DESCRIP: Main Panel3-Luton
  MODEL: K20-6
 SERIAL: 10051
RECORDER_INFO
   PSID: 1
    MIN: 15
 PSDESC:
  RINGS: 2
 CUTOFF: 0
OPTIONA: 0
OPTIONB: 0

K20_CT_TABLE
|CH|DESCRIP        |AMPS |VH|VL|VMULT |VLT|AMP|DLT|PW|
-------------------------------------------------------
 0  SecondFl-1A      70.00 C1 N1 1.0    ON  ON  OFF 0
 1  SecondFl-1B      70.00 C1 N1 1.0    ON  ON  OFF 1
 2  SecondFl-1C      70.00 C1 N1 1.0    ON  ON  OFF 2
 3  FirstFl-1A       100.0 C1 N1 1.0    ON  ON  OFF 3
 4  FirstFl-1B       100.0 C1 N1 1.0    ON  ON  OFF 4
 5  FirstFl-1C       100.0 C1 N1 1.0    ON  ON  OFF 5
 6  GroundFl-1A      100.0 C1 N1 1.0    ON  ON  OFF 6
 7  GroundFl-1B      100.0 C1 N1 1.0    ON  ON  OFF 7
 8  GroundFl-1C      100.0 C1 N1 1.0    ON  ON  OFF 8
 9  Lift-A           50.00 C1 N1 1.0    ON  ON  OFF 9
 10 Lift-B           50.00 C1 N1 1.0    ON  ON  OFF 10
 11 Lift-C           50.00 C1 N1 1.0    ON  ON  OFF 11
 12 Kitchen-A        50.00 C1 N1 1.0    ON  ON  OFF 12
 13 Kitchen-B        50.00 C1 N1 1.0    ON  ON  OFF 13
 14 Kitchen-C        50.00 C1 N1 1.0    ON  ON  OFF 14
 15                0.0   A1 N1 1.0    OFF OFF OFF 15

K20_PW_TABLE
```

```
|PW|DESCRIP        |KW |KWH|KVA|KVH|
-------------------------------------
 0  SecondFl-1A      ON  OFF OFF OFF
 1  SecondFl-1B      ON  OFF OFF OFF
 2  SecondFl-1C      ON  OFF OFF OFF
 3  FirstFl-1A       ON  OFF OFF OFF
 4  FirstFl-1B       ON  OFF OFF OFF
 5  FirstFl-1C       ON  OFF OFF OFF
 6  GroundFl-1A      ON  OFF OFF OFF
 7  GroundFl-1B      ON  OFF OFF OFF
 8  GroundFl-1C      ON  OFF OFF OFF
 9  Lift-A           ON  OFF OFF OFF
 10 Lift-B           ON  OFF OFF OFF
 11 Lift-C           ON  OFF OFF OFF
 12 Kitchen-A        ON  OFF OFF OFF
 13 Kitchen-B        ON  OFF OFF OFF
 14 Kitchen-C        ON  OFF OFF OFF
 15                OFF OFF OFF OFF
```

CR10X Weather Station Files

```
};CR10X
;MET_SU~1.DLD
;$1/6/11/16 2/7/12/17 3/8/13/18        4/9/14/19 5/10/15/20
;:Batt_Volt:latitude :longitude:K_hrAngle:day_ofYr
;:hr_ofYr  :min_ofDay:sec_ofMin:declinatn:EOT
;:ssHrang  :sTotHzWm2:shTotal  :eShade   :fullShade
;:wShade   :ckNoShade:Prog_Sig :AirTC    :RH
;:WS_ms    :SlrkW    :SlrkJ    :psia
;$

;Luton, England
;51 deg 25 min N
;0 deg 26 min W

MODE 1
SCAN RATE 20.0000

1:P10   ;battery voltage in location 1
1:1

;SETUP CONTROL(I/O) PORTS FOR SHADOWBAND
1:P91   ;IF
1:28    ;flag 8 is low
2:30    ;THEN DO
```

```
2:P20   ;set control ports
1:9998 ;C8765: C5 as input HomeSense
2:1109 ;C4321: C4=C3=output C2=low

3:P20   ;set control ports
1:9999 ;C8765
2:9949 ;C4321: C2 for (3)1ms (4)10ms (5)100ms pulse

4:P95   ;ENDIF

;DAILY EOT CALCULATION AND SIGNATURE
11:P92 ;IF
1:0       ;minutes into...
2:1440 ;minute interval
3:28     ;set flag 8 low

12:P91  ;IF
1:28    ;flag 8 is low
2:30    ;THEN DO

3:P19   ;SIGNATURE IN LOC18
1:18

;DUMMY VARIABLES
;30 - N
;31 - DUM1
;32 - DUM2

13:P18
1:2       ;hours into year
2:0       ;no-op
3:5       ;hour of year

14:P30   ;DUM1 = 24
1:24
2:0
3:31

15:P38   ;hours--->days into year
1:5     ;day_ofYr
2:31   ;hrs per day
3:5     ;day_ofYr

16:P45   ;INT part of day of year
1:5     ;day_ofYr
```

```
2:5     ;day_ofYr

17:P30    ;EOT = 0.000075
1:7.5
2:-5
3:10

18:P37    ;N = 360/365*day_ofYr
1:5
2:0.98630
3:30

19:P34    ;DUM1 = N + 90
1:30
2:90
3:31

20:P48    ;DUM1 = sin(DUM1)
1:31
2:31

21:P30   ;DUM2 = 0.001868
1:1.868
2:-3
3:32

22:P36   ;DUM1 = 0.001868*DUM1
1:32
2:31
3:31

23:P33  ;EOT = EOT + DUM1
1:31
2:10
3:10

24:P48   ;DUM1 = sin(N)
1:30
2:31

25:P30   ;DUM2 = -0.032077
1:-3.2077
2:-2
3:32

26:P36   ;DUM1 = -0.032077*DUM1
```

```
1:32
2:31
3:31

27:P33   ;EOT = EOT + DUM1
1:31
2:10

3:10

28:P37   ;DUM1 = 2*N
1:30
2:2
3:31

29:P34   ;DUM1 = DUM1 + 90
1:31
2:90
3:31

30:P48   ;DUM1 = sin(DUM1)
1:31
2:31

31:P30   ;DUM2 = -0.014615
1:-1.4615
2:-2
3:32

32:P36   ;DUM1 = -0.014615*DUM1
1:32
2:31
3:31

33:P33   ;EOT = EOT + DUM1
1:31
2:10
3:10

34:P37   ;DUM1 = 2*N
1:30
2:2
3:31

35:P48   ;DUM1 = sin(DUM1)
1:31
```

```
2:31

36:P30   ;DUM2 = -0.04089
1:-4.089
2:-2
3:32

37:P36   ;DUM1 = -0.04089*DUM1
1:32
2:31
3:31

38:P33   ;EOT = EOT + DUM1
1:31
2:10
3:10

39:P37   ;EOT = 229.2*EOT gives EOT in minutes
1:10
2:229.2
3:10

40:P86   ;DO
1:18     ;Set flag 8 high

41:P95
;END OF DAILY EOT CALCULATION

;CHECK/SEND SHADOWBAND HOME
43:P87
1:0
2:400   ;one revolution at most; then quit if home is not sensed

44:P91 ;IF
1:45     ;port5 (homeSense)
2:31     ;exit loop

45:P86 ;DO
1:72     ;pulse port2 (step)

46:
47:P95 ;end

;3:P30  ;set inputLOC
;1:-20  ;test value
;2:0     ;10exp
```

```
;3:4     ;[K_hrAngle]

;CALC SHADOWBAND POSITION
51:P18
1:1      ;minutes into day (0-1439? or 1-1440?)
2:0      ;no-op
3:7      ;

52:P33 ;Z=X+Y
1:4      ;
2:10     ;equation-of-time correction
3:4      ;min_ofDay

53:P37 ;Z=X*F convert to degrees
1:7      ;X=min_ofDay
2:.25    ;360/1440 degrees/minute
3:4      ;Z=K_hrAngle

54:P34 ;Z=X+F
1:4      ;
2:359.57         ;add 360, then subtract longitude of Luton
3:4      ;Z=K_hrAngle

56:P46 ;Z=X mod F
1:4
2:360    ;must lie between 0 and 360
3:4      ;Z=K_hrAngle

57:P37 ;Z=X*F convert to steps
1:4      ;
2:-1.111;convert to #steps (negative for up-counter: -400/360 steps/revolution
3:4      ;Z=K_hrAngle

;58:P22          ;EXC w/DELAY (only for delay)
;1:0     ;exc chan
;2:0     ;*10ms duration
;3:200   ;*10ms delay after
;4:0     ;volts

;58:P4   ;Excite, delay, measure (only for delay)
;1:1     ;reps
;2:0     ;range code
;3:1     ;channel for measurement
;4:1     ;channel for excitation
;5:100   ;delay in hundredths of a second
;6:0     ;excitation voltage (mV)
```

```
;7:21   ;input location
;8:0    ;mulptiplier
;9:0    ;offset

59:P2   ;unshaded solar flux
1:1
2:32
3:5
4:13
5:0.1962
6:0

20:P89  ;IF
1:13    ;Slr_kW
2:4     ;<
3:0     ;0
4:30    ;DO

21:P30  ;Slr_kW = 0
1:0
2:0
3:13

22:P95  ;ENDIF

;MOVE SHADOW BAND TO EAST-SHADE POSITION
64:P87 ;loop
1:0       ;no delay
2:400   ;count (1 revolution=400 max steps)

65:P89 ;if K_hrAngle>= 0 exit loop
1:4       ;[K_hrAngle]
2:3       ;>=
3:0       ;0
4:31     ;exit loop

66:P86 ;do
1:72     ;pulse C2

67:P32 ;incr
1:4       ;[K_hrAngle]

68:P95 ;end

;69:P22          ;EXC w/DELAY (only for delay)
;1:0      ;exc chan
```

```
;2:0      ;*10ms duration
;3:200  ;*10ms delay after
;4:0      ;volts

;69:P4  ;Excite, delay, measure (only for delay)
;1:1    ;reps
;2:0    ;range code
;3:1    ;channel for measurement
;4:1    ;channel for excitation
;5:100  ;delay in hundredths of a second
;6:0    ;excitation voltage (mV)
;7:21   ;input location
;8:0    ;mulptiplier
;9:0    ;offset

70:P2   ;east-shaded solar flux
1:1
2:32
3:5
4:14
5:0.1962
6:0

20:P89  ;IF
1:14    ;Slr_kW
2:4     ;<
3:0     ;0
4:30    ;DO

21:P30  ;Slr_kW = 0
1:0
2:0
3:14

22:P95  ;ENDIF

;MOVE SHADOW BAND TO FULL-SHADE POSITION
74:P87 ;loop
1:0       ;no delay
2:6       ;6 steps == 5.4 degrees

76:P86 ;do
1:72     ;pulse C2

78:P95 ;end
```

```
;79:P22          ;EXC w/DELAY (only for delay)
;1:0     ;exc chan
;2:0     ;*10ms duration
;3:200  ;*10ms delay after
;4:0     ;volts

;69:P4  ;Excite, delay, measure (only for delay)
;1:1    ;reps
;2:0    ;range code
;3:1    ;channel for measurement
;4:1    ;channel for excitation
;5:100  ;delay in hundredths of a second
;6:0    ;excitation voltage (mV)
;7:21   ;input location
;8:0    ;mulptiplier
;9:0    ;offset

80:P2   ;full-shaded solar flux
1:1
2:32
3:5
4:15
5:0.1962
6:0

20:P89  ;IF
1:15    ;Slr_kW
2:4     ;<
3:0     ;0
4:30    ;DO

21:P30  ;Slr_kW = 0
1:0
2:0
3:15

22:P95  ;ENDIF

;MOVE SHADOW BAND TO WEST-SHADE POSITION
84:P87 ;loop
1:0      ;no delay
2:6      ;6 steps == 5.4 degrees

86:P86 ;do
1:72     ;pulse C2
```

```
88:P95 ;end

;90:P22          ;EXC w/DELAY (only for delay)
;1:0     ;exc chan
;2:0     ;*10ms duration
;3:200  ;*10ms delay after
;4:0     ;volts

;69:P4  ;Excite, delay, measure (only for delay)
;1:1    ;reps
;2:0    ;range code
;3:1    ;channel for measurement
;4:1    ;channel for excitation
;5:100  ;delay in hundredths of a second
;6:0    ;excitation voltage (mV)
;7:21   ;input location
;8:0    ;mulptiplier
;9:0    ;offset

91:P2   ;west-shaded solar flux
1:1
2:32
3:5
4:16
5:0.1962
6:0

20:P89  ;IF
1:16    ;Slr_kW
2:4     ;<
3:0     ;0
4:30    ;DO

21:P30  ;Slr_kW = 0
1:0
2:0
3:16

22:P95  ;ENDIF

;CHECK/SEND SHADOWBAND HOME
92:P87
1:0
2:400   ;one revolution at most; must quit even if home is not sensed

93:P91 ;IF
```

```
1:45     ;port5 (homeSense)
2:31     ;exit loop

94:P86 ;DO
1:72     ;pulse port2 (step)

95:P95 ;end

;96:P22          ;EXC w/DELAY (only for delay)
;1:0      ;exc chan
;2:0      ;*10ms duration
;3:200  ;*10ms delay after
;4:0      ;volts

;69:P4  ;Excite, delay, measure (only for delay)
;1:1    ;reps
;2:0    ;range code
;3:1    ;channel for measurement
;4:1    ;channel for excitation
;5:100  ;delay in hundredths of a second
;6:0    ;excitation voltage (mV)
;7:21   ;input location
;8:0    ;mulptiplier
;9:0    ;offset

97:P2   ;system check: measure unshaded flux again
1:1
2:32
3:5
4:17
5:0.1962
6:0

20:P89  ;IF
1:17    ;Slr_kW
2:4     ;<
3:0     ;0
4:30    ;DO

21:P30  ;Slr_kW = 0
1:0
2:0
3:17

22:P95  ;ENDIF
```

```
;DONE WITH SHADOWBAND MEASUREMENTS

5:P86   ;DO
1:41    ;port 1 high

6:P22   ;excit. w/delay
1:1     ;channel 1
2:15    ;delay 15 ms
3:0
4:0     ;0 V

7:P2    ;voltage differential
1:1
2:35    ;50 Hz, +/-2500 mv
3:3     ;channel 3
4:19     ;AirTC in loc 19
5:0.1
6:-40.0

8:P2    ;voltage differential
1:1
2:35    ;50 Hz, +/-2500 mv
3:4     ;channel 4
4:20    ;RH in loc 20
5:0.1
6:0

9:P86   ;DO
1:51    ;port 1 low

10:P89  ;IF
1:20    ;RH
2:3     ;>=
3:100   ;100
4:30    ;DO

11:P89  ;IF
1:20    ;RH
2:4     ;<
3:108   ;108
4:30    ;DO

12:P30  ;RH=100
1:100
2:0
3:20
```

```
13:P95  ;ENDIF

14:P95  ;ENDIF

15:P3   ;pulse
1:1
2:1     ;channel 1
3:22    ;switch closure
4:21    ;WS_ms in loc 21
5:0.8
6:0.447

16:P89  ;IF
1:21    ;WS_ms
2:4     ;<
3:0.457 ;0.457
4:30    ;DO

17:P30  ;Ws_ms = 0
1:0
2:0
3:21

18:P95  ;ENDIF

19:P2   ;Voltage differential
1:1
2:32    ;50 Hz, +/-7.5 mV
3:2     ;diff. channel 2
4:22    ;Slr_kW in loc 22
5:1
6:0

20:P89  ;IF
1:22    ;Slr_kW
2:4     ;<
3:0     ;0
4:30    ;DO

21:P30  ;Slr_kW = 0
1:0
2:0
3:22

22:P95  ;ENDIF
```

```
23:P37  ;SlrkJ = 2*SlrkW
1:22
2:2.0
3:23

24:P37  ;SlrkW = 0.2*SlrkW
1:22
2:0.2
3:22

25:P2
1:1 ;reps
2:34 ;50Hz rejection, 250mv range
3:6 ;differential channel 6
4:24 ;baro-PSIA in loc 24
5:.13021 ;25PSIA/192mv (16ma*12ohm)
6:-6.25  ;all 4-20ma devices: subtract 25% of span (25psia/4=6.25psia)

25:P92  ;IF time
1:0     ;minutes into...
2:15    ;minute interval
3:10    ;set output flag

26:P80  ;Store Area
1:1     ;Final storage
2:101   ;101

27:P77  ;time stamp
1:1220

101:P71         ;average
1:6
2:12     ;6 solrad measurements (LOC12-17)

102:P73         ;maximum
1:6
2:0
3:12     ;6 solrad measurements (LOC12-17)

28:P71  ;average
1:1
2:19    ;Air_TC

29:P71  ;average
1:1
```

```
2:20    ;RH

30:P70  ;sample
1:1
2:20    ;RH

31:P71  ;average
1:1
2:21    ;WS_ms

32:P73  ;maximum
1:1
2:0
3:21    ;WS_ms

33:P71  ;average
1:1
2:22    ;SlrkW

33:P71  ;average
1:1
2:24    ;psia

34:P92  ;IF time
1:0     ;minutes into...
2:1440  ;minute interval
3:10    ;set output flag

35:P80  ;Store Area
1:1     ;final storage
2:102   ;102

36:P77  ;time stamp
1:1220

37:P74  ;maximum
1:1
2:0
3:1     ;battery voltage

38:P70  ;sample
1:1
2:18    ;signature

39:P78  ;high res.
1:1
```

40:P72 ;total
1:1
2:23   ;SlrkJ

41:P78 ;low res.
1:0

42:P71 ;average
1:1
2:19   ;AirTC

43:P71 ;average
1:1
2:21   ;WS_ms

44:P71 ;average
1:1
2:22   ;SlrkW

MODE 2
SCAN RATE 10.0000
1:P96
1:71

MODE 3

MODE 10
1:96
2:118
3:0

MODE 12
1:0
2:0
3:0

Appendix B: Additional Experimental Results

Single Heated Zone Results

Seven Windows Open: Upper versus Lower Window Location

Table 53. Scaled Temperature Distribution Comparison of Lower and Upper Windows for Seven Window, Three Stack Model Case

7 Windows 3 Stacks	Temperature Location	Lower Windows (°C)	Upper Windows (°C)
Scaled Temperature	Texhaust	13.89	14.19
	Tatrium	13.37	13.72
	Tatrium-lower	12.73	13.05
	Tatrium-upper	13.48	13.81
	Theated-zone	17.12	17.35
	Tcolumn	13.60	13.84
	Tcolumn-lower	10.88	10.62
	Tcolumn-upper	15.63	16.34
	Model Taverage	13.84	14.12
	outlet velocity	0.70	0.77

Table 54. Scaled Temperature Distribution Comparison of Lower and Upper Windows for Seven Window, Three Stack Model Case

7 Windows 2 Stacks	Temperature Location	Lower Windows (°C)	Upper Windows (°C)
Scaled Temperature	Texhaust	15.70	16.37
	Tatrium	15.29	15.95
	Tatrium-lower	14.49	14.99
	Tatrium-upper	15.46	16.10
	Theated-zone	18.26	19.09
	Tcolumn	15.21	16.39
	Tcolumn-lower	12.05	14.02
	Tcolumn-upper	17.37	18.93
	Model Taverage	15.48	16.48
	outlet velocity	0.9	0.8

Five Windows Open: Upper versus Lower Window Location

Table 55. Scaled Temperature Distribution Comparison of Lower and Upper Windows for Five Window, Three Stack Model Case

5 Windows 3 Stacks	Temperature Location	Lower Windows (°C)	Upper Windows (°C)
Scaled Temperature	Texhaust	15.06	14.61
	Tatrium	14.77	14.44
	Tatrium-lower	14.42	14.26
	Tatrium-upper	14.85	14.48
	Theated-zone	18.08	18.10
	Tcolumn	15.06	14.61
	Tcolumn-lower	12.39	11.64
	Tcolumn-upper	16.73	16.41
	Model Taverage	15.17	14.82
	outlet velocity	0.70	0.73

Table 56. Scaled Temperature Distribution Comparison of Lower and Upper Windows for Five Window, Two Stack Model Case

5 Windows 2 Stacks	Temperature Location	Lower Windows (°C)	Upper Windows (°C)
Scaled Temperature	Texhaust	16.60	16.31
	Tatrium	16.23	15.78
	Tatrium-lower	15.77	14.97
	Tatrium-upper	16.31	15.90
	Theated-zone	19.33	18.93
	Tcolumn	16.62	16.45
	Tcolumn-lower	13.85	13.63
	Tcolumn-upper	18.41	19.07
	Model Taverage	16.64	16.38
	outlet velocity	0.8	0.9

Two Windows Open: Upper versus Lower Window Location

Table 57. Scaled Temperature Distribution Comparison of Lower and Upper Windows for Two Window, Three Stack Model Case

2 Windows 3 Stacks	Temperature Location	Lower Windows (°C)	Upper Windows (°C)
Scaled Temperature	Texhaust	16.87	16.16
	Tatrium	16.42	15.76
	Tatrium-lower	15.87	15.55
	Tatrium-upper	16.50	15.81
	Theated-zone	19.94	19.24
	Tcolumn	16.34	15.79
	Tcolumn-lower	13.00	12.87
	Tcolumn-upper	18.78	17.76
	Model Taverage	16.72	16.12
	outlet velocity	0.60	0.65

Table 58. Scaled Temperature Distribution Comparison of Lower and Upper Windows for Two Window, Two Stack Model Case

2 Windows 2 Stacks	Temperature Location	Lower Windows (°C)	Upper Windows (°C)
Scaled Temperature	Texhaust	18.46	17.26
	Tatrium	17.94	16.91
	Tatrium-lower	17.66	16.60
	Tatrium-upper	17.99	16.97
	Theated-zone	21.03	20.43
	Tcolumn	17.84	17.07
	Tcolumn-lower	13.83	14.13
	Tcolumn-upper	20.50	19.13
	Model Taverage	18.15	17.31
	outlet velocity	0.7	0.8

One Window Open: Upper versus Lower Window Location

Table 59. Scaled Temperature Distribution Comparison of Lower and Upper Windows for One Window, Three Stack Model Case

1 Window 3 Stacks	Temperature Location	Lower Windows (°C)	Upper Windows (°C)
Scaled Temperature	Texhaust	16.87	16.12
	Tatrium	16.42	15.83
	Tatrium-lower	15.87	15.43
	Tatrium-upper	16.50	15.90
	Theated-zone	19.94	19.75
	Tcolumn	16.34	16.24
	Tcolumn-lower	13.00	13.45
	Tcolumn-upper	18.78	18.94
	Model Taverage	16.72	16.46
	outlet velocity	0.57	0.6

Table 60. Scaled Temperature Distribution Comparison of Lower and Upper Windows for One Window, Two Stack Model Case

1 Window 2 Stacks	Temperature Location	Lower Windows (°C)	Upper Windows (°C)
Scaled Temperature	Texhaust	20.27	17.44
	Tatrium	19.38	17.20
	Tatrium-lower	18.30	16.73
	Tatrium-upper	19.56	17.27
	Theated-zone	22.60	20.93
	Tcolumn	19.68	17.69
	Tcolumn-lower	15.06	14.75
	Tcolumn-upper	23.45	20.42
	Model Taverage	19.79	17.80
	outlet velocity	0.7	0.7

Single Heated Zone Model vs Building: Lower Windows Open

Table 61. Comparison of Dimensionless Temperature Distribution for Model and Hypothetical Building**:** Seven Window Cases-Lower Window

	Experimental Model Temperatures		Predicted Building Temperatures (Tambient=20 C)	
Ground Floor Column	**7 windows 3 stacks**	**7 Windows 2 Stacks**	**7 windows 3 stacks**	**7 Windows 2 Stacks**
26 cm / 3 m	26.38	29.31	22.90	23.22
19 cm / 2.3 m	25.16	28.38	22.77	23.12
12 cm / 1.4 m	21.90	24.68	22.41	22.71
5 cm / 0.6 m	18.35	20.33	22.02	22.24
Ground Floor Heated Zone	**7 windows 3 stacks**	**7 Windows 2 Stacks**	**7 windows 3 stacks**	**7 Windows 2 Stacks**
27 cm / 3.2 m	27.85	31.15	23.06	23.43
21 cm / 2.5 m	25.33	29.10	22.79	23.20
15 cm / 1.8 m	26.01	27.79	22.86	23.06
9.5 cm / 1.1 m	26.29	24.44	22.89	22.69
3 cm / 0.4 m	38.94	41.63	24.28	24.58
Atrium	**7 windows 3 stacks**	**7 Windows 2 Stacks**	**7 windows 3 stacks**	**7 Windows 2 Stacks**
100 cm / 12 m	22.80	26.08	22.51	22.87
75 cm / 9 m	23.03	26.65	22.53	22.93
50 cm / 6 m	22.59	26.36	22.49	22.90
25 cm / 3 m	21.48	24.46	22.36	22.69

Table 62. Comparison of Dimensionless Temperature Distribution for Model and Hypothetical Building**:** Five Window Cases-Lower Window

	Experimental Model Temperatures		Predicted Building Temperatures (Tambient=20 C)	
Ground Floor Column	**5 Windows 3 Stacks**	**5 Windows 2 Stacks**	**5 Windows 3 Stacks**	**5 Windows 2 Stacks**
26 cm / 3 m	28.23	31.08	23.11	23.42
19 cm / 2.3 m	27.51	30.20	23.03	23.32
12 cm / 1.4 m	24.99	27.53	22.75	23.03
5 cm / 0.6 m	20.91	23.38	22.30	22.57
Ground Floor Heated Zone	**5 Windows 3 Stacks**	**5 Windows 2 Stacks**	**5 Windows 3 Stacks**	**5 Windows 2 Stacks**
27 cm / 3.2 m	29.79	32.18	23.28	23.54
21 cm / 2.5 m	28.55	30.53	23.14	23.36
15 cm / 1.8 m	27.46	29.60	23.02	23.26
9.5 cm / 1.1 m	25.47	27.64	22.80	23.04
3 cm / 0.4 m	41.28	43.19	24.54	24.75
Atrium	**5 Windows 3 Stacks**	**5 Windows 2 Stacks**	**5 Windows 3 Stacks**	**5 Windows 2 Stacks**
100 cm / 12 m	25.00	27.47	22.75	23.02
75 cm / 9 m	25.06	27.71	22.76	23.05
50 cm / 6 m	25.39	27.76	22.79	23.05

25 cm / 3 m	24.33	26.62	22.68	22.93

Table 63. Comparison of Dimensionless Temperature Distribution for Model and Hypothetical Building**:** Two Window Cases-Lower Window

	Experimental Model Temperatures		Predicted Building Temperatures (Tambient=20 C)	
Ground Floor Column	**2 Windows 3 Stacks**	**2 Windows 2 Stacks**	**2 Windows 3 Stacks**	**2 Windows 2 Stacks**
26 cm / 3 m	31.70	34.59	23.49	23.81
19 cm / 2.3 m	29.90	32.70	23.29	23.60
12 cm / 1.4 m	26.78	29.80	22.95	23.28
5 cm / 0.6 m	21.94	23.34	22.41	22.57
Ground Floor Heated Zone	**2 Windows 3 Stacks**	**2 Windows 2 Stacks**	**2 Windows 3 Stacks**	**2 Windows 2 Stacks**
27 cm / 3.2 m	34.59	36.45	23.80	24.01
21 cm / 2.5 m	32.30	33.42	23.55	23.68
15 cm / 1.8 m	30.98	32.81	23.41	23.61
9.5 cm / 1.1 m	27.18	30.54	22.99	23.36
3 cm / 0.4 m	43.20	44.19	24.75	24.86
Atrium	**2 Windows 3 Stacks**	**2 Windows 2 Stacks**	**2 Windows 3 Stacks**	**2 Windows 2 Stacks**
100 cm / 12 m	28.16	30.77	23.10	23.38
75 cm / 9 m	27.95	30.62	23.07	23.37
50 cm / 6 m	28.19	30.29	23.10	23.33
25 cm / 3 m	26.78	29.80	22.95	23.28

Single Heated Zone Model vs Building: Upper Windows Open

Table 64. Comparison of Dimensionless Temperature Distribution for Model and Hypothetical Building**:** Seven Window Cases-Upper Window

	Experimental Model Temperatures		Predicted Building Temperatures (Tambient=20 C)	
Ground Floor Column	**7 windows 3 stacks**	**7 Windows 2 Stacks**	**7 windows 3 stacks**	**7 Windows 2 Stacks**
26 cm / 3 m	27.57	31.95	23.03	23.51
19 cm / 2.3 m	26.05	28.97	22.87	23.19
12 cm / 1.4 m	21.87	26.04	22.41	22.86
5 cm / 0.6 m	17.93	23.66	21.97	22.60
Ground Floor Heated Zone	**7 windows 3 stacks**	**7 Windows 2 Stacks**	**7 windows 3 stacks**	**7 Windows 2 Stacks**
27 cm / 3.2 m	29.70	37.62	23.27	24.14
21 cm / 2.5 m	26.19	33.70	22.88	23.71
15 cm / 1.8 m	24.79	31.13	22.73	23.42
9.5 cm / 1.1 m	22.69	30.01	22.50	23.30
3 cm / 0.4 m	43.03	28.64	24.73	23.15
Atrium	**7 windows 3 stacks**	**7 Windows 2 Stacks**	**7 windows 3 stacks**	**7 Windows 2 Stacks**
100 cm / 12 m	23.27	27.15	22.56	22.99
75 cm / 9 m	24.16	27.54	22.66	23.03
50 cm / 6 m	22.86	27.63	22.51	23.04
25 cm / 3 m	22.03	25.31	22.42	22.78

Table 65. Comparison of Dimensionless Temperature Distribution for Model and Hypothetical Building**:** Five Window Cases-Upper Window

	Experimental Model Temperatures		Predicted Building Temperatures (Tambient=20 C)	
Ground Floor Column	**5 Windows 3 Stacks**	**5 Windows 2 Stacks**	**5 Windows 3 Stacks**	**5 Windows 2 Stacks**
26 cm / 3 m	27.69	32.18	23.05	23.54
19 cm / 2.3 m	27.00	29.66	22.97	23.26
12 cm / 1.4 m	24.30	26.18	22.67	22.88
5 cm / 0.6 m	19.65	23.00	22.16	22.53
Ground Floor Heated Zone	**5 Windows 3 Stacks**	**5 Windows 2 Stacks**	**5 Windows 3 Stacks**	**5 Windows 2 Stacks**
27 cm / 3.2 m	29.82	36.91	23.28	24.06
21 cm / 2.5 m	27.97	32.59	23.08	23.58
15 cm / 1.8 m	26.89	31.07	22.96	23.42
9.5 cm / 1.1 m	24.32	30.01	22.68	23.30
3 cm / 0.4 m	43.77	29.19	24.81	23.21
Atrium	**5 Windows 3 Stacks**	**5 Windows 2 Stacks**	**5 Windows 3 Stacks**	**5 Windows 2 Stacks**
100 cm / 12 m	24.09	27.01	22.65	22.97
75 cm / 9 m	25.35	27.37	22.79	23.01
50 cm / 6 m	24.84	27.35	22.73	23.01

25 cm / 3 m	24.07	25.26	22.65	22.78

Table 66. Comparison of Dimensionless Temperature Distribution for Model and Hypothetical Building**:** Two Window Cases-Upper Window

	Model Temperatures		Predicted Building Temperatures (Tambient=20 C)	
Ground Floor Column	**2 Windows 3 Stacks**	**2 Windows 2 Stacks**	**2 Windows 3 Stacks**	**2 Windows 2 Stacks**
26 cm / 3 m	29.97	32.28	23.30	23.55
19 cm / 2.3 m	28.78	31.34	23.17	23.45
12 cm / 1.4 m	26.10	27.76	22.87	23.05
5 cm / 0.6 m	21.73	23.84	22.39	22.62
Ground Floor Heated Zone	**2 Windows 3 Stacks**	**2 Windows 2 Stacks**	**2 Windows 3 Stacks**	**2 Windows 2 Stacks**
27 cm / 3.2 m	31.74	33.85	23.49	23.72
21 cm / 2.5 m	28.83	32.25	23.17	23.55
15 cm / 1.8 m	29.30	31.01	23.22	23.41
9.5 cm / 1.1 m	27.37	28.70	23.01	23.16
3 cm / 0.4 m	45.09	46.61	24.96	25.13
Atrium	**2 Windows 3 Stacks**	**2 Windows 2 Stacks**	**2 Windows 3 Stacks**	**2 Windows 2 Stacks**
100 cm / 12 m	26.30	28.52	22.89	23.14
75 cm / 9 m	27.61	29.37	23.04	23.23
50 cm / 6 m	27.04	28.94	22.97	23.18
25 cm / 3 m	26.24	28.02	22.89	23.08

Two Heated Zone Results

One Stack Open Temperature Stratification

Table 67. Scaled Temperatures for One Stack Open Model Experiment and Hypothetical Full Scale Building

	Model Temp	**Building Temp**
First Floor Column	**1 Stack Open**	**1 Stack Open**
26 cm / 3 m	54.5	26.0
19 cm / 2.3 m	48.4	25.3
12 cm / 1.4 m	41.6	24.6
5 cm / 0.6 m	37.6	24.1
First Floor Heated Zone	**1 Stack Open**	**1 Stack Open**
27 cm / 3.2 m	63.1	26.9
21 cm / 2.5 m	59.6	26.6
15 cm / 1.8 m	56.6	26.2
9.5 cm / 1.1 m	54.8	26.0
3 cm / 0.4 m	44.7	24.9
Ground Floor Column	**1 Stack Open**	**1 Stack Open**
26 cm / 3 m	37.1	24.1
19 cm / 2.3 m	32.9	23.6
12 cm / 1.4 m	30.3	23.3
5 cm / 0.6 m	26.0	22.9
Ground Floor Heated Zone	**1 Stack Open**	**1 Stack Open**
27 cm / 3.2 m	33.4	23.7
21 cm / 2.5 m	31.2	23.4
15 cm / 1.8 m	31.7	23.5
9.5 cm / 1.1 m	41.6	24.6
3 cm / 0.4 m	40.7	24.5
Atrium	**1 Stack Open**	**1 Stack Open**
100 cm / 12 m	51.7	25.7
75 cm / 9 m	50.5	25.6
50 cm / 6 m	47.7	25.3
25 cm / 3 m	33.6	23.7

Two Stacks Open Temperature Stratification

Table 68. Scaled Temperatures for Two Stacks Open Model Experiment and Hypothetical Full Scale Building

	Model Temperature	**Building Temperature**
First Floor Column	**2 Stacks Open**	**2 Stacks Open**
26 cm / 3 m	49.0	25.4
19 cm / 2.3 m	41.0	24.5
12 cm / 1.4 m	35.2	23.9
5 cm / 0.6 m	34.1	23.8
First Floor Heated Zone	**2 Stacks Open**	**2 Stacks Open**
27 cm / 3.2 m	57.1	26.3
21 cm / 2.5 m	53.2	25.8
15 cm / 1.8 m	49.2	25.4
9.5 cm / 1.1 m	46.9	25.2
3 cm / 0.4 m	37.9	24.2
Ground Floor Column	**2 Stacks Open**	**2 Stacks Open**
26 cm / 3 m	34.0	23.7
19 cm / 2.3 m	30.0	23.3
12 cm / 1.4 m	28.2	23.1
5 cm / 0.6 m	24.2	22.7
Ground Floor Heated Zone	**2 Stacks Open**	**2 Stacks Open**
27 cm / 3.2 m	30.7	23.4
21 cm / 2.5 m	28.5	23.1
15 cm / 1.8 m	29.5	23.2
9.5 cm / 1.1 m	39.7	24.4
3 cm / 0.4 m	38.5	24.2
Atrium	**2 Stacks Open**	**2 Stacks Open**
100 cm / 12 m	45.9	25.1
75 cm / 9 m	44.5	24.9
50 cm / 6 m	41.0	24.5
25 cm / 3 m	30.3	23.3

Three Stacks Open Temperature Stratification

Table 69. Scaled Temperatures for Three Stacks Open Model Experiment and Hypothetical Full Scale Building

	Model Temperature	**Building Temperature**
First Floor Column	**3 Stacks Open**	**3 Stacks Open**
26 cm / 3 m	42.9	24.7
19 cm / 2.3 m	33.2	23.7
12 cm / 1.4 m	31.3	23.4
5 cm / 0.6 m	32.2	23.5
First Floor Heated Zone	**3 Stacks Open**	**3 Stacks Open**
27 cm / 3.2 m	50.1	25.5
21 cm / 2.5 m	46.3	25.1
15 cm / 1.8 m	42.9	24.7
9.5 cm / 1.1 m	39.6	24.4
3 cm / 0.4 m	32.3	23.6
Ground Floor Column	**3 Stacks Open**	**3 Stacks Open**
26 cm / 3 m	30.9	23.4
19 cm / 2.3 m	28.2	23.1
12 cm / 1.4 m	25.9	22.8
5 cm / 0.6 m	22.8	22.5
Ground Floor Heated Zone	**3 Stacks Open**	**3 Stacks Open**
27 cm / 3.2 m	28.6	23.1
21 cm / 2.5 m	27.0	23.0
15 cm / 1.8 m	27.6	23.0
9.5 cm / 1.1 m	37.8	24.2
3 cm / 0.4 m	36.7	24.0
Atrium	**3 Stacks Open**	**3 Stacks Open**
100 cm / 12 m	39.6	24.4
75 cm / 9 m	39.1	24.3
50 cm / 6 m	31.9	23.5
25 cm / 3 m	28.1	23.1

Stacks Closed Temperature Stratification

Table 70. Scaled Temperatures for Stacks Closed Model Experiment and Hypothetical Full Scale Building

	Model Temperature	**Building Temperature**
First Floor Column	**3 Stacks Closed**	**3 Stacks Closed**
26 cm / 3 m	59.9	26.6
19 cm / 2.3 m	53.7	25.9
12 cm / 1.4 m	47.7	25.3
5 cm / 0.6 m	41.9	24.6
First Floor Heated Zone	**3 Stacks Closed**	**3 Stacks Closed**
27 cm / 3.2 m	68.4	27.5
21 cm / 2.5 m	66.0	27.3
15 cm / 1.8 m	62.0	26.8
9.5 cm / 1.1 m	58.0	26.4
3 cm / 0.4 m	50.8	25.6
Ground Floor Column	**3 Stacks Closed**	**3 Stacks Closed**
26 cm / 3 m	40.7	24.5
19 cm / 2.3 m	36.0	24.0
12 cm / 1.4 m	33.5	23.7
5 cm / 0.6 m	27.2	23.0
Ground Floor Heated Zone	**3 Stacks Closed**	**3 Stacks Closed**
27 cm / 3.2 m	36.3	24.0
21 cm / 2.5 m	33.6	23.7
15 cm / 1.8 m	34.2	23.8
9.5 cm / 1.1 m	43.5	24.8
3 cm / 0.4 m	43.1	24.7
Atrium	**3 Stacks Closed**	**3 Stacks Closed**
100 cm / 12 m	55.5	26.1
75 cm / 9 m	54.2	26.0
50 cm / 6 m	51.7	25.7
25 cm / 3 m	36.1	24.0

Full-Model Experimental Temperature Data

Buoyancy-Driven Flow

Table 71. Scaled Temperatures for Buoyancy-Driven Flow

Ground Column			
Height from Floor (m)	3 Stacks Open	1 Stack Open	Stacks Closed
3.0	22.38	22.43	22.46
2.3	21.96	22.04	22.08
1.4	21.75	21.86	21.90
0.6	21.80	21.84	21.87
Ground Heated Zone			
Height from Floor (m)	3 Stacks Open	1 Stack Open	Stacks Closed
3.2	22.47	22.53	22.57
2.5	22.04	22.13	22.16
1.8	22.07	22.17	22.17
1.1	22.02	22.08	22.11
0.4	23.82	23.79	23.78
First Floor South-Column			
Height from Floor (m)	3 Stacks Open	1 Stack Open	Stacks Closed
3.0	23.21	23.43	23.53
2.3	22.69	22.87	22.95
1.4	22.37	22.51	22.53
0.6	22.44	22.54	22.56
First Floor South-Heated Zone			
Height from Floor (m)	3 Stacks Open	1 Stack Open	Stacks Closed
3.2	23.74	23.93	24.02
2.5	23.38	23.56	23.68
1.8	23.23	23.44	23.49
1.1	23.56	23.75	23.81
0.4	22.65	22.75	22.77
First Floor North-Column			
Height from Floor (m)	3 Stacks Open	1 Stack Open	Stacks Closed
3.0	23.30	23.46	23.49
2.3	22.56	22.72	22.78
1.4	22.46	22.58	22.63
0.6	22.48	22.63	22.67
First Floor North-Heated Zone			
Height from Floor (m)	3 Stacks Open	1 Stack Open	Stacks Closed
3.2	22.90	23.03	23.04
2.5	22.63	22.78	22.73
1.8	23.77	23.94	23.93
1.1	23.17	23.34	23.35
0.4	22.74	22.89	22.88
Second Floor Column			
Height from Floor (m)	3 Stacks Open	1 Stack Open	Stacks Closed
3.0	24.86	25.14	25.20

2.3	24.31	24.65	24.78
1.4	23.35	23.65	23.78
0.6	23.38	23.65	23.70
Second Floor Heated Zone			
Height from Floor (m)	3 Stacks Open	1 Stack Open	Stacks Closed
3.2	23.71	24.05	24.19
2.5	24.14	24.51	24.65
1.8	25.26	25.62	25.71
1.1	23.53	23.83	23.92
0.4	24.66	25.05	25.19

Combined Wind-Buoyancy Driven Flow

Table 72. Scaled Temperature Data for Combined Wind-Buoyancy Driven Flow: Stacks Open

Ground Floor-Column								
m	5m/s	4m/s	3m/s	2m/s	1.5m/s	1m/s	0.7m/s	0.5m/s
3	20.39	20.48	20.61	20.86	21.09	21.35	21.64	21.80
2.3	20.40	20.49	20.63	20.86	21.06	21.33	21.55	21.67
1.4	20.46	20.54	20.70	20.92	21.12	21.33	21.45	21.54
0.6	20.51	20.59	20.77	21.02	21.21	21.30	21.33	21.40
Ground Floor-Heated Zone								
	5m/s	4m/s	3m/s	2m/s	1.5m/s	1m/s	0.7m/s	0.5m/s
3.2	20.35	20.43	20.54	20.84	21.10	21.34	21.68	21.91
2.5	20.39	20.45	20.56	20.81	21.07	21.28	21.63	21.92
1.8	20.45	20.52	20.63	20.84	21.06	21.28	21.66	22.04
1.1	20.48	20.56	20.67	20.93	21.78	21.35	22.50	22.78
0.4	20.94	21.10	21.43	21.87	22.07	22.52	22.71	22.88
First Floor-South Column								
m	5m/s	4m/s	3m/s	2m/s	1.5m/s	1m/s	0.7m/s	0.5m/s
3	20.39	20.48	20.70	20.96	21.15	21.43	21.79	22.04
2.3	20.40	20.49	20.70	20.92	21.15	21.37	21.73	21.93
1.4	20.46	20.54	20.69	20.89	21.10	21.34	21.71	21.87
0.6	20.51	20.59	20.72	20.93	21.16	21.40	21.76	21.95
First Floor South-Heated Zone								
	5m/s	4m/s	3m/s	2m/s	1.5m/s	1m/s	0.7m/s	0.5m/s
3.2	20.35	20.43	20.79	21.02	21.32	21.60	22.08	22.75
2.5	20.39	20.45	20.70	20.94	21.22	21.56	22.08	22.80
1.8	20.45	20.52	20.71	20.95	21.22	21.56	22.01	22.76
1.1	20.48	20.56	20.88	21.17	21.44	21.65	22.15	22.70
0.4	20.94	21.10	20.75	20.92	21.05	21.25	21.76	22.01
First Floor-North Column								
m	5m/s	4m/s	3m/s	2m/s	1.5m/s	1m/s	0.7m/s	0.5m/s
3	20.39	20.54	20.70	21.37	21.92	22.56	22.73	22.99
2.3	20.40	20.51	20.65	20.91	21.12	21.90	22.10	22.44
1.4	20.46	20.64	20.80	21.10	21.26	21.28	21.53	21.76
0.6	20.51	20.73	20.92	21.32	21.50	21.67	21.99	22.16
First Floor-North Heated Zone								
	5m/s	4m/s	3m/s	2m/s	1.5m/s	1m/s	0.7m/s	0.5m/s
3.2	20.35	20.84	21.25	21.97	22.17	22.35	22.62	22.67
2.5	20.39	20.70	20.85	21.20	21.45	21.68	22.00	22.14
1.8	20.45	21.07	22.20	22.89	23.10	23.24	23.52	23.72
1.1	20.48	20.70	21.38	22.16	22.34	22.54	22.79	22.94
0.4	20.94	20.69	20.86	21.43	21.69	21.92	22.28	22.39
Second Floor Column								
m	5m/s	4m/s	3m/s	2m/s	1.5m/s	1m/s	0.7m/s	0.5m/s
3	20.42	20.51	20.91	22.45	22.92	23.25	23.86	24.09
2.3	20.40	20.48	20.66	21.16	22.61	22.91	23.62	23.75
1.4	20.42	20.49	20.65	20.86	21.11	21.72	22.26	22.62

0.6	20.56	20.67	20.94	21.22	21.41	21.97	22.21	22.75
Second Floor Heated Zone								
	5m/s	4m/s	3m/s	2m/s	1.5m/s	1m/s	0.7m/s	0.5m/s
3.2	20.56	20.62	20.86	21.21	21.60	22.23	22.67	23.00
2.5	20.68	20.79	21.31	21.42	21.81	22.25	22.78	23.19
1.8	19.81	19.89	19.95	20.08	20.52	20.69	20.98	21.42
1.1	20.58	20.65	20.77	21.34	21.76	22.33	22.81	23.15
0.4	20.51	20.60	21.05	21.36	21.76	22.18	22.68	23.12

Table 73. Scaled Temperature Data for Combined Wind-Buoyancy Driven Flow: Stacks Closed

Ground Floor Column								
m	5m/s	4m/s	3m/s	2m/s	1.5m/s	1m/s	0.7m/s	0.5m/s
3	20.4042	20.48616	20.62966	20.90135	20.97387	21.44434	21.67381	21.81499
2.3	20.41628	20.50198	20.64385	20.90304	20.99325	21.43336	21.58161	21.68081
1.4	20.47502	20.56444	20.70873	20.95848	21.06522	21.43581	21.47392	21.55297
0.6	20.52836	20.61825	20.76384	21.07022	21.17139	21.3823	21.37005	21.44805
Ground Floor Heated Zone								
	5m/s	4m/s	3m/s	2m/s	1.5m/s	1m/s	0.7m/s	0.5m/s
3.2	20.36229	20.42936	20.59156	20.8792	21.02334	21.43322	21.72469	21.88462
2.5	20.40895	20.45982	20.61655	20.84888	20.98346	21.37892	21.66447	21.89513
1.8	20.46531	20.52396	20.68311	20.85359	21.03492	21.3731	21.72087	22.01657
1.1	20.49836	20.56249	20.73126	20.95347	21.65266	21.45834	22.5791	22.83274
0.4	20.95701	21.12217	21.39533	21.96275	21.85942	22.70337	22.79425	22.92543
First Floor-South Column								
m	5m/s	4m/s	3m/s	2m/s	1.5m/s	1m/s	0.7m/s	0.5m/s
3	20.4042	20.48616	20.70985	20.99975	21.1094	21.48456	21.85274	22.05754
2.3	20.41628	20.50198	20.69879	20.95904	21.08482	21.44354	21.78811	21.97138
1.4	20.47502	20.56444	20.68687	20.92943	21.04584	21.41905	21.74203	21.9054
0.6	20.52836	20.61825	20.71896	20.9642	21.09147	21.48599	21.80928	21.99767
First Floor-South Heated Zone								
	5m/s	4m/s	3m/s	2m/s	1.5m/s	1m/s	0.7m/s	0.5m/s
3.2	20.36229	20.42936	20.79884	21.05637	21.2756	21.68704	22.1686	22.74406
2.5	20.40895	20.45982	20.71019	20.98156	21.17434	21.63576	22.15402	22.80652
1.8	20.46531	20.52396	20.7194	20.99262	21.17278	21.64458	22.12434	22.75886
1.1	20.49836	20.56249	20.8833	21.19777	21.38133	21.7439	22.29268	22.72425
0.4	20.95701	21.12217	20.74322	20.96276	21.01231	21.31259	21.89386	22.04307
First Floor-North Column								
m	5m/s	4m/s	3m/s	2m/s	1.5m/s	1m/s	0.7m/s	0.5m/s
3	20.4042	20.55056	20.69713	21.27967	21.8928	22.66036	22.7826	22.97541
2.3	20.41628	20.51624	20.64124	20.92905	21.05882	21.99383	22.20195	22.58265
1.4	20.47502	20.65114	20.76524	21.14041	21.11726	21.36972	21.58857	21.76199
0.6	20.52836	20.73372	20.86522	21.34625	21.42869	21.78635	22.06468	22.21327
First Floor-North Heated Zone								
	5m/s	4m/s	3m/s	2m/s	1.5m/s	1m/s	0.7m/s	0.5m/s
3.2	20.36229	20.829	21.16005	21.99057	22.09135	22.4503	22.68546	22.87444
2.5	20.40895	20.72262	20.83568	21.22341	21.38282	21.75017	22.05164	22.24419
1.8	20.46531	20.96741	22.0705	22.92271	23.01547	23.35441	23.55233	23.77012
1.1	20.49836	20.68262	21.25249	22.18285	22.27848	22.62617	22.83988	23.03755

0.4	20.95701	20.71092	20.8446	21.42993	21.62916	22.03532	22.33537	22.53143
Second Floor Column								
m	5m/s	4m/s	3m/s	2m/s	1.5m/s	1m/s	0.7m/s	0.5m/s
3	20.42305	20.51726	21.15108	22.51273	22.81022	23.47457	23.9934	24.34045
2.3	20.40351	20.49062	20.68986	21.18224	22.42838	22.93748	23.82081	23.99656
1.4	20.40992	20.50469	20.60022	20.8867	21.02792	21.87676	22.37977	22.7074
0.6	20.55857	20.69365	20.87354	21.2143	21.29327	22.11186	22.30511	22.75677
Second Floor Heated Zone								
	5m/s	4m/s	3m/s	2m/s	1.5m/s	1m/s	0.7m/s	0.5m/s
3.2	20.55956	20.63375	20.78265	21.21824	21.52322	22.37115	22.73733	22.99734
2.5	20.67108	20.79137	21.27527	21.45137	21.67425	22.42941	22.87532	23.21107
1.8	19.48527	19.77397	20.35267	20.78637	20.7554	21.22007	21.4495	21.42241
1.1	20.59194	20.66367	21.08523	21.36179	21.66821	22.482	22.88408	23.16113
0.4	20.49822	20.60281	21.55976	21.43167	21.6048	22.35928	22.79913	23.17501